A GEOMETRIC METHOD OF FATIGUE SCF AND FRACTURE SIF ASSESSMENT

BENQIANG LOU

To my Mother

DECLARATION

I declare that, except where explicit reference is made to the contribution of others, that this dissertation is the result of my own work and has not been submitted for any other degree at the University of Strathclyde or any other institution.

SIGNATURE:

PRINT NAME: BENQIANG LOU

ACKNOWLEDGEMENTS

I would like to thank my supervisors, Professor Nigel Barltrop and Professor Atilla Incecik, for their guidance, support and help.

I deeply thank to Mrs. Thelma Will and Mr. Bob McNair for their care. I am grateful to Dr Li Xu for her kind help and valuable discussions, and S. Wang of ABS, London Branch. Thanks to Professor Purnendu K. Das, Professor Colin MacFarlane, Dr Kieran Dodworth and Mr Peter Blackwood (from Safety at Sea Ltd.), and Professor Peilin Zhou for their kind support. I also thank all fellows and students in Department of NAME, for their help and the time we shared together.

I am indebted to my family, for their love and support.

This work has been made possible by scholarships from ORSAS and CSC and support from the EC FP7 RISPECT Project. The financial support is gratefully acknowledged.

ABSTRACT

In modern marine structural design, the fatigue life and fracture prediction of local connection details of the vessel is necessary.

The traditional empirical rules or numerical work has considerably advanced the qualitative and quantitative understanding of fatigue and fracture analysis. Compared with the existing methods, this thesis explores a novel geometric methodology to evaluate the stress intensity and stress concentration factors (SIF and SCF).

The background and special theory was developed to give:

1. A better understanding of the singularities that commonly occur in sharp corners in ship connection details;
2. A quicker method for fatigue life estimation than present methods based on finite element analysis and/or detail classes.
3. A prediction of the stress fields so that more appropriate and reliable finite element meshes can be selected

When dealing with the influence of each connection detail, a “Length Scale” is estimated from the dimensions of the connection detail. This Length Scale can be converted into a Hot Spot Stress Concentration Factor for SN based fatigue calculations or used with (often simply added to) the real crack length to determine, in conjunction with a constant Y value (commonly 1.1) a Stress Intensity Factor for linear elastic fracture mechanics crack growth calculations.

The method is useful both for assessment of existing structures and for design application.

The thesis includes a comparison of the results from the application of this new methodology and existing fatigue analysis guidance.

Within the thesis the methodology is described together with relevant conclusions.

SUMMARY

The nature of ship structures is emphasized: inhomogeneous material, welding residual stresses and length scale characteristics. Imperfections are generally present and affect the fatigue strength characteristics and the fatigue damage. The basic approaches to service life assessment are based on fatigue analysis; and account for fatigue phenomena, influencing parameters, objectives of the assessment, global and local approaches and historical development.

An empirical method from ship classifications rules or FEM is usually required for the calculation. But the FEM process is quite time consuming and the extrapolation method, which is used to determine the stress to use in the fatigue calculations, is still subject to uncertainty, especially at the sharp corners with stress singularities.

A new methodology for fatigue (and possibly fracture) assessment, has been developed, starting from a cruciform model; and then further developed to realistic ship structural components.

The theoretical background involves the determination of a "Length Scale" from the sizes of the components making up the structural detail. This characterizes the stress field in the vicinity of the notch or sharp corner of the un-cracked structure.

The "Length Scale" is estimated from the dimensions of the connection detail. This Length Scale can be converted into a Hot Spot Stress Concentration Factor (SCF) for SN based fatigue calculations or used with (often simply added to) the real crack length to determine, in conjunction with a constant Y value (commonly 1.1) a Stress Intensity Factor (SIF) for linear elastic fracture mechanics crack growth calculations.

In some cases the method, with its capability to directly estimate SCFs and SIFs, may avoid the need for a finite element analysis, but the work also helps in setting up finite element analyses, by understanding the nature of the stress field appropriate mesh refinement can be selected for the type of analysis (that may be trying to model or to avoid the singularity in the notch/corner).

Various methods for SIF prediction are discussed, including the new empirical

Length Scale, approximate weight functions, extrapolation methods and the critical distance method. Relationships between simple and complex geometry shapes are found. Numerical codes are selected supporting SIF calculation, which having good accuracy between FE and analytical derivations.

The work presented here enables easy estimation of service life, including understanding the sensitivity to changes in the detail dimensions. The Length Scale is particularly useful during the early design stage and when attempts to identify fatigue prone locations for inspection planning purposes.

CONTENTS

DECLARATION i
ACKNOWLEDGEMENTS ii
ABSTRACT iii
SUMMARY iv
CONTENTS vi
NOMENCLATURE 1
CHAPTER 1 INTRODUCTION 1
1.1 State of the Art 1
1.2 Industrial Background 4
1.2.1 Case Study: Alexander Kielland Wreck 5
1.2.2 Case Study: Liberty Ship 8
1.2.3 Industrial Demanded Constructions 11
1.3 Reorganization of Assessment Procedures 13
1.4 Objectives and Scope of My Thesis 16
REFERENCES 18
CHAPTER 2 LITERATURE REVIEW 20
2.1 Introduction 20
2.2 Engineering Validation of Novel Methods 30
2.3 Fatigue assessment approaches 31
2.4 SN Curve Approaches 34
2.4.1 Nominal Stress Approach 36
2.4.2 Hot-spot Stress Approach 39
2.4.3 Structural Stress Approach 44
2.4.4 Notch Stress and Strain Approach 46
2.5 Fracture Mechanics Approaches 51
2.5.1 Fatigue failure life prediction 51
2.5.2 Micro-cracks 55

2.5.3 Methods for K Determination (for macro cracks) 57
2.6 Classification Rules 64
2.7 Conclusions 66
REFERENCES 67
CHAPTER 3 THEORETICAL BACKGROUND 80
3.1 Introduction 80
3.2 New Stress Distribution Formula 81
3.2.1 William's Eigen Stress Solution 82
3.2.2 Conformal Mapping Theory 86
3.2.3 Explanation and Solutions for Length Scale 88
3.3 Constant Distance SCF Definition 92
3.4 Transformation for 3D Situations 95
3.5 Conclusions 99
REFERENCES 99
CHAPTER 4 FEA IN FATIGUE and FRACTURE MECHANICS 101
4.1 FEA with SN Predictions 101
4.2 FEA in Fracture Mechanics Calculations 103
4.2.1 Selection of Element Type 104
4.2.2 Sub-modelling 106
4.2.3 Crack Path determination 107
4.2.4 Crack Modelling in ANSYS 108
4.3 FEM Applications in Ship Engineering 114
4.4 Conclusions 115
REFERENCES 115
CHAPTER 5 FRACTURE MECHANICS IN FATIGUE ASSESSMENT 120
5.1 Introduction 120
5.2 SIF Calculation 121
5.2.1 SIF Comparative Calculations for Different Crack Sizes 121
5.2.2 Use of Different Weight Functions for Estimating the Corner SIF 123
5.2.3 SIF Corrections for Early Crack Extensions 126

5.2.4 Small cracks in corners 128
5.3 Cracks approaching an edge 131
5.4 SCF Assessments from LEFM 133
5.5 Conclusions 136
REFERENCES 137
CHAPTER 6 LENGTH SCALE 'as' VERIFICATION 138
6.1 Introduction 138
6.2 Approximate Length Scale 139
6.2.1 Bracket/attachment plate influences 139
6.2.2 Basic plate influences 145
6.3 Comparison of the length scale formula and stress distributions at the corner of a Cruciform Shape 147
6.4 Verification for Geometric Transformation 154
6.5 Conclusions 158
REFERENCES 159
CHAPTER 7 COMPARISON OF LENGTH SCALE SCFs WITH PUBLISHED DATA 160
7.1 Introduction 160
7.2 Selection of Structural Examples 160
7.3 Further Assessment of HHI Specimen 162
7.3.1 Specimen HHI #2: Gussets on the Plate Edge 162
7.3.2 Specimen HHI #5: Plate to I-beam Box 165
7.3.3 Specimen HHI #1 Longitudinal Gussets on the Plate 167
7.3.4 Specimen HHI #3: Two-sided Double Plate Joint 170
7.4 Fatigue Life Assessment 172
7.5 Conclusions 173
REFERENCES 173
CHAPTER 8 COMPARISON OF LENGTH SCALE SCFs AND EXTRAPOLATION METHODS OF REAL SHIP DETAILS 177
8.1 Introductions 177
8.2 Structural Components Study 182

8.2.1 Double Bottom Longitudinal 183
8.2.2 Double Bottom Girders 193
8.2.3 Inner Double Bottom Frames 198
8.2.4 Double Bottom Ballast Tank Longitudinal 205
8.2.5 Ballast Tank Side Shell 216
8.2.6 Cargo Lower Stool Plates 225
8.2.7 Side Shell Frames 234
8.2.8 Top Tank Longitudinals 245
8.2.9 Deck Stiffening Connections 250
8.3 Conclusions 257
REFERENCES 257
CHAPTER 9 CONCLUSIONS AND RECOMMENDATIONS 259
9.1 Achievements 259
9.2 Conclusions 260
9.3 Future Works 263
APPENDIX A ANALYTICAL STRESS FORMULA DERIVATION 264
REFERENCES 269
APPENDIX B Methods Adopted for K Calculations 270
B.1 Weight Function Method 270
B.1.1 Weight Function for double edge crack 273
B.1.2 Weight Function for edge crack in infinite plane 274
B.1.3 Weight Function for edge crack in finite plane 276
B.2 Boundary Collocation Function 277
B.3 Relationship between BCM and WF 283
B.4 Summary of Elasto-Plastic Fracture Mechanics 285
REFERENCES 291
APPENDIX C FEA Applications in LEFM 294
C.1 Terminology of Finite Element Method 294
C.2 Solid and Shell Elements Considerations 297
C.3 MPC Technology 302

C.4 Singular Element in LEFM 304
C.5 J-integral Calculation Path 306
C.6 Fracture FE Case Study 308
REFERENCES 312
APPENDIX D Special Technology in Fatigue and Fracture Analysis 314
D.1 VCCT Technology 314
D.2 Paris Law Formulas 315
D.3 SN Assessment Employing FE-SAFE 316
REFERENCES 319

NOMENCLATURE

Without Specific explanation, the symbols used in this dissertation are referred to as follows:

2D, 3D	Two (Three)-Dimensional
ABS	American Bureau of Shipping
a_e	Additional Crack Size
a_s or Length Scale	Length scale of the corner/notch singularity
ASCE	American Society of Civil Engineers
ASME	American Society of Mechanical Engineers
BCM	Boundary Collection Method
BSI	British Standards Institution
BV	Bureau Veritas
CD	Critical Distance
DNV	Det Norske Veritas
FDA	ShipRightFatigue Design Assessment
FEA	Finite Element Analysis
FEM,FEA	Finite Element Method (Analysis)
GL	Germanischer Lloyd
HAZ	Heat Affected Zone
HHI	Hyundai Heavy Industries. Co., Ltd.
HHS	Hot-spot Stress
IACS	International Association of Classification Societies
IIW	International Institute of Welding
ISSC	International Ships Structure Congress
KI, SIF	Stress Intensity Factor
LEFM	Linear Elasticity Fracture Mechanics
LR	Lloyds' Register
SCF	Stress Concentration Factor

SEC, SEN	Singular Edge Crack, Singular Edge Notch
SN	Stress range – number of stress cycles (SN-curves)
SS	Structural Stress
SSC	Ship Structural Committee
WF	Weight Function
σ_0	Nominal Stress

CHAPTER 1

INTRODUCTION

1.1 State of the Art

Fatigue failure is the main cause of a large number of structural failures in engineering structures, causing many catastrophic accidents; it leads to loss of life and gross environmental pollution, damage of equipment and so on. The fatigue phenomenon is involved many basic disparities in fatigue analysis between the laboratory research and real engineering structures of very difficult and complex.

Experience from industries is relevant, but the structural details may be quite different and the nature of the fatigue damage may be significantly different with random turbulence and regular pressure cycles for aircraft, regular cyclic loads and random ‘bumpy road’ load for vehicles.

Welding strongly affects the material by the process of heating and subsequent cooling, the fusion process with additional filler material and the residual stresses that remain after welding. The weld is usually far from being perfect, containing inclusions, pores, cavities, and undercuts. As a consequence, fatigue failures appear in welded structures mostly at the welds rather than in the base component.

It demonstrates in Figure 1.1 that a failure appears in the ship engineering; fatigue of ships and offshore structures is typically characterized by a large number of cycles of wave induced stresses that are relatively low away from the high stress concentrations.

Figure 1.1 Illustration of a significant failure, involving fracture

However the combination of a weld and a sharp corner frequently occurs in ship structures. Fatigue may also be involved in the final failure associated with the accident, such as collisions, grounding, and wave impact damage.

The research will be arranged starting with a mid-section of the hull girder and side shell in which global structural locations of interest are identified. These regions are particularly prone to cyclic fatigue from stiffener, or overall cross section bending under cyclic pressures. Low fatigue lives may also be found under the effect of cyclic vertical and horizontal wave bending moments (see Figure 1.2).

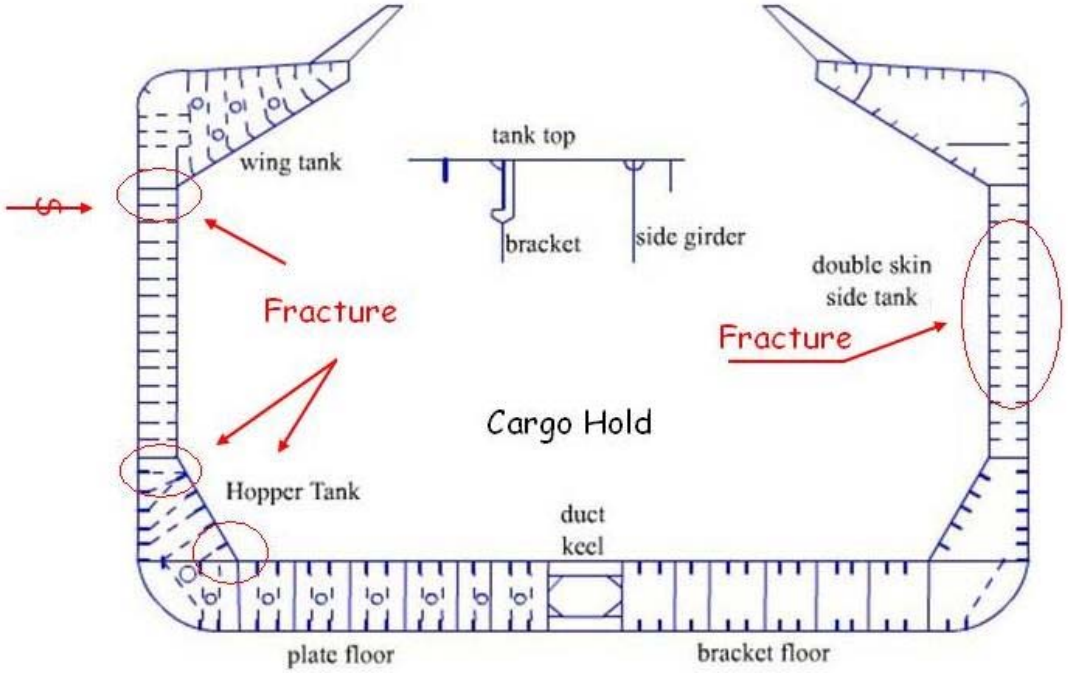

Figure 1.2 Typical fractures connection on double Bulk Carriers, (ABS, 1995)

There is no single agreed methodology for fatigue assessment of ships however some attempts have been made to unify the procedures and to understand differences. Compared with the laboratory study of the components, many factors influence and complicate the real subject e.g. material, load, and environmental corrosion, discontinuous geometry, defect, residual stresses or manufacturing.

In order to investigate the different procedures for fatigue strength assessment of ship structures, the members of ISSC Committee, 'Fatigue and Fracture' (ISSC, 2006, 2009) performed a comparative study.

During 2004 and 2005 common design rules for bulk carriers and tankers were proposed. The rule proposals were developed in two different projects: 1) the rules for bulk carriers were developed in the Joint Bulker Project (JBP, 2005) with participation of the following Classification societies: BV (1999), CCS, GL (1998), NK (1995), RINA, KR (1998) and RS the rules for tankers were developed in the Joint Tanker Project (JTP) with participation of the following Classification societies: ABS (1996), DNV (1999) and LR (1998), and the whole life from building to decommission compared with academic research.

The research is to provide the practicing naval architect with a readily accessible method, for improving the assessment of the fatigue performance of structural connections; however this thesis concentrates on the geometry assessment research of fatigue SCFs and fracture SIFs.

1.2 Industrial Background

The reasons why fatigue leads to structural fractures are various but two factors are important, acting separately or together:

1. Cyclic forces acting on the ship structure;
2. Insufficient resistance of the material.

Fatigue analyse is of high practical interest for all welded ships, ocean platform, and offshore renewable energy devices.

Even now, in the 22nd century, with superior steels and advanced weld processes, many hull structures still fail such as the 'Prestige' accident shown in Figure 1.3, where wave impact probably initiated fracture failures by fatigue loads.

Figure 1.3 Prestige oil tanker breaks in half. (AP, 2002)

Very often, the phenomena are inspected for the purposes of: 1) design philosophy, where fracture failure probabilities and consequences should be considered and controlled, 2) the selection of materials and to improve structure resistance quality and 3) the selection of appropriate periodic inspection and maintenance procedures.

The case studies, by the Ship Structure Committee (SSC) (**http**://www.shipstructure.org/), demonstrate a wide range of structural failures, casualties and analysis, which should increase appreciation of the structural issues, which are common in the shipbuilding industry and provides a forum for the dissemination of information to naval architects.

Depending on the functions of the component and usage in service, the failure impact on the overall system will vary from a minor degradation to catastrophic failure. In order to understand ocean engineering fatigue failures, it is necessary to review these disasters and significant structure damages, semi-submersible Alexander Kielland, Liberty ships and tanker and bulk carriers.

1.2.1 Case Study: Alexander Kielland Wreck

One of the most serious fatigue failures, which resulted in a heavy loss of life, is the semi-submersible pentagon platform ‘Alexander Kielland’ (shown in Figure 1.4). The rig capsized creating the worst disaster in Norwegian waters since World War II; 123 people perished.

Figure 1.4 Platform-pentagon ‘Alexander Kielland’ working in the North Sea

The Alexander Kielland is a Norwegian owned semi-submersible rig (by the Stavanger Drilling Company) in the Ekofisk oil field. The rig, located approximately 320 km east from Dundee, Scotland, hired by the U.S. Company Phillips Petroleum then.

In driving rain and mist, early in the evening of 27 March 1980 more than 200 men were off duty in the accommodation on the Alexander Kielland, and the wind was gusting to 40 knots with waves up to 12m high. About 18:30 the staff on board felt a 'sharp crack' following by 'some kind of trembling'. The rig began to heel over and the heel continued to increase; the anchor cables preventing the rig from capsizing but broke one by one. At 18:53, the only remaining anchor-cable snapped and the whole rig turned upside down. (Later, evidence was put forward indicating that the rig had been deliberately sabotaged with explosives, but the fracture surfaces demonstrated that fatigue loading on the defective welded was the cause.) (http://en.wikipedia.org/wiki/Alexander_L._Kielland)

The investigative report in March 1981 concluded that the rig collapsed owing

to a fatigue crack in one of its bracings, which connected the collapsed leg to the rest of the rig. Cold cracks in the welds, increased stress concentrations due to the weakened flange plate, the poor weld profile, and stress concentrations, collectively worked towards the rig's collapse.

Furthermore, the investigation report showed that considerable amounts of lamellar tearing were found in the flange plate and cold cracks in the butt weld position, which may be also the potential cause. Broken brace that lead to the disconnection of the leg is shown in Figure 1.5.

Figure 1.5 The collapsed leg floating above the sea surface after the accident

The rig was recovered in 1983; it was scuttled later to search for missing bodies, and to determine the cause of the disaster. Part of the bracing failed in accident is displaying in the Norwegian Petroleum Museum (as shown in Figure 1.6).

Figure 1.6 Smashed bracket of Alexander Kielland in Norway museum

After the investigation of Alexander Kielland accidents, it gave rise to several new rules to control the disaster incidents, and a number of measurements have been adopted after the accident to improve offshore safety. Safety courses became mandatory, and all offshore staff had to be issued with survival suits – both on the rig and on helicopter flights over the sea.

Other major structural elements then failed in sequence, destabilizing the entire structure, the rig design flawed owing to the absence of structural redundancy. Design rules following this failure required structural redundancy. The rigs must stay afloat even if one brace collapsed, and all loose equipment had to withstand at least 40 degrees of listing.

1.2.2 Case Study: Liberty Ship

Probably the best well-known examples of ship fatigue failure are Liberty cargo built during World War II. The Liberty ships were purchased for the U.S. fleet and for lend-lease provision to Britain. One report ‘Liberty cargo ship feature article’, written by James Davies (2008), described their histories, names, backgrounds and

contributions to WWII in detail.

During World War II, eighteen American shipyards produced large numbers of petroleum tankers, most of them were the T2 series. But 1941-1945, there were nearly 1,500 instances of significant brittle fractures on the Liberty Ships, shown in Figure 1.7.

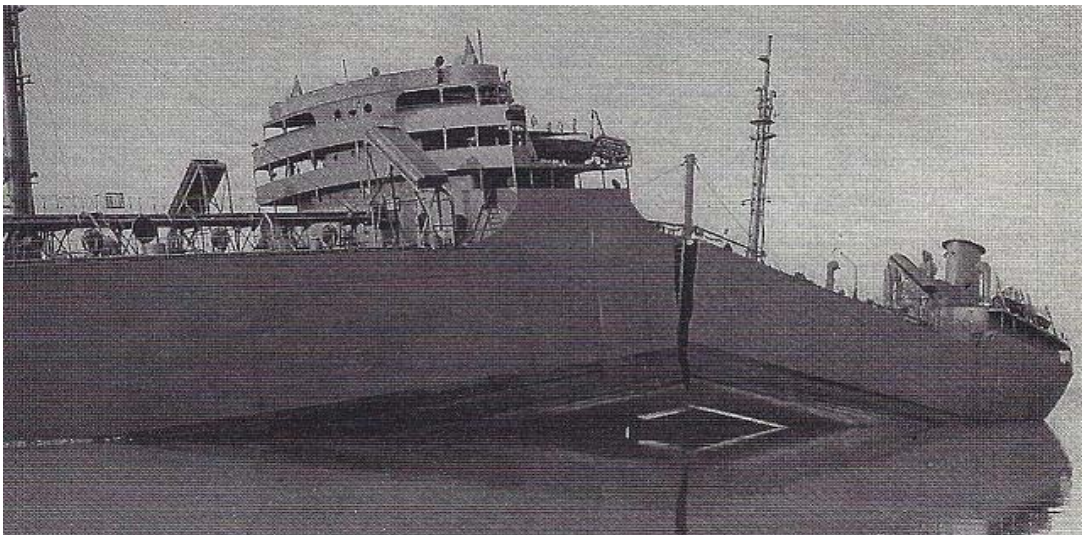

Figure 1.7 Fracture cutting split right across the main deck and down both sides from top to bottom in two amidships

Compared with the immense effort to build Liberty ships, the fact that the ships survived less than the original design life of five years, resulted in them being studied:

Twelve ships, including three of the 2,710 Liberties built, broke in half without warning, including the SS John P. Gaines which sank on 24 November 1943 with the loss of 10 lives, reported by newspaper in Figure 1.8.

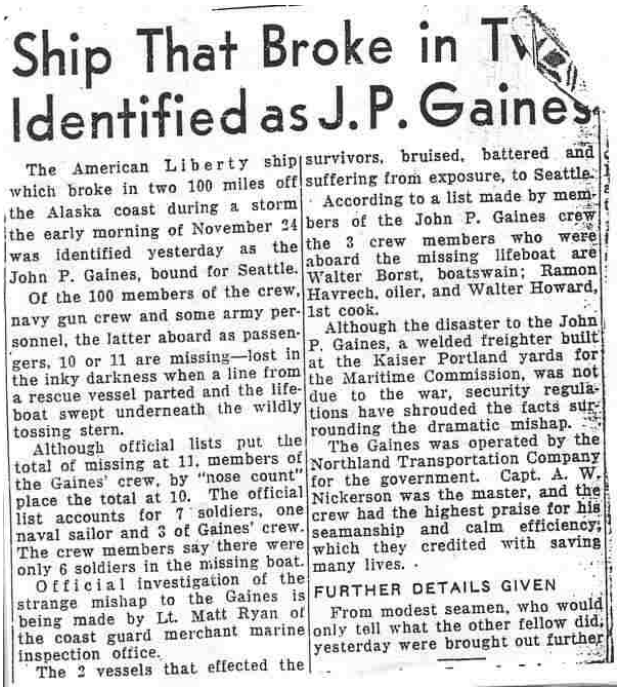

Ship That Broke in Tw Identified as J. P. Gaines

The American Liberty ship which broke in two 100 miles off the Alaska coast during a storm the early morning of November 24 was identified yesterday as the John P. Gaines, bound for Seattle.

Of the 100 members of the crew, navy gun crew and some army personnel, the latter aboard as passengers, 10 or 11 are missing—lost in the inky darkness when a line from a rescue vessel parted and the lifeboat swept underneath the wildly tossing stern.

Although official lists put the total of missing at 11, members of the Gaines' crew, by "nose count" place the total at 10. The official list accounts for 7 soldiers, one naval sailor and 3 of Gaines' crew. The crew members say there were only 6 soldiers in the missing boat.

Official investigation of the strange mishap to the Gaines is being made by Lt. Matt Ryan of the coast guard merchant marine inspection office.

The 2 vessels that effected the survivors, bruised, battered and suffering from exposure, to Seattle.

According to a list made by members of the John P. Gaines crew the 3 crew members who were aboard the missing lifeboat are Walter Borst, boatswain; Ramon Havrech, oiler, and Walter Howard, 1st cook.

Although the disaster to the John P. Gaines, a welded freighter built at the Kaiser Portland yards for the Maritime Commission, was not due to the war, security regulations have shrouded the facts surrounding the dramatic mishap.

The Gaines was operated by the Northland Transportation Company for the government. Capt. A. W. Nickerson was the master, and the crew had the highest praise for his seamanship and calm efficiency, which they credited with saving many lives.

FURTHER DETAILS GIVEN

From modest seamen, who would only tell what the other fellow did, yesterday were brought out further

Figure 1.8 Newspaper report for SS John P. Gaines broken accident

Generally, early Liberty Ship suffered hull and deck cracks. One common type of crack nucleated at the square corner of a hatch which coincided with a welded seam, both the corner and the weld acted as stress concentrators and small fatigue cracks probably become unstable and fractured.

Suspicion fell on the shipyards that often used inexperienced workers and new welding techniques to produce large numbers of ships in great haste. The predominantly welded (as opposed to riveted) hull construction then allowed cracks to run for large distances unimpeded.

However, work by the Engineering Department in Cambridge, Constance Tipper (in Figure 1.9) established that the factor could be critical temperature: If the environmental temperature fell below a critical point, the mechanism of failure changed from ductile to brittle, and thus the hull could fracture relatively easily.

Figure 1.9 Constance Tipper

The studies on the Liberty Ship lead to recommendation for steel manufacture and material selection to reduce the fatigue fracture risk, although, with better steels, fast crack growth is now not so much of a problem but it can still occur. Various reinforcements were applied to the same series ships to arrest the crack problems, and the successor design, was stronger and less stiff to better deal with the fatigue problem.

1.2.3 Industrial Demanded Constructions

Even if the ship does not break in two, fatigue cracks can cause pollution if there is oil on one side of a plate and the sea on the other side. Joint design rules have been developed by classification societies, providing information on two generic ship types: Double Hull Tankers and Bulk Carriers. The hull of a tanker is now of double construction design shown in Figure 1.10, where the bottom and sides of the ship have two complete layers of watertight surface, which forms a redundant barrier

between seawater and oil cargo, so a single plate failure, by cracking, corrosion, collision or grounding will not cause a pollution incident.

Note though that FPSOs (Floating Production, Storage and Offloading tankers) may still be built with a single bottom, because grounding is unlikely. However this increases the consequences of risks associated with bottom fatigue cracking.

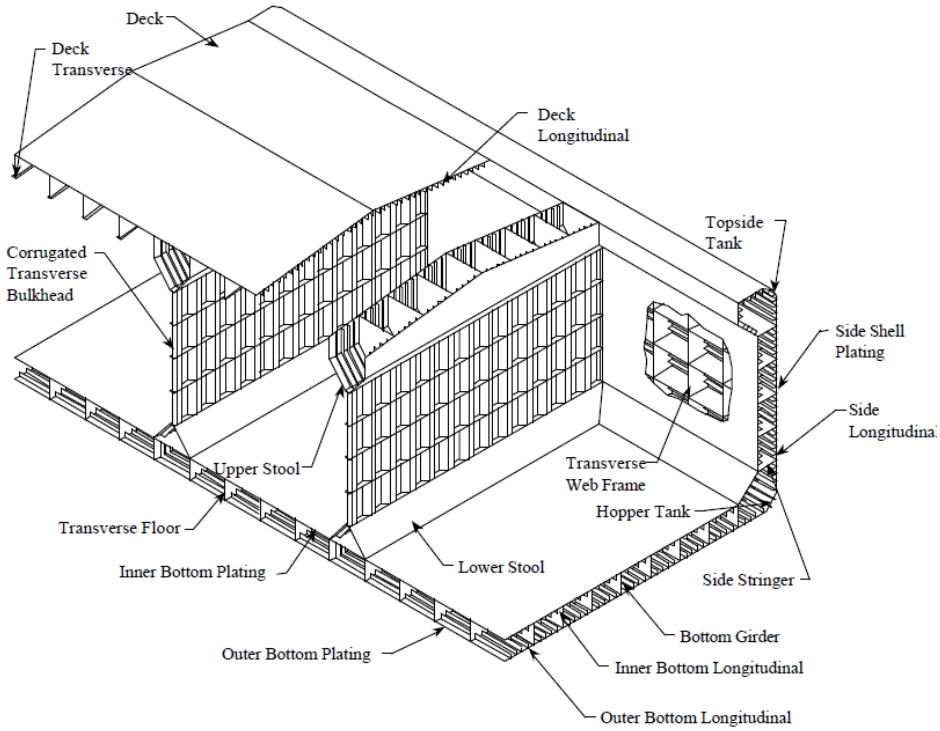

Figure 1.10 Typical Double Hull Tanker Mid-ship Global Structural Arrangement (SSC-405, 1999)

A bulk carrier, or bulker, is a merchant ship specially designed to transport unpackaged bulk cargo, such as grain, coal, ore, or cement in its cargo holds. Bulk cargo can be very dense, corrosive, or abrasive. The typical construction is shown in Figure 1.11; the use of ships that are old and have corrosion problems has been linked to a spate of bulker sinking since the 1990s, as have the bulker's large hatchways, important for efficient cargo handling and under strength hatchcovers and bulkheads.

To improve the safety of the bulk carrier, the strength of hatches has been increased to resist additional green water loading and bulkhead strength and the double bottom has been increased to withstand hold-flooded and alternate hold cargo

loading conditions.

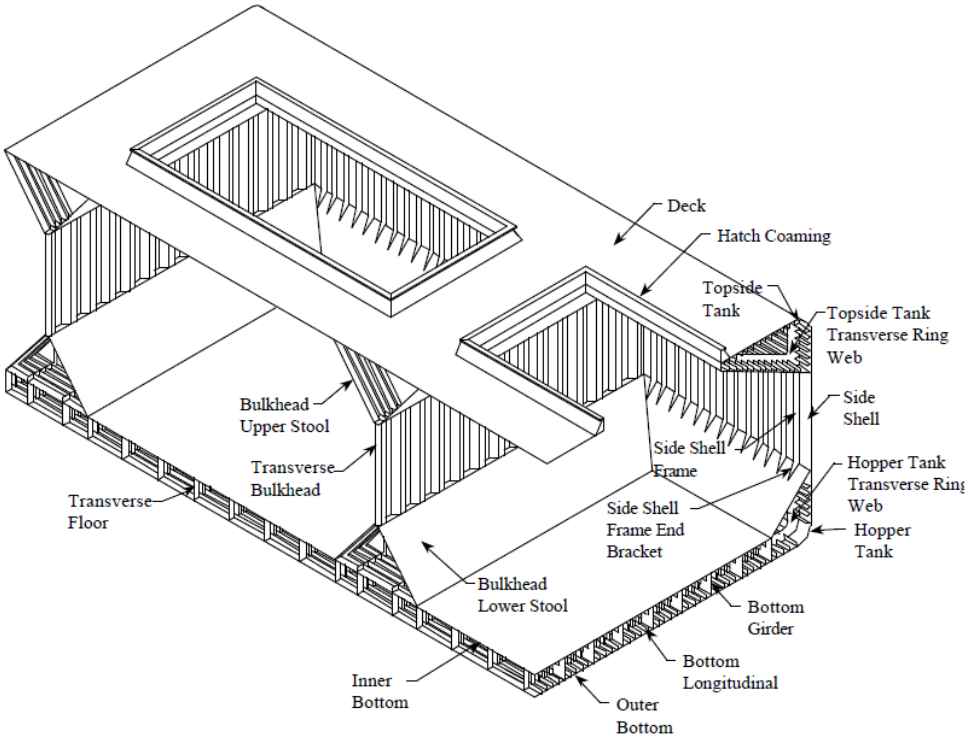

Figure 1.11 Typical Bulk Carriers Mid-ship Global Structural Arrangement (SSC-405, 1999)

For the two generic ship types and the many detaches (SSC 294, 1996 for catalogue), the research presented in this thesis could provide sources of information for practicing designers to use in addressing fatigue issues.

1.3 Reorganization of Assessment Procedures

Many structural details are similar in more than one ship type. At the design stage, the mid-section of ships is documented and submitted to the Classification Society as part of the design review and approval process. The section drawings illustrate the detail for a bulk cargo ship type (then a tanker) so that the user has complete information within mid section.

The rules focus on details associated with the mid-section of the vessel, since

this is generally the most critical area. It is shown in Figure 1.12 (the mid-section of bulk carrier) as good detail practice and is suggested those alternative configurations (shown circled) considered under high risk. (However the high stress concentration associated with the lower left right angled corner of the centre hold would need careful analysis.) All welded connections which are potentially prone to fatigue failure are presented.

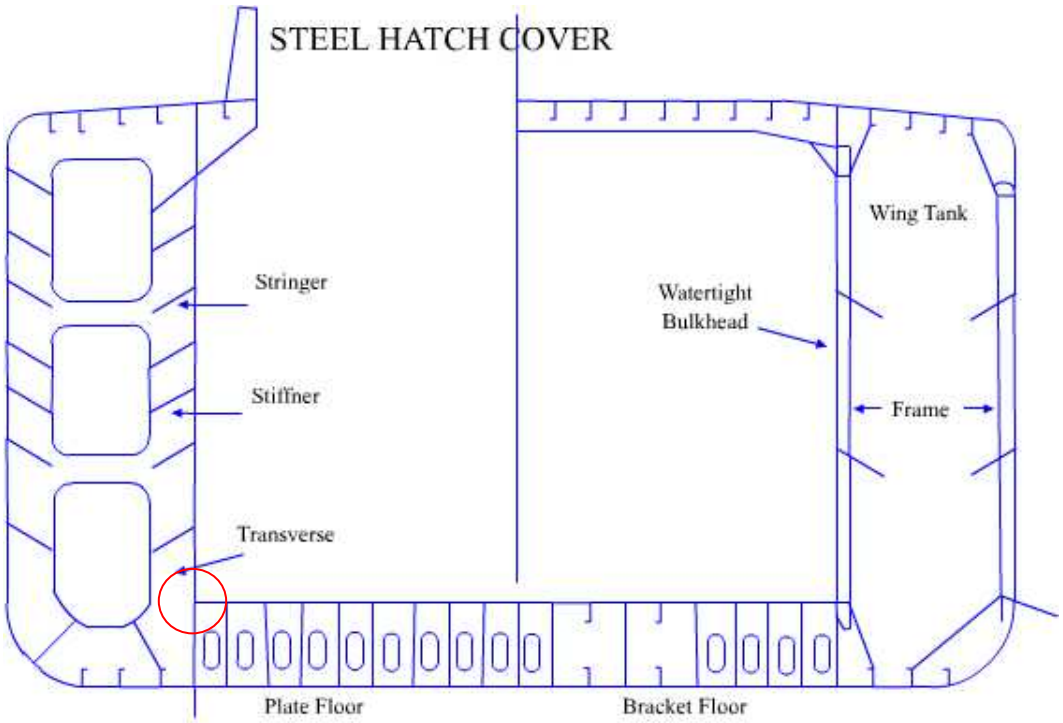

Figure 1.12 Example of Bulk Carrier (RISPECT documents, 2010) Mid-section Drawings

Typical classification Society outline guidance is of the form: the design load combinations should be sufficiently severe and varied so as to encompass all scenarios that can reasonably occur. Hydrodynamic loads should be based on the worldwide scatter diagram. Design load should combine local and global static and dynamic load components to represent identified load situations", (see Figure 1.13).

More detailed guidance will propose stress concentration factors for different types of detail.

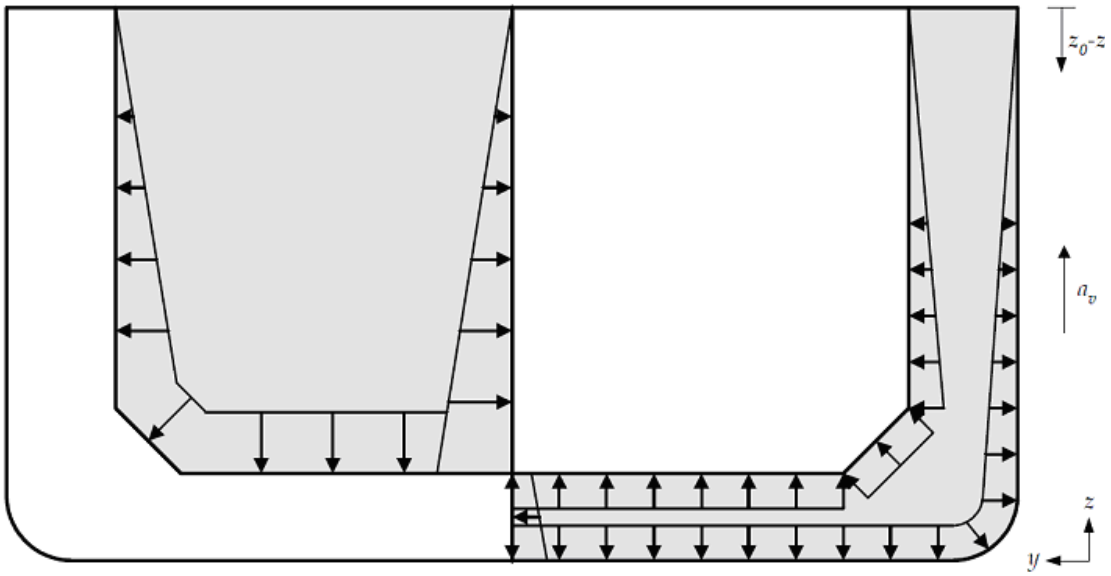

Figure 1.13 Pressure in Cargo Tank (Left) and Ballast Tank (Right) due to Positive and Negative Vertical Tank Acceleration (ABS, 2010)

The severity of the loadings seen by any specific detail will be determined by location-specific factors, and thus an inherently high-risk connection may require modification depending on its application. Accidental design load combination will usually also be considered.

Although the external environment plays an important role in fatigue and final failure are more dependent on the flaws or notches in the structure where fractures originate. To help understand the fatigue issues, we should analyze the fatigue behaviour and view the damage in terms of an intrinsic orderliness rather than an extrinsic problem.

While recent analysis results and guidance have emphasized the possible consequences of fatigue and related that with the geometry of the component, (dimensional shape, open angle, length and local weld connections) the analytic derivation of the geometry contribution to fatigue still needs to be clarified. The Length Scale method is based on the dimensions and shapes of the details and so provides a logical approach.

Several investigations have focused on the discussion of finite element meshing techniques at crack locations and on the fatigue resistance of the local structural

details. In the author's opinion, the combination of defects in the weld, the weld and connection profile shape and non-welded discontinuities in the connection will create stress concentrations that depend on the varying geometry parameters that are not properly accounted for in present guidance; the fatigue strength evaluation of a connection should be based on the stress concentration of the particular geometrical connection. Unless finite element analysis is to be applied to every location then the behaviour and the effect of the influencing factors need to be widely explored so that sensible fatigue analysis decisions can be made.

Starting from scratch a designer might browse a series of structural details, appropriate for the vessel local position, along with suggested "good practice" to improve fatigue performance.

The primary step in the design process for the details involves the selection of suitable sizes and thicknesses; the final aim, from this research is to help industry to better understand and predict fatigue behaviour using the defined Length Scale, so that efficient cycle life design method can be applied in order to optimize levels of risk and cost.

A detail analytical fatigue life assessment system should be developed to indicate the effects of the different geometry properties associated with the ship or offshore structure. Innovation of a new length scale based fatigue resistance procedure should proceed through a series of levels, or steps, like industry background, physical definitions, mathematical derivation, calculation method and time/costs, error performance and engineering application.

1.4 Objectives and Scope of My Thesis

In the thesis, the definition of the Length Scale has been brought out combined with SCF. This should allow fatigue design to be performed more efficiently (if the geometry is use to estimate the Length Scale/SCF directly) and/or more accurately (If the method is used to estimate the stress field in the un-cracked structure, which will provide guidance on the finite element meshing and what parts of the stress singularities are likely to be included in the analysis and what needs to be separately

accounted for.

The scope of my research work is:

Chapter 2 reviews existing literatures, on the fatigue assessment of ship and offshore structures, during the last 40 years. A series of papers are categorized into branches, and the efficiency of the different methods will be compared

In Chapter 3, the elasticity theory is discussed, especially the mathematical derivation and confirmation of the stress distribution formula. The cruciform shape will be used as the starting point.

More energy will be focused on the discussions of Length Scale (as), such as the effect of various in plane angles and the effect of out of plane angles. An innovation is the introduction of a power index into the formula to represent the behaviour of very small cracks.

The relationship between SCF and geometry property can be built by the bridge of Length Scale ‘as’: Based on conformal mapping explanation and mathematical hypothesis of Length Scale ‘as’ has been developed.

The fracture mechanics calculation is the other point. The Additional crack size ‘ae’ is now used and related to Length Scale ‘as’. In Chapter 4 a parametric equation of SIF is estimated from the empirical expressions and related to ‘ae’ by integrating the linear elastic fracture mechanics, crack propagation equations.

FEM is a very effective tool applied in modern design. FE calculation will be discussed in Chapter 5, and more calculations will be simulated. Guidelines for the mesh size will be verified for stress distributions using.

The approach of using Length Scale in fatigue strength prediction is discussed in Chapter 6, and verified by the numerical calculations.

Experimental specimens by Hyundai Heavy Industry (HHI) are used as the models comparison in Chapter 7. SCF results from Length Scale method and LEFM method are used to compare with the existing ones.

In Chapter 8 the SCF values for real ship structural locations predicted by the Length Scale approaches are compared with the traditional extrapolation ones. The numerical SCF employed, applicability of the Length Scale methods is determined.

Both the engineers and analysts urgently need well-founded methods in respect

of fatigue assessment. Based on our new methodology for the preliminary design stage, conclusions and recommendations are offered in Chapter 9, and also outlook for future work.

Appendices

Selected topics are presented in the Appendices: Appendix A explains the classic definition and derivation of the stress formula using complex series theory (main derivation is summarised from the works by Muskhelishvili, Westergaard, Irwin and Williams); Appendix B describes traditional theoretical methods for SIF calculations, and summary of Elasto-Plastic Fracture Mechanics, which will be the future development direction in structural strength analysis; Appendix C mainly described FE technology: introduced theoretical background, explained four special FE skills application in fracture mechanics calculations; and single edge crack model is simulated by ANSYS FE package in this section. Appendix D summaries relevant developments in structural analysis are presented of virtual crack closure technology firstly, and then reviewed two classical formula fistly: SN curve formula and Paris Law.

REFERENCES

1. ABS, Guide for Improvement for Structural Connections and Sample Structural Details - Service Experience and Modifications for Bulk Carriers - 1995
2. ABS. Guide for dynamic based design and evaluation of container carrier structures, American Bureau of Shipping, 1996
3. BV. Rules for the classification of steel ships. NR466A JAP R00 E, Bureau Veritas, Paris, 1999.
4. Davies. James. ‘Liberty Cargo Ship’. ww2ships.com, p. 23, Retrieved 25 March 2008
5. DNV. Fatigue assessment of ship structures, Det Norske Veritas Class Notes No.30. 7, 1999
6. GL. Rules for classification, Fanalysis techniques. Guidelines for fatigue

strength analyses of ship structures, Germanischer Llyod, Hamburg, 1998, [Chapter 2].

7. ISSC committee III.2: Fatigue and fracture［C］// 16th International Ship and Offshore Structure Congress. Southampton, UK, 2006: 445-527.
8. ISSC committee III.2: Fatigue and fracture［C］// 17th International Ship and Offshore Structure Congress. Seoul, Korea, 2009: 475-585.
9. JBP. IACS Common Rules for Bulk Carriers. Second Draft—April 2005
10. KR. Guidance relating to rules for classification of steel ships. Annex 7-8 Guidance for the fatigue assessment of ship structures. Korean Register of Shipping, 1998
11. LR. Ship Right FDA level 3 procedures manual, technical planning and development department, Lloyd's register of Shipping, 1998
12. NK. Guidance for fatigue design of ship structures. Nippon Kaiji Kyokai, 1995
13. Part 5A. Specific Vessel Types (Chapter 1) Common Structural Rules for Double Hull Oil Tankers, ABS, 2010
14. RISPECT documents, 2010
15. SSC-405. Fatigue resistant detail design guide for ship structures.
16. (http://www.guardian.co.uk/environment/2002/nov/19/spain.world)
17. (http://www.weldreality.com/ship-broken-in-two-x.gif)
18. (http://en.wikipedia.org/wiki/Alexander_L._Kielland_(platform))
19. (http://navalmerchantshiparticles.blogspot.com/2010/03/oh-those-famous-cracks.html)
20. (http://www.oilcity.co.uk/home/article.asp?pageid=507)
21. (http://www-g.eng.cam.ac.uk/125/1925-1950/tipper.html)
22. (http://stavanger.clickwalk.no/cgi-bin/seq.cgi?id=134&by=stavanger&lang=1&ttype=)

CHAPTER 2

LITERATURE REVIEW

2.1 Introduction

Fatigue cracks occur and develop if cyclic stresses are too high. The local stresses may be controlled effectively in the design; the locations of crack propagation can be examined and overall stresses reduced or local stresses reduced by improving the structural connection details.

The hull details can be grouped as follows:

Details comprises the discontinuous joints, e.g., bracket connections of longitudinal and transverse girders in bottom constructions, web plate connections of transverse girders in side tank frames has shown in Figure 2.1 (AMSP, 2006)

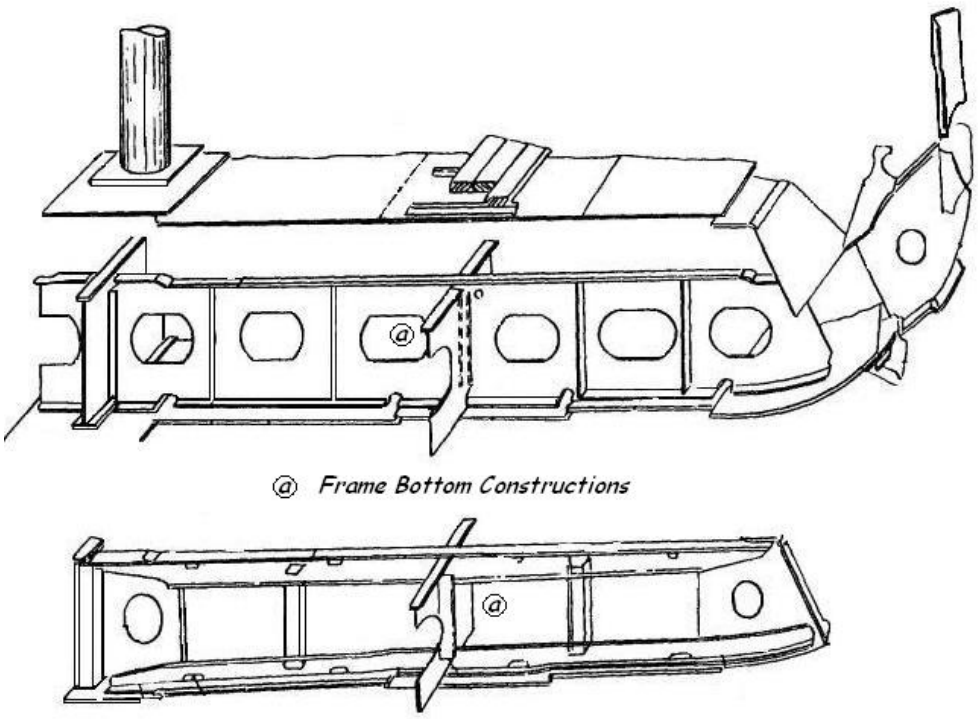

Figure 2.1 Longitudinal Framing Double Bottom Constructions (AMSP, 2006)

Details comprising the continuous welded connections of the hull elements, such as the bulkhead plating and longitudinal shell stiffener are shown in Figure 2.2 (AMSP, 2006)

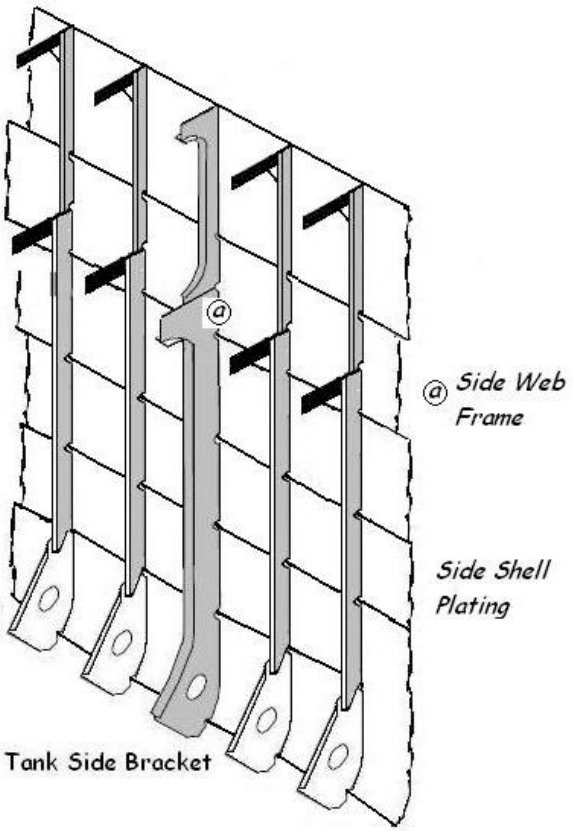

Figure 2.2 Transverse Framing ship Side Constructions (AMSP, 2006)

Details comprising the continuous welded joints[Error! Bookmark not defined.] located at structural discontinuities, at deck bulwark stay and side openings framed, e.g., in connections of supporting to deck plating, shown in Figure 2.3 (AMSP, 2006)

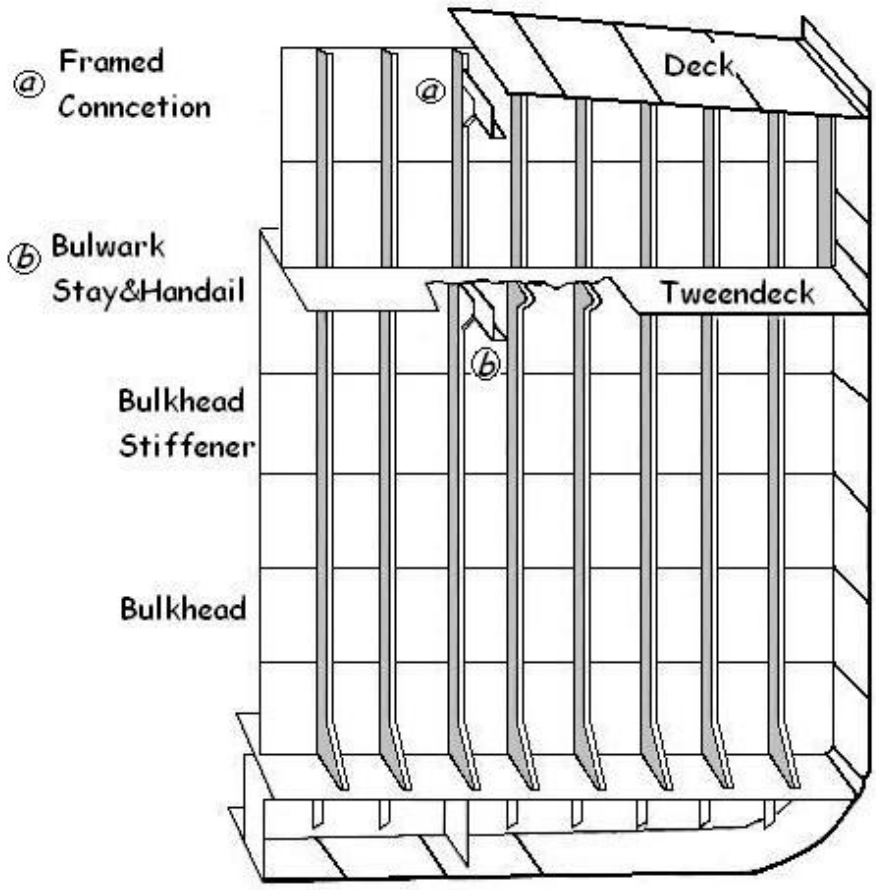

Figure 2.3 Partial Watertight Plane Bulkhead Construction (AMSP, 2006)

A case study has been successfully performed by Eylmann et al, 2005 where a comprehensive fatigue prediction program has been carried out on a ship structural component of a truck deck stiffened by trapezoidal profiles.

Therefore the details of these groups may be regarded as the details with controllable fatigue properties.

Due to the inspection problems, cracks in the beam-web to side-frame connections, which are menacing to the tanker's structural integrity, are often not identified until they are as large as 100-300 mm.

To meet the reliability requirements, the local stresses may be altered through small changes to the geometry of the details, e.g., by smoothing the bracket ends, increasing the hatch corner radius, increasing the stiffener sizes of the structural elements.

However, it is commonly observed that the cracks occur at stiffeners as shown in Figure 2.4.

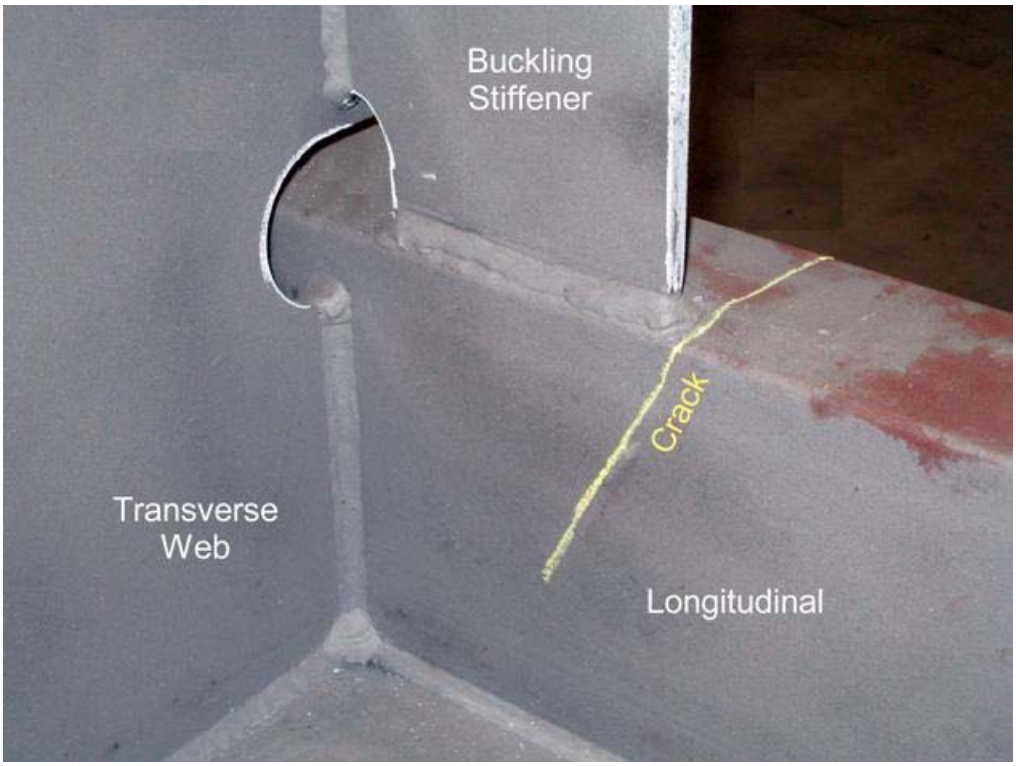

Figure 2.4 Crack propagating along the longitudinal stiffener
(Fricke W., Hans Paetzold, 2010)

Illustrating in Figure 2.5, it is found that the crack also initiates at the end of the bracket of the longitudinal stiffeners.

Figure 2.5 Fatigue crack at the bracket end of longitudinal stiffener

(R.V. Guchisky, S.V. Petinov, 2011)

Cracks also grow along brackets, Figure 2.6.

Figure 2.6 Fatigue cracks growth along the bracket plate

(I. Lotsberg, En Landet, 2005)

During the ship services, cracks are also observed at the inner connection locations shown in Figure 2.7.

Figure 2.7 Material repairing at the inner mouse-hole location
(WU Xiaoyuan, 2007)

The web frames are the primary structural members for the transverse ship sections. Longitudinal web panels are considered particularly for the crack initiation locations. It has shown in Figure 2.8 that the bracket connecting longitudinal and transverse bulkhead stiffener.

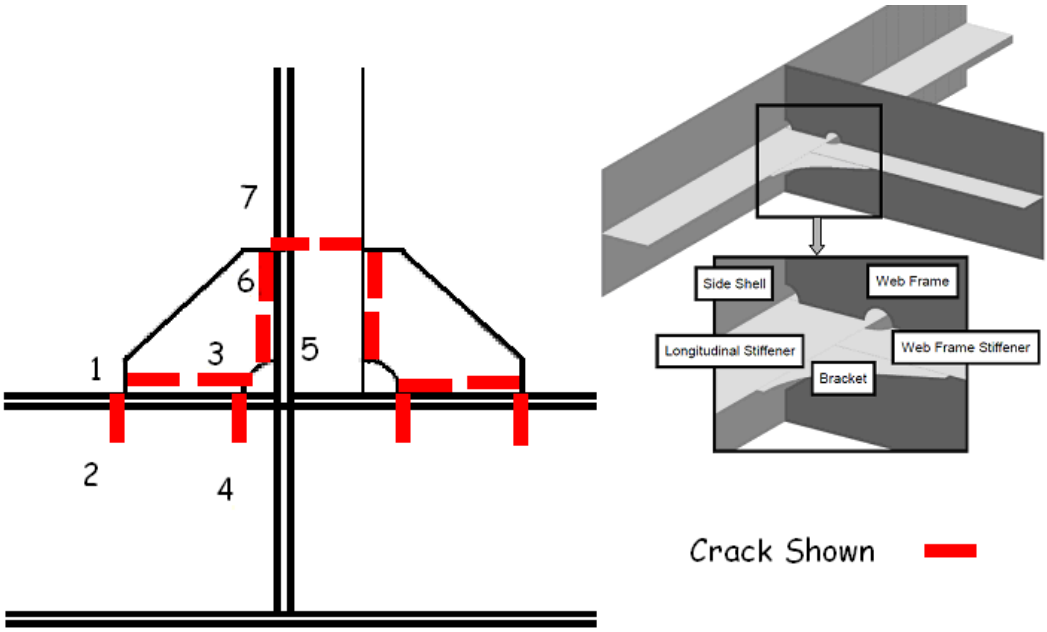

Figure 2.8 Considering crack initiation locations on the longitudinal panel (Brian E. Healy, 2004)

The tests results for the tensile loaded models are given in the form of stress concentration factor distributions at the detail parts where high strains are measured. As the reference value, the nominal stress used is obtained by dividing the applied load in the stiffened panel by the sectional area.

High stress concentrations are found in the stiffener's web, at the circular cutout in it, at a small distance from the bulkhead, where the smooth edge material is affected.

The fatigue strength of the panel structures based on direct fatigue tests may be overestimated in model tests, when transverse deflections of asymmetric stiffeners are not allowed, (S. Petinov, 2003).

Dimensionless principal stress distributions, around the crack initiation positions, are shown in Figure 2.9 are useful for estimating stress concentrations.

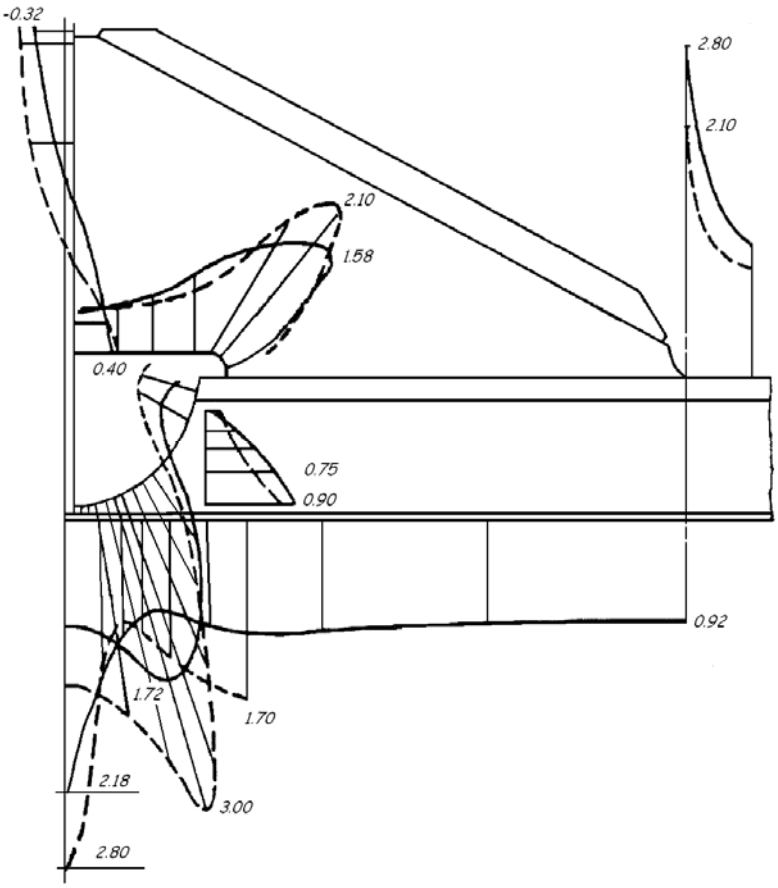

Figure 2.9 SCF of the bracket connection (Ziganchenko et al., 1981);
Solid lines marked for restricted transverse deflections and dashed for unrestricted

The crack propagation from the bracket end into the beam web and flange is a certain complication because standard stress intensity solutions do not exist. Once initiated at the bracket end, the crack propagates in the web beam and enters the connection of the web and beam flange.

A common design case concerns the bracket connection of plating longitudinal at a transverse bulkhead. The local stress elevation at the bracket end results from the hull girder deformation and bottom structure deformation, including the bottom longitudinal bending of the space between neighbouring floor and bulkhead. Being elements of the hull shell, these details sustain high stresses due to hull deformations and pressures imposed on the shell plating. The bracket connections are usually designed to withstand the longitudinal loading and therefore may be less effective in the transferring the local loads and shear stresses. A side longitudinal-flat bar

connection of a single-skin tanker structure under multiple loading; the longitudinal flange at the web plate is one of the potential critical points.

These details are responsible for the hull structural reliability, and their fatigue strength is the most influential factor in defining the hull reliability.

Entering the connection, the crack splits in branches into the flange and its rate is slowed due to essential expansion of the crack front. The problem can be solved by FE modelling of the detail and boundary conditions and simulating the crack extensions.

A series of fatigue test (Lotsberg I, 2001; Bergan PG, Lotsberg I, 2002, 2004) have been carried out as representative of the ship connections. The geometry transformations are needed for structures, and the definitions are given in Figure 2.10. The web frames are primary structural members, which can be transferred to the cruciform shape.

Approaches discussed in previous section are rather approximate and should be refined accounting for the typical structural damage failure.

We will see in later Chapters that we can usually ignore the dimensions of the main plate (a, b), and just the dimensions of flange (H, L) play the decisive role leading to significant influence on the SCF results.

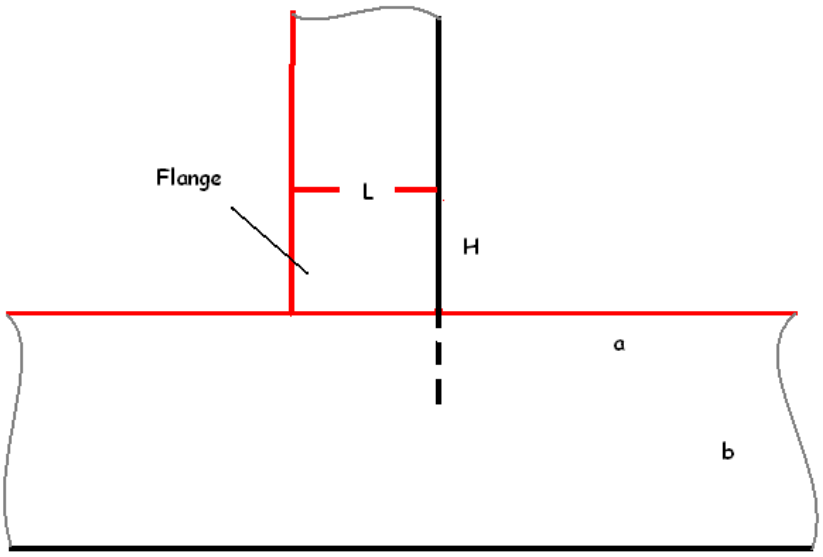

Figure 2.10 Specifying the simple length scale specimen for stress raisers (N. Barltrop, 2011)

It is generally acknowledged that the fatigue strengths of specimen component can decrease with the plate thickness increasing (Gurney, 1979). Further refinement in recommendations (IIW, 1996) is to modify the thickness correction exponent. Some works (Maddox SJ, 1987, 1995) showed the geometry effect depending on the proportions of the geometry details.

2.2 Engineering Validation of Novel Methods

The engineers are unable to produce defect-free components; it is very obvious that many connections can be recognized as defects in the bottom or side frames of the cargo hold.

It should be noted that during design and inspection, the physical criteria of the fatigue damage may be different: in design it should preferably be, as discussed above, the macroscopic crack happen, whereas inspection has to reply on the detectable size of the fatigue crack which depends on the resolution of the monitoring means. (Sergei Petinov, 2003)

To improve the design methods, many studies are particularized for related engineering types of specimens. In order to minimize the prediction proceed during fatigue analysis, crack is assumed to be found during the web frame detail categories, primary supporting stiffener transverse locations. The stress concentration factors are used for the fatigue life assessments.

The proposed structural detail has been surveyed from literature review, relevant work by classification institutions, or discussions with experts. The web frame connections are incorporated by Lotsberg.I, 2005 in shipbuilding community, a schematic of the transverse section are provided in Figure 2.11.

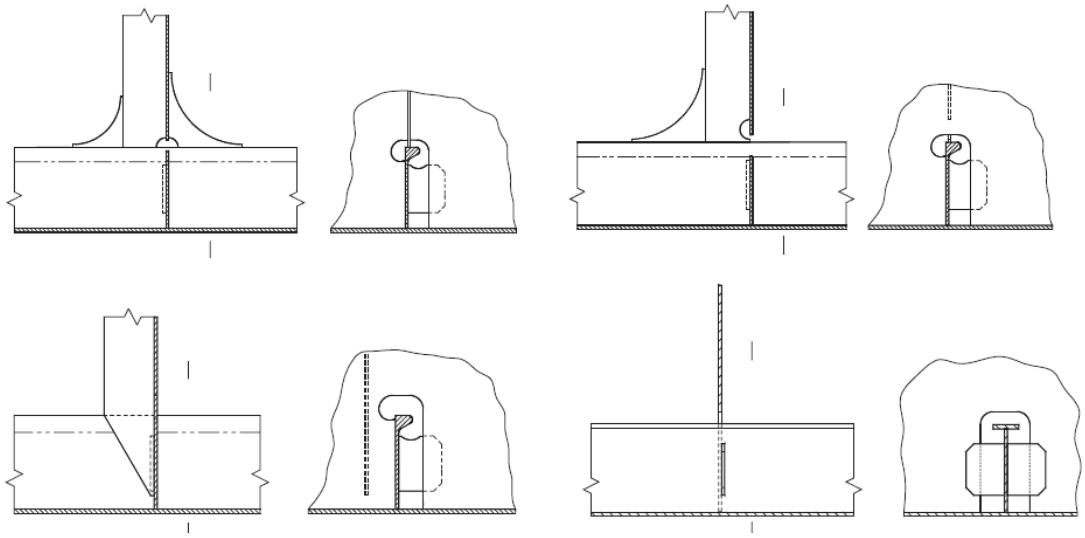

Figure 2.11 Full-scale test specimens (I. Lotsberg, 2005)

In this section, we are trying to consider the fatigue sensitive location from the real engineering project. According to the specimen selections from the tanker and bulk cargo constructions, the stress raisers along the crack propagation path are predicted. The Length Scale is used to investigate the fatigue behaviours of the web frame specimens.

Therefore, proper guideline for the calculation on complex geometry should be required, adhesive connecting applied commonly throughout the marine structures component.

2.3 Fatigue assessment approaches

The accidents caused by cracking failures of the hull are usually with fracture cracks propagations. Following the accidents, many institutes have done component tests and numerical calculation and brought out empirical or analytical formula. A large number of papers and books have been published as guides to the fatigue theory and application.

In view of the complexity of the fatigue subject and the mass of technical papers,

it is not surprising that within the two main branches of 1) SN curves and 2) Paris law / fracture mechanics, plenty of approaches to this topic exist and that even within an overall approach the detail of the methods used may differ. It is impractical to discuss all the possible options for fatigue assessment. However, fatigue analysis approaches may be subdivided, as shown in Figure 2.12 and Table 2.1.

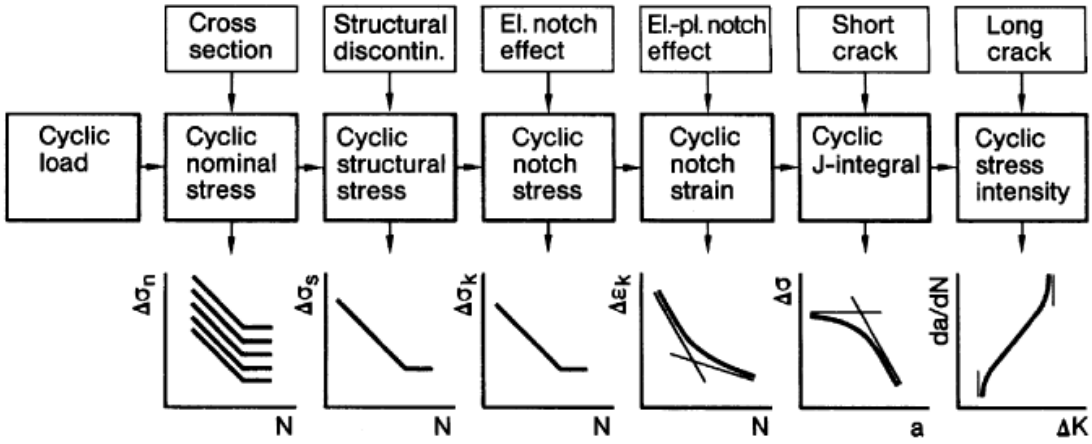

Figure 2.12 Approaches for description of the fatigue strength and life

(D. Radaj, 1995)

For the purpose of division of technical papers, available approaches are picked out to consider particularly. Furthermore, the following areas, each of them can be the subject of similar reviews, have been left out or are only touched. The two main possible approaches are in Table 2.1:

Table 2.1

Consistent application of IIW recommendations

	SN Curve Approach			**Fracture Mechanics Approach**	
Method	SN curve	SN curve	SN curve	Paris Law	Paris Law
Load on component	Nominal stress	Structural hot-spot stress	Notch stress	Notch Stress Intensity	Stress intensity at crack tip
Component	Structural detail	Type of weld	Particular detail	Particular detail	Particular detail

Before different papers on fatigue assessment of ship and offshore engineering components are discussed I note that some classic books provide a background into this subject and summarize the fundamentals as well as recent developments.

In connection with welded joints, the books by Gurney (1979) and Maddox (1991) present fundamentals of the fatigue strength assessment, investigations on fatigue behaviour and design rules and applications. Radaj (1990) presents the fatigue strength characteristics of welded joints and outlines different approaches for their assessment.

2.4 SN Curve Approaches

The SN curve approach prediction is based on fatigue strength of a critical structure detail as a function of the fatigue life.

The SN curve is used in conjunction with Miner's cumulative damage rule for dealing with varying sequential stress ranges, usually defined by a stress histogram.

If the real structure contains stress concentrations that did not occur in the tests that determined the SN curve then the design stress range will need to be multiplied by a stress concentration factor before entering the SN curve.

Different stresses are used with the different SN approaches. These are described briefly here and in more detail in Section 2.4:

- **Nominal stress approach:** This uses the nominal stress range $\Delta\sigma_n$ usually determined by the loads and the section properties at several plate thicknesses from the location of interest. This is used with an SN curve which accounts for the local stress pattern in the detail.

- **Hot spot stress:** This corresponds to a peak stress at the location of interest. A hot-spot stress is either calculated using local finite element calculation or estimated on the basis of tabulated SCF values multiplied by the nominal stress $\Delta\sigma_n$. For sharp notches, where the elastic stress concentration is theoretically infinite, even though the fatigue life is finite, the peak stress predicted by the finite element analysis is very sensitive to the mesh used and is not a reliable stress to use in the fatigue calculation. Instead a linear or quadratic extrapolation of the surface stresses into the corner, from specified distances from the corner is used to define the hot-spot stress. The fact that this is less than infinity can be considered to account for the fatigue crack growing into areas of lower stress. (Even for a round hole the peak elastic stress on the edge of the hole, corresponding to an SCF of 3, is often reduced

in fatigue calculations by using a "Fatigue SCF" of 2.4 to account for the reducing stress away from the corner.) On the basis that the effects of the corner have been taken into account in the calculated stress, this is used with an SN curve representing a welded connection between flat plates.

- **Structural stress approach:** It uses an approximate stress range at the weld to partly consider the effect of the structural discontinuity. A structural stress range $\Delta\sigma_s$ is a local stress range that accounts for the local average axial stress and the local bending moment, based on an approximate, linearly varying stress at the location of interest. Note that in many connections the average axial stress within the structural stress is greater than the average axial stress at some distance from the connection, because the stiffness of the connection draws load towards it. Structural stress range can be useful for interpreting finite element results, particularly if solid elements are used in the finite element model.

- **Notch stress approach:** A notch stress $\Delta\sigma_k$ can be defined if a pre-defined radius e.g. 1mm (not a sharp corner) is assumed at the structural discontinuity. This substitutes a finite stress for the infinite sharp corner stress and allows FEA to converge to a solution as the mesh is refined.

Some of the differences between these stresses, which are also indicative of the difficulty of estimating them, are illustrated in Figure 2.13. This shows the stresses at the end of a bracket, both on the plate surface and through the thickness of the plate.

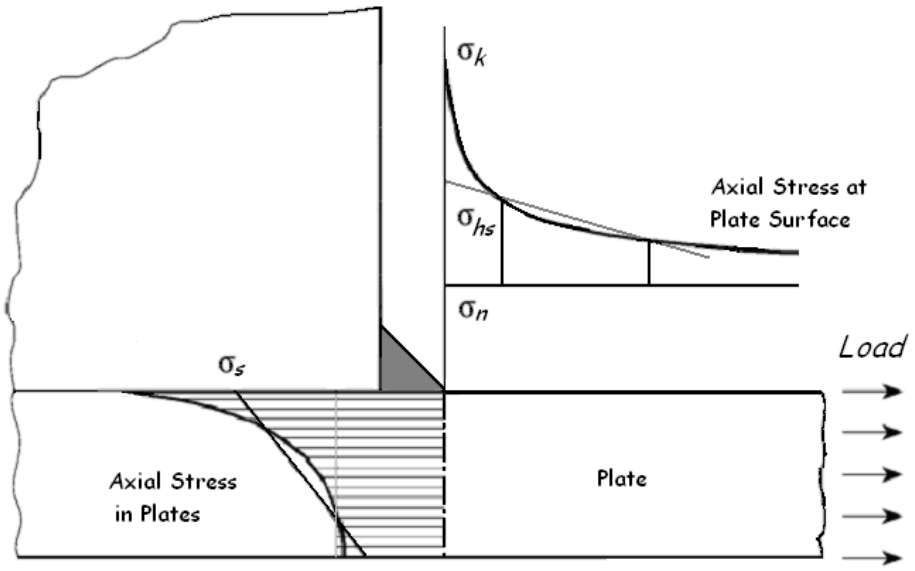

Figure 2.13 Concentrated stress types at a typical plate-type strip

In all cases these stresses characterize the linear elastic stresses in the un-cracked structure and providing they are calibrated with experiments:

- on similar geometry
- of similar sizes

to the real structure, then they should lead to reasonable fatigue life estimates.

2.4.1 Nominal Stress Approach

In a laboratory test, the definition of nominal stress is not complicated and can be calculated from Force/Area with possibly an allowance for bending: Moment/Section modulus, if the structure is eccentrically loaded. The nominal stress approach has been generally applied, mostly in large engineering component fatigue life predictions, by prescribing the related cross section properties of the stress range $\Delta\sigma_n$ histogram together with the number of external and internal load cycles.

Most codes refer to nominal stress range and then leave the engineering assessment of nominal stress to the designer. Modern design workflow (see Figure 2.14) makes increasing use of finite element method (FEM); however it can be difficult to interpret the results of a complicated stress field in terms of a nominal stress.

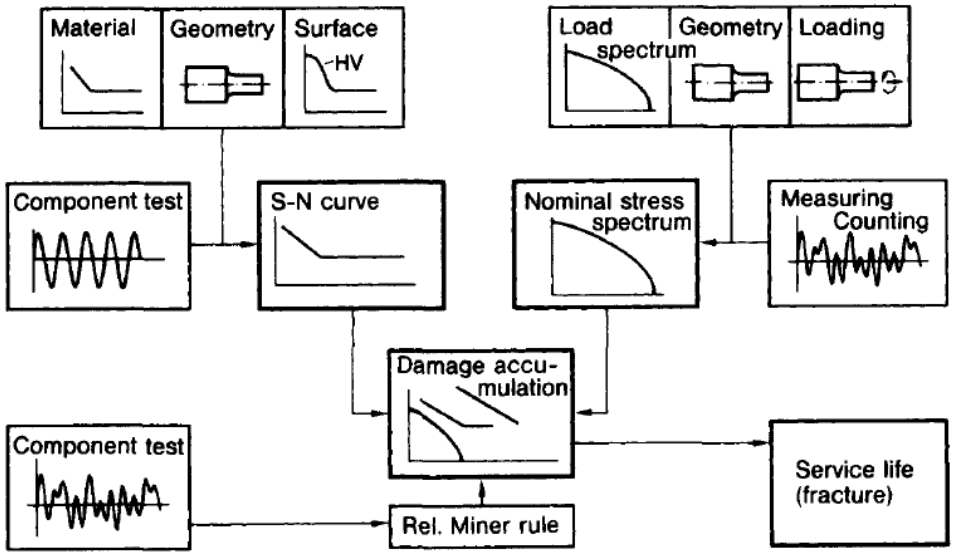

Figure 2.14 Nominal stress approach for assessing the fatigue strength and service life of structural component, according to Kloos, 1989

The nominal stress approach uses standard SN curves together with detail classes of basic joints which can be found in several standards. The appropriate class can be selected using example diagrams. SN curves are mainly based on the statistical evaluation of relevant fatigue tests, where a lower limit (usually -2 standard deviations) to the scatter in the results is used as the design curve. Two example curves are shown in Figure 2.15 and curves, from the International Institute of Welding (IIW) that correspond to a wider range of details, with different fatigue performance caused primarily by the inherent stress concentrations and initial defects, are shown in Figure 2.15.

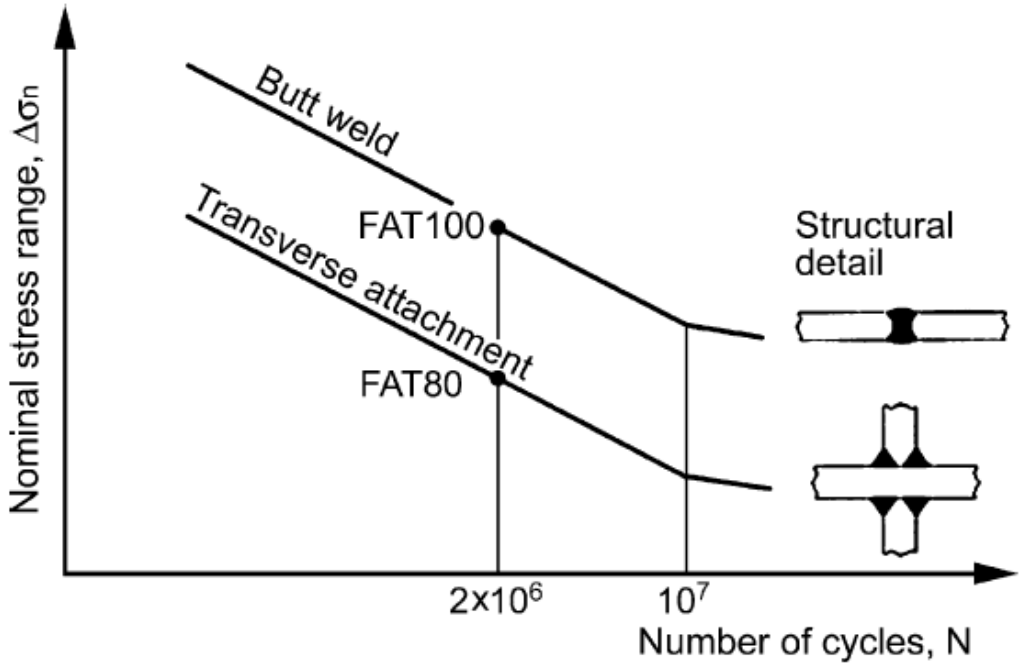

Figure 2.15 Example of design *SN* curves in the nominal stress concept; recommendations refer to fatigue design classes (Hobbacher A, 2007)

There are curves relating with the hot-spot stress concentrations, more and more experimental results up to Giga-cycles and failure experiences with decline of the Woehler SN in Figure 2.16. In traditional codes, the knee point of the SN curve is defined as the transition to infinite life, the fatigue resistance of about 10% per decade is assumed.

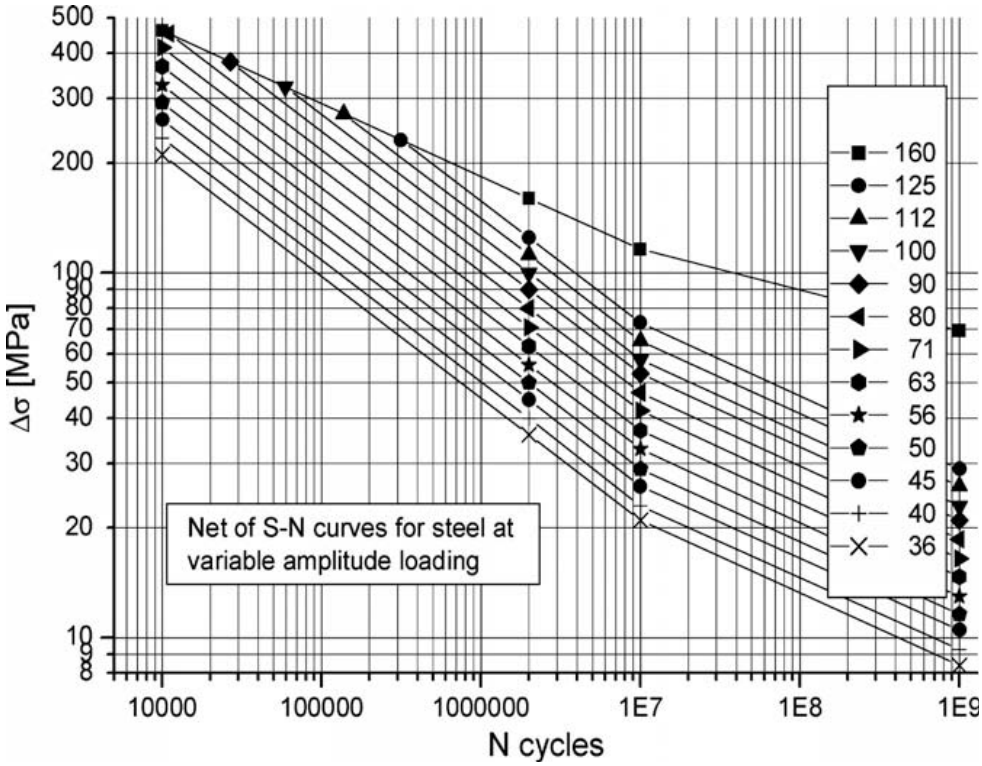

Figure 2.16 Modified net of Woehler SN curves for variable amplitude (A. Hobbacher, 2009)

As well as the general references (Gurney and Maddox) given previously, the following references are useful:

Backstrom and Marquis (2001) re-analyzed different experimental investigations for multi axial fatigue loading and compared the results with different methods of stress estimation.

A. Hobbacher (2009) gives basic guidelines for the design and analysis of welded components loaded by fluctuating forces, relevant to common structural components.

2.4.2 Hot-spot Stress Approach

The Hot spot is a point in a structure where a fatigue crack may initiate due to the combined effect of structural stress fluctuation and the weld geometry. The hot

spot stress excludes the contribution to the stress concentration caused by the local geometry but includes those that result from the overall geometry. The stresses are measured by extrapolating results from surface strain gauges or are obtained from extrapolating surface stresses from finite element analysis. The idea to exclude the local stress concentration is related to experimental investigations performed in the 1960s by Peterson, Manson and Haibach.

An HSS extrapolation method is shown in Figure 2.17.

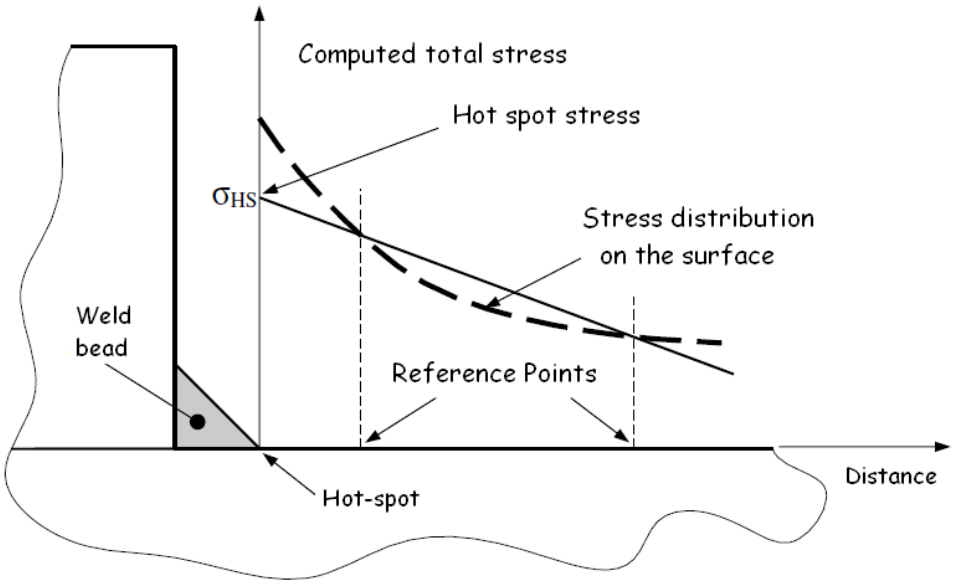

Figure 2.17 Extrapolation to the hot spot (Luca Susmel, 2009)

Several extrapolation procedures (shown in Figure 2.18, linear and quadratic extrapolation approaches) have been suggested for the determination of the local stress raiser.

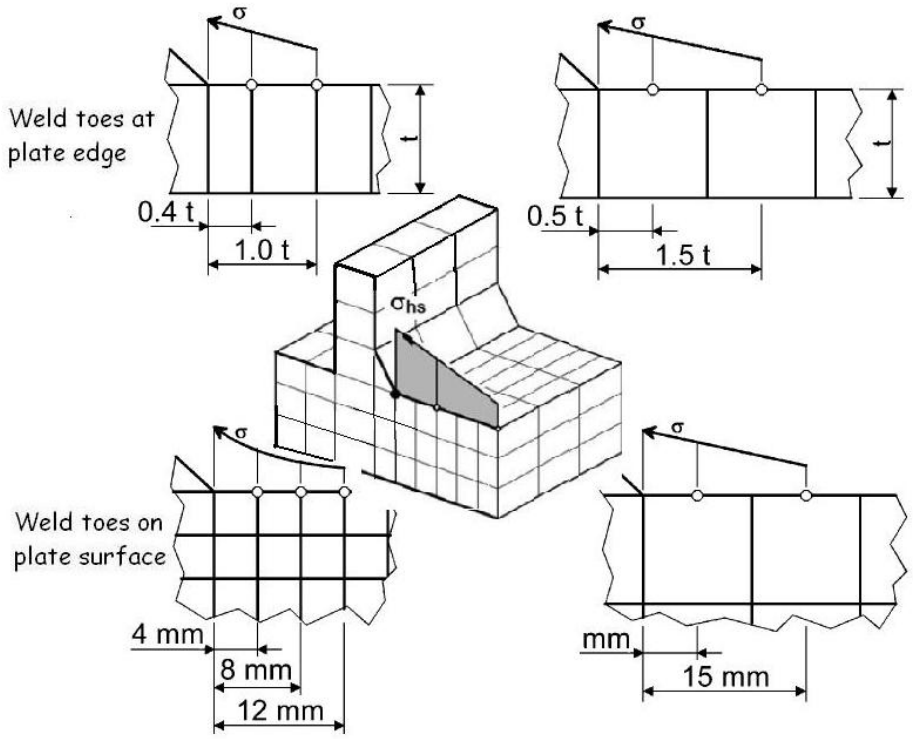

Figure 2.18 Different rules for hot spot stress extrapolation
(A. Hobbacher, 2003; W. Fricke, A. Kahl, 2005)

In the recommendations of the International Institute of Welding (IIW), 2009 the hot-spot stress is derived, using extrapolation, from reference points on the surfaces at distances from the weld toe of 0.4t/1.0t, 0.5t/1.5t or 0.4t/0.9t/1.4t where t is the plate thickness. The hot spot stress is then found from one of the following extrapolation formulae (which require strain gauges or finite element results at the specified distances from the hot-spot:

$$\sigma_{hs} = 1.67 \cdot \sigma_{0.4t} - 0.67 \cdot \sigma_{1.0t} \quad 2.1$$

$$\sigma_{hs} = 1.50 \cdot \sigma_{0.5t} - 0.50 \cdot \sigma_{1.5t} \quad 2.2$$

$$\sigma_{hs} = 2.52 \cdot \sigma_{0.4t} - 2.24 \cdot \sigma_{0.9t} + 0.72 \cdot \sigma_{1.4t} \quad 2.3$$

For attachments to a plate, the plate thickness is considered as a suitable parameter to define the extrapolation locations. However for corners in plates and extrapolation points on the edges of the plate, the plate thickness should not be relevant and IIW recommends reference points at fixed distances from the corner: of 4/8/12 mm or 5/15mm.

$$\sigma_{hs} = 3 \cdot \sigma_{4mm} - 3 \cdot \sigma_{8mm} + \sigma_{12mm} \quad 2.4$$

$$\sigma_{hs} = 1.50 \cdot \sigma_{5mm} - 0.50 \cdot \sigma_{15mm} \quad 2.5$$

Lotsberg from DNV has published a lot of works about fatigue design procedures, for realistic engineering components:

Due to fabrication tolerances for design guidelines, classical shell theory is used by Lotsberg, 1998 to derive the analytic expressions. The design cases include butt welds in tubular, welds at ring stiffeners and bulkheads in shell structures, welds at conical transitions and tubulars subjected to axial tension, as in risers and tethers.

Lotsberg (2004) supplied a design procedure for fatigue assessment of welded pipe penetrations in plated structures, based on SCF from finite element analyses. Numerical examples using the procedure are presented.

Lotsberg (2006) compared 200 fatigue test data, the test specimens were subjected to different loading conditions, with two procedures for calculating fatigue life.

Lotsberg (2008) applied Shell theory to pipes subjected to internal pressure and axial force. He considered circumferential butt welds, welds connecting different wall thicknesses, welds at buckling arrestors, welds at flanged connections, and welds at ring stiffeners on the inside and the outside of the pipes.

In the recommendation, Lotsberg (2009) improved equations for stress concentration factors to be used in fatigue design rules and for butt welded tubular sections and pipelines structures. Eccentricities at plate thickness and with fabrication tolerances gave increased stresses due to local in-plane bending.

Arno M. van Wingerde, et al, (1997) focused on the definition of hot-spot stress, using knowledge gained from experiments and the important fatigue behaviour of 90° T- and X-connections between hollow structural sections.

C.M. Sonsino (1990, 2001, and 2003) from Germany is doing research more works about SN curves of hot-spot stress approach assessment, in which there are

several reviews. His papers can be considered as necessary literature reviews for the automotive industry and ship-offshore structures through the recent approaches:

In C.M. Sonsino's study (2003) the fatigue properties of different types of laser beam welded thin sheet aluminum are examined by experiment. Fatigue test data derived from specimen geometry is transferred to real structures with a master curve concept.

Especially, under a spectrum of variable amplitude loading, the decrease in the permitted stress range from the effect of tensile residual stresses is not as high as under constant amplitude loading; this knowledge benefits light weight design of C.M. Sonsino (2007).

The influence of multi-axial stress/strain is researched, C.M. Sonsino (2007). He researched the fatigue behaviour of hollow cylindrical specimen under elastic-plastic deformations and determined fatigue reliably with un-notched specimens in deformation controlled tests.

C.M. Sonsino (2008) reviewed the fatigue design of components submitted to loadings below the knee point of the SN curve, i.e. in the very high-cycle area. Material and manufacturing dependent recommendations are given; the work revealed a continuous decrease of fatigue strength.

The paper by C.M. Sonsino (2009) describes how spectra and test conditions should be clearly described and how statistics can be applied when variable amplitude test results are presented.

G. Savaidis, M. Vormwald (2000) examined various welded joints from the floor of buses. The numerical and experimental work considered bending and tensional cyclic constant-amplitude loading.

Bard Wathne Tveiten et al (2000) reviewed and verified already published hot-spot stress extrapolation procedures for plate structures, and developed and establish a general method together with a hot-spot design SN curve for aluminium ship structures.

In conclusion, the majority of the effort has been on developing effective hot-spot stress extrapolation procedures and correlated to various available SN curves.

2.4.3 Structural Stress Approach

The definition of such corresponding structural stress approaches can also be referred to as Dong's method or the Battelle method. The feature that distinguishes the structural approaches is the inclusion of the effect of the stress gradient along the anticipated crack path, which is taken into account using fracture mechanics. For completeness the solution technique is applied to the Mode I problems with a discontinuity connection (Dong, 2001), which, it is claimed, can be consistently calculated in a mesh-insensitive manner regardless of finite element models and regardless of element types or loading modes.

The structural stress distribution needs to satisfy equilibrium conditions within the context of elementary structural mechanics theory at the anticipated crack plane. Membrane (σ_m) and bending (σ_b) stress components that are equilibrium-equivalent to the local stress distribution are calculated as illustrated in Figure 2.19 and Figure 2.13.

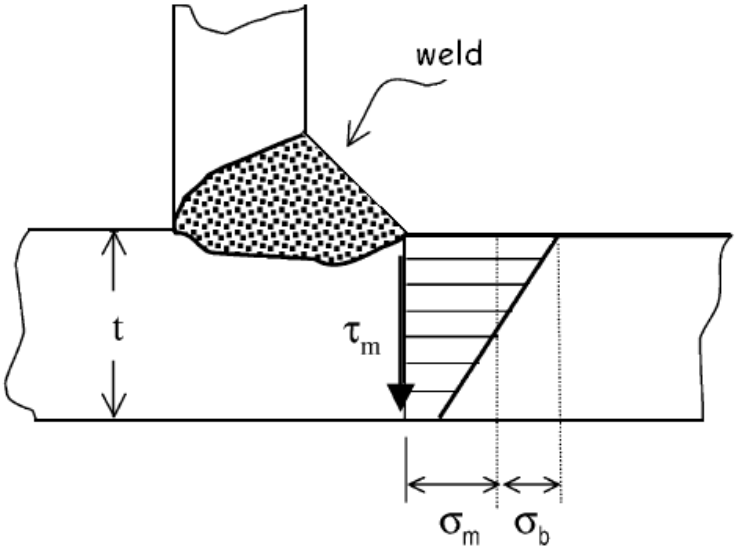

Figure 2.19 Structural stress definition for through-thickness crack: local normal and shear stress at weld toe by Dong (2001)

The structural stress procedure proposed by Dong (2001) linearizes the stress over the plate thickness.

In a recently proposed alternative structural stress approach by Xiao and Yamada (2004) the computed stress at 1mm distance from the crack initiation point and along the expected crack path is compared with the fatigue strength.

In the structural stress method, the SCF is obtained from stress results along the crack path, whereas in the traditional hot-spot extrapolation method the results are obtained from the surface stresses, as shown in Figure 2.20.

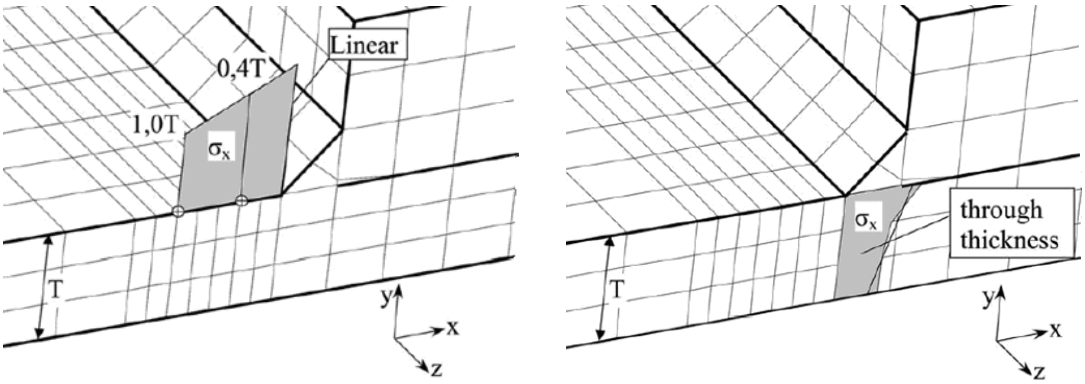

Figure 2.20 Differences comparison between HSS and SS determinations (W. Fricke, A. Kahl, 2005)

There are numerous on-going international efforts addressing the structural stress assessment issue.

Dong (2001) utilized the structural stress definition from Radaj, evaluated the structural stress at the weld toe position by using principles of structural mechanics. Mesh insensitivity is demonstrated by several examples, however, mostly on 2D basic joints.

See also Dong and Hong (2008) for fatigue analysis of welded tubular joints considering the thickness correction in the calculation of the structural stress.

The use of theoretical derivation for stress and displacement solution for the semi-infinite domain is discussed by Radaj and Zhang (1996), and compared with finite-element results.

Soh (1997) found that the stresses in the vicinity of the welded brace/chord

intersections of tubular joints computed with solid elements do not satisfy the free surface conditions and developed a correction procedure to improve the accuracy of computed stresses.

Tveiten and Moan (2000) describe the development and verification of a more general method for the structural stress calculation, being based on the asymptotic behaviour of the stresses adjacent to an idealized notch and the definition of stress extrapolation from points outside the region.

Tovo and Lazzarin (1999) also used a similar approach with fillet welds. The influence of sheet thickness on fatigue strength in thin-walled (less than 5 mm) and welded structures have also been studied numerically and experimentally by Mashiri et al (2001), Fourlaris et al (2006), Gustafsson (2006), Sonsino et al (2007) and Ringsberg et al (2008).

2.4.4 Notch Stress and Strain Approach

The notch stress approach of the fatigue life assessment proceeds from the stress amplitudes at the notch root (which may be artificially radiused) and then uses them with the SN curves for an un-notched comparison specimen.

The idea behind notch stress approach is that the mechanical behaviour of the material at the notch root in respect of local deformation, local damage and crack initiation is similar to the behaviour of a miniaturized, axially loaded, un-notched specimen in respect of global deformation, global damage and complete fracture, as shown in Figure 2.21.

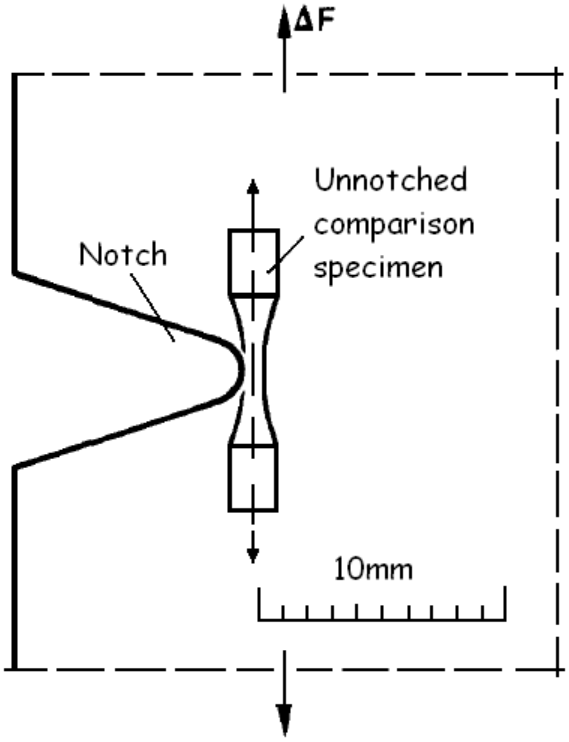

Figure 2.21 Comparison specimen for simulating the cyclic stress strain and crack initiation behaviour at the notch root (Radaj D, 1996)

Different micro-structural support hypotheses exist, which are further described in textbooks (1990) such as: the stress gradient approach according to Siebel and Stieler, the stress averaging approach according to Neuber (1958) and the surface layer approach according to Peterson. Using the Airy stress function, the solution is extended to the region outside the notch bisector.

Filippi's equations which include Williams' solution (1952) for pointed V-notches are shown to be superior. By means of Filippi's equations and considering different failure criteria (Rankine, von Mises and Beltrami), the fictitious notch radius is evaluated for different notch opening angles, and also the micro-structural support length.

A fictitious notch radius is predicted for different geometry shape, plane stress or plane strain conditions by F. Berto, P. Lazzarin and D. Radaj (2009). The support factor is derived.

The severity of the notch stress concentration depends on the notch geometry

configuration, generally referred to as the V-shaped notch open angle.

The ratio of the peak stress and the nominal stress leads to the commonly used definition of the notch-SCF, in Eqn.2.6.

$$K_t = \sigma_{\text{peak}} / \sigma_{\text{norminal}} \qquad 2.6$$

It gives a direct indication of the concentration severity, and an amplification factor on the elastic stress level nominally present in the notch. In the traditional elliptical hole case, the maximum stress, σ_{peak}, occurs at the end (x = a, y = 0); and SCF is a function of the notch geometry in Eqn.2.7:

$$\sigma_{\text{peak}} = (1 + 2\sqrt{\frac{a}{\rho}}) \cdot \sigma_{\text{norminal}} \qquad 2.7$$

As a result, the K_t-expression ($(1 + 2\sqrt{\frac{a}{\rho}})$) for a round hole where a = ρ is equal to 3, which is a classical value.

Taylor and Lawless (1996) extended this idea to include stress concentrations of arbitrary geometry, known as the crack modelling method. The resulting SCF in a modified form is given in Eqn.2.8:

$$K_t = [a / 2r]^{1/2}(1 - \rho / 2r) \qquad 2.8$$

a, reference dimension of a component

r, polar coordinates

ρ, notch tip radius

The SCF of the weld toe notch K_t is determined by Eqn.2.9

Where:

$$K_t = \frac{4(2\tan\alpha/2)^{1-2(1-\lambda_1)}}{2\alpha + \sin 2\alpha}(\frac{t}{2\rho})^{1-\lambda_1} 0.5^{1-\lambda_1} \qquad 2.9$$

λ_1, the first eigen value

α, open angle

t, thickness of plate

In the case of butt welds with partial penetration, the stress concentration factor K_t is determined by Eqn.2.10

Where:

$$K_t = 1 + \frac{2}{\sqrt{\cos(\frac{\pi a}{t})}}\sqrt{\frac{a}{\rho}} \qquad 2.10$$

a, reference dimension of a component

ρ, notch tip radius

t, thickness of plate

The result of an SCF analysis for the tensile-loaded cruciform joint, with load-carrying fillet welds (Radaj D, 2006) is evaluated with respect to the thickness effect.

Complex potentials and conformal mapping can be used for the stress singularity calculation (N. I. Muskhelishvili, 1963). And also the calculation of stress intensity factor for a sharp V-notch is calculated for the limiting case of the stress concentration factors for the same V-notch with rounded root radius by G. Lhermet, G. Vessiere and J. Bahuaud (1987).

The plane elastic-static problems of a lozenge hole and a rigid lozenge inclusion in an infinite plate under tension loading are examined by the conformal mapping and Goursat stress functions (1989).

Seeger et al. (1991, 1993) proposed notch stress approach for welded joints, which also uses a toe radius of 1mm; however, he considers this radius as the mean of real values.

The analogies between crack tip and rigid line tip stresses and displacements are stated by Radaj (1993), in respect of loading modes with singular stresses, with non-singular stresses, distribution of singular stresses, ligament related limit value formulae for stress intensity factors, notch stress related limit value formulae and elementary explicit formulae.

Stress analysis of a semi-infinite plate with a triangular notch and a crack originating from a triangular notch are carried out. Muskheiishvili's method (N. I. Muskheiishvili, 1953) is used for stress analysis and rational mapping functions of a sum of fractional expressions (Newman. Jr and Dowling N, 1998).

With the aim to perform a comprehensive evaluation of the structural support

factor for sharp V-notches, the indispensable theoretical tools, especially the basic stress equations, are reconsidered and amended in respect of accuracy by F. Berto, P. Lazzarin and D. Radaj (2008).

By definition, FEM or BEM determines the effective notch stress; the fatigue assessment is then done using a single universal Woehler curve. Thus besides the weld toe, a possibly present weld root gap can be assessed. Useful are also SCFs available for standard cases, which can be found in papers (Yung JY, Lawrence FV, 1985; Iida K, Uemura T., 1996; Radaj D, Zhang S., 1992).

Using FE models, notch stresses are analyzed, corresponding to the worst case in the approach proposed by W. Fricke (2010), assuming that the maximum value of stress was obtained at the effective notch locations in the fatigue-critical region.

Verreman and Nie (1996) proposed, from observations, to use the related notch stress intensity factor (N-SIF) as a parameter describing the crack initiation life of welds including short crack propagation up to a crack depth of approx. 0.5 mm.

The definition of N-SIF was justified by finite element analyses performed on cruciform joints which confirmed the possibility of using the analytical solution already obtained by Williams for open V-shaped cracks; local stress distribution in the neighbourhood of a weld toe is linear in a log–log plot, and its slope corresponded to the analytical solution valid for V-shaped sharp notches with the same opening angle as the severe V-notched geometry of the welds. The idea of estimating the fatigue strength of welded joints (the weld toe radius being zero or tending towards zero) on the basis of the stress fields represented by straight lines in log–log diagrams was proposed previously by Atzori (1985), and largely used in fatigue life predictions. (Lazzarin and Tovo, 1998)

Lazzarin and Tovo (1998) quantified the contributions of the symmetric and anti-symmetric loading modes for different geometries of welds and re-analyzed experimental data in terms of the new stress field parameter.

Further applications of the approach demonstrate the limits (applicability to real structures, not sufficient for evaluation of the local stress field, and the difficulty in defining the geometrical parameters) of the structural stress approach (Tovo R, Lazzarin P., 1999) and of local strain measurements close to the weld toe (Atzori B, Meneghetti G., 2001).

2.5 Fracture Mechanics Approaches

Today, fracture mechanics analysis has been well established particularly for fatigue assessment, where the crack propagation phase is typically longer than the crack initiation phase. The fracture mechanics approach is useful for assessment of cracks or crack-like imperfections.

The elements of the crack propagation approach are the crack propagation equations, normally according to Paris and Erdogan; when the range of the stress intensity factor ΔK, (or possibly the range of the J-integral) is used to describe the increase of the crack length per cycle, i.e. the crack propagation rate da/dN.

The history of the fracture mechanics approach for fatigue assessment has been reviewed by Smith (1986) and more recently also by Paris (1998), both giving some insight into the dramatic development during the past 40 years. George Irwin, 1956, firstly drew attention to the elastic stress field surrounding crack tips in loaded bodies and the intensity factor of that unique field, K, as a tool to analyse abrupt failures (Smith RA., 1986). Following the work by Maddox (1991) in the 1970s, several investigations have been performed on cracks varying the geometry and loading parameters.

The fracture mechanics approach (W Fricke, 2003) often offers the only way for fitness for purpose assessment of structural members with flaws or other crack-like defects.

Where stress intensity factors (SIFs) from standard handbooks are not applicable to the locations of interest, rising computing power has encouraged the widespread use of FEA for the determination of K values and the simplicity of the method makes fracture mechanics a widely used tool.

2.5.1 Fatigue failure life prediction

Crack growth can be divided into 4 main phases: crack nucleation, short or micro-crack growth, macro-crack growth, and failure, as shown in Figure 2.22.

New striations will be produced by the initial grains. It can be imagined that the slip traces accumulate on the slip bands and propagate into adjacent grains with intensive slip bands. Coarsened, the slip bands will transform into micro-tears. Some adjacent slip bands will accumulate the micro cracks and grow under cyclic loading, the process may require large numbers of the loading cycles. Consequently, the fatigue life comprises the micro-structural crack initiation life and the short-crack propagation life up to a final crack length. In welds the first and second stages are not needed as the welding effectively puts macro cracks into the structure.

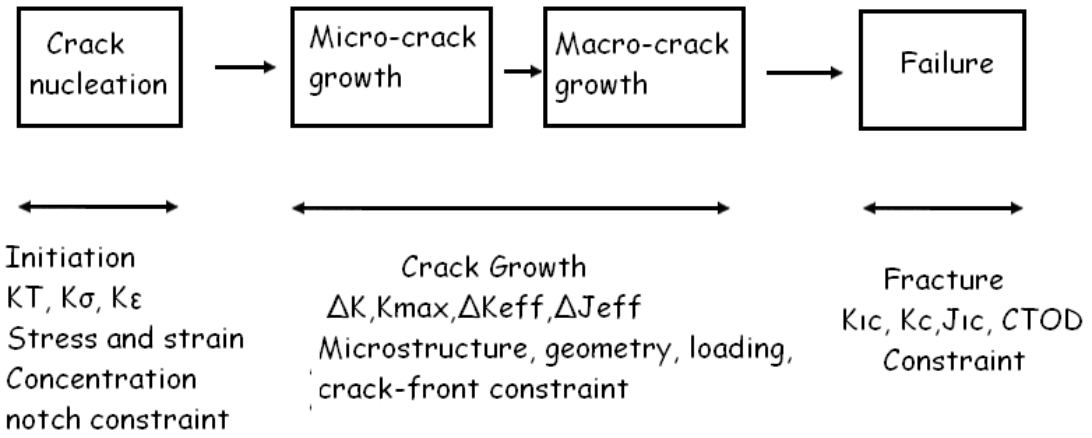

Figure 2.22 Different phases of crack growth life and relevant factors
modified after Schijve (2001)

Service fatigue life estimates use analytical or numerical solutions for K for the macro stage of crack growth.

Fatigue life prediction is well established, particularly for the fatigue strength assessment of the structural components where the crack propagation phase is longer than the crack initiation phase.

The procedure is shown schematically in the flow chart in Figure 2.23.

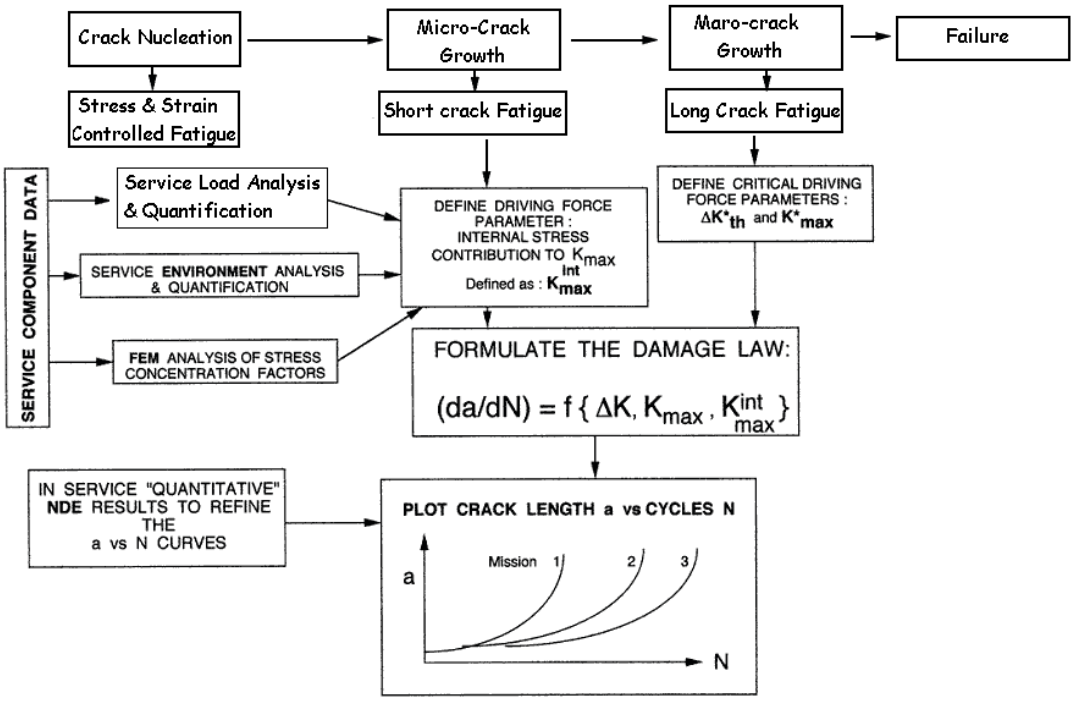

Paris Law: $\frac{da}{dN} = C_0 \cdot \Delta K^m$ for $\Delta K > K_{th}$

Figure 2.23 Flow chart showing various stages of modelling fatigue damage with the integrated use of inputs from experiment
(A.K. Vasudevan, K. Sadananda and G. Glinka, 2001)

The rate of fatigue crack growth under cyclic loading can be expressed in terms of the range of stress intensity factor (ΔK). Or the range of stress intensity factor (ΔK) can be modified to an effective stress intensity factor (ΔK_{eff}) to allow for the effect of various parameters on the fatigue crack growth rate.

The crack propagation approach has been applied to investigate the effect of various geometrical influences on fatigue life, e.g. the effects of a longitudinal attachment, the misalignment of load-carrying cruciform joints and the effects of undercuts and residual stresses at misaligned butt-joints.

Based on the success of the stress intensity factor concept for static fracture, Paris et al. (1957) postulated that the rate of fatigue crack propagation per cycle, da/dN, should be determined by the range of stress intensity factor ΔK .

$$\frac{da}{dN} = C_0 \cdot (\Delta K)^m$$

Below a threshold level of ΔK there is no crack growth: 2.11

$$\Delta K < \Delta K_{th} \quad \text{then} \quad \frac{da}{dN} = 0$$

For preliminary screening assessments, hand-calculations or assessments that can be compared directly with calculations based on fatigue design rules; the following curve is recommended in Figure 2.24.

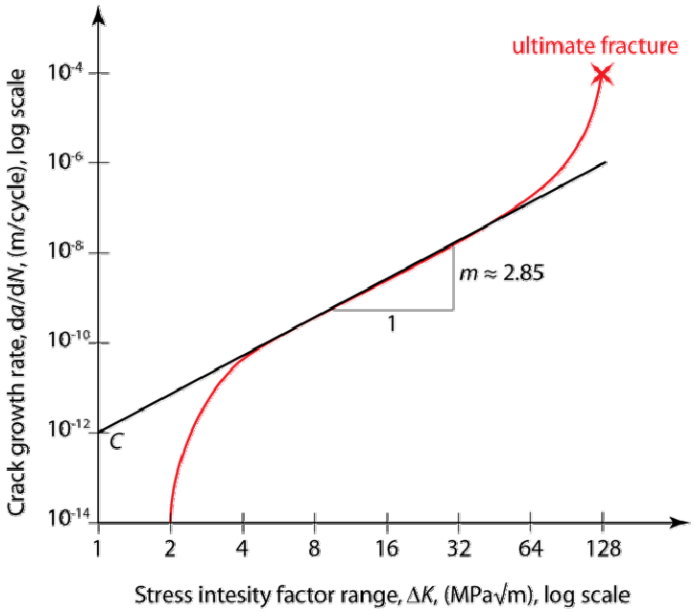

Figure 2.24 Schematic representation of fatigue crack growth rate curves

(P Paris, F Erdogan, 1963)

In Paris' law, C_0 and m depend on various factors such as material properties, environment conditions, frequency of applied load, temperature, stress ratio. In BS 7608 and BS 7910 (British Standard guide of methods for assessing the acceptability in metallic model) the recommended simple values are.

$$m = 3, \quad C_0 = 5.21 \times 10^{-13} \qquad 2.12$$

For steels (excluding austenitic stainless steels) operating in marine environments at temperatures up to 20 °C, the following values are recommended:

$$m = 3\,,\quad C_0 = 2.3\times10^{-12} \qquad 2.13$$

for da/dN in $mm/Cycle$ and K in $N/mm^{3/2}$

The fatigue crack growth data can be used to estimate the remaining fatigue life of a cracked component. A critical crack size is specified or estimated and the number of cycles to failure of the component is then predicted as:

$$N_f = \int_{a_0}^{a_c} \frac{da}{(da/dN)} = \int_{a_0}^{a_c} \frac{da}{A(\Delta K)^m} \qquad 2.14$$

In this form and with modifications (e.g. including explicit power law dependence on another parameter) Paris law has served the engineering design community well.

2.5.2 Micro-cracks

For the micro-crack stage of fatigue the SN curve approach is often used. Small cracks grow together, and then form larger cracks, a process which is not easily represented by calculation. Even when the micro-crack is detectable and immediate crack propagation can be assumed, the stress intensity factor is unsuited for describing micro-crack growth.

Micro-cracks can be initiated at several positions simultaneously and united to a single crack in a later stage as shown in Figure 2.25.

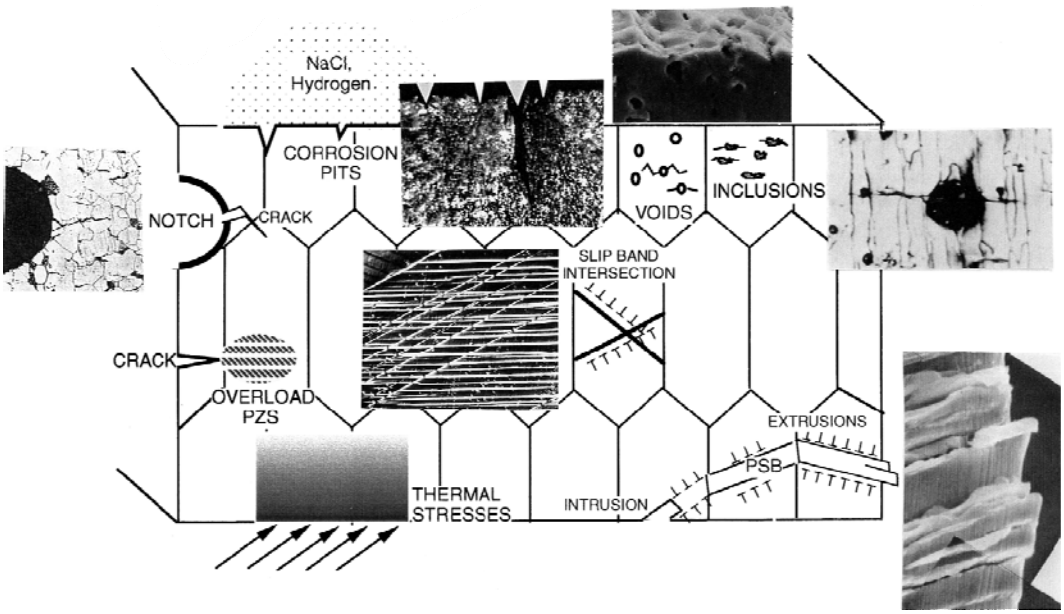

Figure 2.25 Examples of microcosmic stresses affect K (1963)

Micro crack behaviour is always related to the notch stress and strain approach as well as to crack closure effects (K. Hussaint, 1997). The geometry correction factor cannot simply be determined for cracks at the notch. It is necessary to describe short crack propagation in the plastically deformed area based on the cyclic J-integral (L. Lawson, E.Y. Chen, M. Meshii, 1999); the procedure is laborious in respect of numerical procedures.

As demonstrated by Newman et al. (1998), the growth behaviour including threshold value of micro cracks differs considerably from that of large cracks. In the paper, they review the capabilities of crack-closure model to predict fatigue lives of metallic materials using ‘small-crack theory’.

2.5.3 Methods for K Determination (for macro cracks)

Weight Function Method

The Weight Function Method (WFM) originally developed by Buckner (1987, 1989), is a useful procedure for the determination of stress intensity factors in complex stress distributions. The weight function is the stress intensity factor caused by a force on part of the crack surface. The method separates the influences of a stress field and the geometry of a cracked body on a stress intensity factor.

K is calculated using the weight function method by simple integration of the weight function $m(x,a)$ and the stress distribution $\sigma(x)$ for the un-cracked body, as shown in Eqn.2.15:

$$K_I = \int_0^a \sigma_r(x) \cdot m(x,a) \cdot dx \qquad 2.15$$

The method is shown in Figure 2.26.

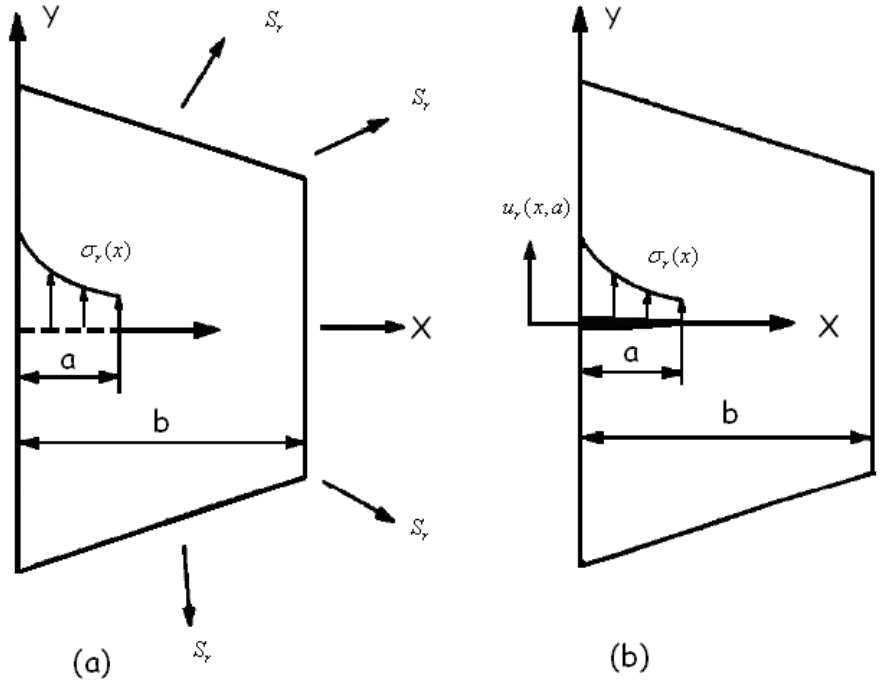

Figure 2.26 Weight function notation under mode I loading: (a) applied reference stress system S_r and the corresponding local stress distribution $\sigma_r(x)$ in the prospective crack plane; (b) and corresponding crack opening displacement $u_r(x,a)$ (G. Shen and G. Glinka, 1991)

The determination of weight function $m(x,a)$ requires complex elastic analysis for a specific geometry and applied stress system; however, it can be simplified by using the relationship in Eqn.2.16:

$$m(x,a) = \frac{\kappa}{K_r} \cdot \frac{\partial u_r}{\partial a} \qquad 2.16$$

$m(x,a)$, weight function;

κ, E for plane stress and $E/1-\nu^2$ plane stain;

K_r, reference stress intensity factor;

u_r is $u_r(x,a)$, corresponding crack opening displacement;

a crack depth

Weight functions calculation can be simply to determine by the Petroski-Achenbach method in the paper (Fett T, 1987). However it has been found

that the crack opening displacement function proposed by Petroski and Achenbach ware not accurate for discontinuous and high gradient reference stress fields.

The displacement fields of edge cracks under tensile stress (Fett T, Munz D and Yang, 2000) can be described by approximation given by Petroski and Achenbach. Using approximation and the weight function method, the displacement fields for single forces and varying stress distributions can be obtained.

Weight functions have been derived by Niu and Glinka (1987), for a variety of crack configurations they have the same general mathematical form.

A numerical technique for simple and efficient integration of weight functions is presented in the paper (Moftakhar A and Glinka G, 1992). The method enables the stress intensity factors to be calculated with the aid of a hand calculator for any non-linear stress distribution normal to the crack surfaces. The proposed integration routine is validated against accurate numerical and analytical solutions.

An algorithm for crack growth analysis of planar cracks under arbitrary Mode I loading was presented in the paper (JC. Newman, 1971). The method is based on the point-load (2D) weight function used for the calculation of stress intensity factors. Validation results supporting the entire methodology are discussed. Application examples of the proposed method for crack growth analysis under arbitrary Mode I stress fields are presented.

An effective approach which can be used to solve stress intensity factors for crack problems with built-in end boundary conditions was summarized by Marchand etc (1986).

An approximate weight function for embedded elliptical cracks was deduced from the properties of weight functions and available analytical weight functions for penny shape and half plane cracks (Niu X and Glinka G, 1989). The weight function is then validated against available exact stress intensity factor solutions for embedded elliptical cracks for several linear and non-linear stress distributions.

Parametric formulae for the determination of SIF (or weight functions) have been developed for a multitude of structural details (Albrecht P, Yamada K, 1977). An additional function $M_k(a)$ considers the non-linear stress peak and the special geometrical conditions of the different structural details and joint types. The numerical integration and the determination of the $M_k(a)$-values can be performed in

parallel using a simple algorithm.

A procedure is discussed that allows the determination of weight functions from a number of known reference stress intensity factors and two geometrical conditions, namely vanishing second and third derivatives of the weight function at the crack mouth (Fett T, 1992).

A convergence consideration is included in the paper (T. Fett, H-A. Bahr, 1999), in order to provide weight function solutions including displacement boundary conditions, rectangular plates with different length-to-width ratios are studied using the boundary collocation method. It was found from the numerical data that weight function results are independent of Poisson's ratio ν for mixed boundary conditions at the plate ends, but depend on ν in case of pure displacement conditions.

Weight functions for one-dimensional cracks in plates are given for the special case of loadings along the crack line. The solution for an edge crack in a rectangular plate is given by interpolated by cubic splines (Fett T, 1995).

Weight functions are derived for edge cracks and internal cracks in the vicinity of interfaces of dissimilar materials. The first terms of a power series representation are determined by directly adjusting the weight function to reference stress intensity factors and geometric conditions (Fett T, Munz D etc, 1997).

Mode I weight functions (Zheng XJ, Kiciak A and Glinka G, 1997) are derived for the deepest and surface points of an internal, radial-longitudinal, surface, semi-elliptical crack in an open-ended, thick-walled cylinder with internal radius to wall thickness ratio R/t=2.0. This paper complements a set of previously published weight function solutions for cracks in cylinders with other radius to thickness ratios. Another research group lead by D. Munz and T. Fett (1997) has provided a significant contribution to the derivation of SIF through the weight function method.

Boundary Collocation Method

The Boundary Collocation Method (BCM), originally developed for plane isotropic analysis, depends on the selection of a stress function describing the stress

field and matching boundary portions at the vicinity of the crack tip in the crack anisotropic plates. The simplicity of computation is attractive compared with other methods.

Successive additions of stress fields which remove the stresses along the crack path can be visualized as an infinite repetition of additive stress fields. Each stress removal along the crack path provides a corrective contribution to the value of K. Thus an approximate estimate of K is given by $K \propto \sigma\sqrt{\pi a}$.

$$K = F \cdot \sigma_o \cdot \sqrt{\pi a} \qquad 2.17$$

Where: F is geometric function;

σ_0 is nominal stress

The method results in closed-form stress intensity factor solutions in various types of specimens.

In order to correlate the results of geometry, the process is considered as determination of the related geometric function F. The function can be defined by Eqn.2.18

$$F = K / \sigma_0 \sqrt{\pi a} \qquad 2.18$$

Coefficients for the corrective function are determined by fitting the general solution to the geometry, and resulted in the functional form for F given in Eqn.2.19

$$F = F\left(\frac{a}{H}, \frac{H}{W}\right) \qquad 2.19$$

For the cases of a central crack in a plate, boundary collocation formulas have been applied; the stress intensity factor calculation can be considered as the result of a combination of the crack lengths.

Despite the fact that several stress intensity factor handbooks (H. Tada, P. Paris and G. Irwin, 1985; Y. Murakami et al., 1987) have been published, it is still difficult to find adequate solutions for many practical problems. Recently, Fett (2005) presented the numerical solutions of stress intensity factor for edge-cracked plate with built-in ends using the boundary collocation method.

The results provide geometric functions in terms of normalized half specimen width and normalized half effective specimen length using Zhang's analytical solutions (S. Zhang, 1997).

For the determination of the stress intensity factor solutions for edge-cracked plates with built-in ends under complex stress distributions (Fett T, Rizzi G and Diegele E, 2004). Ted L and G Glinka (2006) develop an alternative technique for surface and corner cracks, which greatly improves both efficiency and accuracy of K estimation.

The single edge-cracked plate (SECP) is one of the most commonly used specimens, the weight functions for stress intensity factor have been summarized by Wu (1991), Shen and Glinka (1991), and compared with FEM by Wang (1996).

Critical Distance Method

The Critical Distance Method (CDM), originally proposed by Neuber (1958), defines failure criteria based on the stresses within a critical region surrounding the stress concentration, the size depending on the material. D. Taylor subsequently has discovered a new reinterpretation (Taylor, 1999) and shown that the same approach first proposed by Neuber (1936) and Peterson (1959) had been used for over 50 years.

Theories of fracture generally accept the need for a material length scale, i.e. a parameter with the dimensions of length by ElHaddad's (1980), which is incorporated into the theoretical model.

Using the stress intensity factor together with a_o, successful correlation was demonstrated by El Haddad (1979) between growth rates at notches and long crack elastic growth rate curves.

$$\Delta K_{th,a} = \Delta K_{th}\sqrt{\frac{a}{a+a_0}} \qquad 2.20$$

Where: a_D is the parameter of the critical defect.

This equivalent stress intensity factor calculation turns out to be equal to formula proposed by D. Taylor (1996).

$$\Delta K_I = \Delta\sigma \cdot \sqrt{\pi(a+ae)} \qquad 2.21$$

The distance size effects are capable of predicting this effect, which is similar in both monotonic fracture (Whitney JM, Nuismer RJ, 1974) and fatigue of metallic materials (Taylor D, 1999). Another example of size effects is the variation in specimen strength which occurs when the size of the entire specimen is changed, without changing its shape (C. Berger etc, 2002).

The authors have shown that complications arise when the size of the specimen becomes similar to L, (L is half length of the rectangular cut-out longer edge) necessitating a modified form of the approach in which L becomes a variable quantity (D. Neal, 1970).

It is surprising that the graphs (G. Crupi etc, 2005) have similar forms considering that the underlying mechanisms are so different, indicating short-cracks and small defects.

A particularly interesting case study is a vehicle suspension component for which the location of fatigue failure was not the same as the location of the maximum stress, an effect which CD anticipates (Taylor D etc, 2000). The CD has also been applied to cases in which high local stresses arise due to contact between bodies, such as fretting fatigue (Vallellano C etc, 2003, Araujo JA etc, 2007). The characterization of notch effects in fatigue is an area of great practical concern; several investigators have demonstrated the value of the sharp notches (Lazzarin P etc, 1997; Susmel L etc, 2003; Taylor D etc, 2000). Further research revealed other, independent, inventions of the theory, in slightly different forms, for the prediction of brittle fracture (Niu X and Glinka G, 1989), in composite materials (Y. Murakam, 1978) and polymers (Kinloch AJ etc, 1982).

The work described in Chapter 6 of this thesis involves an equation that is identical to equation 2.22. However the interpretation of ‘ae’ in this thesis is of an increased effective defect size caused by a sharp notch singularity. This thesis follows on from Xu and Barltrop (2007) who investigated stress singularities with the aim to allow the estimation of hot spot stresses or stress intensity factors by considering the geometry of the structural detail in conjunction with simple formulae. According to elastic stress analysis, structural sharp corners are singularities and may be classified by singularity type and strength. The authors pointed out that, once a correspondence has been determined between these characteristics and the

geometrical characters under consideration, it provides guidance both on the mesh size needed to analyze a structure and on the size-dependent stress concentration factors.

Others

The stress intensity factors at keyhole seam welds of overlap joints are derived from the outer surface deformations of the joined plates (Zhao. W, Newman Jr etc, 1997). Relations between forces and stresses are given which avoid the measurement of curvature. Unequal thickness of the plates and dissimilar materials are taken into account. The analysis for a circular hole (H. Nisitani and M. Isida, 1973; Y. Murakamj, 1978), an elliptical hole (G. Savaidis, M. Vormwald, 2000) and a square hole (D. M. Neal, 1970; M. Isida, 1978) can be found. A crack originating from a square hole is analyzed as a plane elastic problem (Nprio Hasebe, Minoru Ueda, 2003).

2.6 Classification Rules

Fatigue analyses performed according to current (July 2012) rules and guidelines from the several classification societies are individually considered below. The initial scantlings are often based on strength (structural capacity) considerations, fatigue being checked afterwards.

The fatigue analysis procedures from LR, DNV, ABS, and NK have been applied, within a comparative study, to the fatigue assessment of a pad detail on a tanker, bulk cargo ship and an FPSO.

The Lloyd's Register, the Ship Right Fatigue Design Assessment Level 3 procedure (LR, 2004) was applied. The objective of the FDA procedure is to analyze the ship's structural response due to applied static and dynamic loads. This procedure

effectively increases confidence that the ship's structural integrity will be maintained throughout its service life. FDA Level 3 is a spectral approach where, in this case, a scaled hull form and weight distribution from a similar ship is used for generation of the vertical bending moment response amplitude operator from 2D strip theory.

ABS also supports both the nominal and the hot-spot stress approaches in their simplified fatigue strength assessment method (ABS, 2003). The fatigue stress ranges are assumed to follow a Weibull probability distribution. The effect of mean stress has been ignored. SN curves are used to describe the fatigue strength of the details. The structural requirements in Part 5A (ABS, 2010) of ABS Rules are applicable for double hull oil tankers of 150 m in length and upward, with structural arrangements as specified in Part 5A.

Generally, for double hull tankers of less than 150m in length, the Rules of the individual Classification Society are to be applied. The structural requirements in Part 5B (ABS, 2010) of ABS Rules are applicable for single side skin and double side skin bulk carriers of 90m in length and upward, with structural arrangements as specified.

The procedure from DNV (1999) for fatigue strength assessment is based on the hot-spot stress approach. The stress concentration factor is obtained from a table of standard details which contains doubled plates. The stress range is further reduced by a factor of 0.80 to account for worldwide operation. The stress concentration factor is obtained from local FE analysis of the patch detail or experimental standard details containing double plates (by DNV). By the rules of DNV, the stress range is multiplied by a stress concentration factor for the weld (notch stress) before entering the Woehler SN curve. The DNV Recommended Practice (2010) presents recommendations in relation to fatigue analyses based on fatigue tests and fracture mechanics. The aim of Recommendation is to ensure that the structure has an adequate fatigue life. In terms of DNV design rules (2010), a design cycle may be considered as consisting of two distinct phases: Preliminary Design Phase and Fatigue Design Phase for FPSO.

The stresses and SN curve, by the BV rules (1998, 1999), are based on the notch stress approach. The calculation included the stress component from the IACS (1989, 1999) head sea vertical bending moment, transferred to a probability of 10e-5 using a

Weibull distribution with a shape parameter of 0.943 combined with a horizontal bending moment. Parametrical SN curves may also be used to fit the results from component fatigue tests.

A comparative study between the rules of classification and FE extrapolation has been performed as part of the work of Committee III.2, 'Fatigue and Fracture', of the International Ship and Offshore Structures Congress (ISSC) during the working period 1997–2000, and a technical paper was published in 'Marine Structure' (W. Fricke, W. Cui, etc., 2002).

It has been shown that there is high scatter: the fatigue lives vary considerably between 1.8 and 20.7 years on the panamx container ship; in a parametric study several assumptions and input parameters have been modified, resulting in calculated fatigue lives, ranging from 2.9 to 6.2 years, and a relatively short fatigue life of 5.3 years, assuming the North Atlantic wave climate and a certain speed profile.

2.7 Conclusions

In view of the complexity of the subject and the wide area of application it is not surprising that different approaches exist for fatigue analysis. The fatigue literatures review above demonstrates both existing experienced and mature results and new ideas. However there is no universally correct or best method. The circumstances of the considered special case determine the choice of approaches.

The nominal stress approach (by Hobbacher, Gurney, British Standard and IIW) is considered as robust as far as it is statistically founded. However it is only valid for details similar to those tested so it cannot represent all structural details.

The main drawback of the HHS method (by Maddox, Lotsberg, Sonisino and Classification Societies) is the limitation to surface crack failures and the uncertainty of extrapolation procedure, which varies depending on the particular codes used. And incorrect extrapolation will result in a poor estimate of this important parameter. FE analyses are performed to evaluate the hot-spot stress but the results depend on the mesh and elements used.

The supporters of the structural stress approach (by Dong, Marquis and Yamda)

hold against the notch stress approach (Lazzarin, Radaj and Lawrence) that the scattering of the notch geometry cannot be accurately evaluated and that it is not well suited for the notch stress analysis. However there are also critics of the structural stress approach.

The notch stress approach and the fracture mechanics approach (Glinka, Fett and Taylor), have the main disadvantage that there are a very large number of possible geometrical forms, and it is time consuming to set up the required finite element analyses for industrial application.

It is easy to understand why experts still disagree on the best approved to the fatigue problem assessment approaches, but any approach can be adjusted to the engineering requirements in a restricted field of application.

Disregarding the limitations, fatigue analysis is well established in ship and offshore engineering, to simplify the ways for fatigue strength assessment.

This thesis continues work started by Xu and Barltrop (2007) in order to allow the estimation of hot spot stresses and the stress field from the geometry of the structural detail. The hot spot stress can be used directly in fatigue analysis and the stress field can be characterized to provide guidance on the required mesh size in finite element analysis and, with suitable weight functions, it can be used directly in fracture mechanics based assessment.

The novel research direction will be discussed to give fatigue guidelines to designers. The simplicity and clearness of the method will be in contrast to the difficulty of practical application of some other methods.

REFERENCES

1. AMSP, Study Guide for Applicants to the Fourth-class Engineer Certificate with STCW Endorsement, 2007
2. A. Hobbacher, Recommendations for fatigue design of welded joints and components (update), IIW doc(revision 2003), XIII-1965-03/XV-1127-03
3. A.F. Hobbacher, The new IIW recommendations for fatigue assessment of

welded joints and components – A comprehensive code recently updated. International Journal of Fatigue Volume 31, Issue 1, January 2009, Pages 50–58

4. A.K. Vasudevan, K. Sadananda, G. Glinka. Critical parameters for fatigue damage. International Journal of Fatigue 23 (2001) S39–S53
5. ABS. Guide for dynamic based design and evaluation of container carrier structures. A simplified method for fatigue strength assessment. American Bureau of Shipping, Houston, 2003
6. ABS. Part 5A Specific Vessel Types (Chapter 1) Common Structural Rules for Double Hull Oil Tankers, 2010
7. ABS. Part 5B Specific Vessel Types (Chapters 3 and 4) Common Structural Rules for Bulk Carriers, 2010
8. Albrecht P, Yamada K. Rapid calculation of stress intensity factors. J Strut Div ASCE 1977;103(ST2):377–89.
9. Araujo JA, Susmel L, Taylor D, Ferro JTC, Mamiya EN. On the use of the theory of critical distances and the modified Wohler curve method to estimate fretting fatigue strength of cylindrical contacts. Int J Fatigue 2007; 29: 95–107.
10. Arno M. van Wingerde, et al. SCF formulae for fatigue design of K-connections between square hollow sections. J. Construct. Steel Res. 43 (1997) 87-118
11. Atzori B, Meneghetti G. Fatigue strength of fillet welded structural steels: finite elements, strain gauges and reality. Int J Fatigue 2001;23:713–21.
12. Bard Wathne Tveiten et al. Determination of structural stress for fatigue assessment of welded aluminum ship details. Mar Struct 13 (2000) 189-212.
13. Bergan PG, Lotsberg I, Fricke W, Francois, M, Pisarski H. Overview of phase II of the FPSO Fatigue Capacity JIP. OMAE Conf Oslo; 2002
14. Bergan PG, Lotsberg I. Advances in fatigue assessment of FPSOs. International Conference Houston, OMAE-FPSO'04-0012, 2004.
15. Brian E. Healy, A case study comparison of surface extrapolation and Battelle structural stress methodologies, Proceedings of OMAE Specialty Conference on FPSO systems (2004), OMAE-FPSO'04-51228, Houston TX, ASME

International Petroleum Technical Institute.

16. Bueckner H. Observations on weight functions. Engineering Analysis with Boundary Elements, 1989, Vol. 6, 3-17 1989
17. Bueckner H. Weight functions and fundamental fields for the penny-shaped and the half-plane crack in three-space. Int. J. Solids Structure Vol 23, 57-93 1987.
18. BV. Fatigue strength of welded ship structures. Bureau Veritas Document NI 393 DSM ROIE; July 1998.
19. BV. Rules for the classification of steel ships. NR466A JAP R00 E, Bureau Veritas, Paris, 1999.
20. C. Berger, K.-G. Eulitz, P. Heuler, K.-L. Kotte, H. Naundorf, W. Schuetz, C.M. Sonsino, A. Wimmer, H. Zenner. Betriebsfestigkeit in Germany — an overview. International Journal of Fatigue 24 (2002) 603–625.
21. C.M. Sonsino, E. Moosbrugger. Fatigue design of highly loaded short-glass-fibre reinforced polyamide parts in engine compartments. International Journal of Fatigue 30 (2008) 1279–1288
22. C.M. Sonsino. Course of SN-curves especially in the high-cycle fatigue regime with regard to component design and safety. International Journal of Fatigue 29 (2007) 2246–2258
23. CM. Sonsino. Effect of residual stresses on the fatigue behaviour of welded joints depending on loading conditions and weld geometry. International Journal of Fatigue 31 (2009) 88–101
24. CM. Sonsino. Fatigue testing under variable amplitude loading. International Journal of Fatigue 29 (2007) 1080–1089
25. CM. Sonsino. Influence of load and deformation-controlled multiaxial tests on fatigue life to crack initiation. International Journal of Fatigue 23 (2001) 159-167
26. D Radaj, S. Zhang. Analogies between crack tip and rigid line tip stresses and displacements. Engineering Fracture Mechanics Vol. 44, No. 6, pp. 913-919, 1993
27. D Radaj, S. Zhang. Stress concentration at fictitiously rounded sharp notches in shear loading. Engineering Fracture Mechanics Vol. 55, No. 4, pp. 675-676,

1996

28. D Radaj. Design and analysis of fatigue-resistant welded structures. Cambridge: Abington Publishers, 1990.
29. D. M. Neal, Stress intensity factors for cracks emanating from rectangular cutouts. Inf. J. Fracture Mech. 6,393-400 (1970).
30. D. Radaj. Design and analysis of fatigue-resistant welded structures. Cambridge: Abington Publishers, 1990
31. D. Radaj. Review of fatigue strength assessment of nonwelded and welded structures based on local parameters, International. J. Fatigue Vol. 18, No. 3, pp. 153–170, 1995
32. DNV. DNV-RP-C203 Fatigue Design of Offshore Steel Structures, 2010.
33. DNV. Fatigue assessment of ship structures, Det Norske Veritas Class Notes No.30. 7, 1999
34. Dong P. A structural stress definition and numerical implementation for fatigue analyses. Int J Fatigue 2001;23(10):865–76.
35. Dong P. and Hong J.K. Fatigue of tubular joints: hot spot stress method revisited. In: Soares C.G., ed. ASME 27th International Conference on Offshore Mechanics and Arctic Engineering (OMAE 2008), Estoril, Portugal, OMAE2008-57914 on CD-ROM.
36. El Haddad MH, Topper TH, Smith KN. Prediction of non propagating cracks. Engineering Fracture Mechanics 1979;11(3):573–84.
37. ElHaddad MH, Dowling NF, Topper TH, Smith KN. J integral applications for short fatigue cracks at notches. Int J Fract 1980;16:15–24
38. Eylmann S., Fricke W. and Paetzold H. Investigation of news designs for wheel loaded truck decks in ferries. International Fatigue Design Conference Cetim 2005, Senlis (France)
39. F. Berto, P. Lazzarin, D. Radaj. Fictitious notch rounding concept applied to sharp V-notches Evaluation of the microstructural support factor for different failure hypotheses. Part I. Engineering Fracture Mechanics 75 (2008) 3060–3072.
40. F. Berto, P. Lazzarin, D. Radaj. Fictitious notch rounding concept applied to sharp V-notches Evaluation of the microstructural support factor for different

failure hypotheses. Part II. Engineering Fracture Mechanics 76 (2009) 1151–1175.

41. Fett T, Munz D et.al. Weight functions for sub-interface cracks. Int. J. Solids Structures Vol. 34, No. 3, pp. 393-400, 1997.
42. Fett T, Munz D, Yang YY. Limitations of the Pelroski-Achenbach crack opening displacement approximation for the calculation of weight functions. Engineering Fracture Mechanics 65 (2000) 393-403.
43. Fett T, Rizzi G amd Diegele E. Weight functions for cone cracks. Engineering Fracture Mechanics 71 (2004) 2551–2560.
44. Fett T, Rizzi G. Weight functions for stress intensity factors and T-stress for oblique cracks in a half-space. Int J Fract 2005;132:L9–L16.
45. Fett T. A weight function for the single edge crack based on approximative displacement fields. Theoretical and Applied Fracture Mechanics 8 (1987) 169-172.
46. Fett T. Direct determination of weight functions from reference loading cases and geometrical conditions. Engineering Fracture Mechanics Vol. 42, No. 3, pp. 435-444, 1992.
47. Fett T. Weight function for an edge crack with tractions at arbitrary locations in the body. Engineering Fracture Mechanics Vol. 51, No. 2, pp. 225-232, 1995.
48. Filippi S, Lazzarin P, Tovo R. Developments of some explicit formulas useful to describe elastic stress fields ahead of notches in plates. Int J Solids Struct 2002;39:4543–65.
49. Fourlaris G., Hambling S.J. and Jones T.B. Influence of steel strength and loading mode on fatigue properties of resistance spot welded H section specimen. Materials Science and Technology 22:1, 39-44, 2006
50. Fricke W., Hans Paetzold, Full-scale fatigue tests of ship structures to validate the S–N approaches for fatigue strength assessment, Marine Structures 23 (2010) 115–130
51. G. Crupi, V. Crupi, E. Guglielmino, D. Taylor. Fatigue assessment of welded joints using critical distance and other methods. Engineering Failure Analysis 12 (2005) 129–142.

52. G. Lhermet, G. Vessiere and J. Bahuaud. Determination of stress intensity factors from stress concentrations for V-notched beams. Engineering Fracture Mechnics. Vol. 28. No. 3. pp. 331-343, 1987

53. G. Savaidis, M. Vormwald. Hot-spot stress evaluation of fatigue in welded structural connections supported by finite element analysis. Int. J. Fatigue 22 (2000) 85-91.

54. G. Shen, G. Glinka, Determination of weight functions from reference stress intensity factors, Theoretical and Applied Fracture Mechanics 15 (1991) 237-245

55. Gurney TR. Fatigue of welded structures. Cambridge: Cambridge University Press, 1979

56. Gurney TR. The influence of thickness on the fatigue strength of welded joints. Proceedings of the Second International Conference on Behaviour of Offshore Structures, London, 1979.

57. Gustafsson M. A study of thickness effect on fatigue in thin welded high strength steel joints. Steel Research Journal 77:12, 873-881, 2006

58. H. Nisitani and M. Isida, Stress intensity factor for the tension of an infinite plate containing an elliptical hole with two symmetrical edge cracks. Trans. JSME 39(317), 7-14 (1973).

59. H. Tada, P. Paris and G. Irwin, The Stress Analysis of Cracks Handbook, 2nd edn, p. 8.3. Paris Productions incorporated, St. Louis, Missouri (1985).

60. Hobbacher A, editor. Recommendations for fatigue design of welded joints and components. IIW Doc XIII-2151r1-07/XV-1254r1-07. Int Inst Welding; 2007

61. I. Lotsberg, Einar Landet, Fatigue capacity of side longitudinals in floating structures, Marine Structures 18 (2005) 25-42

62. IACS R 56. Fatigue assessment of ship structures. Recommendation of the International Association of Classification Societies, 1999.

63. IACS UR S11. Longitudin al strength standard, Unified Requirement of the International Association of Classification Societies, 1989.

64. Iida K, Uemura T. Stress concentration factors formulae widely used in Japan. Fatigue Fract Eng Mater Struct 1996;19(6):779–86.

65. IIW. Fatigue design of welded joints and components. Abington, Cambridge: Abington Publishing; 1996.

66. J. C. Newman, An improved method of collocation for the stress an analysis of cracked plates with various shaped boundaries. NASA TN D-3676 (1971)

67. K. HUSSAIN. Short fatigue crack behaviour and analytical models: a review. Engineering Fracture Mechanics Vol. 58, No. 4, pp. 327-354, 1997

68. Kinloch AJ, Shaw SJ, Hunston DL. Crack propagation in rubber-toughened epoxy. In: International conference on yield, deformation and fracture. London: Cambridge Plastics and Rubber Institute; 1982. p. 29.1–6.

69. Kottgen VB, Olivier R, Seeger T. Fatigue analysis of welded connections based on local stresses (in German). In: DVS-Report No 133, DVS-Verlag, D. usseldorf 1991; English translation in IIW-doc. XIII-1408-91/XV-802-92, International Institute of Welding.

70. Kottgen VB, Olivier R, Seeger T. The damage of the large wind energy converter GROWIAN—fatigue strength analysis of the critical welded joints (in German). Konstruktion 45, 1993, p. 1-9, and partly in: IIW-Doc. XIII-1497-1993, International Institute of Welding.

71. L. Lawson a, E.Y. Chen, M. Meshii. Near-threshold fatigue: a review. International Journal of Fatigue 21 (1999) S15–S34.

72. Lazzarin P, Tovo R, Meneghetti G. Fatigue crack initiation and propagation phases near notches in metals with low notch sensitivity. Int J Fatigue 1997;19:647–57.

73. Lazzarin P, Tovo R. A notch intensity factor approach to the stress intensity of welds. Fatigue Fract Eng Mater Struct 1998;21:1089–103.

74. Li Xu and Nigel Barltrop. Analysis of Sharp Corners in Structural Details. Universities of Glasgow and Strathclyde, 2007, UK.

75. Lotsberg I, Landet E. Fatigue capacity of side longitudinals in floating structures. Marine Struct 2005;18:25–42.

76. Lotsberg I. Assessment of fatigue capacity in the new bulk carrier and tanker rules. Marine Structures 19 (2006) 83–96

77. Lotsberg I. Fatigue design of welded pipe penetrations in plated structures. Marine Structures 17 (2004) 29–5

78. Lotsberg I. Overview of the FPSO—fatigue capacity JIP. OMAE, Rio de Janeiro; 2001.

79. Lotsberg I. Stress concentration factors at circumferential welds in tubulars. Mar Struct 11 (1998) 207-230

80. Lotsberg I. Stress concentration factors at welds in pipelines and tanks subjected to internal pressure and axial force. Mar Struct 21 (2008) 138-159

81. Lotsberg I. Stress concentrations due to misalignment at butt welds in plated structures and at girth welds in tubulars. International Journal of Fatigue 31 (2009) 1337–1345

82. LR. Ship Right FDA level 3 procedures manual, technical planning and development department. Lloyd's register of Shipping, 2004.

83. Luca Susmel, Three different ways of using the Modified W?hler Curve Method to perform the multiaxial fatigue assessment of steel and aluminium welded joints, Engineering Failure Analysis 16 (2009) 1074–1089

84. M Eibl, C.M. Sonsino, H. Kaufmann, G. Zhang. Fatigue assessment of laser welded thin sheet aluminium. International Journal of Fatigue 25 (2003) 719–731.

85. M. Backstrom, G. Marquis, Evaluation of interaction equations for multiaxial loaded welded structures. Proceedings of the Sixth International Conference on Biaxial/Multiaxial Fatigue and Fracture, Lisbon, Vol. 1. European Structural Integrity Society (ESIS) 2001, p. 65–72

86. M. Isida, Analysis of stress intensity factors of plates containing an arbitrary array of line and branched cracks. Trans. JSME 44(380), 1122-1132 (1978)

87. Maddox S. Fatigue strength of welded structures. Cambridge: Abington Publishers, 1991

88. Maddox SJ. Scale effect in fatigue of fillet welded aluminium alloys. Proceedings of the Sixth International Conference on Aluminium Weldments, Cleveland, OH, 3–5 April 1995. Miami, FL: American Welding Society; 1995 [ISBN 0-87171-458-2].

89. Maddox SJ. The effect of plate thickness on the fatigue strength of fillet welded joints. Abington, Cambridge: Abington Publishing; 1987.

90. Marchand N, Parks DM, Pelloux RM. KI-Solution for single edge notch

specimens under fixed end displacements. Int J Fract 1986;31: 53–65.

91. Mashiri F.R., Zhao X.L. and Grundy P. Effects of weld profile and undercut on fatigue crack propagation life of thin-walled cruciform joint. Thin-walled Structures 39:3, 261-285, 2001
92. Moftakhar A and Glinka G. Calculation of stress intensity factors by efficient integration of weight functions. Engineering Fracture Mechanics Vol. 43, No. 5, pp. 149-756, 1992
93. N. I. Muskheiishvili, Some Basic profess of the mathematical Theory of Elasticity. Noordhoff, Groningen (1953).
94. N. I. Muskhelishvili, Some Basic Problems of the Mathematical Theory of Elasticity. Noordhoff, Amsterdam (1963).
95. Neuber H. Theory of notch stresses: principles for exact calculation of strength with reference to structural form and material. 2nd ed. Berlin: Springer Verlag; 1958.
96. Newman Jr and Dowling N. A crack growth approach to life prediction of spot-welded lap joints. Fatigue and Fracture of Engineering Materials and Structures 1998; 21: 1123–1132
97. Niu and G. Glinka, On the limitations of the Petroski-Achenbach crack opening displacement approximation for the calculation of weight fimctiondo they really exist. Engng Fracture Mech. 26, 701-706 (1987).
98. Niu X and Glinka G. Stress-intensity factors for semi-elliptical surface cracks in welded joints. International Journal of Fracture 40: 255-270, 1989.
99. Norio Hasebe and Jiro Iida. A crack originating from a triangular notch on a rim of a semi-infinite plate. Engineering Fracture Mechnics. Vol. 10, pp. 773~782
100. Nprio Hasebe, Minoru Ueda. Crack originating from a corner of a square hole. Engineering Fracture Mechnics. Vol. 13, 2003. pp. 913-923
101. P Paris, F Erdogan, A critical analysis of crack propagation laws, Journal of Basic Engineering, Transactions of the American Society of Mechanical Engineers, (1963), 528-534
102. Paris PC. Fracture mechanics and fatigue: a historical perspective. Fatigue Fract Eng Mater Struct 1998;21(5) 535-40.

103. PC Paris. The mechanics of fracture propagation and solutions to fracture arrester problems The Boeing Company Document D-2-2195

104. Peterson RE. Notch sensitivity. In: Sines G, Waisman JL, editors. Metal fatigue. New York: McGraw Hill; 1959. p. 293–306.

105. R.V. Guchisky, S.V. Petinov, Fatigue of Fillet-welded Joint Assessment by the FEA Simulation of Damage Accumulation, Magazine of Civil Engineering, 4 (2011) 5-9

106. Radaj D, Zhang S. Notch Effect of welded joints subjected to antiplane shear loading. Eng Fract Mech 1992;43(4):663–9.

107. Radaj D. Review of fatigue strength assessment of nonwelded and welded structures based on local parameters. International Journal of Fatigue 1996(18):153–70

108. Ringsberg J.W., Orvegren O., Henrysson H.-F. and ?kerstr?m G. (2008). Sheet metal fatigue near nuts welded to thin sheet structures. International Journal of Fatigue 30:5, 877-887.

109. Sergei V. Petinov. Fatigue Analysis of Ship Structures. Backbone Publishing Company, 2003, ISBN 0-9644311-8-1.

110. Shen G, Glinka G. Weight functions for a surface semi-elliptical crack in a finite thickness plate. Theor Appl Fract Mech 1991;15(2):247–55.

111. Smith RA. Thirty years of fatigue crack growth—a historical review. Smith RA, editor. In: Fatigue Crack Growth, 30 Years of Progress. Oxford: Pergamon Press, 1986. p. 1-16.

112. Soh AK. Improved procedure for the determination of hot spot stresses in tubular joints. Fatigue Fract Eng Mater Struct 1997;20(12):1709–18.

113. Sonsino C.M., Radaj D. and Fricke W. Advanced local concepts for assessing the fatigue durability of welded joints. In: Alfaiate J., Aliabadi M.H., Guagliano M. and Susmel L., eds. 6th International Conference on Fracture and Damage Mechanics. Trans Tech Publications LTD, Zürich, Switzerland, Madeira, Portugal, 565-568, 2007.

114. Susmel L, Taylor D. Fatigue design in the presence of stress concentrations. Int J Strain Analysis 2003;38:443–52

115. T. Fett, H-A. Bahr. Mode I stress intensity factors and weight functions for

short plates under different boundary conditions. Engineering Fracture Mechanics 62 (1999) 593±606.

116. Taylor D, Bologna P, Bel Knani K. Prediction of fatigue failure location on a component using a critical distance method. Int J Fatigue 2000;22:735–42.
117. Taylor D, Lawless S. Prediction of fatigue behaviour in stress-concentrators of arbitrary geometry. Eng Fract Mech 1996;53:929–39
118. Taylor D, Wang G. The validation of some methods of notch fatigue analysis. Fatigue Fract Engng Mater Struct 2000;23:387–94
119. Taylor D. Crack modelling: a technique for the fatigue design of components. Engineering Failure Analysis 1996;3:129–36.
120. Taylor D. Geometrical effects in fatigue: a unifying theoretical model. Int J Fatigue 1999;21:413–20.
121. Taylor D. Geometrical effects in fatigue: a unifying theoretical model. Int J Fatigue 1999;21:413–20.
122. Ted L and Glinka G. A closed-form method for integrating weight functions for part-through cracks subject to Mode I loading. Eng Fract Mech 73 (2006) 2153-2165.
123. The new IIW recommendations for fatigue assessment of welded joints and components-A comprehensive code recently updated. International Journal of Fatigue 31 (2009): 50–58
124. Tovo R, Lazzarin P. Relationship between local and structural stress in the evaluation of the weld toe stress distribution. Int J Fatigue 1999;21:1063–78.
125. Tveiten BW, Moan T. Determination of structural stress for fatigue assessment of welded aluminium ship details. Mar Struct 2000;13:189–212.
126. Vallellano C, Dominguez J, Navarro A. On the estimation of fatigue failure under fretting conditions using notch methodologies. Fatigue Fract Engng Mater Struct 2003;26:469–78.
127. Verreman Y, Nie B. Early development of fatigue cracking at manual fillet welds. Fatigue Fract Eng Mater Struct 1996;19:664–81.
128. W Fricke Review: Fatigue analysis of welded joints state of development. Mar Struct 16 (2003) 185-200.
129. W. Fricke, A. Kahl, Comparison of different structural stress approaches for

fatigue assessment of welded ship structures, Marine Structures 18 (2005) 473-488

130. W. Fricke, H. and H. Paetzold. Full-scale fatigue tests of ship structures to validate the S–N approaches for fatigue strength assessment. Marine Structures Volume 23, Issue 1, January 2010, Pages 115-130
131. W. Fricke, W. Cui, etc. Comparative fatigue strength assessment of a structural detail in a containership using various approaches of classification societies, Marine Structures, Volume 15, Issue 1, January 2002, Pages 1-13.
132. Wang, X. J. and Lambert, S. B., Stress intensity factors and weight functions for longitudinal semi-elliptical surface cracks in thin pipes. International Journal of Pressure Vessels and Piping, 1996, 65,75-87.
133. Whitney JM, Nuismer RJ. Stress fracture criteria for laminated composites containing stress concentrations. J Compos Mater 1974;8:253–65.
134. Williams M L, 1952, Stress singularities resulting from various boundary conditions in angular plates in extension, Journal of Applied Mechanics, 19, pp526-528
135. WU Xiaoyuan, Study on the Fatigue Life Prediction Methods for FPSO Structures, PhD thesis, 2008
136. X. R. Wu, Study of influence of the reference load case on the crack face weight functions. Znt. J. Fracture 48(3) (1991).
137. Xiao Z-G, Yamada K. A method of determining geometric stress for fatigue strength evaluation of steel welded joints. Int J Fatigue 2004;26:1277–93.
138. Y. Murakami et al. (Eds), Stress Intensity Factor Handbook. Pergamon Press, oxford (1987).
139. Y. Murakamj, A method of stress intensity factor calculation for the crack emanating from an arbitrary shaped hole or the crack in the vicinity of an arbitrary shaped hole. Trans. JSME 44(378), 423-432 (1978).
140. Yung JY, Lawrence FV. Analytical and graphical aids for the fatigue design of weldment. Fatigue Fract Eng Mater Struct 1985;8(3):223–41.
141. Zhang, S., 1997, Stress intensities at spot welds. International Journal of Fracture 88, 167–185.
142. Zhao. W, Newman Jr, Sutton. M, WU. X and Shivakumar K. Stress intensity

factor for corner cracks at a hole by a 3-D weight function method with stresses from the finite element method. Fatigue Fracture Engineering Material. Structure. Vol. 20, No. 9, pp, 1255-1267, 1997

143. Zheng XJ, Kiciak A and Glinka G. Weight functions and stress intensity factors for internal surface semi-elliptical crack in thick-walled cylinder. Engineering Fracture Mechanics Vol. 58, No. 3, pp. 207-221, 1997

144. Ziganchenko, PP. Kuzovenkov. BP. Tarasov. Hydrofoil crafts: Strength and Construction. Sudostroenie Pubs, Leningrad, 1981.

CHAPTER 3

THEORETICAL BACKGROUND

3.1 Introduction

Compared with the nominal stress fatigue prediction method, the drawback with the finite element based hot spot, structural stress and fracture mechanics methods is that they require significant time to set up finite element analyses and require good insights into the structural behaviour. It is important to understand how much of the local singularity is included in the analysis but that is often unclear. For 2D problems of attachments to plates, the structural stress approach does avoid the singularity but for 2D corner problems and 3D problems the structural stress approach still requires an understanding of what is and is not included in the calculated stresses.

The methodology developed in this work considers the nature of the stress singularity and provides a theoretical background when sets up an analysis, about the scale singularity relative to the used elements size and hence how much of the singularity might be resolved by the analysis. It can also give preliminary estimates of the intensity of the singularity which can be used directly within a stress concentration calculation and fracture mechanics calculation.

It should be mentioned that the treatment of fatigue failure uses continuum-mechanics approaches, and fatigue damage is a localised phenomenon resulting from repeated stress application. The knowledge of elasticity theory built up in the applied mechanics framework is necessary for describing the behaviour of structures' fatigue behaviour. This chapter will briefly highlight the theoretical

background and relevant mathematical formula relevant to the 'Length Scale method'.

3.2 New Stress Distribution Formula

The elasticity solutions have the advantage of being extended to cracks at the interface of homogeneous isotropic materials and applicable for V-notch problems. It is necessary to bring out the theory of elasticity analysis of preparation for the stress derivation (S. Timoshenko, 1951; E. E. Sechler, 1952; N. I. Muskhelishvili, 1953).

Just as both Kolosoff (1910) and Inglis (1913) independently discovered the elasticity stress problem with defect, there are several classical solutions for it. The first ones are proposed by Westergaard (1937), the later by Williams (1961); and the original development of complex variable was done by a series of Russian elasticians of Muskhelishvili (1953).

Developments have proceeded on parallel tracks, there being little overlap between the study of the notches and cracks shown in Table 3.1.

Table 3.1

Original development for the singular stress solutions

Problem	Coordinate System	Real/Complex	Solution	Date
Circular Hole	Polar	Real	Kirsh	1898
Elliptical Hole	Curvilinear	Complex	Inglis	1913
Crack	Cartesian	Complex	Westergaard	1939
V notch	Polar	Complex	Williams	1952
Isotropic Materials	Cartesian	Complex	Muskhelishvili	1953
Dissimilar Materials	Polar	Complex	Williams	1959
Anisotropic Materials	Cartesian	Complex	Sih	1965

In this part we propose a semi-empirical corner stress formula that is based on the geometry. That this formula seems to be useful may be partly due to the fact that the stress functions above allow the use of conformal mapping and more fundamentally that stress patterns scale with the size of the structural detail.

3.2.1 William's Eigen Stress Solution

Using the method of separation of variables, M L Williams (1952) proposed the solution for Airy's stress function (detail elasticity stress problem derived in Appendix A); note that the problem originally considered is not a crack, but rather a plate under tension with angular corners, making an angle 2θ :

$$\Phi(r,\theta) \equiv r^{\lambda+1} F(r,\theta) \qquad 3.1$$

For θ=0 we recover the crack problem of Westergaard. Substituting Eqn. 3.2 into the bi-harmonic equation give:

$$\frac{\partial^4 F(\theta,\lambda)}{\partial\theta^4} + 2(\lambda^2+1)\frac{\partial^2 F(\theta,\lambda)}{\partial\theta^2} + (\lambda^2-1)^2 F(\theta,\lambda) = 0 \qquad 3.2$$

However, using the method of eigenfunction expansion, the stress at the crack tip cannot be determined but has a 1 over distance (r) to the power ½ singularities, or asymptotic solution, as r becomes small and approaches the notch tip.

Williams (1952) demonstrated that in the context of the elasticity theory, the asymptotic stress state near a sharp corner is singular and its degree of singularity is a function of the angle of the corner (Fig 3.1).

The asymptotic state at the singularity of a sharp open corner is defined by the root of the eigenvalue function, the exponent value 'p' for the stress distribution is the first solution of following expression by M L Williams (1958):

$$(p+1)\sin(2\pi-\alpha) + \sin((p+1)(2\pi-\alpha)) = 0 \qquad 3.3$$

Where: α is the corner angle; p is the factor for different corner angles.

Results for different angles are shown in Figure 3.1

Table 3.2

Typical coefficients values from the eigenvalue functions

α	0^o	60^o	90^o	100^o	120^o	135^o	140^o	160^o
p	0.5	0.488	0.455	0.437	0.374	0.326	0.303	0.181

Based on analysis of linear elastic fields at a sharp open corner, Williams stated that the stress distribution in a re-entrant V-shaped corner is similar to the Mode I stress distribution of a crack.

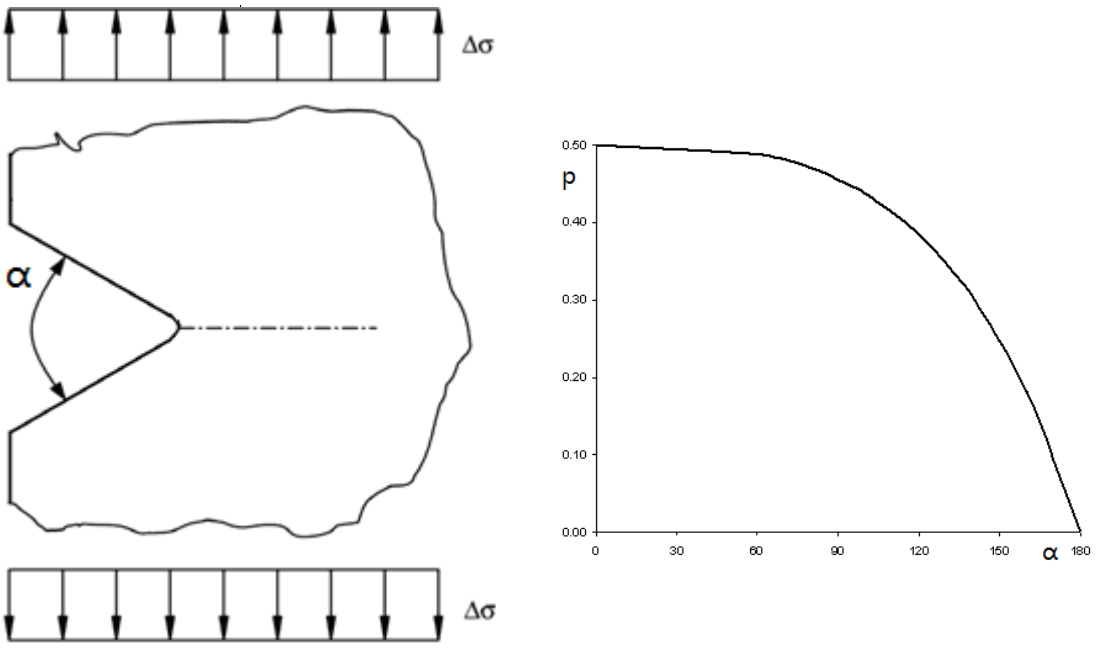

Figure 3.1 a) Plot of applied stress with notch, and
b) the '*p*' value curves relating with the notch angles

This permits geometric simplification to be made. The cruciform is the most suitable shape for initial study as it offers a similar geometry to many details found in classical ship components, from simple joints shown in Figure 3.2, the singularities are out of the plane of the members to more complex components, where the singularities are also out of the plane of the members itself.

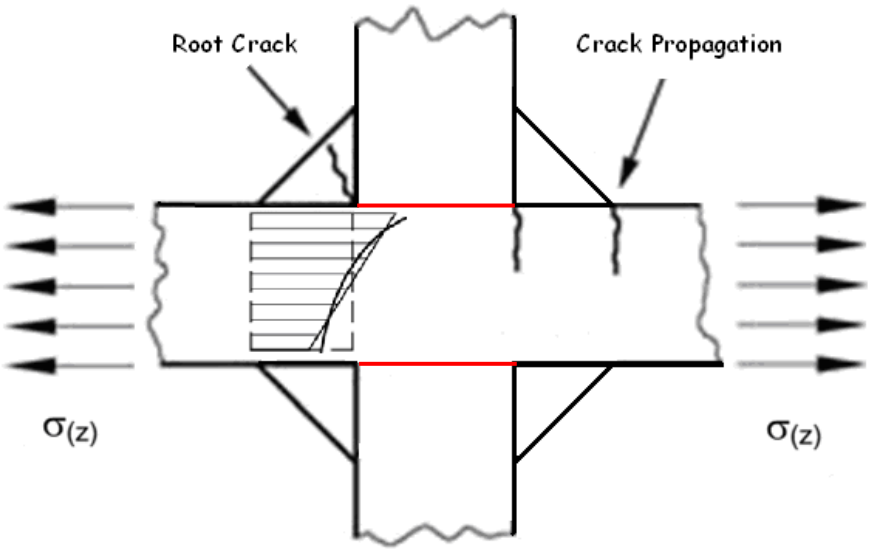

Figure 3.2 Cruciform shape for connection section modelling

From the power singularity just illustrated, it can be seen that the solution of a singular stress field can be visualized, for more functions, we can also check in handbook (Tada etc, 1973).

Lazzarin and Tovo (1998) investigated a theoretical framework and formal definition of the Notch-SIF, and directly correlated fatigue life with N-SIF values taking into account different welded joints.

$$K_I^V = \sqrt{2\pi}\lim_{r\to 0} r^{1-\lambda_1}[\sigma_\theta(r,0)]$$
$$K_{II}^V = \sqrt{2\pi}\lim_{r\to 0} r^{1-\lambda_2}[\tau_{r\theta}(r,0)] \qquad 3.4$$

Where: λ_1 is singularity exponent of Mode I (opening mode) notch,

$1-\lambda_1$ is equal to the 'p' value in William's formula (1952)

λ_2 is singularity exponent of Mode II (sliding mode) notch

The exponent values for the stress distributions are the eigenvalues defined from the solutions of William's (1952), which relate to the opening angle of notch.

The N-SIF approach has the capability to describe the stress gradient along a free edge. For example that the radial stress distribution for $\alpha = 135^\circ$ and $\theta = 120^\circ$ can be determined from the stress formula of Williams', which is shown as following:

$$\sigma_r = K_1 \cdot 0.423 \cdot r^{-0.326} - K_2 \cdot 0.553 \cdot r^{0.302} \qquad 3.5$$

Note: the positive exponent of second term is correct. (Lazzarin and Tovo,1998)

A problem with the simple asymptotic formula is that it predicts the stress decays to zero at a large distance from the crack. To obtain a stress which decays to a nominal value at some distance from the crack tip Xu and Barltrop (2007) proposed the formula in Eqn.3.6. This empirical formula was adapted from the formula by Paris and Sih (1965) which, with p = 0.5, is exact for a centre crack in an infinite sheet.

$$\sigma(x) = \frac{\sigma_0 (a_s + x)}{\left[\left(2^{(\frac{1}{2p})} \cdot x \cdot a_s^{(\frac{1}{p}-1)} \right)^q + x^{(\frac{q}{p})} \right]^{\frac{p}{q}}} \qquad 3.6$$

where: q = 3p – 0.5, 'x' is the distance from the crack tip;

σ_0 is nominal stress;

and a_s is a characteristic size of the singularity with units of length, that characterizes the stress field from the notch.

Non-dimensional stress plots for different corner angles (actually based on a unit nominal stress and an 'as' value of 10mm) are shown in Figure 3.3. Note that the stress at any non-dimensional distance x/as from a crack tip is proportional to the applied stress $\Delta\sigma_0$.

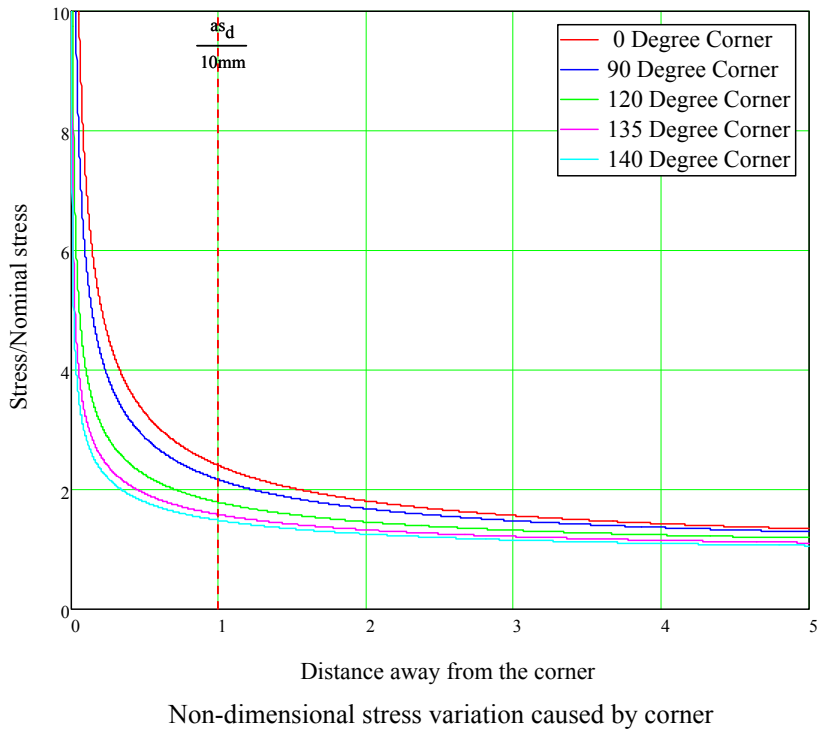

Figure 3.3 Stress distribution of different cruciform angles (and hence *p* vales) (Drawn for an 'as' value of 10mm)

In practice the as value depends on the geometry features and the dimensions of the structure containing the sharp corner, usually the effect of the singularity is at the

distances range of as/3 or less from the crack tip.

3.2.2 Conformal Mapping Theory

The rational mapping function of the sum of fractional expressions can be formed for comparatively arbitrary shapes and is particularly efficient for obtaining the stress distributions (it is also used for many other problems such as in fluid mechanics).

The semi-infinite plate with a triangular notch (and with a crack originating from a triangular notch) on a rim of a semi-infinite plate is analyzed for an angle of the notch, under uniform tension as shown in Figure 3.4.

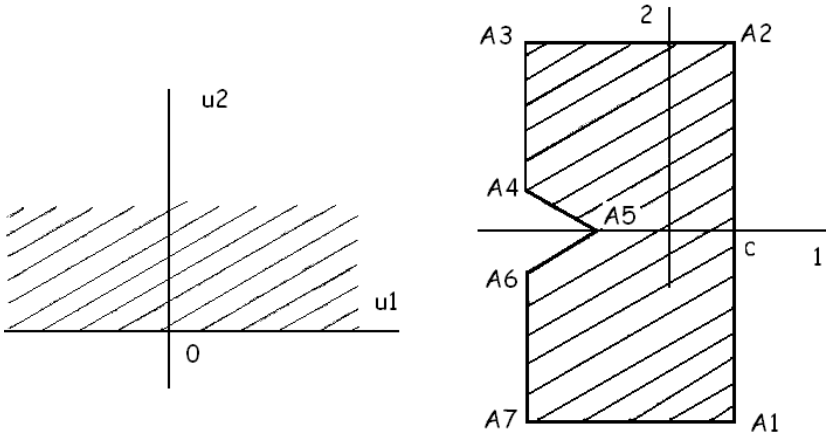

Figure 3.4 The semi-infinite region mapping to a triangular notch

Conformal mapping of an infinite region with a corner can be obtained by Schwarz-Christoffel transformation. The transformation function is defined by:

$$f(w) = A\int_{w_0}^{w} \prod_{k=1}^{n} (w - w_k)^{\alpha_k - 1} dw + B \qquad 3.7$$

where: A and B could be constants

Let the seven vertices A1, A2…A7 of the plate enumerated in a counter clockwise order, be the points $z_1, z_2 ... z_7$ with corresponding exterior angles

$\alpha_1, \alpha_2 ... \alpha_7$ respectively and let their image points on the real axis be $\alpha_2 ... \alpha_7$ respectively.

Thus, we can apply a Schwarz-Christoffel transformation in order to map the interior of this polygon onto the upper half plane with the polygon on the points, of the real axis of the semi-infinite plane.

The values of the exterior angles are:

$$\begin{aligned} &\alpha_1 = \alpha_2 = \alpha_3 = \alpha_7 = \pi / 2 \\ &\alpha_4 = \alpha_6 = \pi / 2 - \varphi / 2 \\ &\alpha_5 = \varphi - \pi \end{aligned} \qquad 3.8$$

The polynomial mapping function may be expressed as:

$$m(\zeta) = C_1 (\sum_{n=0}^{N} \frac{\varepsilon}{n+1} \zeta^{n+1}) \qquad 3.9$$

where C_1 is a new constant

A solution by Aifantis (1978) uses the conformal mapping technique, for a convenient Mode III stress solution of the semi-infinite domain.

The solution holds for each point in the linear elastic, homogeneous isotropic material. It is shown that the limiting case of the V-notch collapses to the stress functions independently of the edge-cut.

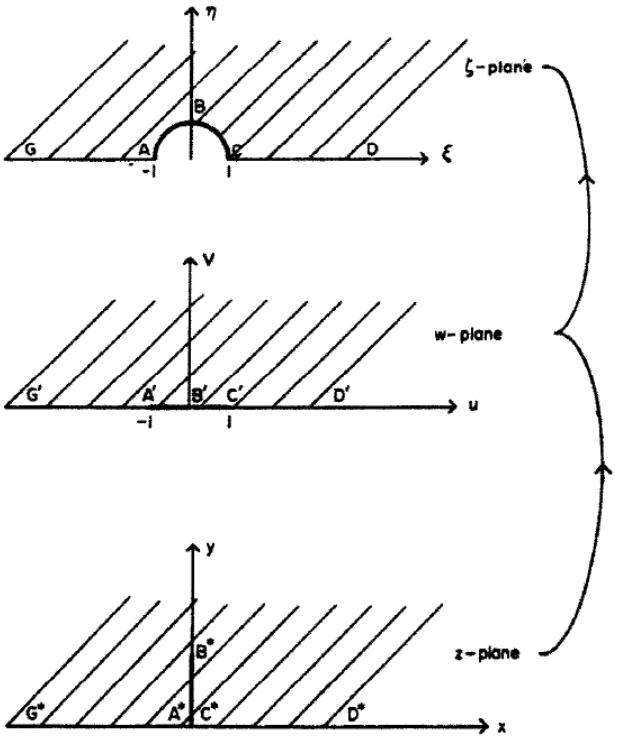

Figure 3.5 Transformation example among the planes by Aifantis, 1978

It is necessary to map the upper-half z plane to the upper-half y with a unit semicircle removed requiring the slit $0 < 2 < a_i$ to be mapped on the being of the unit semicircle.

The appropriate inverse transformation is taken by

$$\zeta = \frac{1}{a}(z + \sqrt{z^2 + a^2}) \qquad 3.10$$

3.2.3 Explanation and Solutions for Length Scale

The Length Scale is a practical parameter dealing with problems of interest to industry. It will be shown later that if this value can be determined then SCFs for hot spot fatigue analysis and SIFs for fracture mechanics analysis can be determined.

The physical reality must be clearly understood in order to propose formulae which will be connected to the essence of the phenomena. The cruciform is considered to be a main plate with an outstand of length L and height H. Important influences on the behaviour are:

The corner angle (often 90 degrees implies that the singularity is likely to be of the form $1/r^{0.455}$. Relevant dimensions are:

The length of the outstand, L;

The height of the outstand, H;

The width of the plate, a;

The length of the plate, b

Providing the plate is sufficiently long and wide the most important influences will be the angle and the length and height of the outstanding.

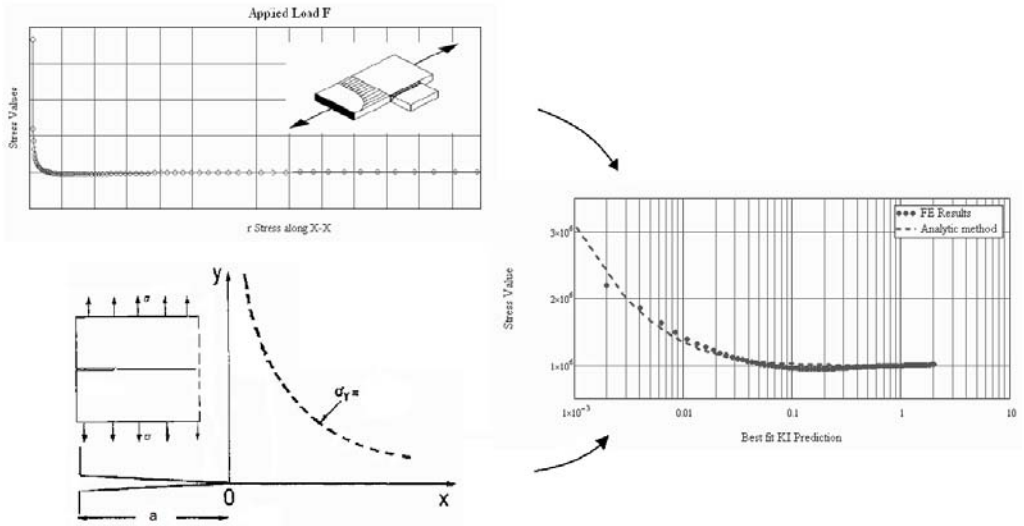

Figure 3.6 Summary of the crack modelling technique

(stress field of right corner is similar to the stress field of an edge crack, suggesting that the corner appears to be an additional length of crack)

The Length Scale 'a_s' expression (Eqn. 3.11) is obtained by applying finite element analysis to numerous cruciform joints and fitting Eqn. 3.6 of the stress distribution along the line from the corner and at right angles to the applied load, as shown in Figure 3.7:

$$a_s = Function(geometry) \qquad 3.11$$

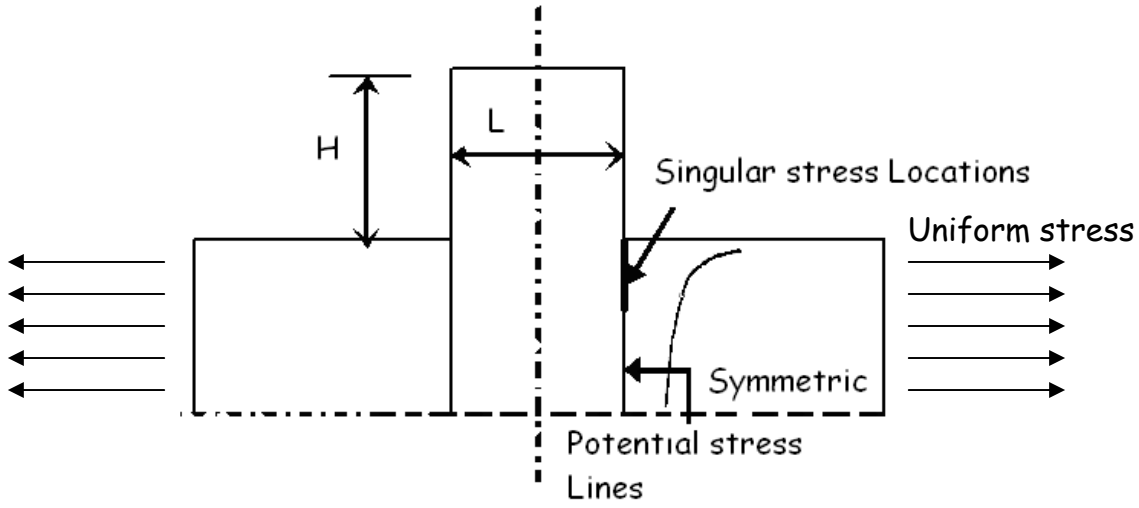

Figure 3.7 Traditional cruciform plate with corner leading to stress singularity

Ten thousand different combinations of cruciform dimensions were computed using FE calculation. The singularity power p was found, as theoretically predicted, to be approximately 0.455.

Values of the as factor were least-squares fitted with a polynomial of second order and the 'as' results non-dimensionalized by dividing by H or by L are shown in Figure 3.8. This was done using the MATHCAD 'genfit' function.

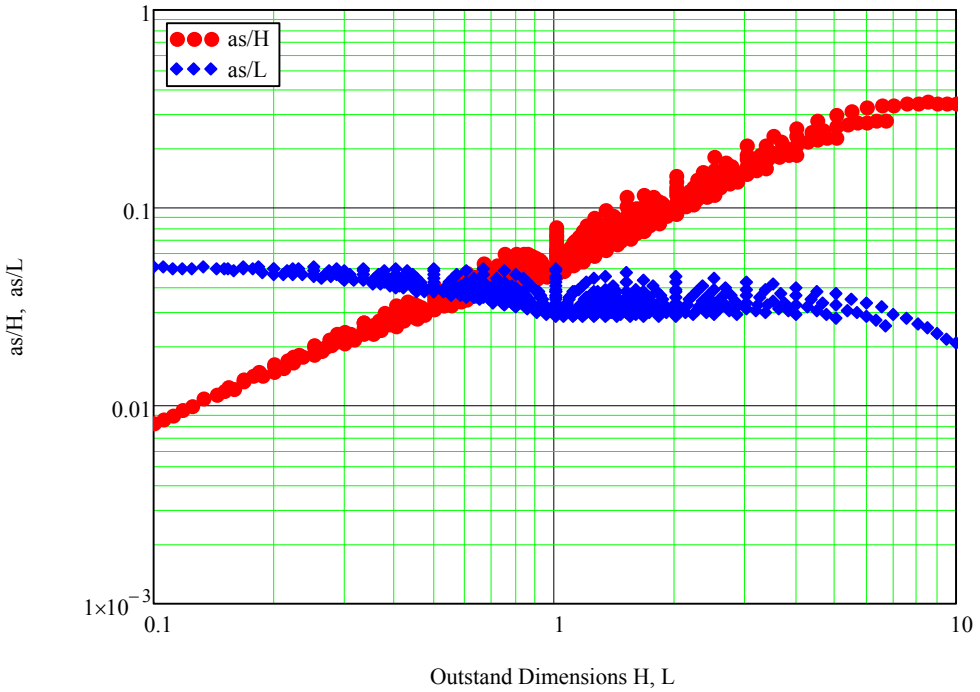

Figure 3.8 'Length Scale' values converting from FE calculations of different geometry dimensions

Drawing means curves through the data Figure 3.9 are obtained. The significance of the scatter will be discussed in Chapter 6.

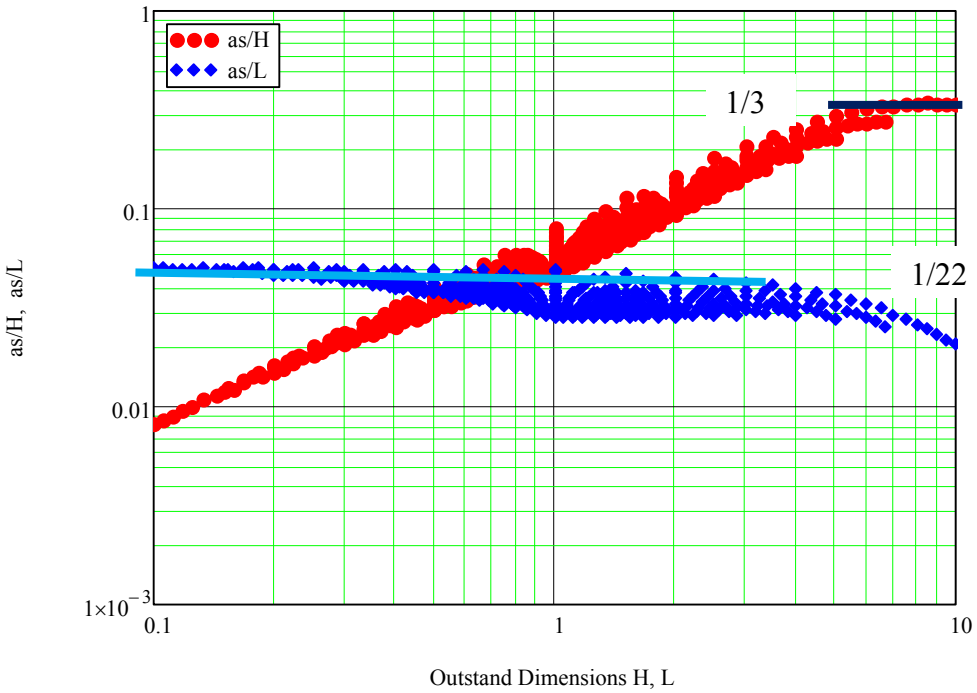

Figure 3.9 Trend of prediction of Length Scale '*as*'

From Figure 3.9, we can see that:

When L/H is less than 0.5, as is approximately H/3.

When L/H is greater than 5, as is approximately L/22.

In between L/H values, the simple approximations above over estimate the as value but the smaller of either estimate is a useful approximation to the as value.

Therefore a simple estimate of as (that will be a little high for L/H between 5 and 10) can be obtained from Eqn. 3.12a.

$$a_s = smallest\ of \quad (L/22, \quad H/3) \tag{3.12a}$$

where L is the length of the bracket, and H is its height (shown in Figure 3.7).

This applies for constant plate thickness ($t_o = t_{bp}$)

For the case where the thickness of the outstand arms (to) of the cruciform have a different thickness to the thickness of the main load carrying plate (t_{bp}) the following formula 3.12b fitted the results:

$$a_s = smallest\ of \quad (L/22 \cdot (t_o/t_{bp})^{0.5}, \quad H/3 \cdot (t_o/t_{bp})^{0.87}) \tag{3.12b}$$

Furthermore, if a bracket of length l is fitted into the corner, so effectively increasing the length of the connection, the equation is simply modified as follows:

$$a_s = smallest\ of \quad ((L+l)/22, \quad H/3) \tag{3.13}$$

Note that this typically means that the as value (and hence the SCF) increases.

3.3 Constant Distance SCF Definition

Stress concentrations leading to high local stress result in objects failing quickly through fatigue. The stress concentrations are usually introduced by geometric discontinuities. (It is very important for engineers to carefully consider the geometry at the design stage.

The relevant stress is termed the ‘concentration stress’ to avoid confusion with the design stress which may exclude stress concentration effects.

For the case of stress concentration caused by a central circular hole in a thin plate is shown in Figure 3.10, the elastic stress concentration factor is finite and for

uniform applied stress =3. However it is sometimes argued that this is too pessimistic and that a value of 2.4 is more consistent with the observed fatigue life, so the peak stress value may not be the important value for fatigue.

This at least partly explains why the infinite elastic stresses at sharp corners lead to finite rather than zero fatigue lives. So a method is needed for determining a fatigue SCF for a sharp corner.

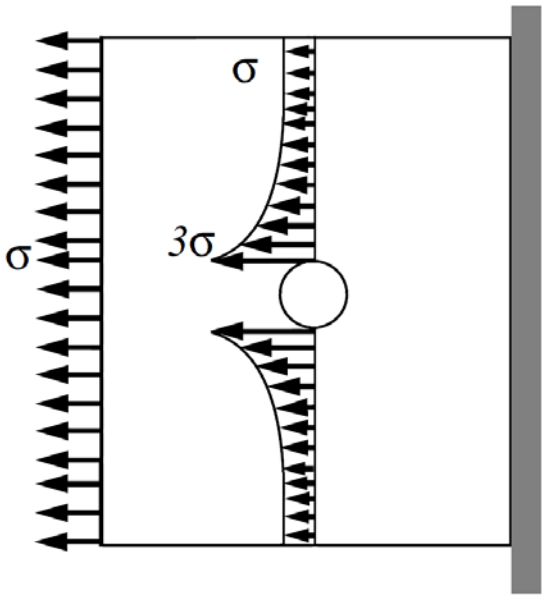

Figure 3.10 The concentration effect of a circular hole on the stress component (S. Timoshenko, 1951)

In the structural stress method proposed by Dong (2001), the fatigue-effective "structural stress" over the cross section replaces the non-linear singular stresses by the sum of a membrane stress and a shell bending stress. As explained previously. This method is not suitable for in-plane corners but it does provide a method of reducing the singular stress to a finite value.

Another method of calculating fatigue stress concentrations is to calculate the stress at some specified 'critical distance' from the singularity. For a critical distance normal to the applied nominal stress this is straightforward if 'as' is known because Eqn. 3.6 will defines the stress at the required through thickness position. As shown previously the length, 'as' is obtained from geometry, and 'da' is recognized as the critical distance away from the corner. Eqn.3.6 then becomes Eqn.3.14.

$$SCF = \frac{(as + da)}{\left[\left(2^{(\frac{1}{2p})} \cdot da \cdot as^{(\frac{1}{p}-1)}\right)^q + da^{(\frac{q}{p})}\right]^{\frac{p}{q}}} \qquad 3.14$$

This will not be satisfactory if the critical distance is in the direction of the stress surface and e.g. 1 or 1.5 times thickness. Xiao and Yamada (2004) proposed that the concentration stress is measured at a point of 1 mm below the longitudinal surface; Haibach (1970) proposed the concentration stress is determined at the surface 2 mm from the corner.

By trial and error a critical distance of 1.2 mm, Eqn. 3.15 gives similar results to linear extrapolation from the corner, as shown in Figure 3.11.

$$SCF = \frac{(as + 1.2)}{\left[\left(2^{(\frac{1}{2p})} \cdot 1.2 \cdot as^{(\frac{1}{p}-1)}\right)^q + 1.2^{(\frac{q}{p})}\right]^{\frac{p}{q}}} \qquad 3.15$$

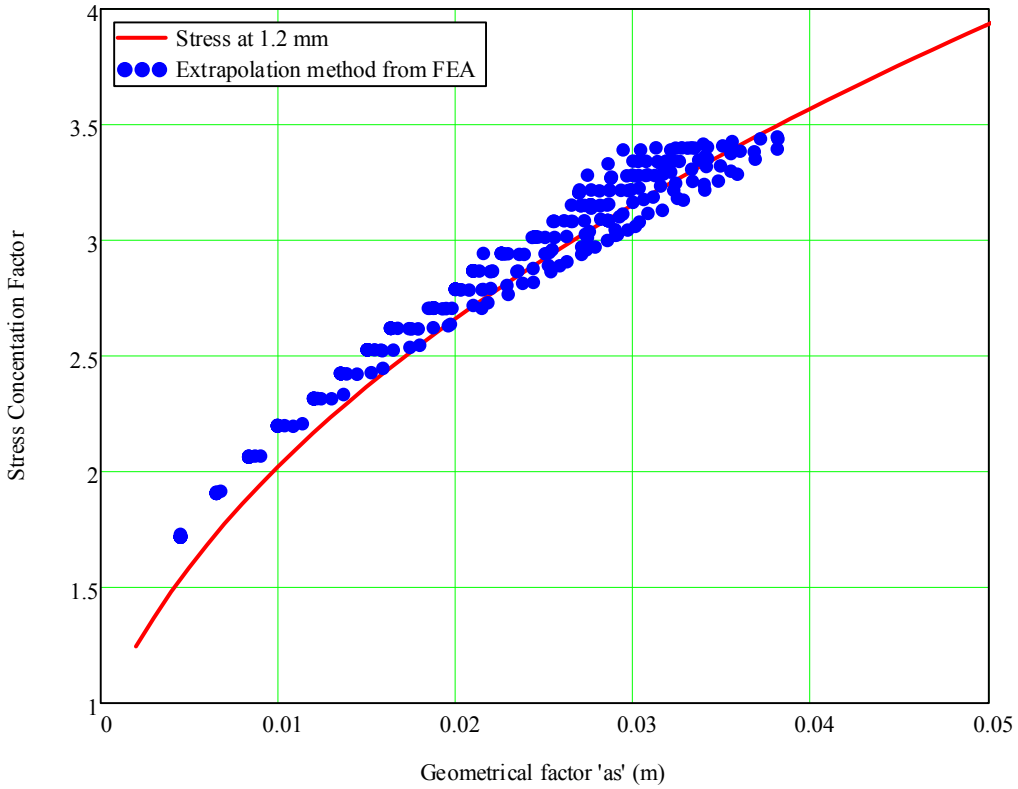

Figure 3.11 Comparison of *SCF* according to different approaches

In Chapter 4 further (and similar) SCF comparisons are made with fracture mechanics simulations where the as value will be used within the fracture mechanics or LEFM formulation.

Note: the advantage of the use of as over the other methods is that it allows a quick estimate of the results without the need for finite element analysis, and/or it can be used to help check the finite element analysis and interpret the results.

3.4 Transformation for 3D Situations

The results so far are all for the 2D, planar cruciform plates, however real engineering connections are more complicated than the 2D plate. For example, the flat bar or bracket attached to the web of the longitudinal stiffener shown in Figure 3.12. We will consider how to apply the Length Scale SCF to real ship engineering.

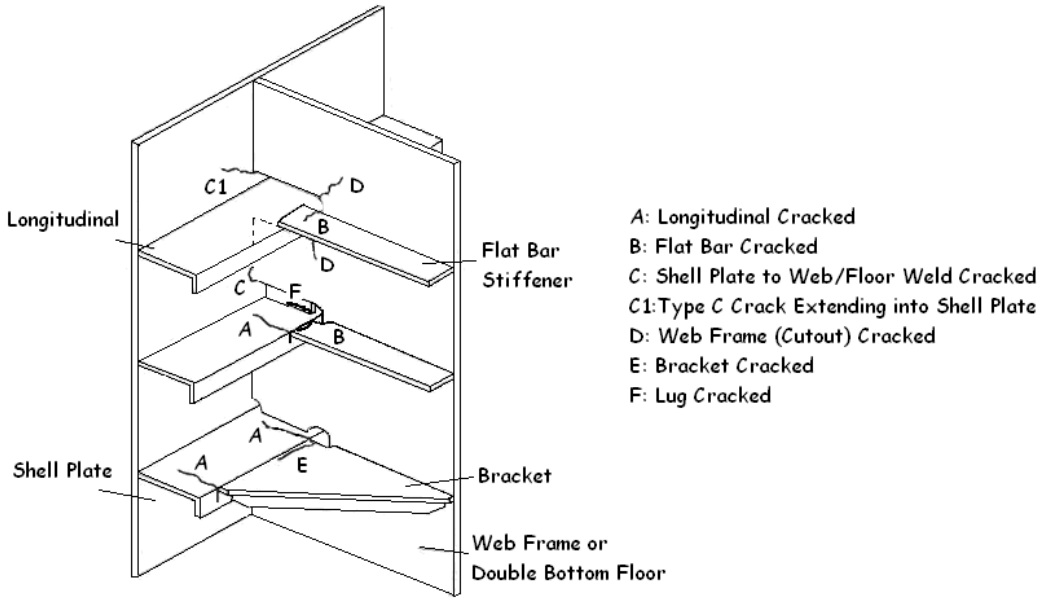

Figure 3.12 Illustration of a ship structural connection

For the commonly occurring cracks A, B and E initiation occurs at the intersection of the stiffener web and flange. The web and flat bar or bracket are similar to the cruciform but the flange at right angles to these plates adds some further complexity.

It is useful to consider a simpler case where the longitudinal stiffener is simply a flat bar and the plane of the flat bar web stiffener or bracket can be changed.

We can see that the problem will go from 2D to 3D; the determination of the peak stress becomes more complicated because the Poisson's ratio effect is different when there is a right angle connection. Also equilibrating local moments are different for the out of plane case.

Numerical results have shown that Poisson's ratio does not have a significant effect on the stress distributions but changes in the pattern of the moment equilibrium are important. The outstand (flat bar or bracket) connection supports the longitudinal stiffeners but introduces an eccentricity in the resistance to the axial loads on the stiffener. It follows that the axial load eccentricity will produce a secondary bending. This bending can be resisted by moments between outstand and stiffener (MX) or by moments within the outstand (MN), see Figure 3.13.

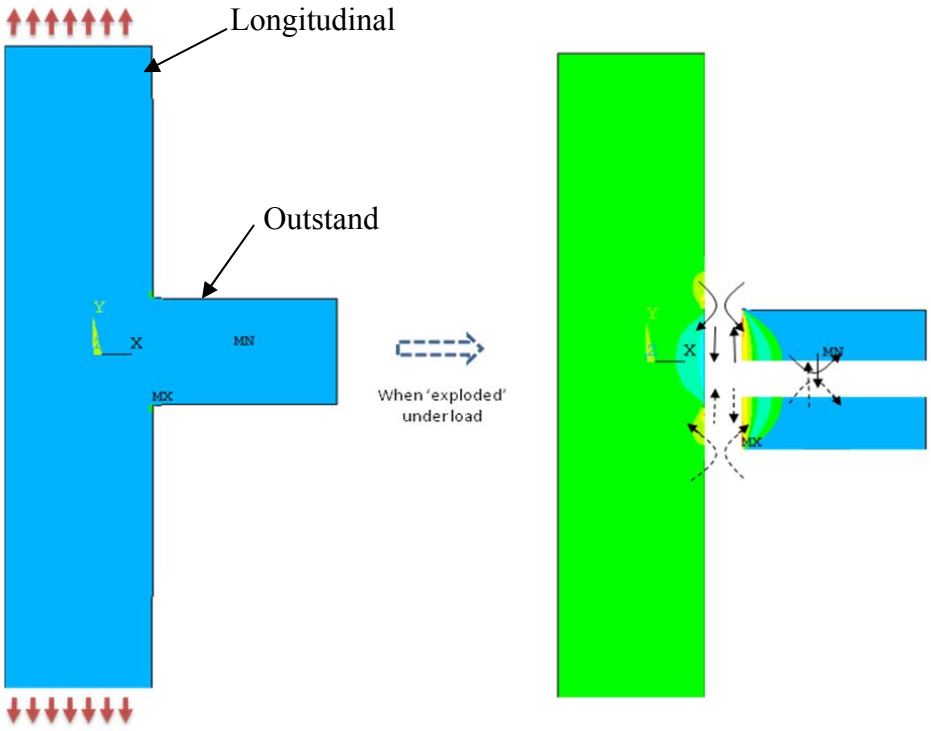

Figure 3.13 Details of the bending moment at the connection between the main plate and the outstanding plate due to the need to balance the eccentric y-direction stress within the outstanding plate (Li, B. Lou and N Barltrop, 2012)

If we imagine folding the outstand from the planar, 0 degree, case shown in Fig 3.13 back through 90 degrees to a right angle and then to 180 degrees so that it is lying against the stiffener, as shown in Figure 3.14.

For the 90 degree case, the moment MX changes to zero (as a result of the small out of plane bending stiffness of the outstand) and the moment has to be resisted primarily by MN.

For the 180 degree case the MX moments applied to the outstand are the same for the 180 degree case as for the 0 degree case but the sign has reversed for the moment applied to the longitudinal. This substantially reduces the stress concentration in the corner.

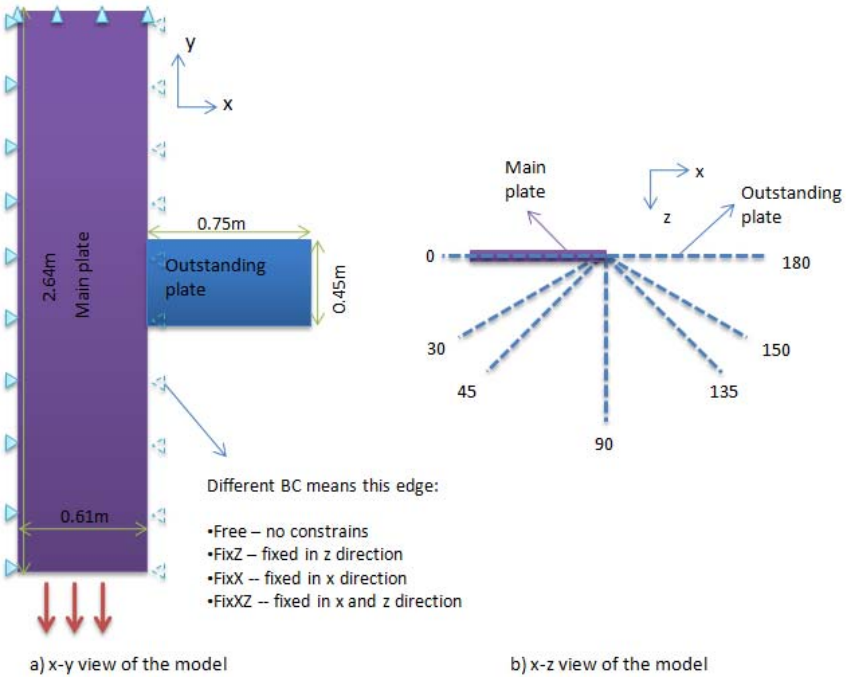

Figure 3.14 Dimensions and constraints of the model with outstanding plate attached at different angles (L. Xu, B. Lou and N Barltrop 2012)

In practice there is usually an in plane connection with the addition of a flange out of plane. This provides an opportunity for the 0 degree type of moment equilibrium even when some of the eccentricity results from the longitudinal stiffener flange being at right angles to the outstand.

It has been found that the 3D connections problem can be transferred to the planar stress by folding plate thickness: the ratio of the thickness of the outstand and the sum of the longitudinal web and flange thicknesses allows, the Length Scale to be determined using the formula of Eqn.2b with relative thickness corrections:

$$a_s = smallest\ of \quad (L/22\cdot(t_o/t_{bp})^{0.5}, \quad H/3\cdot(t_o/t_{bp})^{0.87}) \qquad 3.16$$

Here, L is the length of the outstand attachment, and H is the height

For different plate thicknesses ($t_o \neq t_{bp}$);

t_o is the thickness of the outstand plate, and t_{bp} is the sum of the thicknesses of the longitudinal flange and web.

Understanding the stress flow inside the system for different cases will allow the clear estimation of stress concentration factors for fatigue assessment. Numerical

calculations are needed to prove the length scale method for more complicated realistic details.

3.5 Conclusions

The influence of geometry on stresses has been considered in detail in this chapter. The amount of material affected by the geometry is rather localized in comparison with the size of the geometric characteristics.

The effect of geometry will be fundamental to the stress distributions and hence the overall life of the joint. For an outstand on the edge of a structural member (as found in a typical shell to frame connection) the Length Scale of the local stresses are determined by the outstand height and the outstand length, the relative thicknesses and the characteristic nominal stress.

From the Length Scale of geometry a new definition of Stress Concentration Factor can be defined using Eqn 3.14. With this information the design fatigue strength is easily calculated. For the case of equal outstand and longitudinal member thickness the Length scale is the lesser of H/3 or L/22.

In the Chapter 5, the length scale is linked to the Stress Intensity Factor for fracture mechanics calculations; as well as providing a direct crack growth calculation method, which links the Length Scale to SCF values.

REFERENCES

1. Dong P. A structural stress definition and numerical implementation for fatigue analyses. Int J Fatigue 2001;23 (10):865-76.
2. E. C. Aifantis and W. W. Gerberich. A new form of exact solutions for Mode I, II, III crack problems and implications. Engineering fracture mechanics. 1978, Vol. 10. pp. 95-106
3. E. E. Sechler, Elasticity in Engineering, Dover Publications, New York, 1952
4. H. Tada, P.C. Paris and G.R. Irwin, The stress analysis of cracks, Heilertown,

Pennsylvania (1973)

5. Haibach, E., Modified linear damage accumulation hypothesis considering the decline of the fatigue limit due to progressive damage, Laboratorium fur Betriebsfestigkeit, Darmstadt, Germany, Techn. Mitt. Tm 50/70, 1970
6. Lazzarin, P. and Tovo, R. (1998). A notch intensity approach to the stress analysis of welds. Fatigue and Fracture of Engineering Materials and Structure 21, 1089–1104
7. Li Xu and Nigel Barltrop. Analysis of Sharp Corners in Structural Details. Universities of Glasgow & Strathclyde, UK
8. Li Xu, Benqiang Lou and Nigel Barltrop, Considerations on the fatigue assessment methods of floating structure details, Journal of Engineering for the Maritime Environment 0(0) 1–12
9. M. L Williams. The bending stresses distribution at the base of a stationary crack. ASME Journal of Applied Mechanics, 1961
10. Muskhelishvili NJ: Singular Integral Equations, trans. JRM Radok and P Noordhoff, Groningen, The Netherlands, 1953.
11. N. I. Muskhelishvili, Some Basic Problems of the Mathematical Theory of Elasticity, Noordhoff, Leiden, 1953
12. S. Timoshenko and J. N. Goodier, Theory of Elasticity, McGraw-Hill, New York, 1951
13. Westergaard HM: Bearing pressures and cracks, J. Appl. Mech., vol 6, pp. A49-53, 1937.
14. Williams M L, 1952, Stress singularities resulting from various boundary conditions in angular plates in extension, Journal of Applied Mechanics, 19, pp526-528.
15. Xiao, Z and Yamada K A method of determining geometrical stress for fatigue strength evaluation of steel welded joint, International Journal of Fatigue, volume 26, 2004, pp 1277-1993
16. P.C. Paris and G.C. Sih, in: Stress Analysis of Cracks, ASTM STP 381 (1965) 30-83

CHAPTER 4

FEA IN FATIGUE and FRACTURE MECHANICS

Mathematical analytical derivations or simple formula often will not be sufficient for the fatigue analysis of real engineering problems, and numerical analysis of finite element analysis (FEA) will often be required.

This chapter discusses the application of FEM to fracture mechanics problems.

4.1 FEA with SN Predictions

Applications of FEA calculation are typically:

- local (i.e. of a fine mesh analysis of the area in the vicinity of the actual or possible crack) static analysis ($x = K^{-1}F$) where K here is the stiffness matrix and x is the local displacement vector, or
- local quasi static analysis ($x = K^{-1}(F - M \cdot x_{dg}'')$): a static analysis but where the acceleration vector x_{dg}'' is approximately pre-calculated in a separate dynamic global analysis.

The finite element mesh will depend on the results required.

For SN curve approach the stress distribution calculation is required, so that either the stress concentration or a nominal stress can be estimated. Commonly the corner singularity is not properly modelled depending on the element size near the

corner.

If the stress concentration is to be obtained, the elements will need to be small enough to model the increasing stress within a distance of 'as' from the corner. A curve fit to determine a more accurate 'as' value is then used to determine the SCF that is compared with the parabolic or linear extrapolation method.

If a nominal stress is required, the stresses need to be calculated at a distance of at least 2as from the corner. A much coarser mesh should be satisfactory. Clearly care is required if effects, other than the corner, are causing the stress to vary in this region.

If the details of the stress field in the vicinity of the singularity are required, then a more detailed mesh will be required:

The limiting mesh size value is defined as convenience, and then comparing refined-mesh study is needed to determine the peak stresses (shown in Figure 4.1).

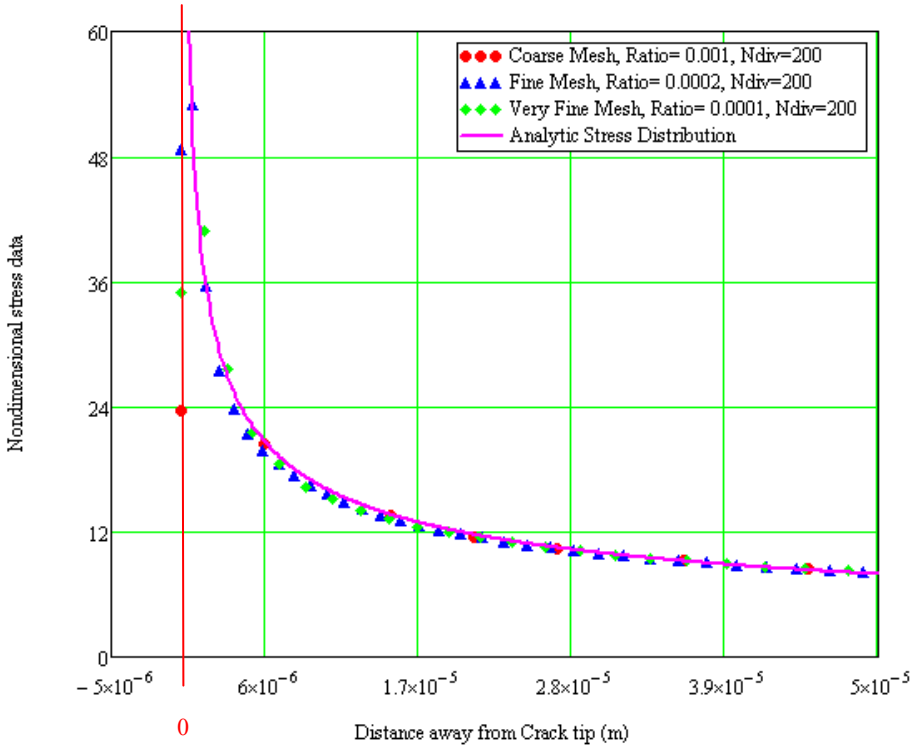

Figure 4.1 Infinite stress distribution on the vertical path with constant thickness of plate (t=10 mm) away from the corner

(Stress singularity happened at 0-line; the results under different finite element meshes are very mesh except for the ones away a short distance from the singularity.)

Clearly, from the figures, the stress distribution has a dramatic stress raiser with the fine mesh density. This diagram needs to be plotted on a horizontal axis of x/as and the mesh sizes given in terms of element size/as. Then we can justify the recommendation for minimum element size = as/10.

It was observed that the stress values found from the FE analysis are highly related to the mesh density within a distance of about as/3 from the crack tip, especially in the case of the flange geometry, while the stresses outside as/3 are far less affected by the density of mesh. At least 10 4-noded elements are required to properly resolve the SN approach, the singularity will depend on the estimation of the power value and 'as' value. (Except for the area near the crack tip, the work was based on the 4 noded FE formulations, having approximate constant stress. If the 8 nodes elements had been used, they could have modelled and had approximately linearly varying stress. This would allow a coarse mesh for the same accuracy.)

The imposition of the equilibrium conditions in the context of elementary mechanics with the self-equilibrating stress distribution need to be eliminated in the stress fitting calculations.

The limitation of element size from the corner is accepted as $as/10$ that will plot the stress raise correctly, and avoid the slow convergence of the Length Scale prediction. Fortunately, with the performance of modern computers, the required fine meshes can be realized easily.

4.2 FEA in Fracture Mechanics Calculations

In this section, numerical values of the stress intensity factors are compared to the analytical solutions.

Based on an extensive parametric study (by Saouma and Schwemmer, 1984) the following recommendations were obtained for the use of the singular quarter point elements (See Appendix C.4 Singular Element in LEFM) in general fracture mechanics calculation, where the applied stress field is uniform.

1. Use 2×2 (reduced) integration scheme;

2. Use at high order singular elements around a crack tip;

3. Have the internal angles of all the singular elements around the crack tip approximately equal to 45 degrees or less;

4. Unless an excessively small element side length to overall crack length ratio l / a ratio is used, little improvement is achieved by using transition elements;

5. For problems with uniform non-singular stress distribution, little improvement is achieved by using small l / a ;

6. For problems where a non-singular, stress gradient is expected, l / a should be less than 0.5.

4.2.1 Selection of Element Type

For the calculation of stress raisers the mesh density and the element type are important. For the 2D elements, the mesh insensitivity has been confirmed in my method. It is also noted that, for 3D problems neglects the influence of element side shear forces. For 3D situation, the stress evaluation area is strongly affected by FE modelling, so whether mesh insensitivity remains questionable of them. The theoretical comparisons between shell and solid element have been given in Appendix C.2 Solid and Shell Elements Considerations.

The first series of FE results used in ANSYS are the 8-node solid element (Solid45), the model can describe the real geometry properly; the stress contour plots are shown in Figure 4.2. Furthermore, the solid element can be simplified to 4-noded shell element (Shell63).

This shell element (Shell63) can work as a multi-layer elements; the shell element can calculate and display every layer simultaneously. However in these calculations it is assumed that the crack behaviour is determined by the mid-layer stress values. This assumption would clearly be poor if there was a significant bending stress relative to the membrane stresses.

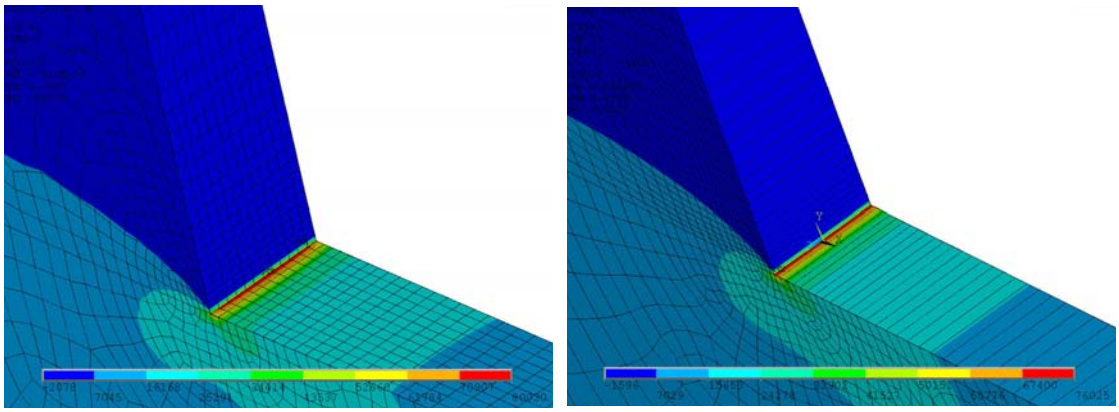

Figure 4.2 Stress distribution plots at the corner location by

a) Solid 45 elements and b) Shell 63 elements

Due to the symmetry of the cruciform plate, only a quarter sector of plate is modelled (L=0.3, H=0.6; a=1.0, b=1.0), the diagram is selected from the cruciform model shown in Figure 3.2, showing the local stress distributions at the corner. Mesh refinement is applied at the corner location. The results from 3D elements have been compared with 2D elements, and the fine mesh density results are compared with the coarser mesh results.

A comparison of non-dimensional x-component in the mid-plane stresses (stress on the mid-plane of the plate), σ_x / σ_0, computed by the solid model and by 2D finite elements model plotting in Figure 4.3.

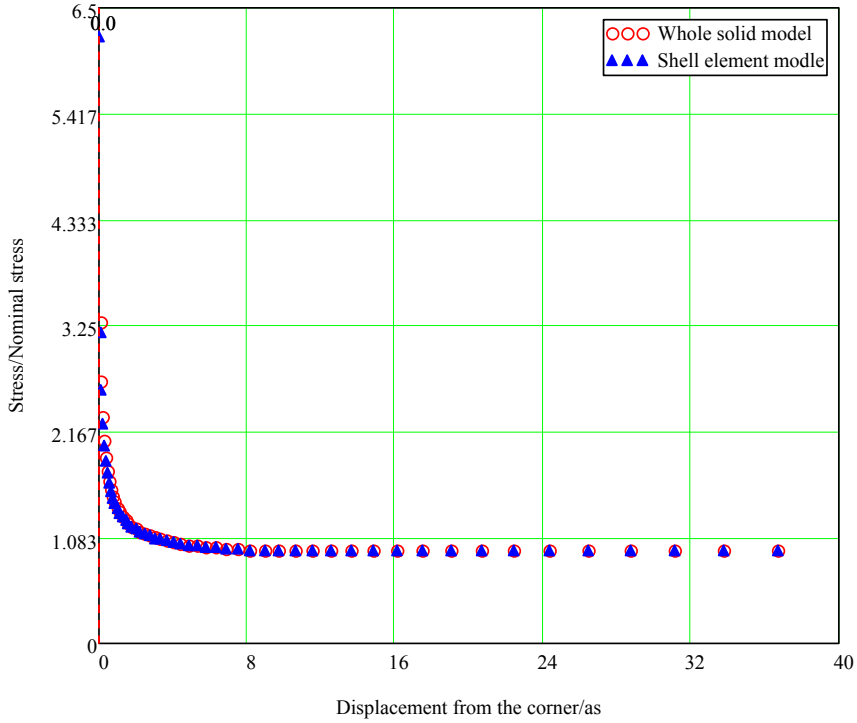

Figure 4.3 Stress distribution values along crack growth path

The nominal points along vertical path fit each other very well using both 2D and 3D elements, the peak stresses are more clearly marked (the effect can be explained with the fact the contribution of membrane stresses to the total peak stress varies with the angular imperfection).

According to the discussions above, cracks usually start from a plate edge, then it is unnecessary (and the calculation cost is higher) to model ship structure plates by solid elements which can include the bending effect. This is because the thickness is small compared with the other two dimensions. However for some details where cracks grow through the through-thickness direction then solid elements would allow better modelling, especially when cracks are also to be modelled because the crack tip plate element in ANSYS cannot determine the stress intensity factor in bending.

4.2.2 Sub-modelling

To conveniently allow different crack sizes to be analyzed, sub-modelling is often used. On the boundary of the sub and main model the coarse mesh and the sub-model should have identical mode patterns. (No need to revise and reanalyze the entire FE model.) Mesh refinement band modification can be strictly local shown in following in Figure 4.4.

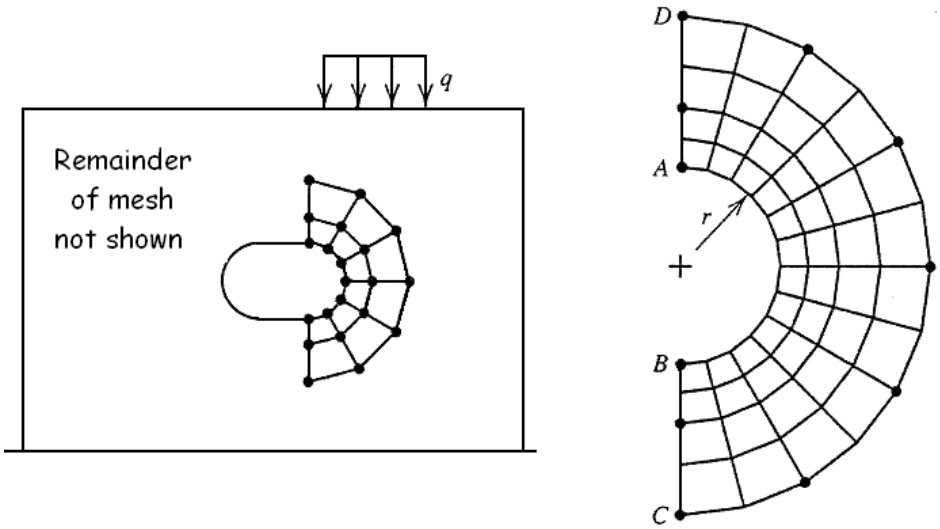

Figure 4.4 Portion of *FEA* in a coarse-mesh model and fine mesh sub-model

Robert D. Cook (P137)

4.2.3 Crack Path determination

Various techniques have been developed with finite element analysis to solve the crack propagation problem. If the crack path is known prior to the analysis then the crack can be modelled at various sizes. If the crack path is to be calculated this requires an analysis, starting from the smallest crack, at each stage estimating the preferential direction of cracking, extending the crack in the defined direction, calculating K value by repeating the process. One of the best methods for estimating the preferential crack propagation direction is to map the discontinuous near-tip field of curved cracks.

4.2.4 Crack Modelling in ANSYS

Methods of performing FEA for fracture mechanics in ANSYS, including the J-integral method are compared with known solutions for an edge crack, as shown in Figure 4.5.

The FE models are built with (for steel) a very high tensile steel material, which has a Young's modulus of $210GPa$, Poisson's ratio of 0.30 and yield strength of $670MPa$.

The geometry is the same as the analytical model of handbook (Tada, H., Paris, P.C. and Irwin, G.R, 2000); the length L of specimen geometry model is 2000mm, the height H is 1000mm; and the edge crack is assumed perpendicular to the loading direction, having crack length ratio from 0.05 of the plate height through to the half height of plate. The thickness of the steel plate specimen is 10 mm. Plane stress conditions are applied.

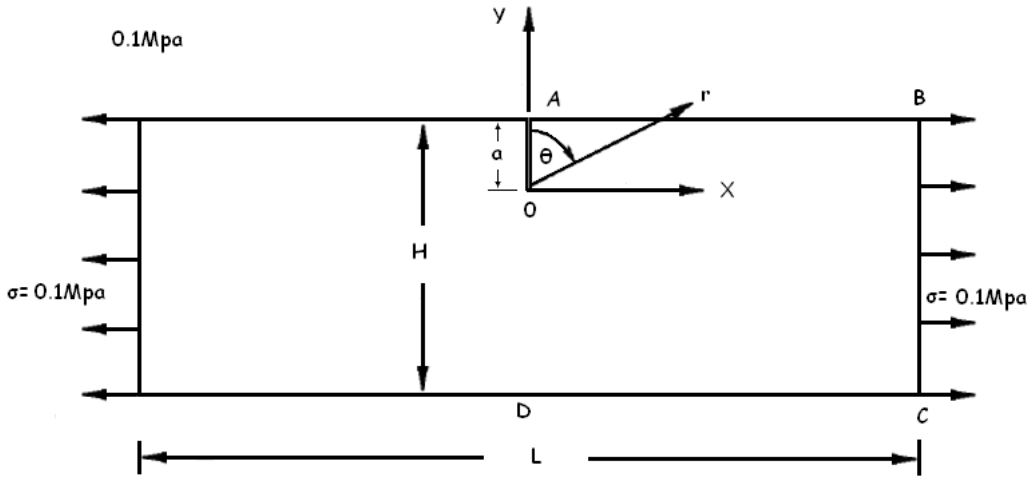

Figure 4.5 Single edge crack originating through 10 mm thickness plate

In general, the relationship between crack-tip element size and accuracy is complicated and depends primarily on the crack-tip mesh. The convergence behaviour is studied by reducing the size of the crack tip elements as shown in Figure 4.6.

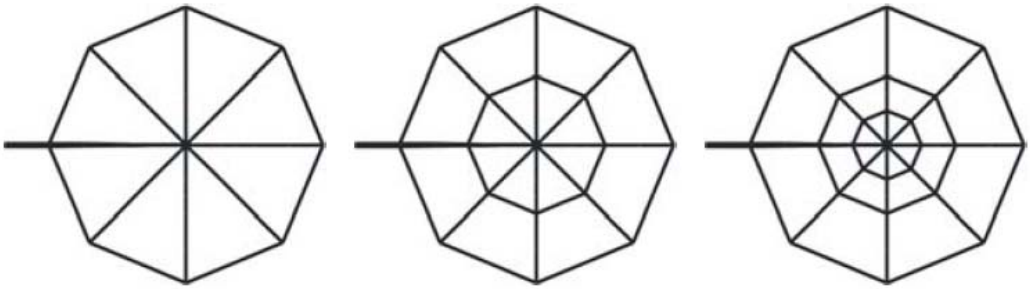

Figure 4.6 Illustration of the pattern of mesh refinement around crack tip

The in-built technology for the crack definition places elements around the "key-point" of the crack tip and creates transition zones between the crack tip and the surrounding plate area.

The geometry building surrounds the arc-shaped mesh transition zone by a hexagon, which is useful for the J-integral integration path selection. Finally the global specimen FE model is simulated and connects to the crack area shown in Figure 4.7.

Figure 4.7 Specific geometric global model of the edge cracked tension plate

A critical issue that must be addressed in 2D FE fracture mechanics analysis is that of mesh generation. Software implemented in conjunction with ANSYS is presented, for topology and meshing in relation to crack (in Appendix C.6 Fracture FE Case Study).

In the geometry of a single edge crack, it is possible to utilize standard mesh generation tools to produce a crack tip surrounded by the required singular elements. Around the node at the crack tip a circular area is meshed by a designated number of triangular singular elements with quarter nodes. The mid-node element meshing model generation (using 8 nodes Shell93) can be created automatically by the programs; and stress intensity factor calculation just becomes an input-output process, although the process is a little time-consuming. The plate area was meshed using ordinary 4-node isoparametric elements except for the vicinity of the crack tip with series of singular elements shown in Figure 4.7. Parabolic isoparametric shell elements were used, the models containing up to 8000 elements at the crack front.

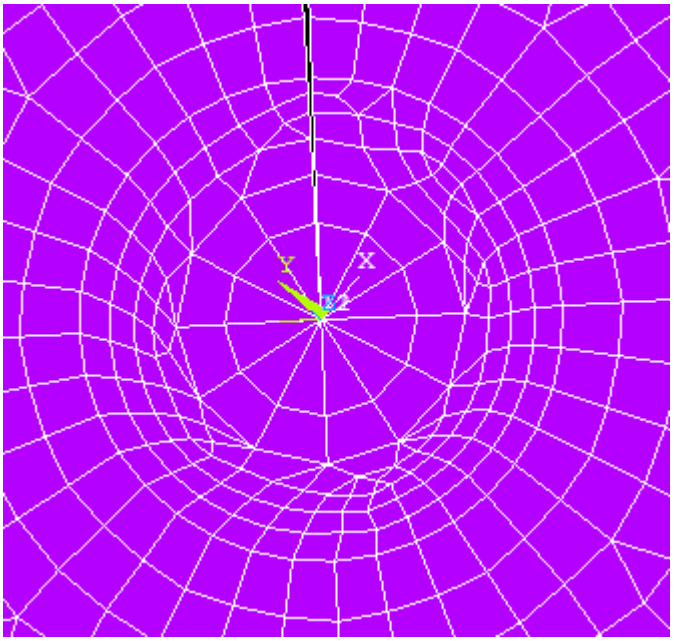

Figure 4.8 Plate *FE* model meshed by ordinary and singular elements

In Figure 4.9, it is an enlarged view of the singular elements showing that triangular elements are placed in a radial manner and that the size of the second row of elements equals half the radius of the first, crack tip, row of elements.

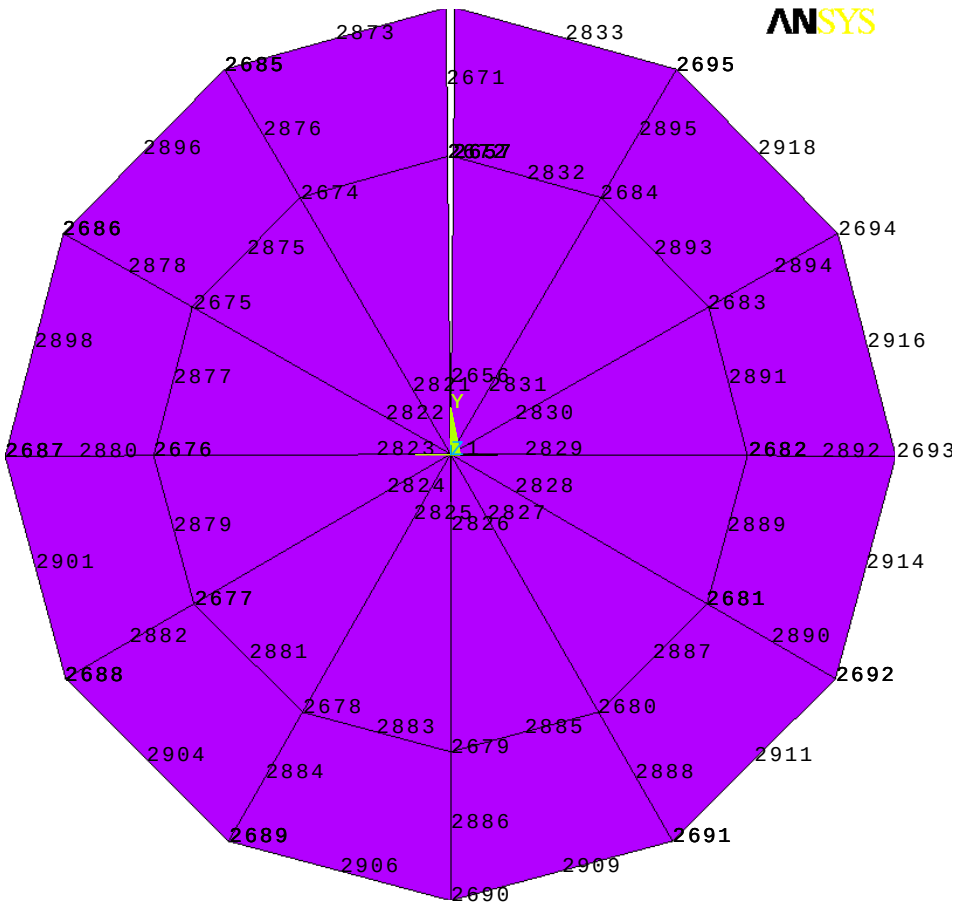

Figure 4.9 Enlarged view of the triangle singular elements (with quarter point nodes) at the crack tip

The results are presented as a function of the ratio of the crack-tip element size along the crack length. The K values can be calculated from the crack surface deformation. Alternatively the FE-calculated J value can be used, together with a relationship of K-J. The calculated stress intensity factors compared favourably with theoretical solutions published in the literature (PC. Paris and GC. Sih, 1965) in Table 4.1.

Stress intensity factors, considering step increases in crack length, have been calculated using FEA. The single edge crack model is investigated according to FEM with a refined mesh in ANSYS using shell elements (SHELL93) and solid elements (SOLID95) of ANSYS.

The non-dimensional geometry (Y) factors for KI are obtained by FE and published analytical solutions. A very good correspondence is found between the

analytical solutions and the numerical points.

$$Y = K_I / \sigma\sqrt{\pi a} \qquad 4.1$$

The theoretical and numerical SIF estimates are compared in Table 4.1.

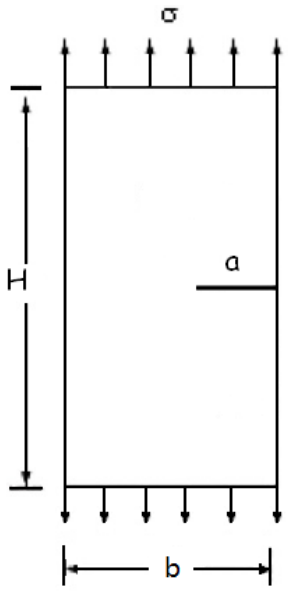

Table 4.1

Y value of single edge crack strip plate of width w

	Bowie	Gross	Numerical results (2D)	
a/b	Strip with edge crack		KI	J-integral
0.05	1.15	1.14	1.137	1.185
0.1	1.20	1.19	1.186	1.237
0.15	1.29	1.29	1.263	1.316
0.2	1.37	1.37	1.366	1.424
0.25	1.51	1.50	1.498	1.561
0.3	1.68	1.66	1.662	1.733
0.35	1.89	1.87	1.867	1.947
0.4	2.14	2.12	2.121	2.213
0.45	2.46	2.44	2.441	2.547
0.5	2.86	2.82	2.849	2.972

The KI estimates are consistently closer to the analytical solutions than those derived from the J-integral values.

The trend for different crack lengths is shown in Figure 4.10.

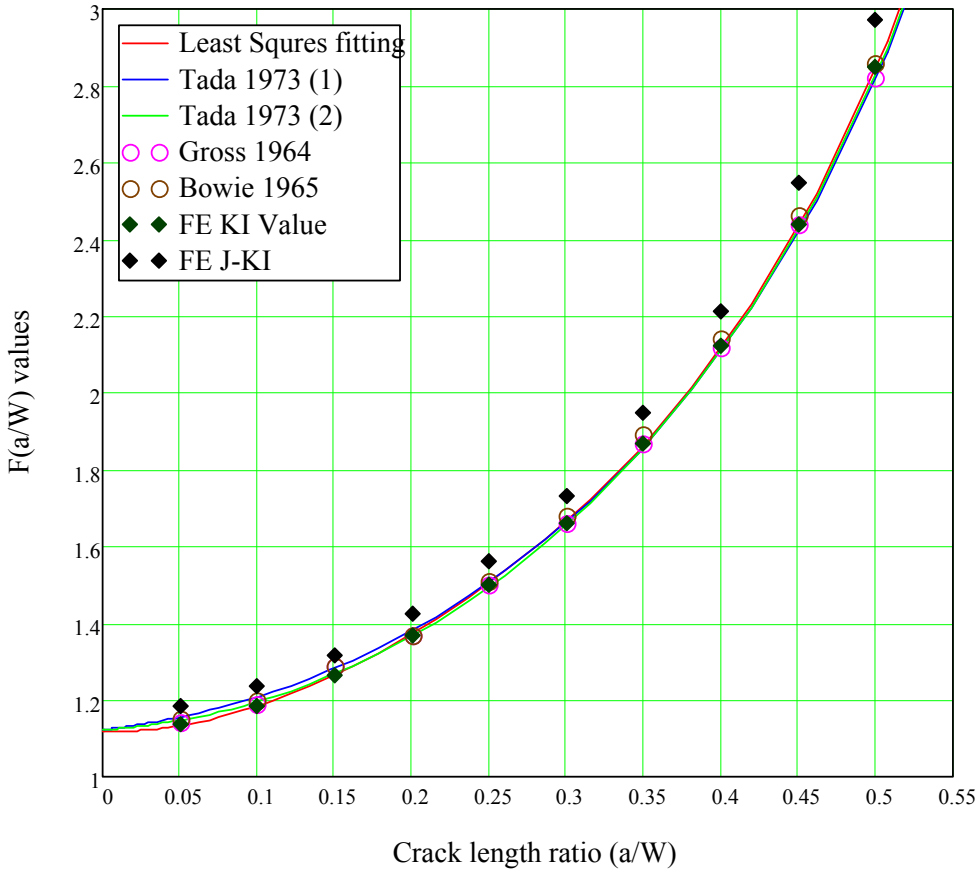

Figure 4.10 SIF factors comparison between the existing approaches (this is the data from Table 4.1)

It is seen from the figure that FE calculation can match the analytical points quite well; with a maximum error 6%. This simple modelling should precede more complex models.

4.3 FEM Applications in Ship Engineering

Stress concentrations are usually calculated by linear or quadratic extrapolation from predefined extrapolation points on the plate surface. These usually depend on the plate thickness and have been developed by research institutes and classification societies. The final fatigue life assessment is performed using Woehler SN curves.

This section compares different methods from different rules.

The numerical results were obtained using ANSYS. The unit system was defined consistently as length—m, time-s, mass-kg, force-N and stress-Pa. Complete columns of the element size, element type and the results are provided. The ship component analysed is shown in Figure 4.11. 2D elements (Shell63) were used. Around the structural connections the mesh had a very fine density.

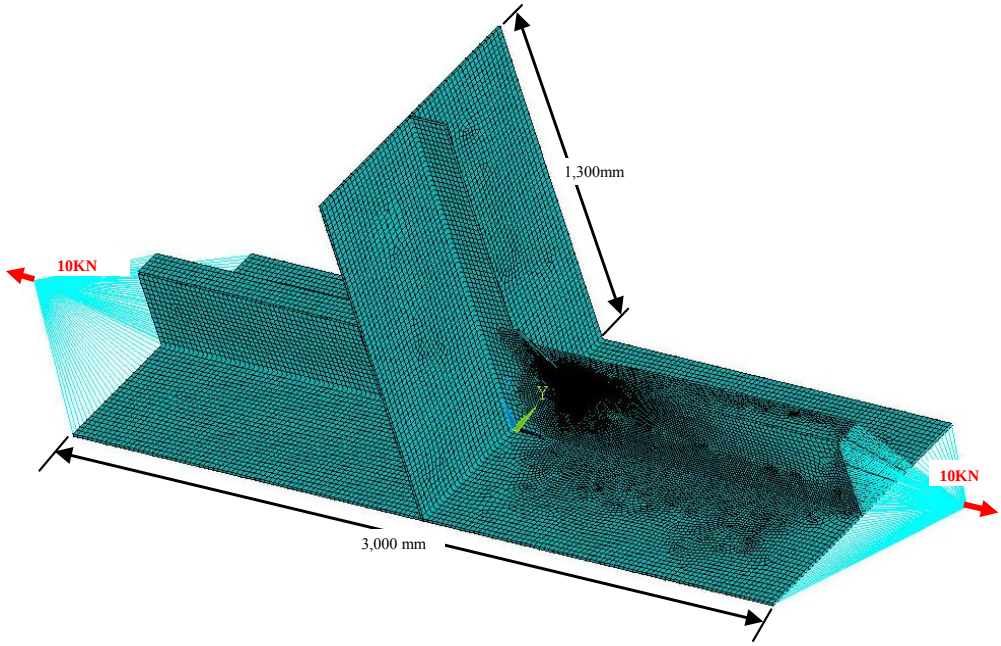

Figure 4.11 Principal fine mesh model of the ship components

Preceding finite element analyses have shown that large stresses occur around the corners.

The recommendations by classifications societies (LR, ABS, BV/RINA, GL, KR and NK were compared in a comparative study, W. Fricke, W. Cui, etc, 2002). The predicted lives varied considerably; between 1.8 and 20.7 years, as shown in Table 4.2. This is clearly unsatisfactory.

4.4 Conclusions

In this Chapter, FE analysis is used to calculate KI values for an edge crack and the results are found to agree, to within less than 6% difference with analytical solutions:

- Singular stress field
- Nominal stresses
- SCFs
- Stress intensity (K) values

The use of the Length Scale, when selecting mesh size or locations for taking stresses from the analysis, is discussed.

SCFs calculated by different organizations and using different rules are compared and found to differ very considerably. Results from the Length Scale method were also compared with these results and showed in Chapter 6.

REFERENCES

1. P.C. Paris and G.C. Sih, in: Stress Analysis of Cracks, ASTM STP 381 (1965) 30-83
2. Saouma, V. and Schwemmer, D., Numerical evaluation of the quarter point singular element, International Journal of Numerical Methods in Engineering 20, 1629–1641
3. Tada, H., Paris, P.C. and Irwin, G.R. The Stress Analysis of Cracks Handbook,

2nd edition, Paris Productions and Del Research Group, 2000, Missouri

4. W. Fricke, W. Cui, etc. Comparative fatigue strength assessment of a structural detail in a containership using various approaches of classification societies, Marine Structures, Volume 15, Issue 1, January 2002, Pages 1-13.

Table 4.2

Results comparison of the comparative study from classifications

Rules and guidelines	Types of stress approach	Elem. type	Size long./transv./vert.	Ref. points (t)	SCF (hot spot/weld)	Fatigue life (yr)
ABS[a]	Nominal	Solid 20-nodes	$30\times30\times30mm^3$	0.5/1.5	-/-	8.9
	Hot spot				1.736/-	7.0
BV/RINA[b]	Notch	Solid 8-nodes	$30\times30\times10mm^3$	0.5/1.5	1.63/1.84	6.0
DNV[c]	Notch				1.47/1.5	20.6
GL[d]	Nominal	Solid 20-nodes	$30\times30\times30mm^3$	0.5/1.5	-/-	13.4
	Hot spot				1.9/-	20.7
KR[e]	Hot spot	Solid 8-nodes	$30\times30\times30mm^3$	0.5/1.5	1.66/-	6.5
LR[f]	Hot spot	Shell	$30\times30mm^2$	0.5	1.81	12.0
NK[g]	Hot spot	Solid 8-nodes	$30\times30\times15mm^3$	0.5/1.5	2.15/-	1.8
RS[h]	Hot spot	Solid 20-nodes	$30\times30\times7.5mm^3$	0.5/1.5	1.80/-	15.2

a **ABS**. Guide for dynamic based design and evaluation of container carrier structures. A simplified method for fatigue strength assessment. *American Bureau of Shipping*, Houston, 1999.

b **BV**. Rules for the classification of steel ships. *NR466A JAP R00 E*, Bureau Veritas, Paris, 1999.

c **DNV**. Fatigue assessment of ship structures, *Det Norske Veritas Class Notes* No.30. 7, 1999.

d **GL**. Rules for classification, IFship technology, Part 1, seagoing ships, Hull Structures, *Germanischer Lloyd, Hamburg*, 1998 [Chapter 1]

e **KR**. Guidance relating to rules for classification of steel ships.Annex 7-8 Guidance for the fatigue assessment of ship structures. *Korean Register of Shipping*, 1998

f **LR**. Ship Right FDA level 3 procedures manual, technical planning and development department. *Lloyd's register of Shipping*, 1998

g **NK**. Guidance for fatigue design of ship structures. *Nippon Kaiji Kyokai*, 1995

h **Boitsov GV** et al. New norms of ship hull strength realized by software system 'RUSLAN'. *Transactions of Russian Register of Shipping*, 22nd ed., RS, St. Petersburg, 1999.

Table 4.3

FE calculated SIF with different crack length

a/w	0.1	0.2	0.3	0.4	0.5	0.6	0.7	0.8	0.9	1.0
SIF	4517.05	6668.25	8853.20	10856.76	13290.03	16111.41	19603.81	23759.14	29004.20	35334.50
2D J	9.7E-05	2.12E-04	3.60E-04	5.63E-04	8.45E-04	1.25E-03	1.84E-03	2.72E-03	4.05E-03	6.12E-03
2D J KI	4695.07	6930.25	9033.23	11288.58	13834.68	16822.20	20414.24	24801.48	30276.25	37233.25
Error (%)	3.94%	3.93%	2.03%	3.98%	4.10%	4.41%	4.13%	4.39%	4.39%	5.37%
3D J	9.84E-05	2.15E-04	3.72E-04	5.76E-04	8.48E-04	1.27E-03	1.86E-03	2.74E-03	4.11E-03	6.15E-03
3D J KI	4718.76	6976.70	9181.88	11414.55	13851.39	16979.21	20540.05	24896.15	30497.77	37325.75
Error (%)	4.47%	4.63%	3.71%	5.14%	4.22%	5.39%	4.78%	4.79%	5.15%	5.64%

CHAPTER 5
FRACTURE MECHANICS
IN FATIGUE ASSESSMENT

5.1 Introduction

This chapter considers the usage of the Length Scale confirmed in Chapter 3 and 4 in Linear Elastic Fracture Mechanics. This section aims to find a simple expression for K, applying to cruciform plate directly, extend to realistic components.

The fracture mechanics concept is applicable to the assessment of crack imperfections, and the simplicity and clearness of the theory are in contrast to the difficulty of application for many practical details.

Fracture mechanics usually consider the elastic stress intensity factor and energy release rate, or non-linear CTOD and J-integral. In crack propagation analysis: LEFM is the usually applied.

Fatigue analyses carried out by LEFM requires the Stress Intensity Factor calculations. Then the fatigue crack growth rate can be calculated using Paris' Law: Eqn. 5.1:

$$\frac{da}{dN} = C_0 \cdot (\Delta K)^m \qquad 5.1$$

The Paris equation initiated widespread research activities. However, both in

this form and with modifications (e.g. including explicit power law dependence on parameters), Paris Law has served the engineering design community well.

5.2 SIF Calculation

The calculation of SIF is needed and it can be obtained by using finite element (FE) analysis, unfortunately numerical simulation is too complex for quick prediction of the likely behaviour and too time-consuming for the repeated analysis that would be required for reliability analysis of a complete ship.

There are other methods for stress intensity factor, such as analytical methods (Westergaard method, and complex functions method), Numerical method (Green's function (H.G. Maschke, 1985), weight function (Bueckner H, 1987), boundary collocation, integral method, continuous dislocations, or experimental methods (photoelasticity, holography and caustics). All these methods are also difficult or time-consuming to apply to realistic structures.

5.2.1 SIF Comparative Calculations for Different Crack Sizes

The crack is assumed to start at the sharp corner and then to propagate along the direction perpendicular to the loads (the former assumption is clearly good, the latter assumption involves some approximation as the true crack path is likely to be curved).

Numerical results for a cruciform geometry are obtained from the FE program ANSYS; the results are plotting in Figure 5.1. In the figure, the x-axis values are the crack length ratio of height of the cruciform flange and the y-axis values are the non-dimensional mode of SIF values ($K/\sigma\sqrt{\pi a}$). As one check on the results two kinds of elements (shell and plate element) are used for the KI calculation; however, there are no distinguishing differences, as shown in Figure 5.1.

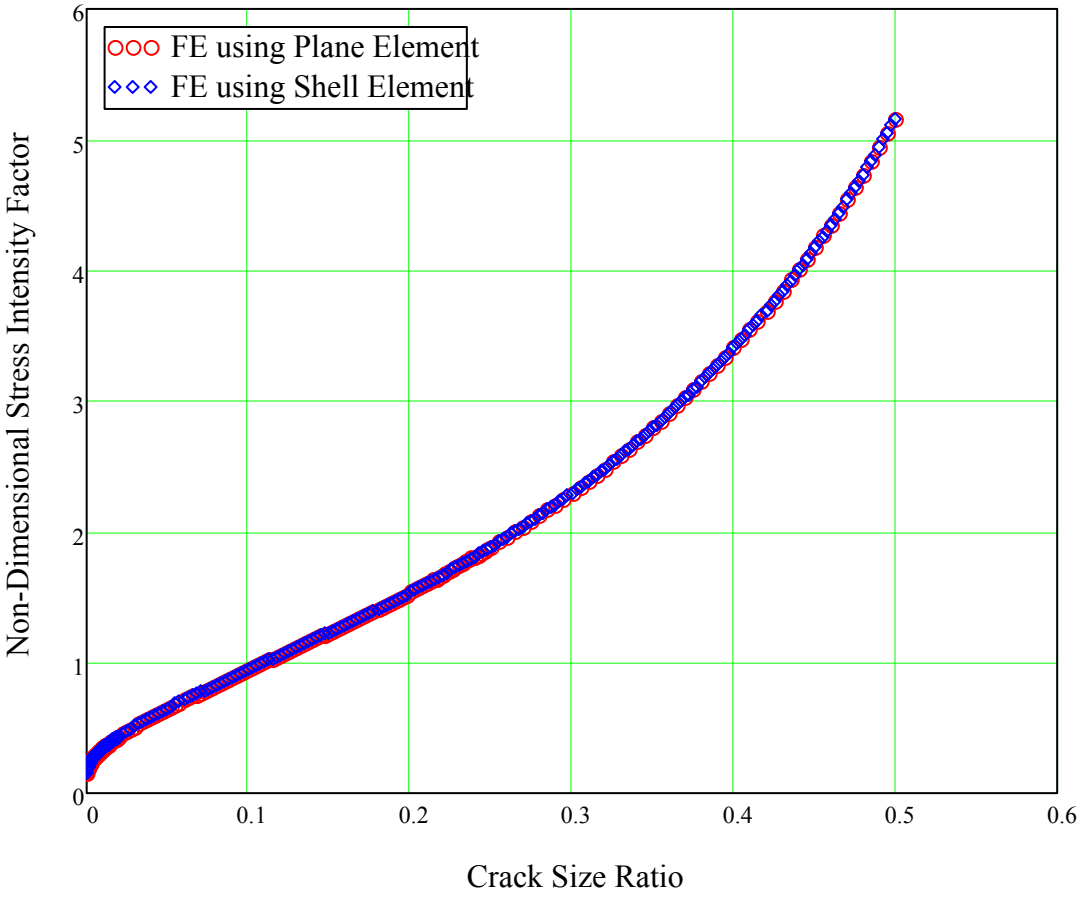

Figure 5.1 Non-Dimensional FE KI results along the crack growth path

It is possible to predict this behaviour using the equations for the stress singularity (as developed in Chapter 3) in conjunction with weight functions of crack in the cruciform plate. This weight function could be calculated using FEA but that would not be very helpful when, as discussed above, there is an advantage from avoiding FEA.

5.2.2 Use of Different Weight Functions for Estimating the Corner SIF

Firstly, the confirmation of corner weight function was checked by different weight functions results and FEA results in Figure 5.2. The use of the weight function for an edge crack in a semi-infinite plate gave the best approximate results. (More detailed background to the weight functions used is given in Appendix B.1 Weight Function Method.

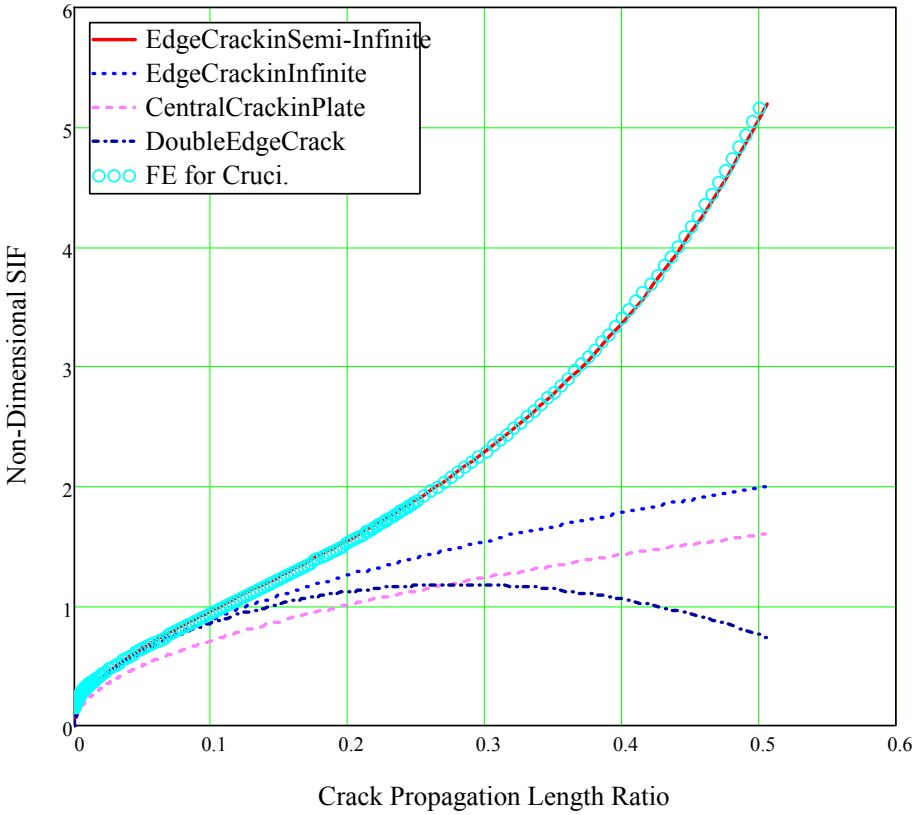

Figure 5.2 Comparisons of various weight function curves

non-dimensional SIF is $K/\sigma\sqrt{\pi a}$

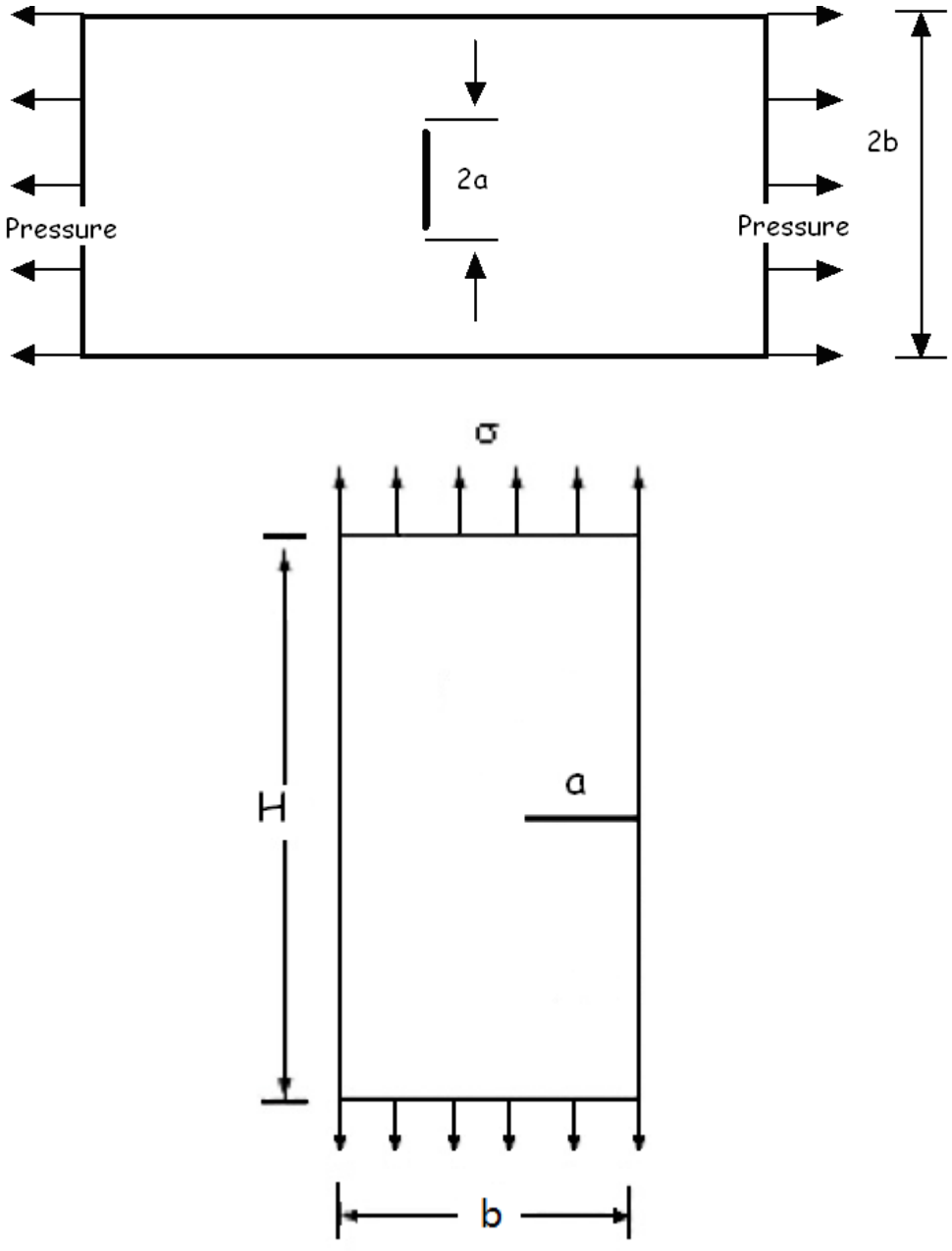

Figure 5.3 a) Plate dimensions with center crack; b) plate dimensions with edge crack

It has been shown that the weight function of semi-infinite plate can be used for a single edge crack, in conjunction with the singular stress field of un-cracked plate, to predict the single edge crack in the cruciform; the trend of the results fit very well and the error between the analytical curve and the numerical points is less than 0.1%

within the crack length ratio range 0.1~0.5.

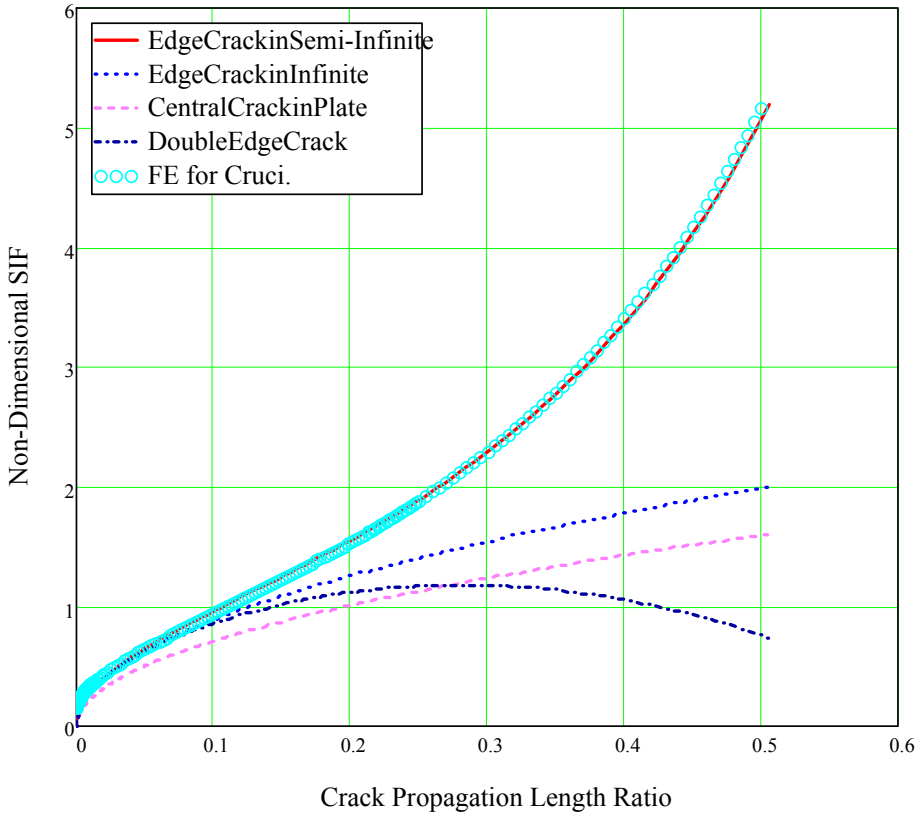

Figure 5.4 KI comparisons of cruciform plate in the allowance crack stage

The results, in Figure 5.4, calculated by using the analytical functions within the range of crack sizes, around 0.05 - 0.2, however for short cracks (shown in more detail in Figure 5.5), the difference between the values based on the stress distributions for weight functions and finite element results differ considerably.

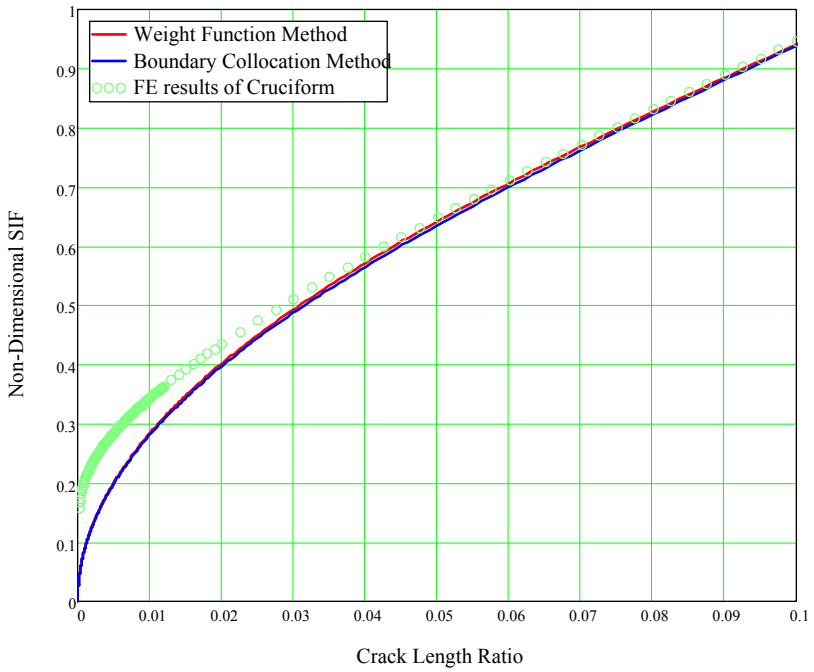

Figure 5.5 KI comparisons of cruciform shape during the short crack stage

The shape in the Figure 5.4 and Figure 5.5 is interesting, with the rapid increase of SIF for small crack sizes and for large crack sizes. The rapid increase of large crack size relate to the crack growing through a large proportion. It will be shown that the rapid increase at small crack size is related to

- the effect of the corner singularity; and
- the corner being a weaker singularity than that of the crack

5.2.3 SIF Corrections for Early Crack Extensions

In the results comparisons of FEA (see Chapter 4) and the additional crack size

analysis are compared. It is apparent that the except for the smallest cracks the additional crack size method provides a good fit to the finite element results.

For small (though not the smallest) cracks, an additional crack size can also be defined to represent the effect of the singularity. As the crack becomes smaller, the additional crack size 'ae' constitutes an increasing fraction of the effective overall crack length. Conversely as the crack propagates into the interior of the specimen the effect of 'ae' reduces.

$$K = F(a)\sigma_0\sqrt{\pi(a+ae)} \qquad 5.2$$

As an alternative to use the weight function, the geometry factor can be added to the crack size. A similar concept has been applied to fatigue crack growth thresholds. (The relationship or links between the fatigue limit and threshold SIF was proposed by Kitagawa and Takahashi (1976) using Kitagawa diagram. For the concept of threshold stress intensity factor, it is often used with damage tolerant design, which defines a loading criterion under which the cracks will not grow significantly (Lawson L, Chen EY, Meshii M, 1999).

By investigating plastic threshold effects, El Haddad (1980) proposed the use of an additional crack size 'l_0' in Eqn. 5.3.

$$K = F(a)\sigma_0\sqrt{\pi(a+l_0)} \qquad 5.3$$

It is shown differences between FE results and WF and BC methods existing, the reason can explained as the structural shape differences: FEA is applied on the cruciform plate and the WF and BC methods are different. It is obvious that the differences are found at the initial length outside of the large crack length.

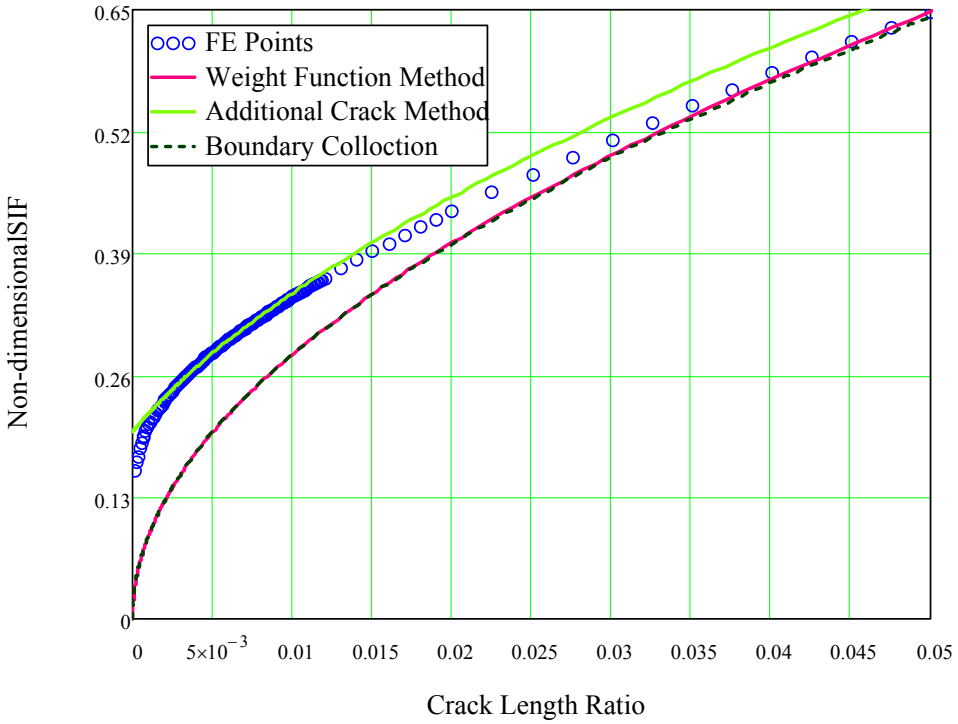

Figure 5.6 Fatigue crack SIF comparisons at threshold crack length

It is found empirically that for right angled corners 'ae' is approximately equal to as in Eqn. 5.4, which has shown to be reasonable in Section 6.4.

$$ae = as \qquad 5.4$$

In order to check the application of the empirical expression, it is useful to research the behaviour of different crack size of as ranges. The additional crack size method works particularly well for crack sizes greater than as (or than the distance to a significant change in thickness).

5.2.4 Small cracks in corners

Because a corner singularity is weaker than crack singularity (e.g. $1/r^{0.455}$ for a 90^o corner, $1/r^{0.5}$ for a crack, the stress intensity factor for a crack in a corner starts at 0, for no crack but increased rapidly; so the Mode I solution for very short stage can be approximated from the power index expressions shown in Eqn. 5.5

$$K = \sigma_0 \cdot (C_1 \cdot a / b)^{C_2} \qquad 5.5$$

a is the crack length on the cruciform

b describe the geometry characterics, can be considered as the Length Scale 'as'

Suitable fitted values are given in Eqn. 5.6

$$C_1 = 0.765, \text{ and } C_2 = 0.225 \qquad 5.6$$

To calculate the stress intensity factor the small crack formula can be used for a < as, which also includes results from Eqn.5.6.

The fit is shown in Figure 5.7; a better fit with Eqn. 5.6, and a relation to the previously calculated as value can be obtained by including an additional term:

$$K = 1.1\sigma_0 \cdot \sqrt{\pi \left[C_1 \cdot \left(\frac{a}{as} \right)^{C_2} + C_3 \cdot \frac{a}{as} \right]} \qquad 5.7$$

$$C_1 = 1.24, \text{ and } C_2 = 0.075, \text{ C}_3 = 0.94 \qquad 5.8$$

Note the constant of 1.1 could be combined with C1 and C2 but it is convenient to keep it separate as it relates to an edge crack.

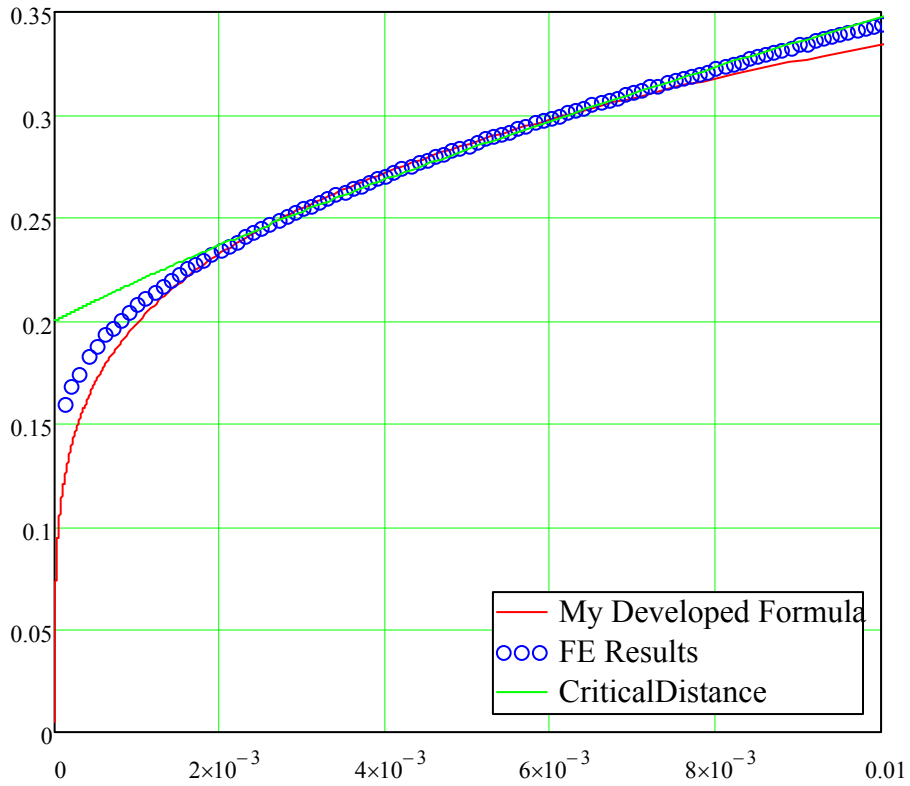

Figure 5.7 Illustration of approximation power index formula with the FE results

For larger cracks approaching a plate edge, the K value depends on the crack length, a, to the plate width, b, as shown in Eqn. 5.8.

$$K_I = \begin{cases} K_I = 1.1\sigma_0 \cdot \sqrt{\pi \left[C_1 \cdot \left(\frac{a}{as} \right)^{C_2} + C_3 \cdot \frac{a}{as} \right]} & \text{for } a \le as \\ 1.1\sigma_0 \sqrt{\pi (a + ae)} & \text{for a > as, } a/b \le 0.1 \\ WF \text{ or } BCM & \text{for } 0.1 < a/b \le 1.0 \end{cases} \qquad 5.9$$

For the middle range ‘ae’ is approximately equal to ‘as’ and a constant Y value of 1.1 fits finite element analysis results quite well.

5.3 Cracks approaching an edge

Several attempts have been made to find the general analytical form for edge crack model. Bowie (1964) and Gross (1967) treated the single edge crack using Williams' eigenfunction representation of the Airy stress function.

Author of this thesis developed a further equation by modified the geometry function of Tada's (1985), which also accounts for the effect of a nearby singularity with power factor 'p' shown in Eqn. 5.10.

$$F(a/b)=\left\{\frac{\pi(b/2)}{a}\cdot[\tan(1.325\frac{a}{b/2}) -0.65\sin(1.40(\frac{a}{b/2})-0.16(\frac{a}{b/2})^{2})]\right\}^{0.455} \quad 5.10$$

A number of empirical formulas dealing with edge or central crack problems are given for any a/b are given in Appendix B.2 Boundary Collocation Function, and the classical results shown in Table 5.1.

Table 5.1

Correction factors of single edge crack plate

a/b	F(a/b) by Gross, 1967	F(a/b) by Bowie, 1964	F(a/b) Eqn5.10
0.05	1.14	1.15	1.153
0.1	1.19	1.20	1.204
0.15	1.29	1.29	1.276
0.2	1.37	1.37	1.371
0.25	1.50	1.51	1.488
0.3	1.66	1.68	1.632
0.35	1.87	1.89	1.813
0.4	2.12	2.14	2.048
0.45	2.44	2.46	2.381
0.5	2.82	2.86	2.926

In their works (Bowie1964 and Gross1967), they found the collocation was required to obtain convergence; the correction factors are given in Figure 5.8 curves show good agreement with each other. The excellent agreement is obvious, especially, the classical solution is determined comparing with my empirical formula of Eqn. 5.9.

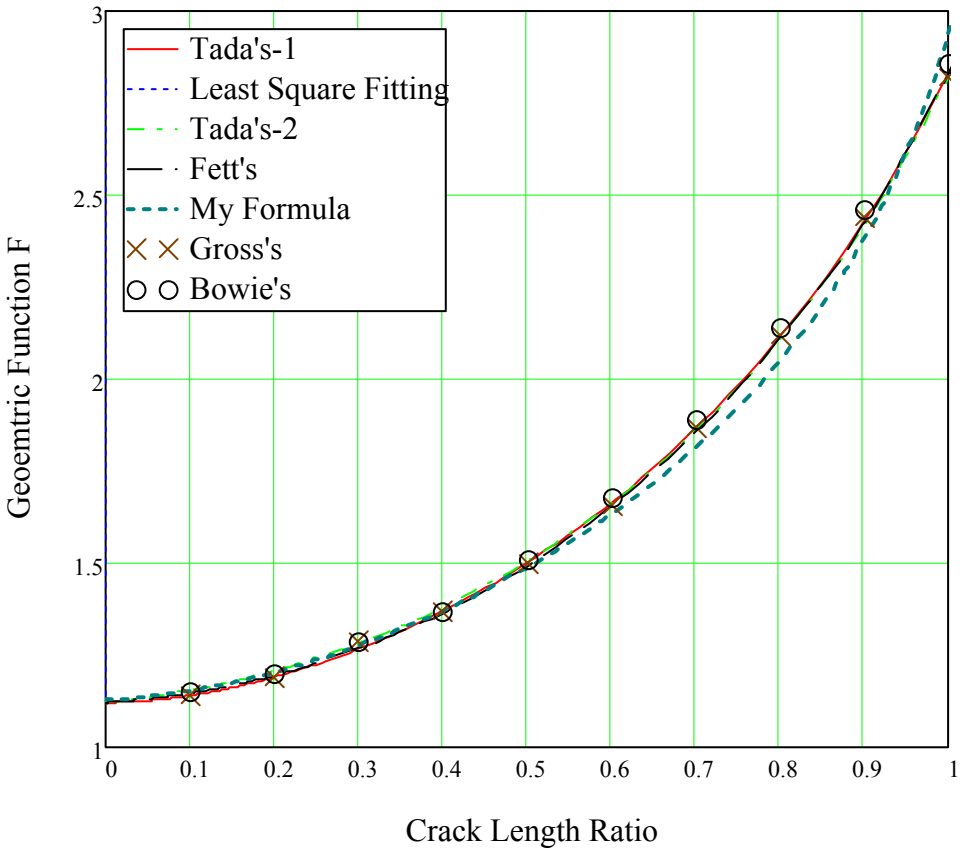

Figure 5.8 Values by *BCM* of single edge crack of strip specimen

5.4 SCF Assessments from LEFM

Cruciform is accepted as typical model analyzed by FEA with edge crack propagating from sharp corner, midline symmetry on single side.

The resulting K values were fitted equations of the form:

$$K = F(as) \cdot \Delta\sigma_0 \cdot \sqrt{\pi(a + ae)} \qquad 5.11$$

The SCF prediction methodology, from the LFEM results, is illustrated in the method of a crack propagating from a likely initial size (0.25mm) to a size corresponding to design failure of the component.

Several definitions are possible for the final crack depth. 25 mm seemed reasonable, representing the thickness of the ship hull plates applied in practice. This final crack size is referred as a_f and the initial crack size as a0 in Eqn. 5.11.

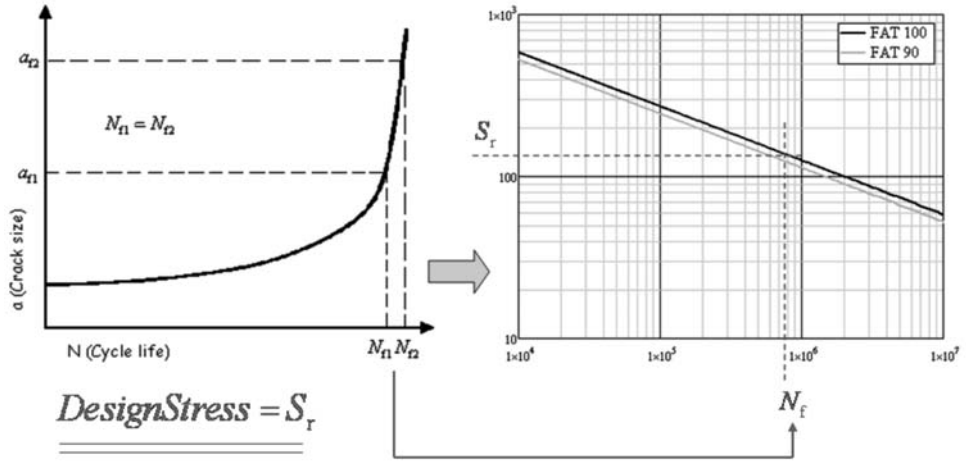

Figure 5.9 Typical fatigue design stress concerning crack growth approach (-2 standard deviation SN curves)

The crack propagation can be simulated with LEFM adopting the Paris law in5.12.

$$dN = \frac{da}{C_0 \cdot (\Delta K)^m} \qquad 5.12$$

Where

$$dN = \frac{da}{C_0 \cdot (F(as) \cdot \Delta\sigma_0 \cdot \sqrt{\pi(a+ae)})^m} \quad 5.13$$

$$dN = \frac{(\pi(a+ae))^{-\frac{m}{2}} \cdot da}{C_0 \cdot (F(as) \cdot \Delta\sigma_0)^m} \quad 5.14$$

$$N = \int_{a_0}^{a_f} \frac{(\pi(a+ae))^{-\frac{m}{2}} \cdot da}{C_0 \cdot (F(as) \cdot \Delta\sigma_0)^m} = \frac{(-2\pi(a_f+ae))^{-\frac{1}{2}} - (-2\pi(a_0+ae))^{-\frac{1}{2}}}{C_0 \cdot (\Delta\sigma_0)^m} \int_{a_0}^{a_f} \frac{da}{F(as)} \quad 5.15$$

The crack growth constants, C_0 and m, were mean or -2 standard deviation values taken from BS7910 (2005) and the SN curves are mean or -2 standard deviation curves from BS 7608 (1993). A single slope SN curve and the simplified constant crack growth coefficients were selected

The decisions taken regarding these issues are based on the two basic data presented: crack propagation calculation and the SN curve transitions, and then the subsequent crack growth is modelled by a 2D stress situation with an edge crack using LEFM based on British guidance.

The SCF (appropriate for a given S-N curve class, typically D or E is given either by:

$$\frac{\text{The stress from the Class D or E (-2 standard deviation SN curves)}}{\text{The nominal stress for the fracture mechanics calculation}}$$

or by the ratio of cycles to failure at the same stress:

$$N_D = C_D \cdot S_{\text{nominal}}^{-\text{m}}$$
$$SCF_{\text{Design}} = \sqrt[m]{N_D / N} \quad 5.16$$

The new methodology provides a simplified way of estimating SCFs or K values for fracture mechanics calculation. In particular we can determine SCF values

directly from the geometry by estimating the scale factor from a function based on these results (Eqn. 5.16).

$$SCF = Function(as) \tag{5.17}$$

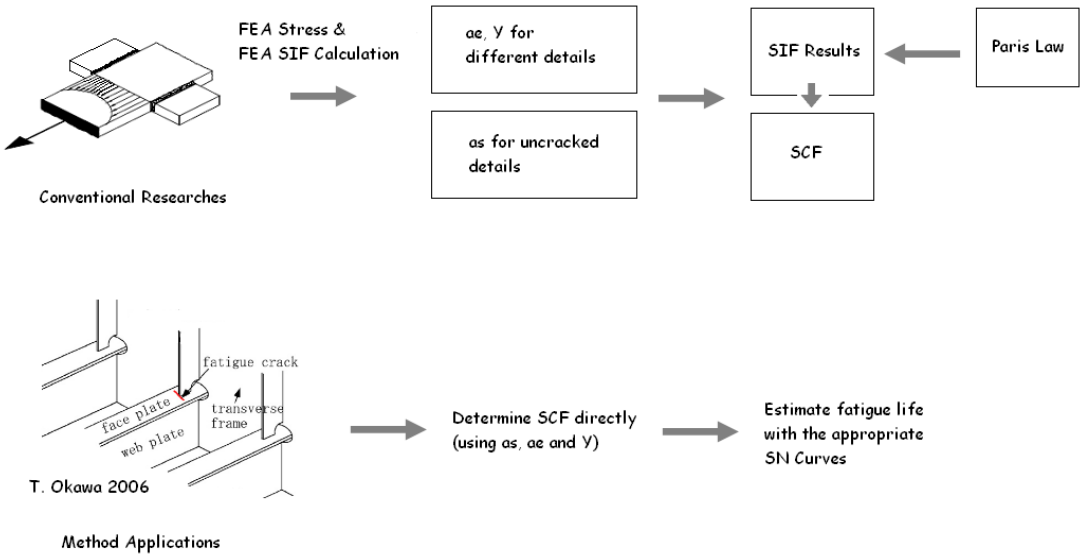

Figure 5.10 Length Scale approach for assessing the stress concentration factor of pointed engineering structural component

We can also fit a curve get SCF against as value by LFEM, conveniently shown in Figure 5.11.

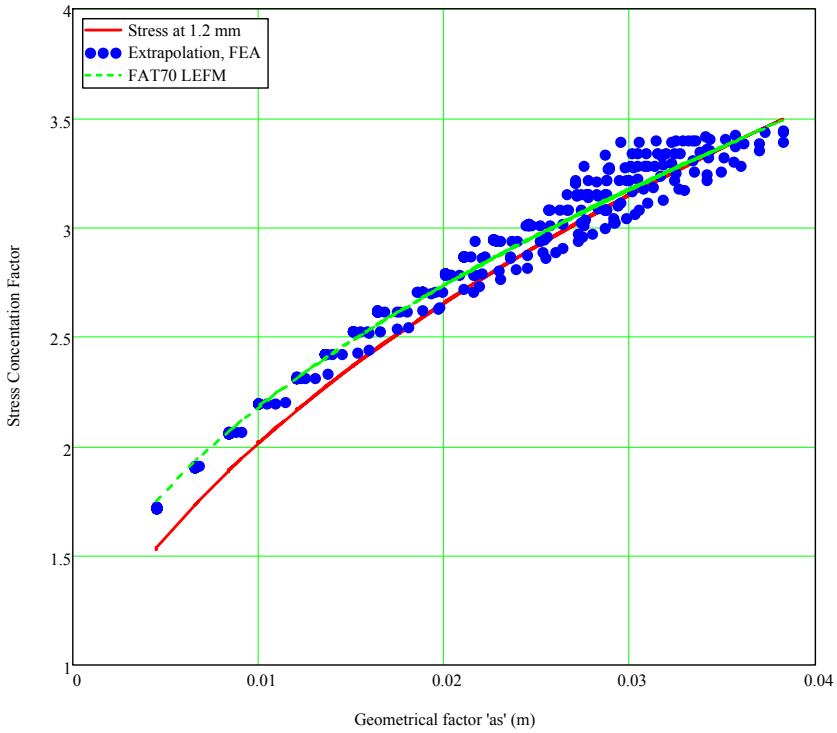

Figure 5.11 Comparison of *SCF* according to different approaches

5.5 Conclusions

The method presented here provides an effective direct or screening method for solving general fatigue problems, may justify more careful consideration.

Understanding the nature of the stress field as categorized by 'as' will also help the FE analyst set up a better model because they can estimate location from the corner that is significantly influenced by the right angled corner singularity:

- Stresses are about 10% greater than the nominal value at a distance of as.
- Stresses are about twice the nominal value at a distance of as/10.

The results also demonstrate the shortcomings of conventional extrapolation techniques used for determining SCFs from FE analyses that are often based on extrapolation from specified multiples of the plate thickness. This is clearly wrong but the IIW (2007) provide a more logical extrapolation rule and BS7608 is being

updated (with input studies used within this work helping to justify the new extrapolation rule).

REFERENCES

1. A. Hobbacher, editor. Recommendations for fatigue design of welded joints and components. IIW Doc XIII-2151r1-07/XV-1254r1-07. Int Inst Welding; 2007
2. B. Gross, J.E Srawley and W.F Brown Jr., Stress-intensity factors for a single-edge-notch tension specimen by boundary collocation of a stress function, NASA Tech. Note, No. Nasa TN D-2395 (1964)
3. H. Bueckner, Weight functions and fundamental fields for the penny-shaped and the half-plane crack in three-space. Int. J. Solids Structure Vol 23, 57-93 1987
4. H.G. Maschke, Anwendung der Randintegralmethode auf ebene RiBprobleme in F3111en beliebiger elastiseher Anisotropie, Technische Mechanik 6 (3), 17-24 (1985)
5. Kitagawa H, Takahashi S. Applicability of fracture mechanics to very small cracks or the cracks in the early stage. In: Proceedings of the Second International Conference on Mechanical Behavior of Materials. Metals Park, OH: ASM; 1976. p. 627–31.
6. Lawson L, Chen EY, Meshii M. Near-threshold fatigue: a review. Int J Fatigue 1999;21:15–34.
7. O.L. Bowie, Rectangular tensile sheet with symmetric edge cracks, J. Appl. Mech. 31 (1964), pp. 208–212

CHAPTER 6

LENGTH SCALE 'as' VERIFICATION

6.1 Introduction

The Length Scale concept has been developed to provide:

- a simple method of roughly assessing the stress patterns and hence the fatigue life in structural details containing sharp corners with, theoretically, infinite stress;
- guidance, on the stress patterns to expect, when setting up a finite element analysis;
- estimates of stress intensity factor : SIF or K for fracture mechanics calculations

It is generally acknowledged that the fatigue strengths failing from the 'weak' locations can decrease with increase in plate thickness (Gurney TR, 1979). Some works (Maddox SJ, 1987, 1995) showed that there was an affect of the overall sizes of the components.

This section considers how the length scale varies with different geometry and provides some background to the analyses used to develop the approximate form of Length Scale.

6.2 Approximate Length Scale

The approximate 'as' formula, derived in Chapter 3 for the simple cruciform specimen having constant thickness plate, serves as a very valuable estimator for the Length Scale:

$$a_s = smallest\ of \quad (L/22, \quad H/3) \tag{3.12}$$

6.2.1 Bracket/attachment plate influences

FEA was performed to determine the influence of the attachment geometry; the lengths (L, H) of the attachment were changed from 0.05m to 0.95m, the dimensions of the main plate (a, b) are both fixed at 2.0 m, the equivalent thickness of the plate is accepted as 10 mm.

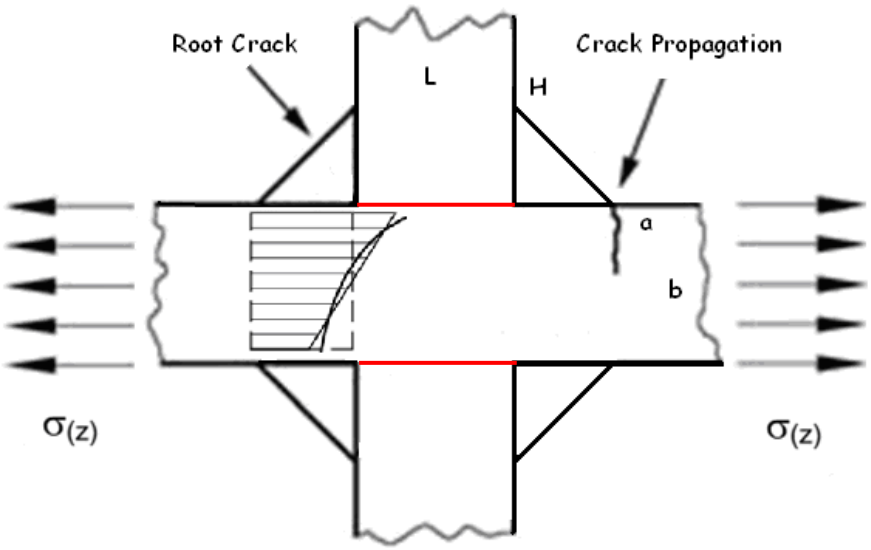

Figure 6.1 Cruciform diagram of the connection section

Finite element analysis is employed for the stress calculation on the perpendicular loading direction. If the width of the flange is fixed as constant (L=0.1m, 0.3m, 0.5m, 0.7m, 0.9m), the stress values are plotted with different height values shown in Figure 6.2:

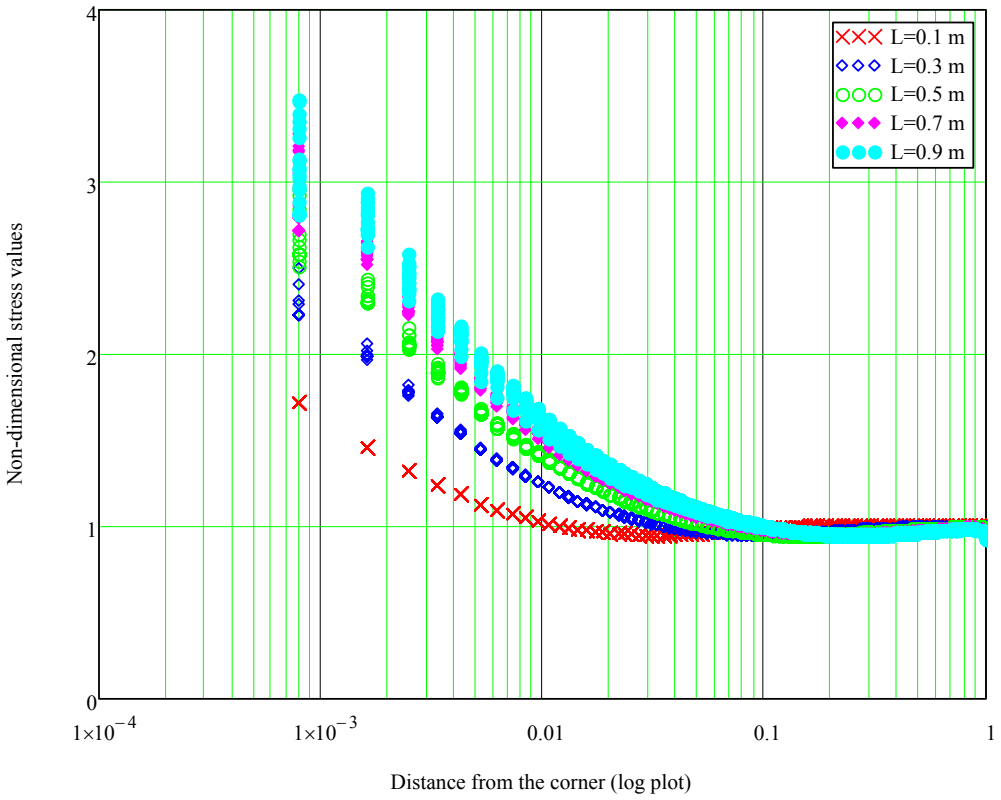

Figure 6.2 Stress distribution plots

Each colour represents the effect of changing H from 0.05 to 0.95 for the noted length of cruciform *L*. The higher curves correspond to the higher values of H (Changing H values and a=2.0m, b=2.0m, t=10mm)

From the points plotting in Figure 6.2, the curves for different heights convergence to same stress curve line, even the width of attachment is very short. If the length of the attachment is increased, then the height of the attachment becomes important. Note that these results are for the same range of H for each L. If the range of H/L had been kept constant then there would have been some variation of stress with H, even for the smaller L values.

If the length of the attachment is varied with constant height of flange (H=0.5m, 0.9m), the stresses increase with the length of the attachment shown in Figure 6.3.

It can be seen the influence of the geometry is such that usually the length of the attachment will affect the stress singularity more than the height of the attachment.

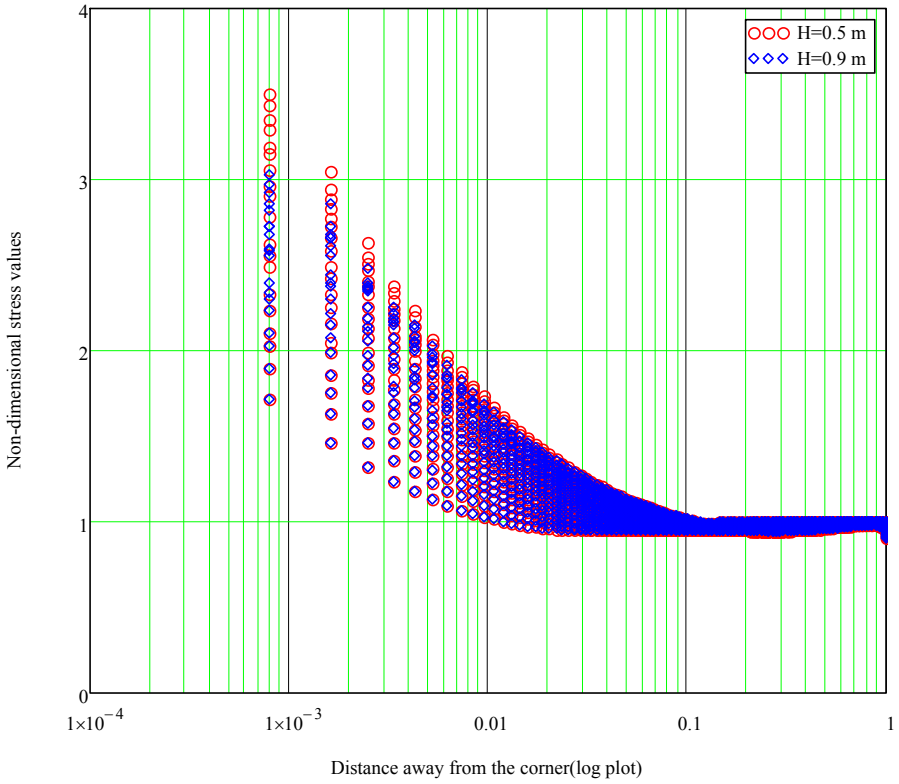

Figure 6.3 Stress distribution plots of constant height H of cruciform
The higher curves at each H correspond to longer L
(Changing L from 0.05 to 0.95, a=2.0m, b=2.0m, t=0.01m)

Each stress distribution can be fitted to equation 3.12. It can be done by using MATHCAD and the function 'genfit'. Examples of fit calculation are shown in following figures.

The resulting Length Scales are plotted out as a contour surface in Figure 6.4. The reason for the lack of smoothness for large H and L is not clear, it may be caused by a poorer mesh used for these analyses, and it may be caused by the finite width or

length of the cruciform.

Most of this surface shows the relationship between as and the length L of the bracket. The fold downwards on the left side represents the area where the height H of the attachment is dominating the as value**.** The approximate formula is shown in Figure 6.4

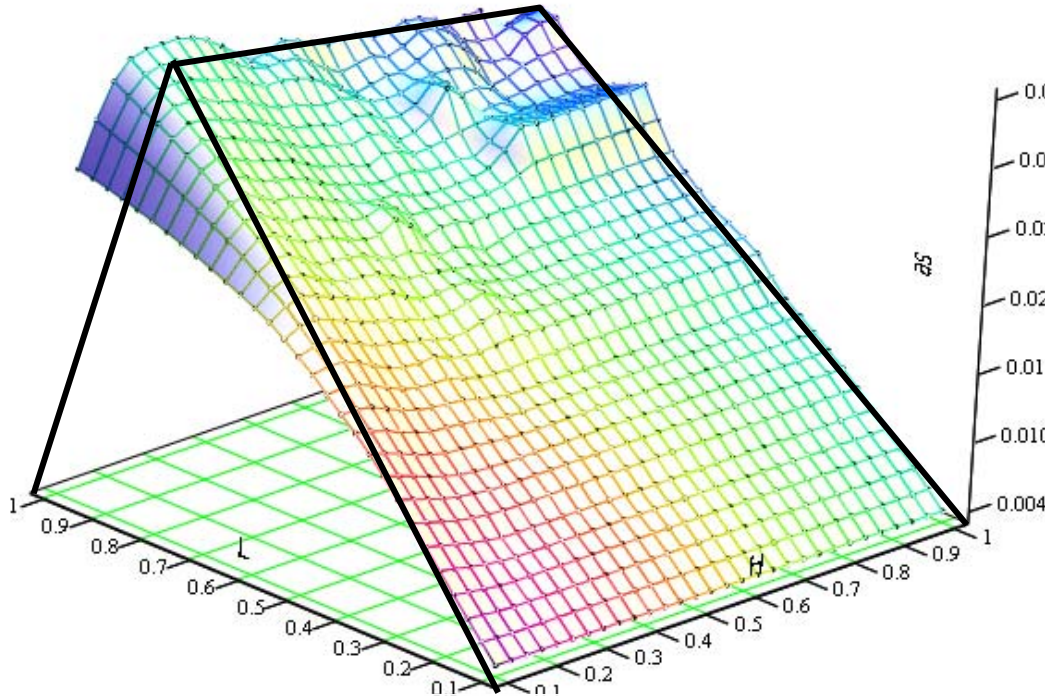

Figure 6.4 'as' changing with the *L* and *H* for cruciform component

The solid black lines represent the surface defined by the approximate formula of Eqn. 3.12

Sections through the surface are shown in Figure 6.5 and Figure 6. 6.

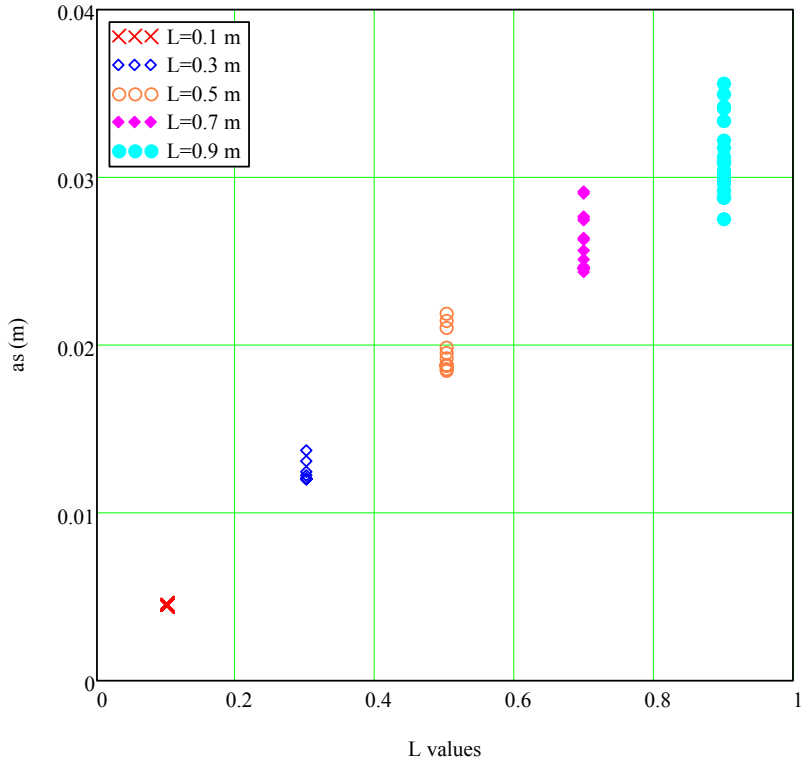

Figure 6.5 Sections through Figure 6.3 for constant H

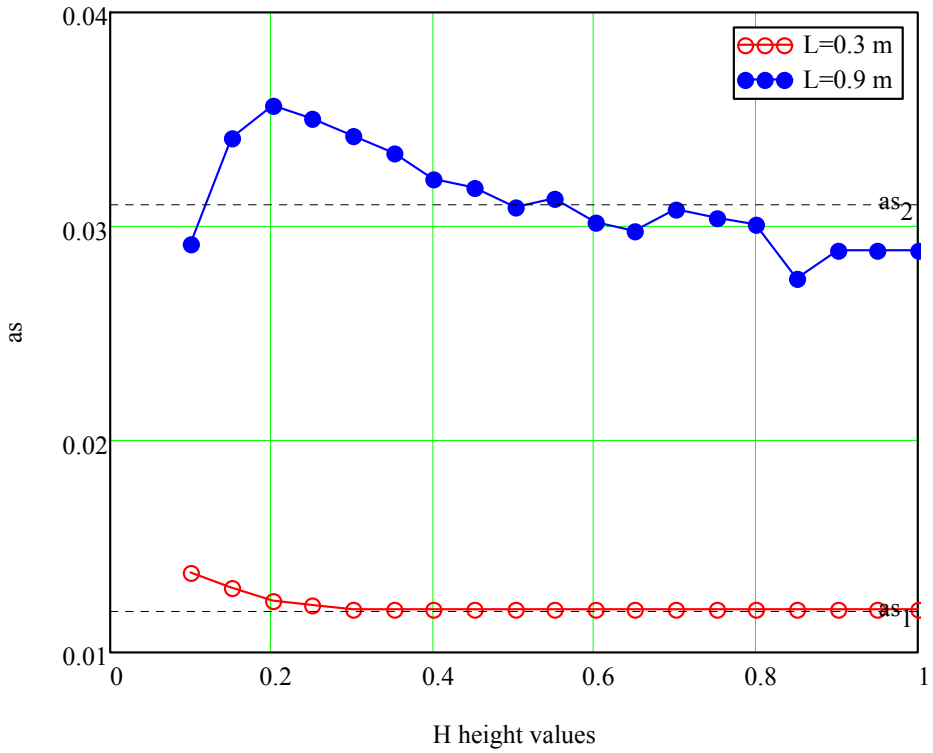

Figure 6.6 Sections through Figure 6.3 for constant L

By analyzing a large number of cruciform types, Figure 6.7 and Figure 6.8 represent a summary of the typical Length Scale as results graphically. It is again evident in Figure 6.7, that the 'as' values are only dependent on H values, for the larger lengths L.

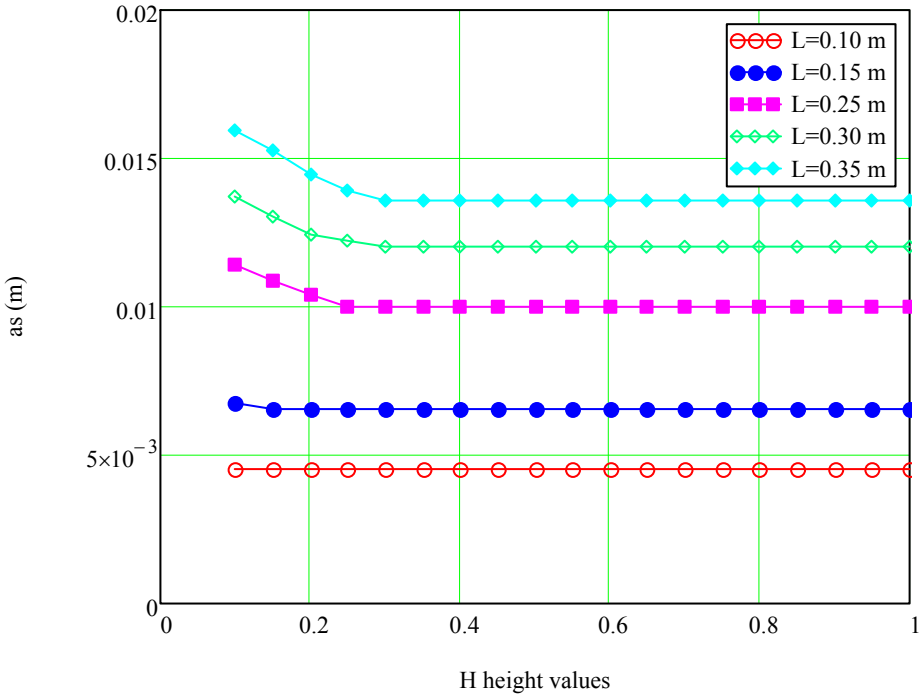

Figure 6.7 The effect of short width *L* influence on the '*as*' value

For the higher height and Length values, the numeric 'as' results are as shown in Figure 6.8, which again shows the irregular shapes.

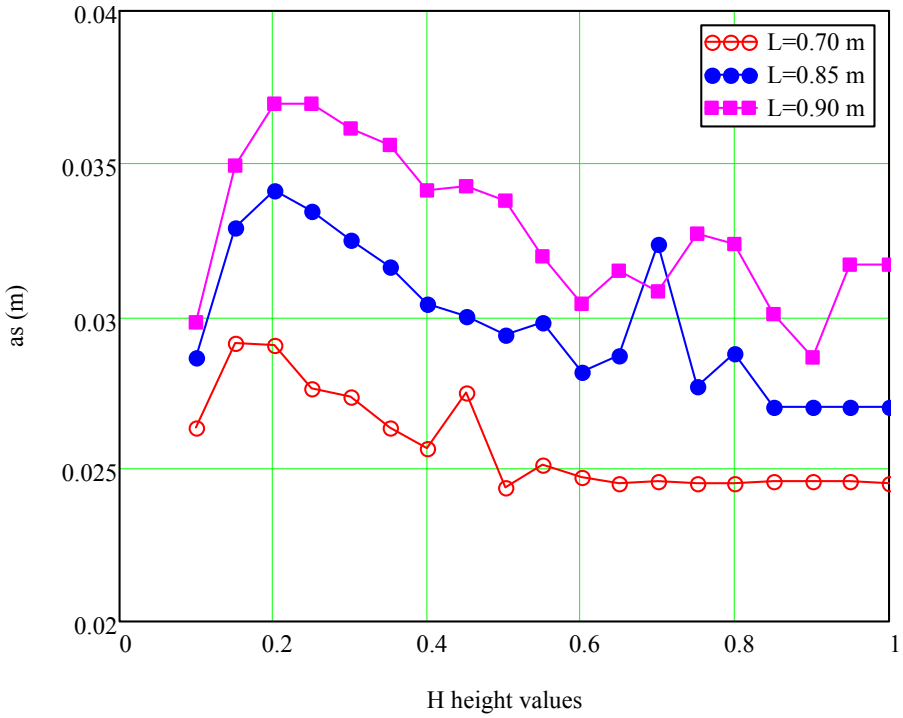

Figure 6.8 The effect of longer width *L* influence on the '*as*' value

6.2.2 Basic plate influences

According to the simplistic idea of the length scale for geometrically similar shaped details the length scale should change in proportion to the size of the detail. If the attachment dimensions are kept constant, while the main plate changes may have insignificant effect on the 'as' value

To check this the main plate size (a, b) is increased in steps (2×2m, 4×4m, 6×6m, 8×8m, 10×10m) but the same range of the attachment sizes are used.

The resulting 'as' values are shown in Figure 6.9, these suggests that there is a small effect of the main plate size, except where the attachment size become similar to the plate size (for the case of smaller a, b and larger L)

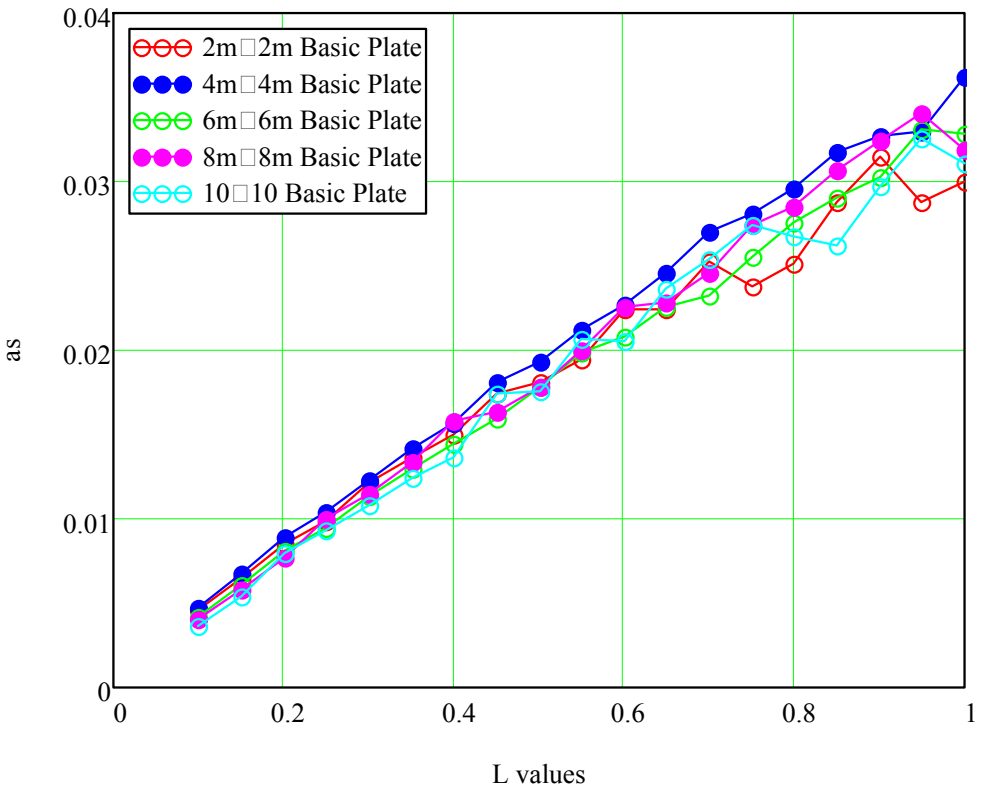

Figure 6.9 'as' results of assumed large main plates

Figure 6.10 shows the SCF values that are derived from the as values. Again there is little effect of the size of the base plate.

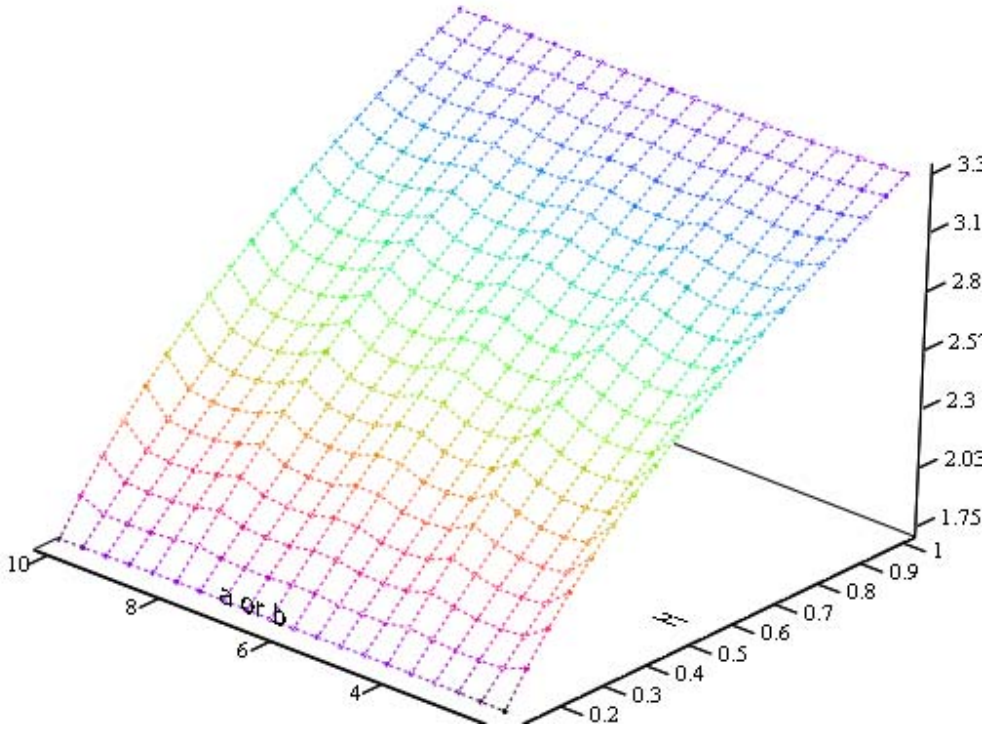

Figure 6.10 SCF changing with the cruciform geometries (H, a or b)

The results show that the stress raiser rarely depends on the geometry of main plate, and for most cases it will be the geometry of the attachment that is important. Note that the 'as' formula can be applied to real component evaluations, this will be the subject of later sections.

6.3 Comparison of the length scale formula and stress distributions at the corner of a Cruciform Shape

To check the quality of the fit, the stress distribution from FEA is compared with a stress distribution estimated from Eqn. 3.6 with the singularity power p taken as the theoretical value 0.455 and the as value the lesser of H/3 and L/22.

$$\sigma(x) = \frac{\sigma_0 (as + x)}{\left[\left(2^{\left(\frac{1}{2p}\right)} \cdot x \cdot as^{\left(\frac{1}{p}-1\right)} \right)^q + x^{\left(\frac{q}{p}\right)} \right]^{\frac{p}{q}}} \qquad 3.6$$

Results for L varying from 0.2m to 0.9m are shown in Figure 6.11.

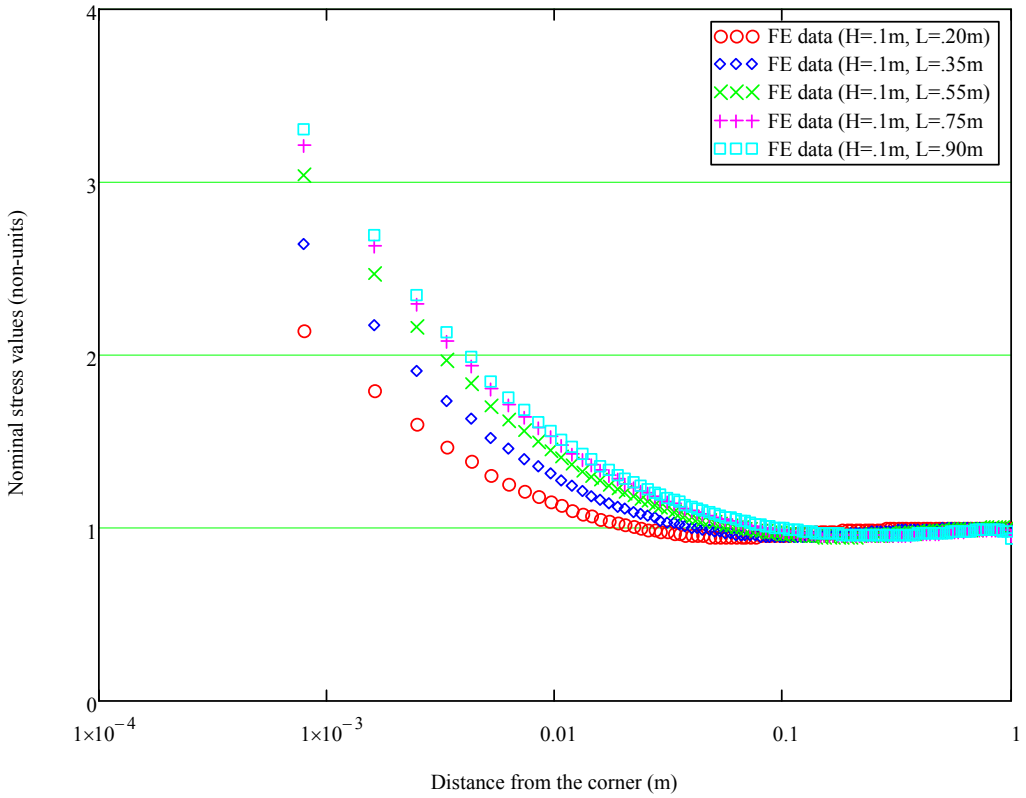

Figure 6.11 *FE* Stress values for various constant height *H* (=0.1m) specimen

The geometric effects can be seen more clearly, for H = 0.1 with L = 0.2 and L = 0.9 in Figure 6.12 and Figure 6.13. In Figure 6.12, the length of the attachment is 0.2m and height is 0.1m; the Length Scale is calculated as 9.091E-3m. The formula for the stress distribution exhibits a reasonable approximate fit to the numerical results as shown on the log plot. Note that the stress from the FEA dips down below the mean level. This may be caused by the moments needed to equilibrate the eccentricity of the force that transfers into the outstand.

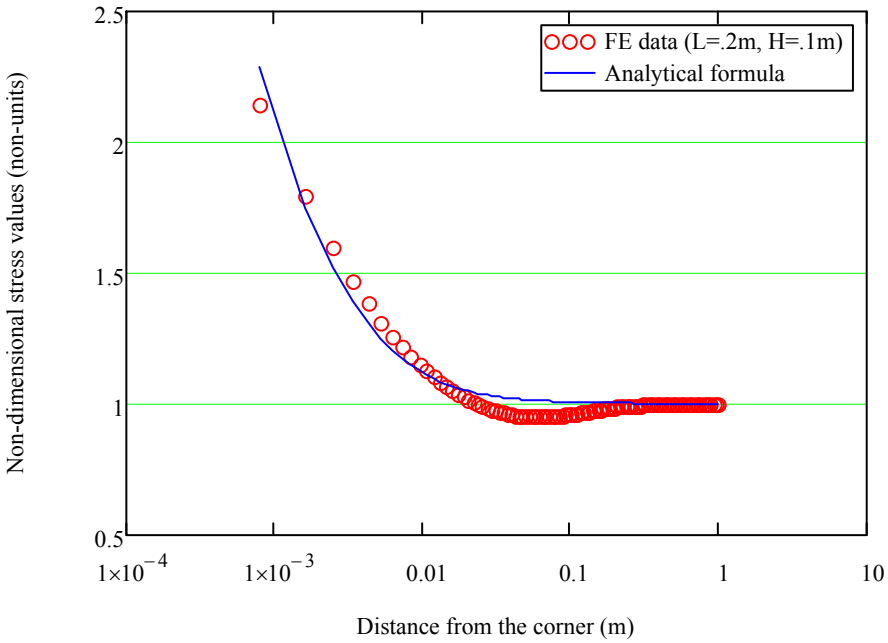

Figure 6.12 Stress comparisons for cruciform specimen (*L*=0.2m and *H*=0.1m); analytical Length Scale, *as*=9.091E-3m (**min(L/22, H/3 = 9.091E-3)**)

In Figure 6.13, it shows the other extreme of the cases considered. Again the fit is slightly better than for the shorter outstand. Maybe because the stresses require balancing the eccentric moment are smaller.

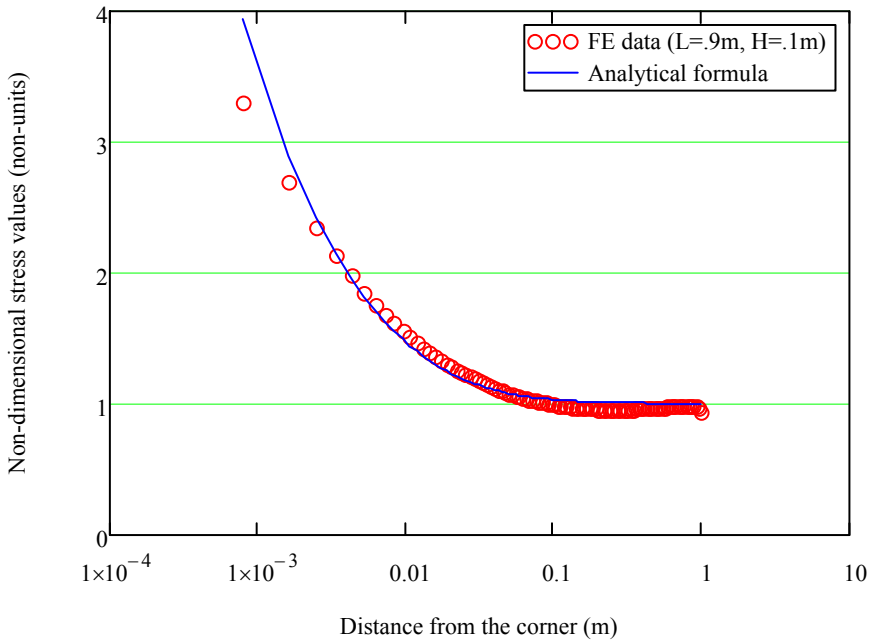

Figure 6.13 Stress comparisons for cruciform specimen (*L*=0.9m and *H*=0.1m); analytical Length Scale, *as*=0.033m (**min(L/22, H/3 = 0.033)**)

The numerical and analytical curve of 3 kinds of different geometry attachments, each having the same 'as', are checked in Figure 6.14, showing that as can be a good indicator of the likely stress pattern. The results are shown separately in Figure 6.15; with attachment (L=0.5 m and H=0.7m) in Figure 6.16; with attachment (L=0.5 m and H=0.9m) in Figure 6.17.

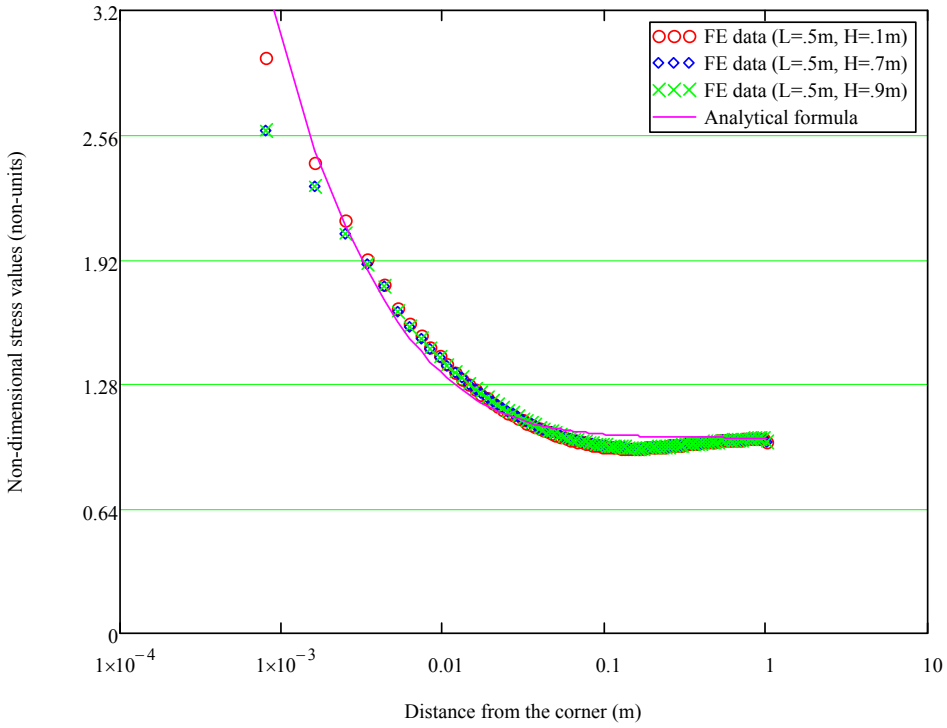

Figure 6.14 Stress comparisons for cruciform specimen;
analytical Length Scale, *as*=0.023m (**min(L/22, H/3 = 0.023)**)

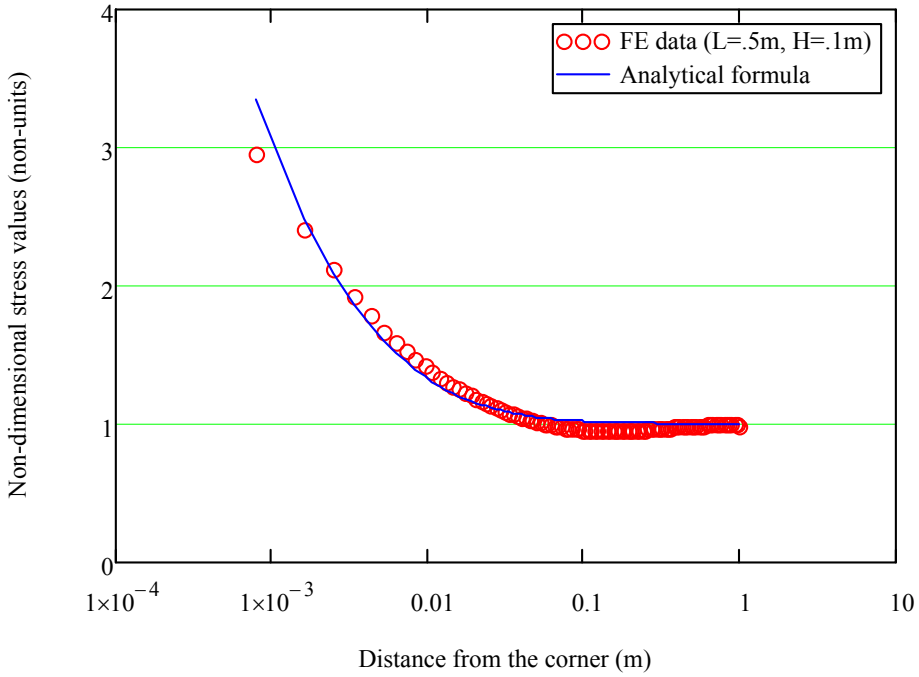

Figure 6.15 Stress comparisons for cruciform specimen (*L*=0.5m and *H*=0.1m); analytical Length Scale, *as*=0.023m (**min(L/22, H/3 = 0.023)**)

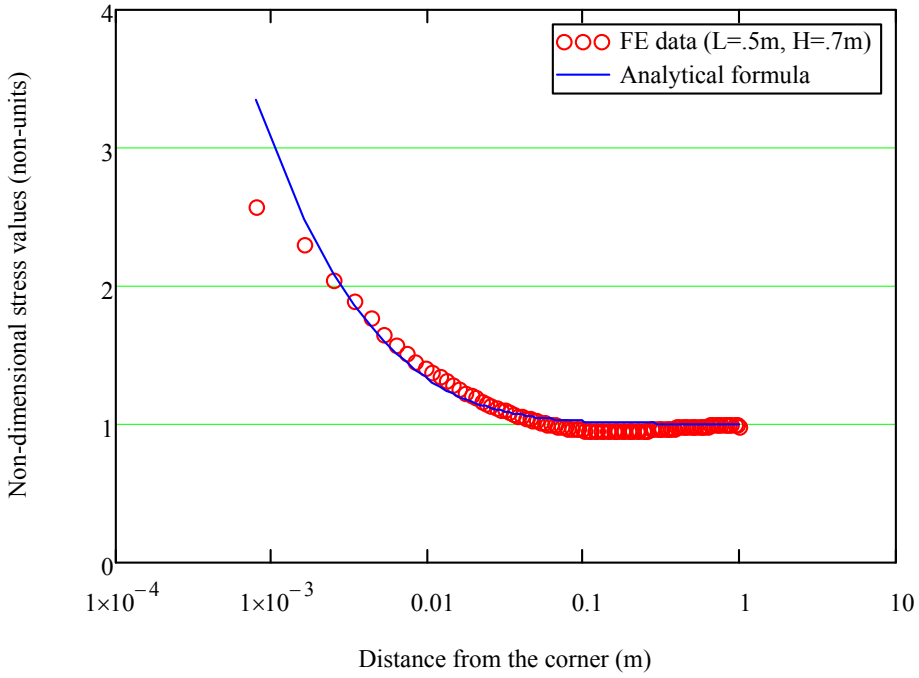

Figure 6.16 Stress comparisons for cruciform specimen (*L*=0.5m and *H*=0.7m); analytical Length Scale, *as*=0.023m (**min(L/22, H/3 = 0.023)**)

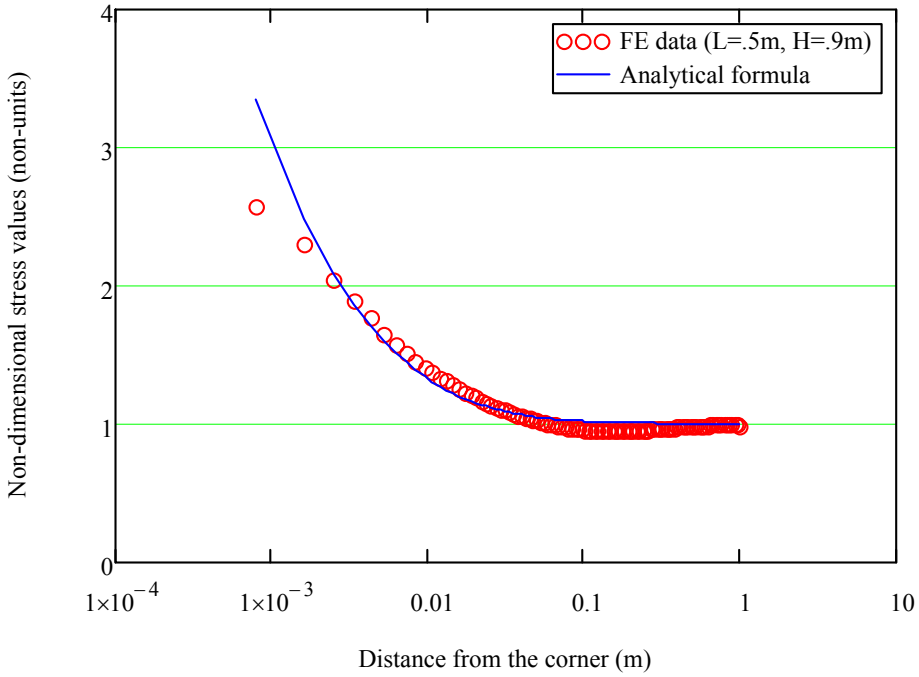

Figure 6.17 Stress comparisons for cruciform specimen (*L*=0.5m and *H*=0.9m); analytical Length Scale, *as*=0.023m (**min(L/22, H/3 = 0.023)**)

It is evident that with Length Scale the curves do exactly coincide with the FE results, except for the tip locations where the stress singularity points.

In Figure 6.18, the results for a constant length L (=0.1m) are plotted for values of height H (from 0.2m to 0.9m). These curves are all the same, and again show the stresses dipping down to 10% less below the nominal stress. The Length Scale is from about 0.012m or 0.5as to 0.1m or 4.4as.

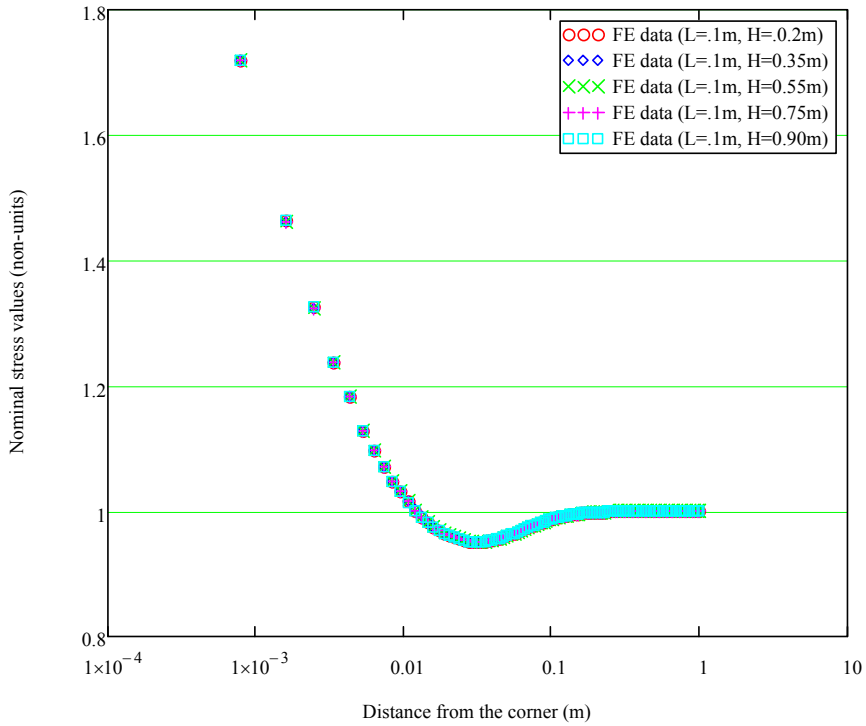

Figure 6.18 *FE* Stress values for various constant width *L*(=0.1m) specimens analytical Length Scale, *as*=0.023m (**min(L/22, H/3 = 0.023)**)

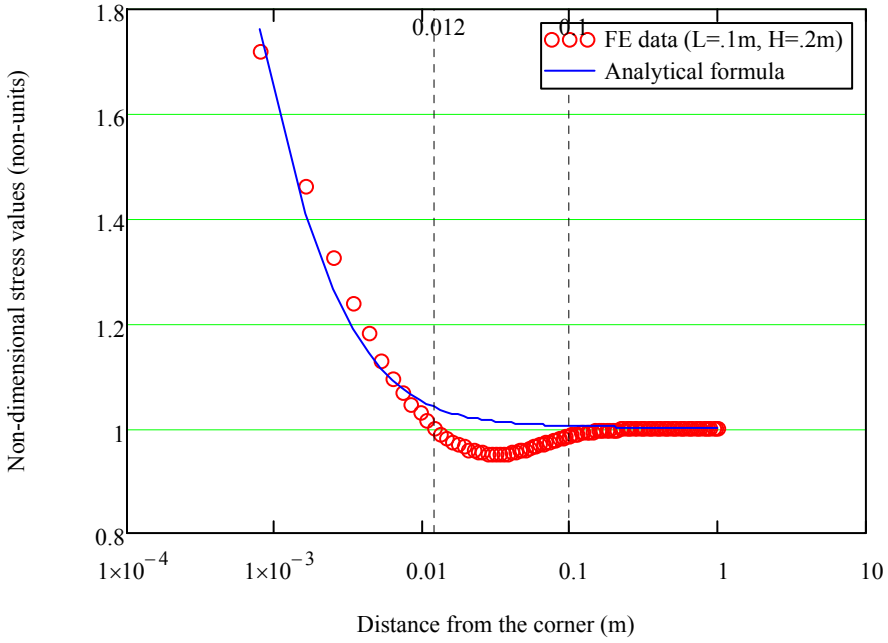

Figure 6.19 Stress comparisons for cruciform specimen (*L*=0.5m and *H*=0.7m) analytical Length Scale, *as*=4.545E-3m (**min(L/22, H/3 = 4.545E-3)**)

It is clear that the stress trends are similar, though not exactly the same as the approximate formula. Nevertheless, the stress distribution is still acceptable for a stress concentration factor or crack growth calculation with an acceptable error between the approximate formula and the FEA result.

It can be recognized that the geometry will affect the stress raises by discussing the Length Scale 'as' for different attachment shapes. The good matches between our formula and numerical results do show significant applications of the Length Scale approach, particularly considering that Length Scale can be taken as a measurement of stress concentrations.

6.4 Verification for Geometric Transformation

Structural details are not simple cruciform; however the cruciform research provides a method for assessing many other details in Figure 6.20.

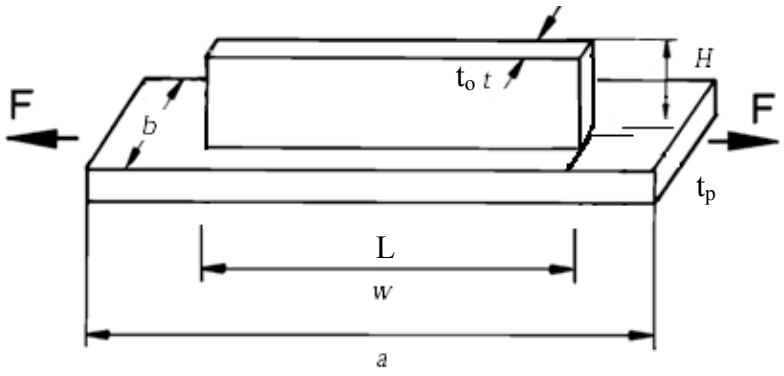

Figure 6.20 Longitudinal stiffener plates in fatigue analysis

For the attachment shown in Figure 6.21, the attachment can be converted to the cruciform shape, with the main plate (for a one sided attachment) being considered to be thickness 2tp (tp for a single sided attachment) and folded downwards. Note that this excludes any bending of the main plate from the eccentricity of asymmetric attachments.

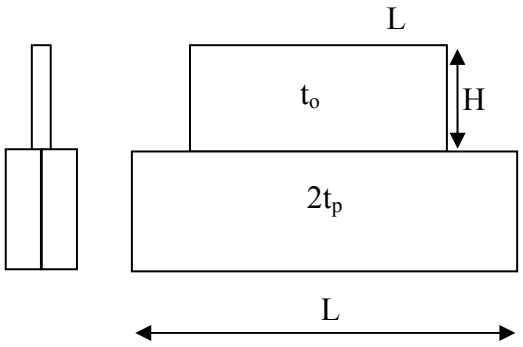

Figure 6.21 Cruciform equivalent plate to Figure

The mid-layer stress along the longitudinal direction of the main plate is compared with the stress from Equation 3.6. The thickness factor is found from Eqn. 3.16.

$$a_s = smallest\ of\ \ (L/22\cdot(2t_p/t_0)^{0.87},\quad H/3\cdot(2t_p/t_0)^{0.5}) \qquad 3.16$$

To position the surface evaluation points, the stress distributions are obtained by verifying the stress formula. We just need top-layer stress distribution (or hot-spot SCF values) to compare the two geometry specimens.

The Length Scale 'as' was derived from the attachment (L, H), and then applied in the empirical stress distribution formula. The models have the following dimensions L=0.25m/ H=0.55m, L=0.45m/ H=0.20m, L=0.95m/ H=0.35m and L=0.55m/ H=0.15m.

The results are compared in Figure 6.22 to Figure 6.25; the distance away from corner is plotted by log.

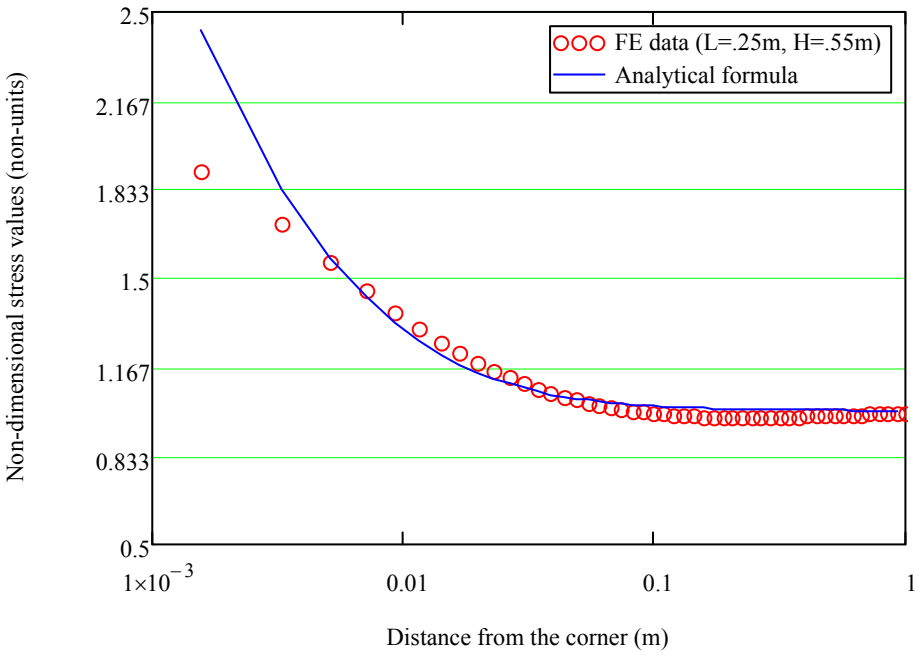

Figure 6.22 Stress comparisons for cruciform specimen (*L*=0.25m and *H*=0.55m); analytical Length Scale, *as*=0.021m (**min(L/22, H/3 = 0.021)**)

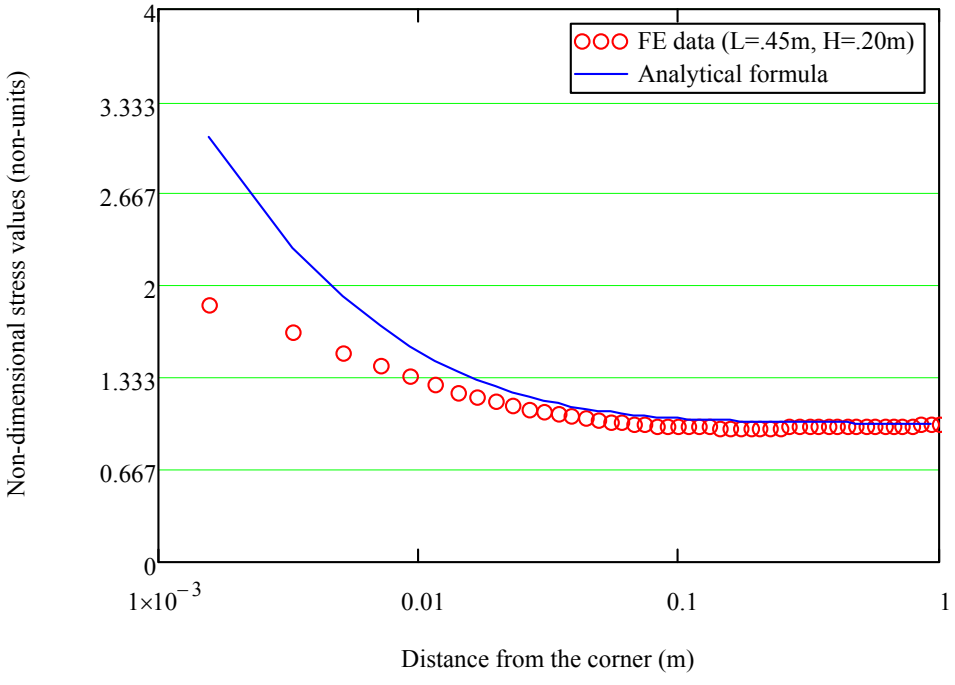

Figure 6.23 Stress comparisons for cruciform specimen (*L*=0.45m and *H*=0.20m); analytical Length Scale, *as*=0.037m (**min(L/22, H/3 = 0.037)**)

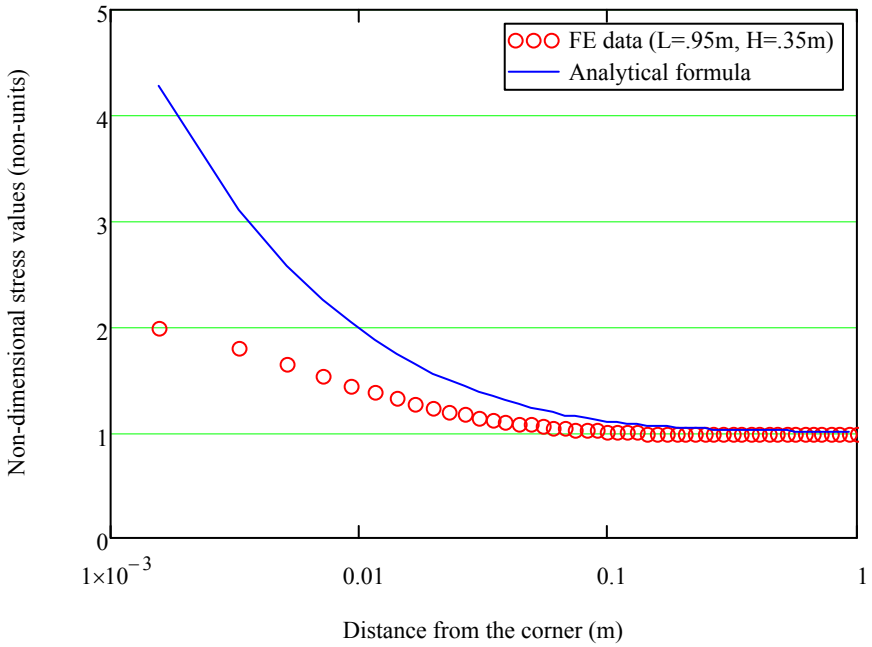

Figure 6.24 Stress comparisons for cruciform specimen (L=0.95m and H=0.35m); analytical Length Scale, as=0.079m (**min(L/22, H/3 = 0.079)**)

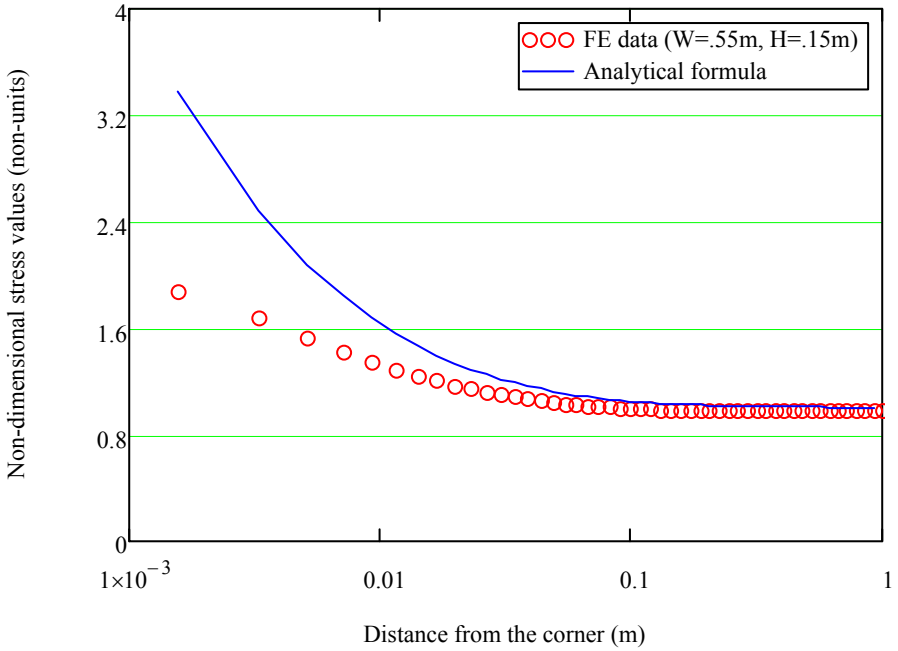

Figure 6.25 Stress comparisons for cruciform specimen (L=0.55m and H=0.15m); analytical Length Scale, as=0.046m (**min(L/22, H/3 = 0.046)**)

The gusset thickness plays a main leading role to decrease the stress singularity, comparing the stress flow goes across the gusset, the peak stress will be cut to flat floor. SCF can be introduced by geometric application; the decisive issue is how to obtain the significant Length Scale from the thickness corrections.

It was shown that the influence of the thickness can be separated from that of gusset dimensions by checking the singularity. By comparing the numerical results derived from ANSYS and scaling the stress distribution values, the geometry correction (by folding the thickness of plate) can apply on the transformation of shape categories very well.

The raise stress distribution is still influenced by the width of gusset dominantly, although the equivalent thickness can be compared with the folded plate thickness, however the thickness correction can not ignore during the calculation of Length Scale.

6.5 Conclusions

The new Length Scale concept and associated stress patterns has been compared with FEA using ANSYS. The comparison has shown:

1. For the cruciform the factor 'as' is a useful way of characterizing the singularity.

2. For many practical cases the stress singularity is strongly dominated by the length of the attachment.

2. The size of the main plate will generally be sufficiently large that it does not affect the prediction of Length Scale 'as'. Therefore we do not need to introduce main plate information into the formula for determining the Length Scale.

3. At the cruciform corner, the stresses from the Length Scale based formula and the numerical results show an agreement that is acceptable for preliminary and screening purposes.

4. As well as the cruciform shape, other more complex components can be assessed using the length scale method.

REFERENCES

1. Gurney TR. The influence of thickness on the fatigue strength of welded joints. In: Proceedings of the Second International Conference on Behaviour of Offshore Structures, London. 1979.
2. Maddox SJ. Scale effect in fatigue of fillet welded aluminium alloys. In: Proceedings of the Sixth International Conference on Aluminium Weldments, Cleveland, OH, 3-5 April 1995. Miami, FL: American Welding Society; 1995 [ISBN 0-87171-458-2].
3. Maddox SJ. The effect of plate thickness on the fatigue strength of fillet welded joints. Abington, Cambridge: Abington Publishing; 1987.

CHAPTER 7
COMPARISON OF LENGTH SCALE SCFs WITH PUBLISHED DATA

7.1 Introduction

In laboratory tests and during the service life of ship structures, cracks are observed at the connection locations. The stiffener is the frequent location owing to the severe angular discontinuity in the ship (or shell-plate) structure.

This chapter considers the structural connections in the HHI report (W. Kim and I. Lotsberg, 2004). A comparative study of the guidelines of IIW recommendations (IIW, 2002; Hobbacher, 2004) and BS7910 (1999), and the length scale method is performed to find the SCF predicted by each approach.

7.2 Selection of Structural Examples

The various specimens investigated by Hyundai Heavy Industries. Co., Ltd is defined as HHI#1-5 specimen and is shown in Figure 7.1. ISSC (1997), and the FPSO JIP (reference) also studied of these structural details.

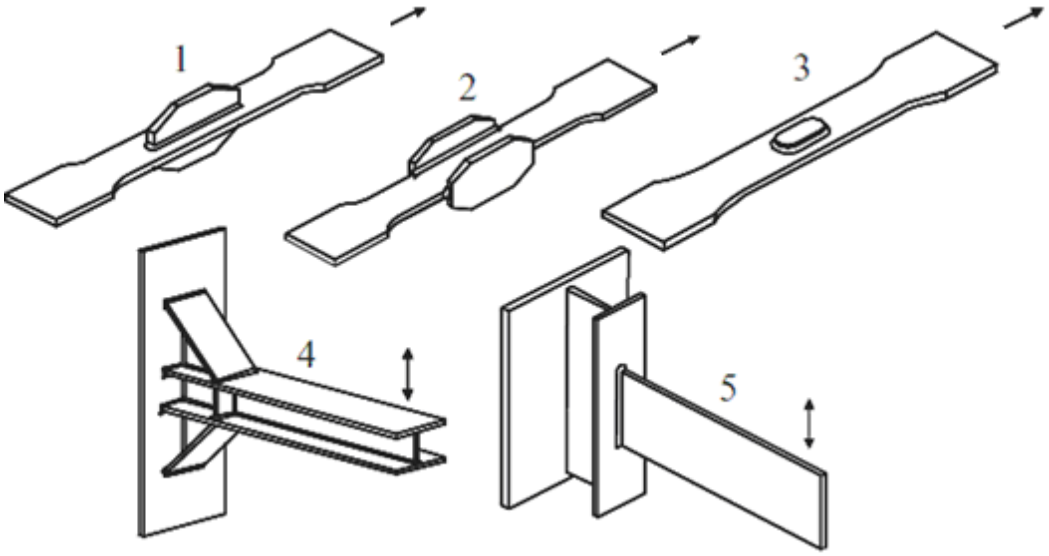

Figure 7.1 Specimens fatigue tested by HHI and analyzed by FE (Lotsberg, 2006)

It could be seen in Figure 7.1 that HHI#1 is a well known detail frequently fatigue tested considering to be one of the most reliably categorized details (Zettlemoyer and Fischer, 1978); HHI#3 has two doubling plates of an oblong shape during the FPSO JIP (W.S Kim, I. Lotsberg, 2004) and the HHI#5 is considered to be the most severe for out of plane bending. These details are fabricated with a full penetration weld without plate fillets, which increases the corner discontinuity.

Parallel to the experimental investigations, extensive finite element analyses were performed. The typical hot spot positions (or failure positions) are classified according to geometric characteristics, at the end of attachment and connection around the plate edge.

Lotsberg (1998), decided to perform analyses of the HHI specimens and the specimen with the severe discontinuity at crossing plates where measurements of stress gradient region have been performed in a DNV project.

W. Fricke (2001) used the conventional hot-spot stress approach. He compared models with thin plate shell elements and solid elements.

Based on the investigation by the previous authors, stress concentration values were evaluated in the 5 specimens. These stress concentration factors are summarized in Table 7.1.

Table 7.1

Typical stress concentration values (Lotsberg, I. and Sigurdsson, 2004)

Specimen	Fricke (2001)	Lotsberg.I (2004)	Difference
HHI #2	1.85	1.96	5.95%
HHI #1	1.77	1.69	0.00%
HHI #3	1.32	1.32	9.02%
HHI #5	1.22	1.33	-4.52%
HHI #4	1.96	1.64	-16.33%

The structural stress procedure is investigated in fatigue strength assessment of the HHI specimens by P. Dong (2004), the similarities and differences between the surface extrapolation procedure and the structural stress method are discussed.

7.3 Further Assessment of HHI Specimen

In Figure 7.1, specimens HHI #2 and HHI #5 may be classified as edge details, according to the works by Dong (2001) for the corner crack initiate. The joint types and categories of HHI #1, HHI #3, and HHI #4 are classified by Yagi etc (1991) as the symmetric component. It should be noted that HHI #1, HHI #3 and HHI #4 posses the symmetry in joint geometry and loading with respect to the mid-thickness direction.

Although there are 5 specimen tests, four of details are selected for the refinement of length scale stress approach. These investigated specimens are HHI#2, HHI#5, HHI#1 and HHI#3 (in the order presented below)

7.3.1 Specimen HHI #2: Gussets on the Plate Edge

The first detail has gussets, 150 mm long and 80 mm high, on the plate edges, as shown in Figure 7.2. The size for the main plate is 60×570 mm. For the analysis the

main plate is subjected to tensile loading $\sigma = 1.0MPa$.

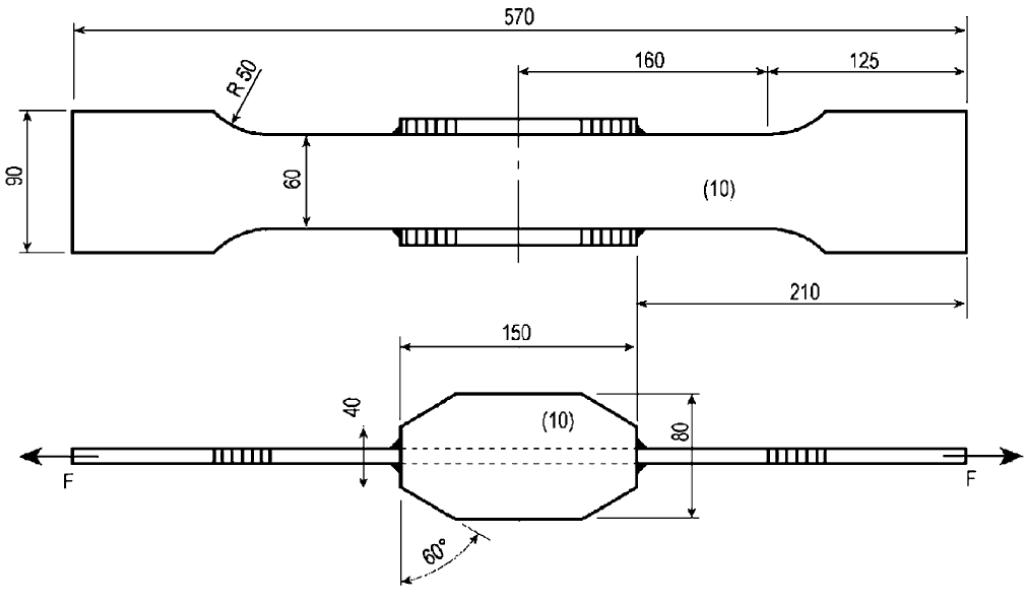

Figure 7.2 Specimen *HHI*#2 with edge gussets investigated
(W.S Kim, I. Lotsberg, 2004)

To apply the length scale methodology the structure is represented by a folded flat equivalent plate, see Figure 7.3.

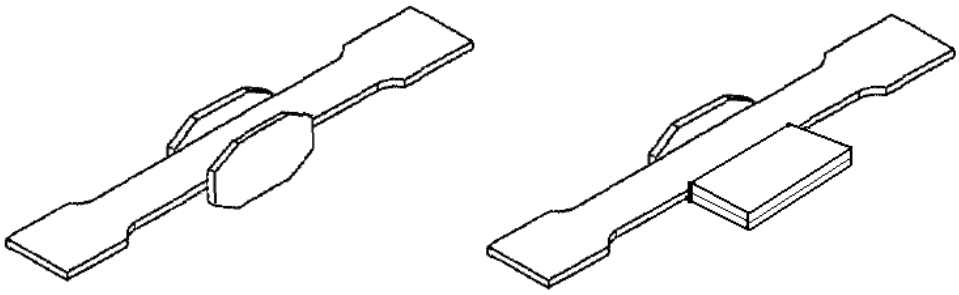

Figure 7.3 Gusset conversion to an equivalent cruciform

A thickness equal 2 times the thickness of the plates is used for modelling of the transverse plates.

Using Eqn. 3.16, we have the Length Scale:

$$as = smallest\ of \quad (150/22\cdot(2.0)^{0.5}, \quad 40/3\cdot(2.0)^{0.87}) \qquad 7.1$$

Here L is the length of gusset 150mm, and H is the height 40mm

From the formula, the predicted Length Scale, $as = 9.642mm$, which will be used for the prediction of SCF for the case.

The surface stress distributions from all ABAQUS 2D shell finite element models with different mesh sizes and element types are summarized by (Dong and Hong, 2004) (using about txt, 0.5tx0.5t, 1/4tx1/4t and 1/8tx1/8t; four and eight node elements respectively) are summarized for comparison purposes. As element sizes were further refined, the HSS values using extrapolation from 0.5/1.5t, 0.4/1.0t and 0.5t showed convergence to a stable value when the element sizes approached 1/8t.

The structural stress results were calculated according to Dong from the fine corner mesh. The shell element models provided only a membrane stress for this case, therefore they did not capture any thickness direction bending component, which is largely restrained by the geometry.

The approach of Xiao and Yamada, 2004 was applied to a model with solid elements having a size of 1mm in the critical region. Therefore, one value representing the stress concentration at the node 1mm below the weld toe was given.

It has been acknowledged that the approach of SCF by LEFM against ‘as’ is right. Here we employ the LEFM research result diagram to predict the SCF directly.

Using the length scale estimated in Equation 7. 1 the SCF was estimated, from Figure 3.11, to be the function of Length Scale: 1.99.

Using FEA to calculate the stress distribution and applying the Paris Law and calculating the SCF for a Fat 90 curve the SCF from Figure 5.11 was found to be: 2.16.

The SCFs from the various approaches are shown in Figure 7.4.

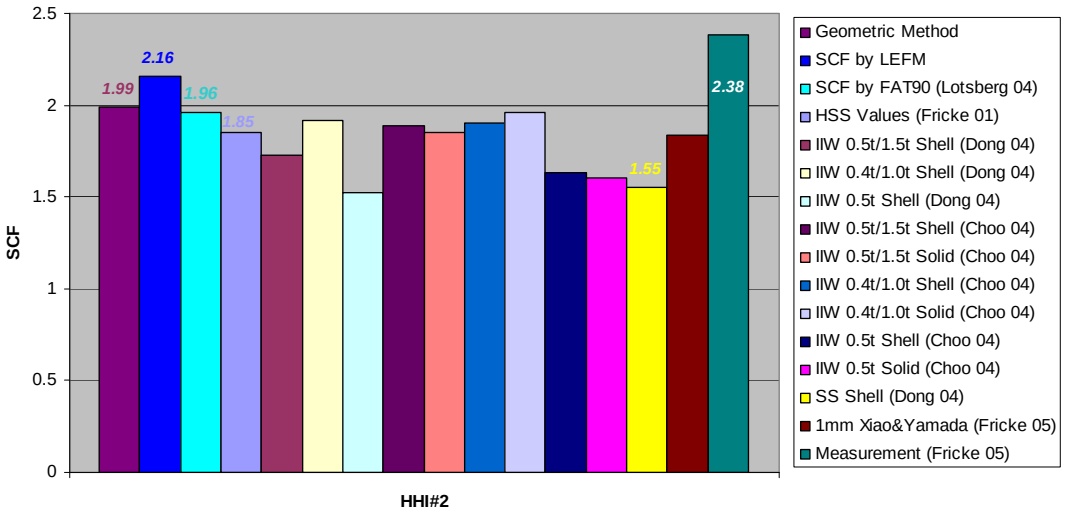

Figure 7.4 Summary of converged Length scale, *HSS*-based and *SS*-based *SCF* (*HHI*#2)

The results from calculating as and from LEFM are both a little higher than the results obtained by the other analysis methods. All of the calculated results are lower than the experimental results (2.38) by Fricke (2005).

7.3.2 Specimen HHI #5: Plate to I-beam Box

The second edge detail is the specimen 5 from the HHI tests, representing a stiffener connection being subjected to shear and bending loads. In my opinion, the HHI#5 is a little similar with the tensile loading case, and the bending loading direction should be converted to that of the tensile loads. The fatigue critical position is the weld toe on the upper plate edge of the flat bar, as shown in Figure 7.5.

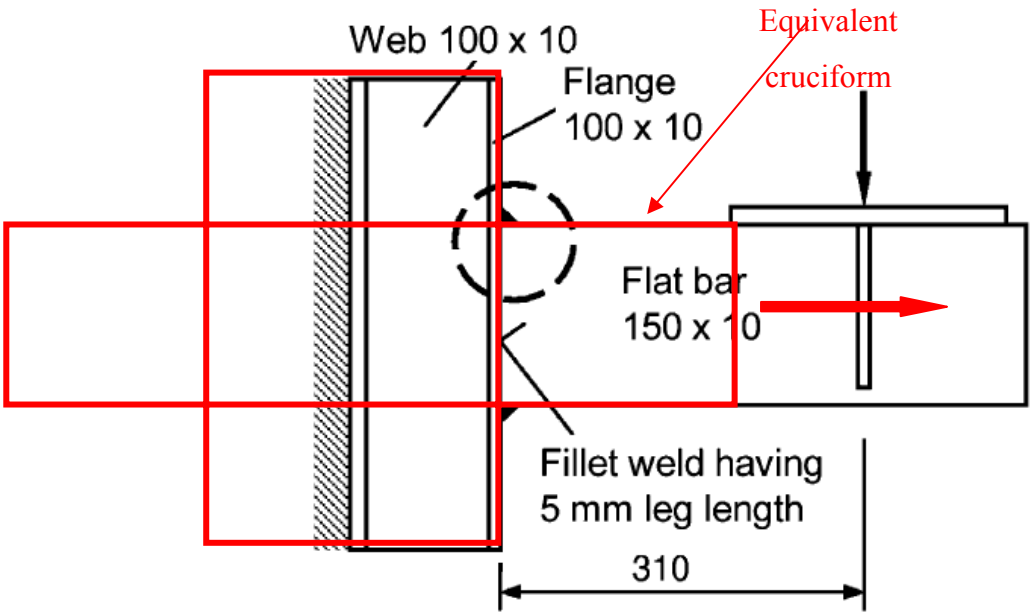

Figure 7.5 Loaded stiffener on I-beam box joint and the critical area

The width (L, 200mm) and height (H, 100mm) of the flat plate are varied to factors for dimensional factor 'as', considering the stiffer plate as flange in the cruciform form. The thicknesses of the all plates are considered as 10mm, and also need to add thickness terms into the calculation. It would then be smallest of 200/22 and 100/3 =9mm with no thickness correction.

$$as = smallest\ of\ \ (200/22,\ \ 100/3) = 9.1mm \qquad 7.2$$

Here L is the length of flat bar 200mm, and H is the height 100mm

The flanges contribute in this case should be ignored. In the previous case the folded elements were stressed whereas here if the flat bar is considered the main stressed plate (see superimposed diagram above) then the flange is not doing anything except providing a moment restraint for the vertical member.

From Length scale method (from Figure 3.11), this as corresponds to an SCF of 1.947; and from the LEFM method (Figure 5.11), the SCF is around the value of 2.12.

The detail has also been investigated in a round-robin analysis with finite element models by the (Dong and Hong 2004, Choo 2004, Fricke, 2001). The stress

concentration factors were derived from surface stress extrapolation according to IIW (2007) specifies the formula.

The SCF results at the hot spot region are shown in Figure 7.6.

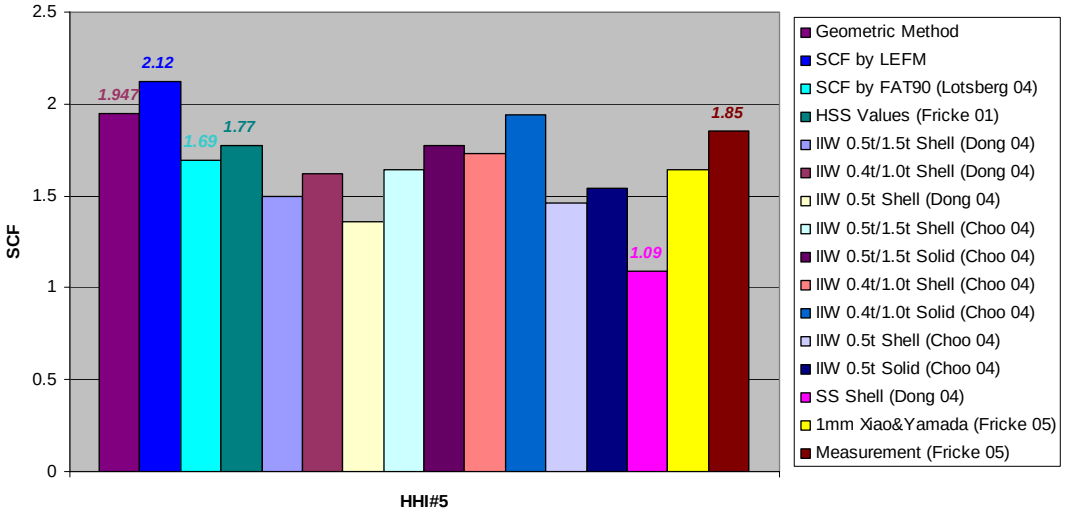

Figure 7.6 Summary of converged Length scale, *HSS*-based and *SS*-based *SCF* (*HHI#5*)

The SCF values show a wide range. The LEFM result is higher than the experimental results. The SCFs estimated by the length scale are about 1.947, when alternative length scale method is tried, compared with the measured SCF value of 1.85 by Fricke (2001).

7.3.3 Specimen HHI #1 Longitudinal Gussets on the Plate

This specimen involves the gusset plate attachments on the top (and bottom) surfaces at the middle of the main plate as shown in Figure 7.7. (The design yield stress equals to 235MPa corresponding to a ship-structural mild steel according to the classification societies' specifications.)

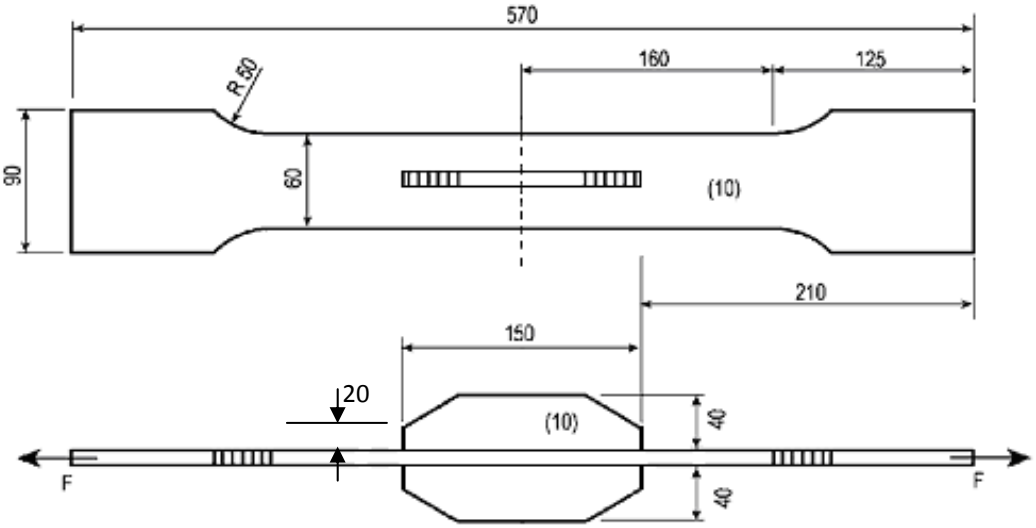

Figure 7.7 Specimen *HHI*#1 with longitudinal gussets investigated

The length of flange and distortions in each fabricated specimen were measured before fatigue testing. The attachment lengths were 150mm; with overall height 40mm and the height from the main plate to the chamfer is 20mm. The length and width dimension of main plate are the same as for the HHI#2 specimens. The thicknesses of the base plate and doubling plates are 10mm, respectively.

The value of the Length Scale as is derived in Eqn. 7.3.

$$as = smallest\ of \quad (150/22\cdot(1/2)^{0.5},\quad 20/3\cdot(1/2)^{0.87}) = 3.648mm \qquad 7.3$$

Here L is the length of gusset 150mm, and H is the height 20mm

The structural stress procedure employs the base plate width W as the reference depth in the structural stress calculations using solid element models. An alternative particularly for this HHI#1 case could be to use solid elements to determine the steep stress gradients in the plate thickness direction.

As element sizes were further refined, the HSS values used 0.5/1.5t, 0.4/1.0t and 0.5t extrapolation for various element mesh level.

The structural stress concentration calculated along the through-thickness direction of the base plate, is shown large differences comparing with other values. Note the values are read from the OMAE paper by Dong, 2004.

Note that due to symmetry with respect to x-y plane, the mid surface of the base plate, the stress gradients near the hot spot are expected to be relatively localized and were ignored. Typical FE model used by Dong and Hong (2004) is shown in Figure 7.8.

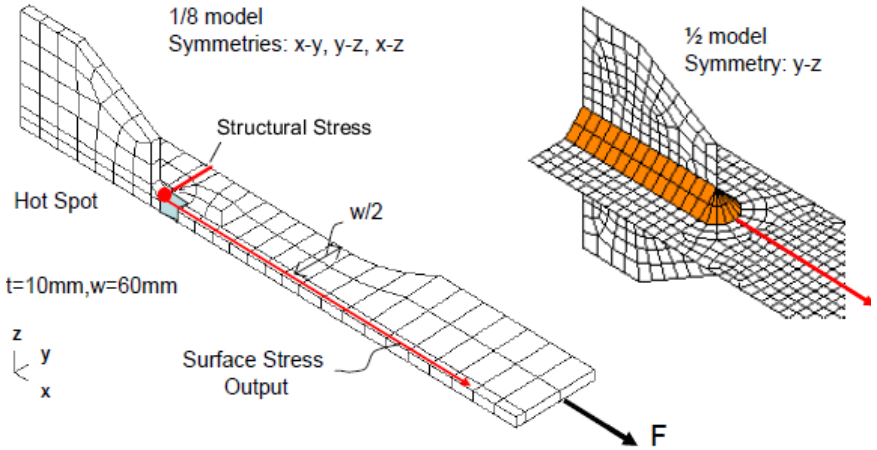

Figure 7.8 Representative *FE* models of Specimen *HHI* #1 (Dong and Hong 2004)

The SCF resulting from length scale (Figure 3.11) is 1.439. The results from other Authors are shown in Figure 7.9 and Table 7.2.

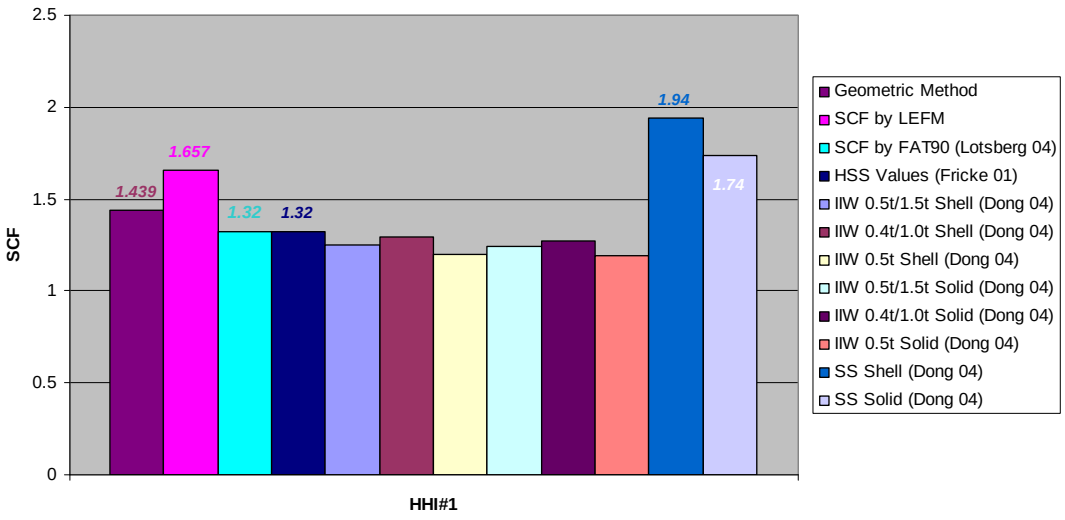

Figure 7.9 Summary of converged Length scale, *HSS*-based and *SS*-based *SCF* (*HHI*#1)

It can be seen that the value from the length scale method (1.439) is one of the lower estimates of the value derived from LEFM (Figure 5.11) is 1.657.

7.3.4 Specimen HHI #3: Two-sided Double Plate Joint

The last detail is HHI#3: one- sided double plate joint is similar to specimen detail #3 (single doubling plate joint), subjected to tensile forces. It should be noted that in the earlier publications, the two joint types are not distinguished. In the author's opinion, there are distinguishing differences between the specimens, especially when comparing the results. The difference is that the joint plate surface of HHI#3 is pasted on the surface of the main plate as shown in Figure 7.10. The specimen has been investigated in a Japanese research project.

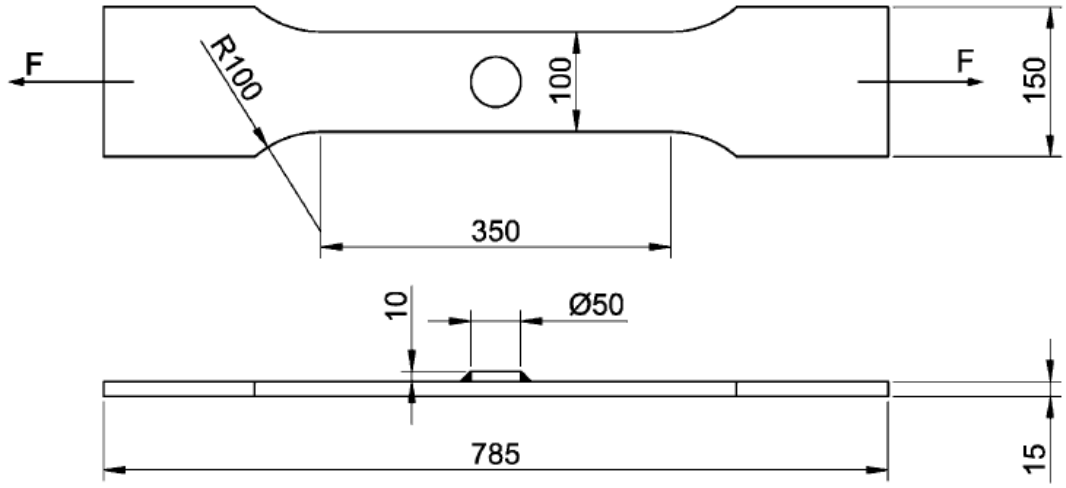

Figure 7.10 Specimen *HHI*#3 with one-sided double plate investigated

The fatigue critical position is at the connection end between the plates oriented transversely to the loading. The circular double plate causes a non-uniform stress distribution in the transverse direction shown in Figure 7.11.

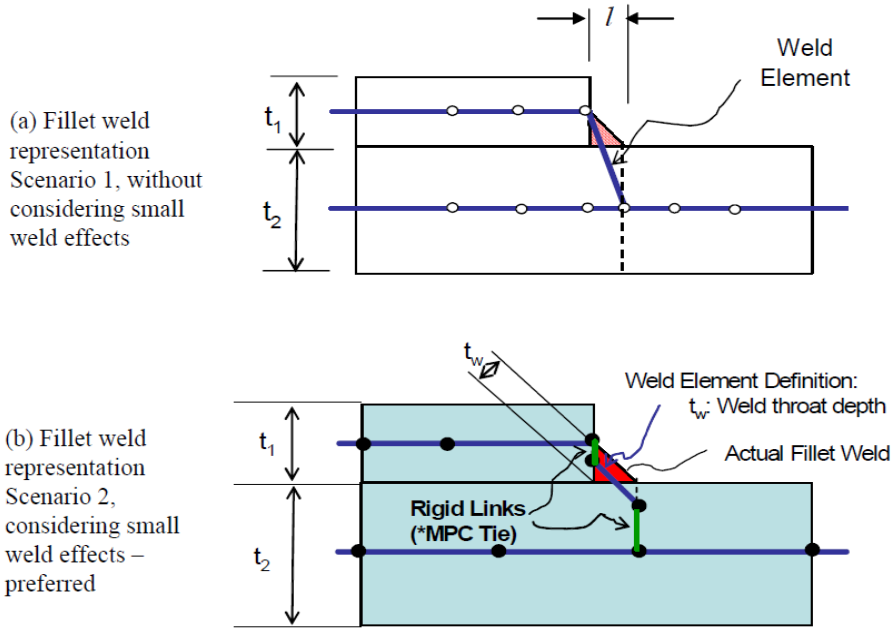

Figure 7.11 Stress steep location of *HHI*#3

(Doerk, O., Fricke, W., and Weissenborn, C, 2002)

The width (50mm) and height (10mm) of the double plate varied for the Length Scale 'as', considering the cross are as the cruciform plate.

$$as = smallest\ of \quad (50/22, \quad 25/3) \tag{7.4}$$

Here L is the length of double plate 50mm, and H is radius of plate 25mm, the thickness correction factor is assumed folding the doubler and the basic plate.

The above does not allow for the transverse in plane stress concentration

The Length Scale of HHI#3 specimen is determined as 2.273mm. The stress concentration factor derived by length scale method is 1.276 from Figure 3.11.

The values derived from the performed analyses supplemented by surface extrapolation stress in Figure 7.12 average 1.278, slightly lower than the values from the length scale method. Dong's method (2004) is applied using solid and three shell FE models in ABAQUS, yielding the stress concentration factors given for through-thickness linearization. In the study by (Dong, 2004 solid elements are used, from which a stress magnification factor of 1.78 was derived. All the results are included and together shown in Figure 7.12.

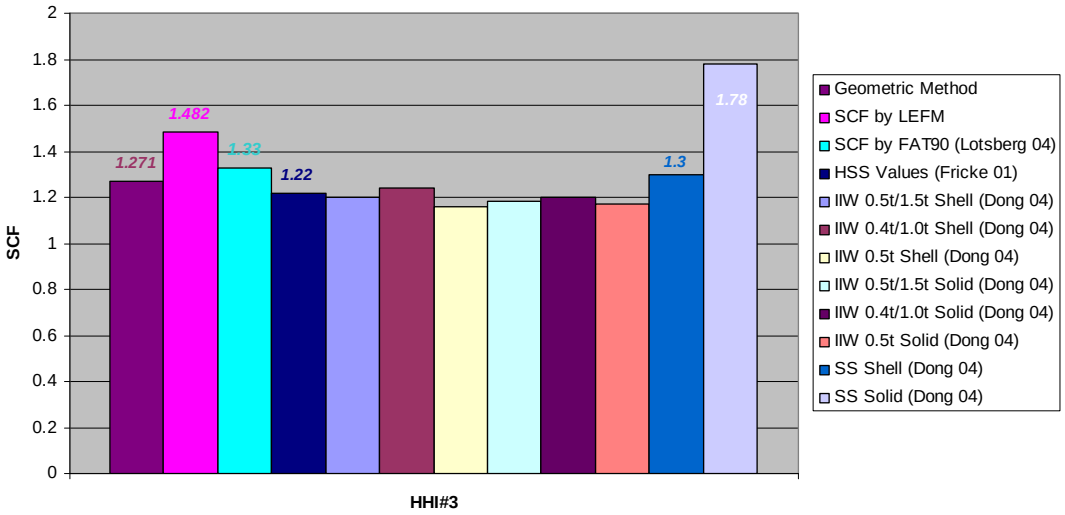

Figure 7.12 Summary of converged Length scale, HSS-based and SS-based SCF (HHI#3)

The longitudinal stresses are measured in front of the critical connection and linearly extrapolated using IIW (2009) guidelines, yielding a hot-spot stress concentration factor ranging from 1.15 to 1.25.

The equation provides stress concentration factors that are in good agreement with hot spot and structural SCF values. The advantage is that the 'as' is that the SCF is obtained with minimal analysis. However some skill may be required to apply the method well.

7.4 Fatigue Life Assessment

In this chapter, the fatigue life is assessed for the 4 different structural details described above. The nominal stress range (important for physical experiments) was $\Delta\sigma = 150MPa$ for the specimen of HHI#1, HHI#3 and HHI#5 and $\Delta\sigma = 80MPa$ for the specimen of HHI#2. My predicted lives were compared with estimates from other researchers and the test results. This is a considerable data base with useful FE analyses results, correlating SN data from all the joint types.

The investigation has shown that the SCFs obtained from the length scale

approach are good estimates of the SCFs from FE analysis combined with LEFM

7.5 Conclusions

This chapter gives an overview of HHI test specimens. Recommendations with respect to definition of Length Scale (for stress concentration factors prediction) are given based on the types of geometry.

From the results comparisons with FEA and tests results, the following conclusions are drawn:

Uncertainties in the computed stresses raisers are mainly due to the element properties and sizes in surface extrapolation method, and in particular to the FE modelling, however, the Length Scale can be successfully and easily obtained.

Stress concentration changes with the dimensions of gussets. The Length Scale plays an important role during in the prediction of concentrations.

Compared with numerical and experimental estimates of stress concentration, it is shown that the novel Length Scale approach gives conservative results.

As extensively discussed above, the comparisons have shown that the length scale and LEFM methods can be applied on the fillet geometric form very well, and with one exception reconsider when that case is recalculated-are slightly conservative compared with fatigue tests and/or linear elastic fracture mechanics assessment.

REFERENCES

1. BS 7910:1999. Guide on methods for assessing the acceptability of flaws in metallic structures. London: BSI; 1999.
2. Choo, Y.S. and Zahidul Hasan, Md. “Hot Spot Stress Evaluation for Selected Connection Details”. OMAEFPSO' 04-0028 Int. Conf. Houston.
3. Doerk, O., Fricke, W., and Weissenborn, C., “Comparison of different calculation methods for structural stresses at welded joints,” IIW Doc.,

XIII-1919-02/XV-1124-02, June, 2002.

4. Dong P, Hong JK. Hot spot stress and structural stress analyses of FPSO fatigue details. Proceedings of OMAE Specialty Conference on FPSO systems, OMAE-FPSO'04-0023, Houston TX, ASME International Petroleum Technical Institute; 2004
5. Dong P, The mesh-insensitive structural stress and master S-N curve method for ship structures. Proceedings of OMAE Specialty Conference on FPSO systems, OMAE-FPSO'04-0021, Houston TX, ASME International Petroleum Technical Institute; 2004
6. Dong P. A structural stress definition and numerical implementation for fatigue analyses. Int J Fatigue 2001;23(10):865–76.
7. Fricke, W. , "Recommended Hot Spot Analysis Procedure for Structural Details of FPSO's and Ships Based on Round-Robin FE Analyses". Proc. 11th ISOPE, Stavanger. Also Int. J. of Offshore and Polar Engineering. Vol. 12, No. 1, March 2002.
8. Fricke, W., Recommended Hot Spot Analysis Procedure for Structural Details of FPSOs and Ships Based on Round-Robin FE Analysis. ISOPE, 2001.
9. Hobbacher A, editor. Recommendations for fatigue design of welded joints and components. IIW Doc XIII-2151r1-07/XV-1254r1-07. International Institute of Welding; 2007.
10. IIW, International Institute of Welding. Recommendations for fatigue design of welded joints and components (March 2002): XIII-1539-96/XV-845-96 and (July 2004): XIII-1965-03/XV-1127-03.
11. ISSC. Report of Committee II.1 "Quasi-static Response". Proc. Of 13th Int. Ship and Structures Congress (ed. By T. Moan and S. Berge, 1997), Vol. 1, Elsevier Science.
12. Kim WS, Lotsberg I. Fatigue test data for welded connections in ship-shaped structures. Proceedings of OMAE Specialty Conference on FPSO systems, OMAE-FPSO'04-0018, Houston, TX, ASME International Petroleum Technical Institute; 2004.
13. Lotsberg I. Fatigue design of plated structures using finite element analysis. J Ships Offshore Struct 2006; 1(1):45–54.

14. Lotsberg, I. and Sigurdsson, G. Hot Spot S-N Curve for Fatigue Analysis of Plated Structures. OMAEFPSO' 04-0014, Int. Conf. Houston.

15. Lotsberg, I. Müsch, K., M?seide, M. O., Solland, G. and Storesund, W., Tested Capacity of Welded Connections made of High Strength Steel. OMAE 1998, Lisabon.

16. W. Kim, I. Lotsberg, Fatigue test data for welded connections in ship-shaped structures, Proceedings of OMAE Specialty Conference on FPSO systems (2004), OMAE-FPSO'04-0018, Houston, TX, ASME International Petroleum Technical Institute.

17. W.S Kim, I. Lotsberg, Fatigue test data for welded connections in ship-shaped structures, Proceedings of OMAE Specialty Conference on FPSO systems (2004), OMAE-FPSO'04-0018, Houston, TX, ASME International Petroleum Technical Institute.

18. Xiao, Z and Yamada K A method of determining geometrical stress for fatigue strength evaluation of steel welded joint, International Journal of Fatigue, volume 26, 2004, pp 1277-1993

19. Yagi, J., Machida, S., Tomita, Y., Matoba, M., and Kawasaki, T., "Definition of Hot Spot Stress in Welded Plate Type Structure for Fatigue Assessment (1st Report)," Journal of the Society of Naval Architects of Japan, Vol.169, p.311-318, 1992 (in Japanese), IIW-XIII-1414-91, International Institute of Welding, 1991.

20. Zettlemoyer, N. and Fischer, J. W. Stress Gradient Correction Factor for Stress Intensity at Welded Gusset Plates. Welding Research Supplement, February 1978, pp. 57-62.

Table 7.2

Structural stress concentration factors obtained for the details by different methods and FE models

Structural Details	SCF FAT90	1	2	Dong's work 2004 [c] ABAQUS 0.5t/1.5t Shl[a]/Sld[b]	0.4t/1.0t Shl/Sld	0.5t Shl/Sld	Dong's SS	Choo's 2004 [d] 0.5t/1.5t Shl/Sld	0.4t/1.0t Shl/Sld	0.5t Shl/Sld	Wolfgang Fricke 2005 [e] 1-mm stress	Measure
HHI#2	1.96	1.99	2.16	1.73 (shl)	1.92 (shl)	1.52 (shl)	1.55 (shl)	1.89[a] /1.85[b]	1.90[a] /1.96[b]	1.63[a] /1.60[b]	1.84	2.38
HHI#5	1.69	1.756	1.95	1.50-1.52[a]	1.62-1.66[a]	1.35-1.37[a]	1.09	1.64[a] /1.77[b]	1.73[a] /1.74[b]	146[a] /1.54[b]	1.64-1.95	1.85
HHI#1	1.32	1.471	1.688	1.25[a] /1.24[b]	1.29[a] /1.27[b]	1.20[a] /1.19[b]	1.94[a]/1.74[b]					
HHI#3	1.33	1.276	1.482	1.20[a] /1.18[b]	1.24[a] /1.20[b]	1.16[a] /1.17[b]	1.28-1.32 [a] /1.78[b]					

[a] Extrapolated HSS SCF using shell element type;

[b] Extrapolated HSS SCF using solid element type;

[c] Dong P, Hong JK. Hot spot stress and structural stress analyses of FPSO fatigue details. Proceedings of OMAE Specialty Conference on FPSO systems, OMAE-FPSO'04-0023, Houston TX, ASME International Petroleum Technical Institute; 2004

[d] Choo, Y.S. and Zahidul Hasan, Md. "Hot Spot Stress Evaluation for Selected Connection Details". OMAEFPSO' 04-0028 Int. Conf. Houston.

[e] Fricke, W., Recommended Hot Spot Analysis Procedure for Structural Details of FPSOs and Ships Based on Round-Robin FE Analysis. ISOPE, 2001.

CHAPTER 8
COMPARISON OF LENGTH SCALE SCFs AND EXTRAPOLATION METHODS OF REAL SHIP DETAILS

8.1 Introductions

Bulk carriers and tank oil carriers are usually constructed of mild steel. The use of high tensile steel can reduce the rigidity of the ship hulls and may develop earlier fatigue cracks. It is also important to identify the holds designed for partial filling as this affects the maximum allowable corrosion diminution that can be applied to the cargo hold plates.

Be grateful to the checks by the surveyors, the ship components surveyed are located in the building environments shown in Figure 8.1, frames and connections can be made accessible to surveyed. Details in way of the bulk carrier contractures are most exposed to fatigue cracks. CSR (Common Structural Rules) require 25 years operational life in North Atlantic.

(http://3.bp.blogspot.com/-l3YstQq4VRc/UFLbkptxsII/AAAAAAAABbI/mVJZv2KCmDI/s1600/Midship_A.jpg)

(ABS, Classification, Certification & Related Services Tank, 2008)

Figure 8.1 Bulk Carrier Ship Constructions

Some typical details of Oil Tanker are selected in Figure 8.2.

(http://marineinsight.com/wp-content/uploads/2011/04/coverStory_maritimeEconomy_tanker3D_280.jpg)

(ABS, Classification, Certification & Related Services Tank, 2008)

Figure 8.2 Oil/Chemical Tanker Ship Constructions

The details of ship structural components are usually concluding primary longitudinal connections at double bottom shell, side shell frame end bracket at the side shell, structural gunwale connections at the deck girders, gusset edge stiffening at the cargo holds, stiffener ends and panel stiffeners, and overall gusset shape (tripping brackets, tight collars, non-tight collars and stanchion ends).

Critical problem in structural fatigue analysis is to determine the differences between the fatigue damage of laboratory specimens and the full scale structural details. The principles of mechanics, the similar initial defect size imply that the fatigue damage is not identical at different scales of structural detail. Extensive experiments have been performed, mainly on small simple specimens and these are the basis of most rules.

Research work has been converted to guidance by the International Institute of

Welding (IIW, 1991 and Hobbacher A, 2007) and International Association of Classification Societies (IACS, 2006). Technical reports such as by Yagi (1991) and Lotsberg (2004) also provide updated methodology for the hull fatigue analysis. Account should also be taken of the chemical environment in which the cracks occur (Burnside etc, 1984; Bea etc, 1995), large scale testing shown in Figure 8.3 (Lotsberg, 2004).

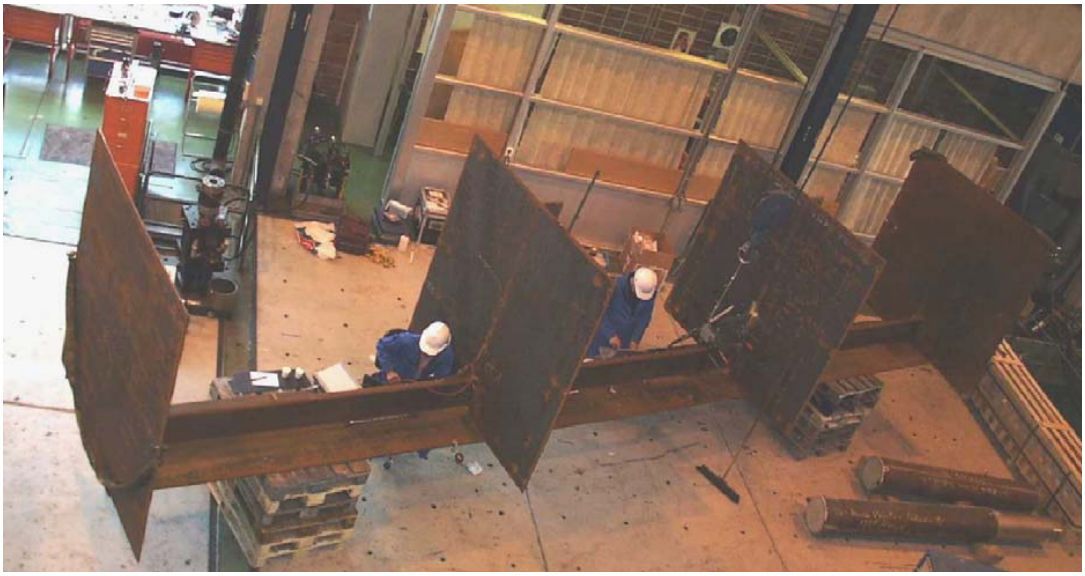

Figure 8.3 Full-scale test specimen (Lotsberg, I. and Einar L 2004)

Recently, the novel fatigue assessment methodologies and ideas have been brought out. Based on numerical comparison and theoretical discussion, it was found that the method could be applied on the relative simple shape efficiently; moreover, in a sole operation, it is extended in realistic components, requiring definitions of crack locations.

$$a_s = smallest\ of \quad (L/22, \quad H/3)$$

$$a_s = smallest\ of \quad (L/22 \cdot (t_0/t_{bp})^{0.5}, \quad H/3 \cdot (t_0/t_{bp})^{0.87})$$

where L is the length of the bracket, and H is its height;
and t0 is the thickness of the outstand arms;
(t_{bp}) is the thickness of the main load carrying plate.

For the purpose of the design recommendation improvement, it is therefore important that a proper link between geometry property and fatigue capacity in design standards. Moreover, the realistic components should be concluded into several categories by the locations and discontinuity locations. In this chapter, I will select ship detail locations from the existing drawings referring to the experimental cases, apply the Length Scale method and LFEM curves to the selected components.

However, more engineering examples will be needed to clarify the method and engineers will have to understand the methodology and structural behaviour in order to properly apply it.

8.2 Structural Components Study

In the following, the fatigue strength of critical members of Panamax Bulk Carrier (Piano Delle Cpacita) and 50.000DWT Oil/Chemical Tanker (SHELL EXPANSION) is listed. The ship detail locations from the existing drawings are referred as the experimental cases, applying the Length Scale measurement. In a sole operation, it is going to extend to engineering guides, requiring definitions of critical locations.

Moreover, the components should be concluded into categories by the discontinuity locations, where usually from the ship's side or deck the cracks may occur and propagate relatively easily. Probably it is also needed specify bottom frames, deck orientate stiffeners and brackets to particular sides of e.g. a bulkhead plate. Finite element can be used as an alternative to compliance with the requirements of direct calculation procedures, including in cases of unusual side structure arrangements or framing to which the applications of this approach can be directly applied. In such cases, the analysis criteria and the strength check criteria are to be in accordance with the Rules of each Society's.

Finally, the peak / reference stress is used to calculate SCFs. The SCF are compared with FE extrapolation methods, including the results convergence studies.

8.2.1 Double Bottom Longitudinal

The first case study is double bottom construction detail. The web frame stiffener is selected from the bottom constructions where the bracket attachment adhesive to the longitudinal stiffener.

The double bottom details are shown in Figure 8.4, the location often experiences fatigue cracking as the result of stress fluctuations; and detail description of principal and secondary crack initiation positions is shown in Figure 8.5.

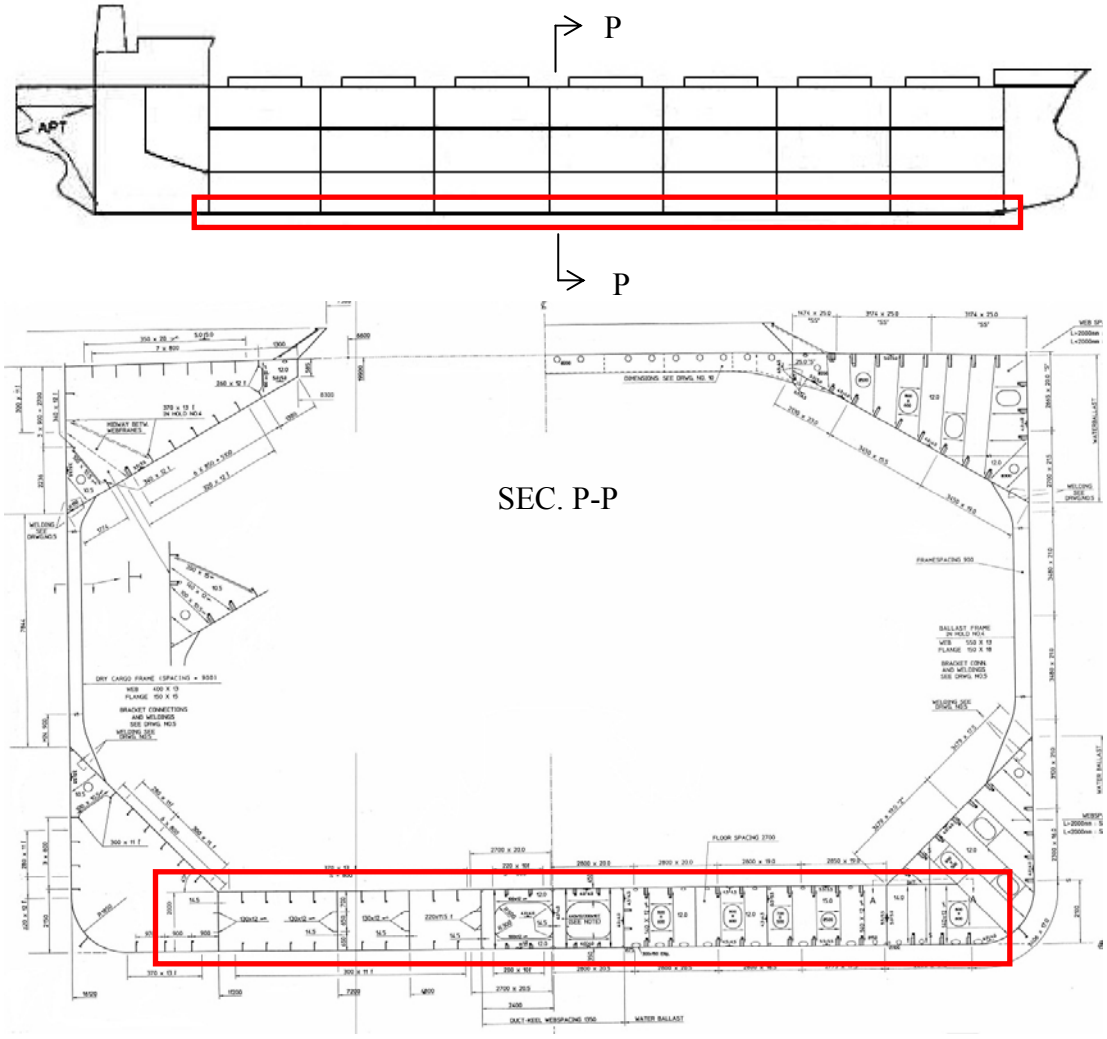

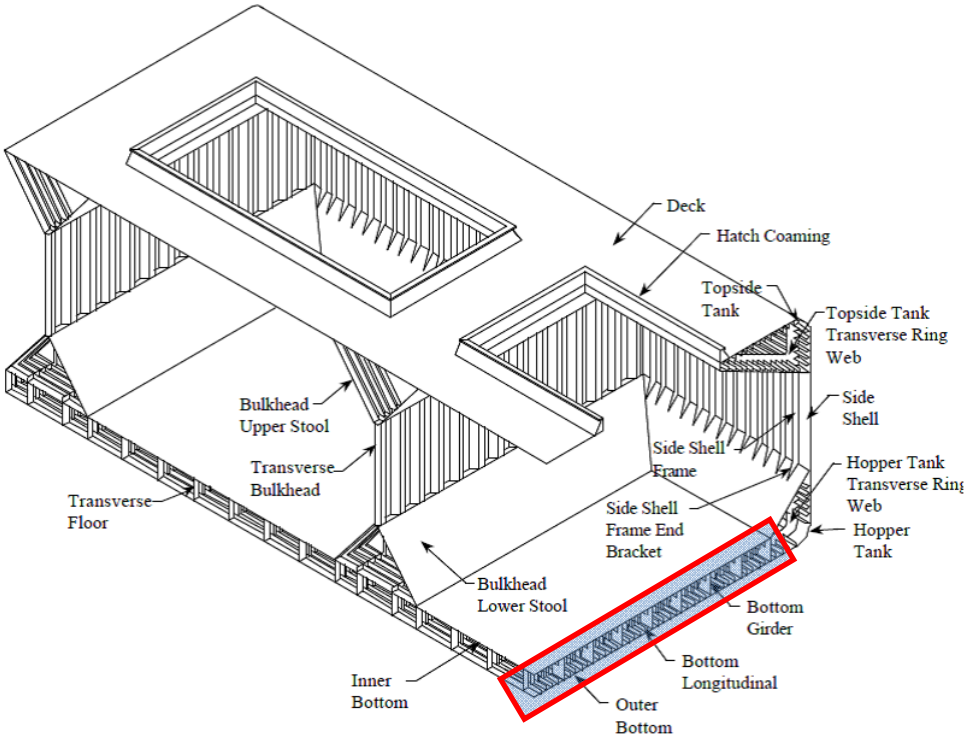

Figure 8.4 Sketch of ballast tank bottom longitudinal

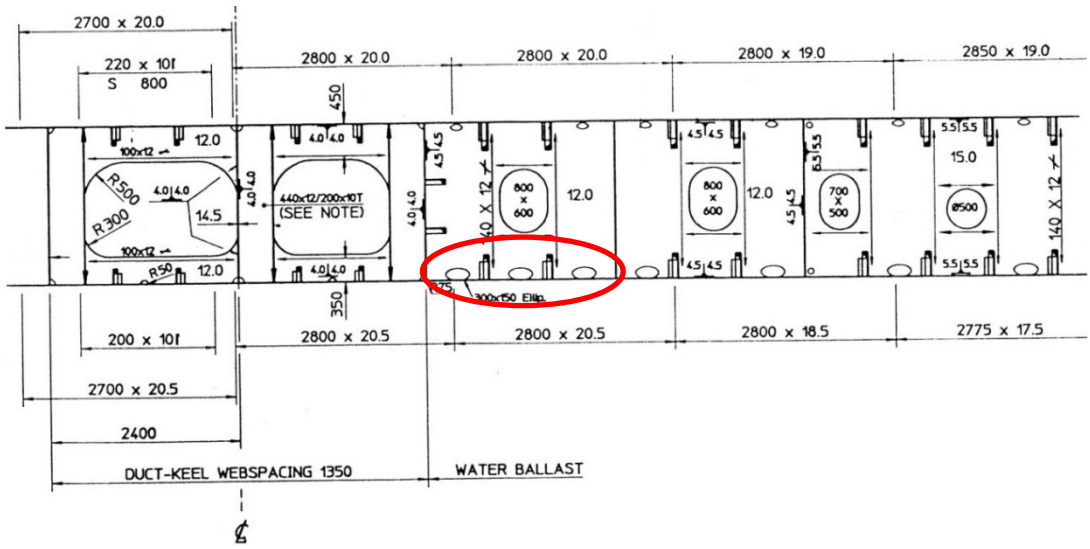

Figure 8.5 Detail description of Bottom Shell of Bulk Carriers

The hydrodynamic pressure acting on the bottom shell is due to local wave loading, in Figure 8.6.

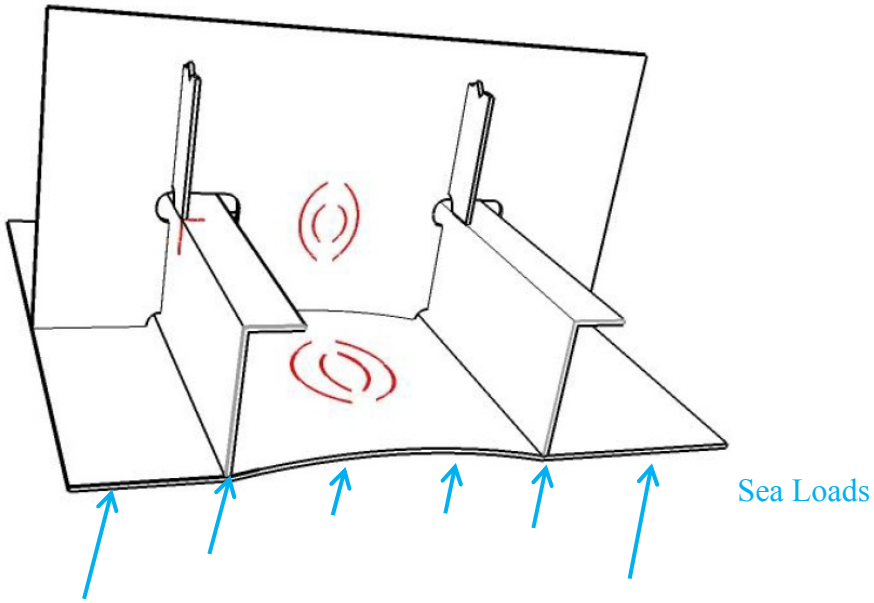

Figure 8.6 Sea Loads on the bottom shell of Bulk Carriers

Situation I: Bottom Longitudinal Frame Cracks

As shown in Figure 8.7, the crack is recognized as that initiated from the connection of the flange and girder, and then propagates along the flange plate and longitudinal frames. It is implicitly assumed that the corner position is enough to prevent root cracking of bottom longitudinal fatigue problems, as situation I.

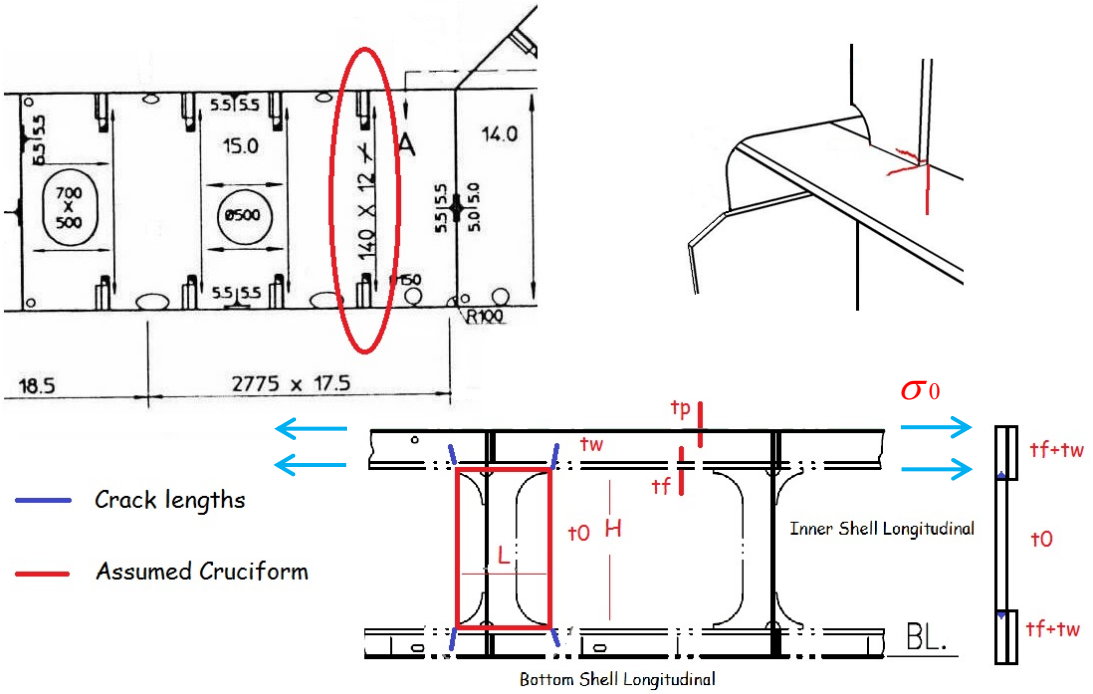

Figure 8.7 Situation I of cracks at bottom longitudinal frames

The stress concentration will be found at the connection end, and the geometry of bracket is the key factor affecting the crack initiations. For the case study of edge crack in the bottom longitudinal frames, the major loading can be recognized as the tensile load on the longitudinal. Even though, the bottom longitudinal can be addressed as the case of cruciform corner crack, for typical length scale measurements; and conversion rules have been given in Figure 8.7**Error! Reference source not found.**.

Table 8.1

Dimensions of the longitudinal stiffener frame

Component	Dimensions (mm)
Bottom Shell Plate	1000.0×3000.0
Girder	1000.0×1300.0
Longitudinal Frame	*L* 300.0×100.0×10.0
Triangle Bracket	100.0×100.0×10.0

Mouse Hole *R* 35.0

Dimensions of the longitudinal detail are listed in Table 8.1, and also marked in Figure 8.8; the longitudinal stiffener is a web frame stiffener on flat plate.

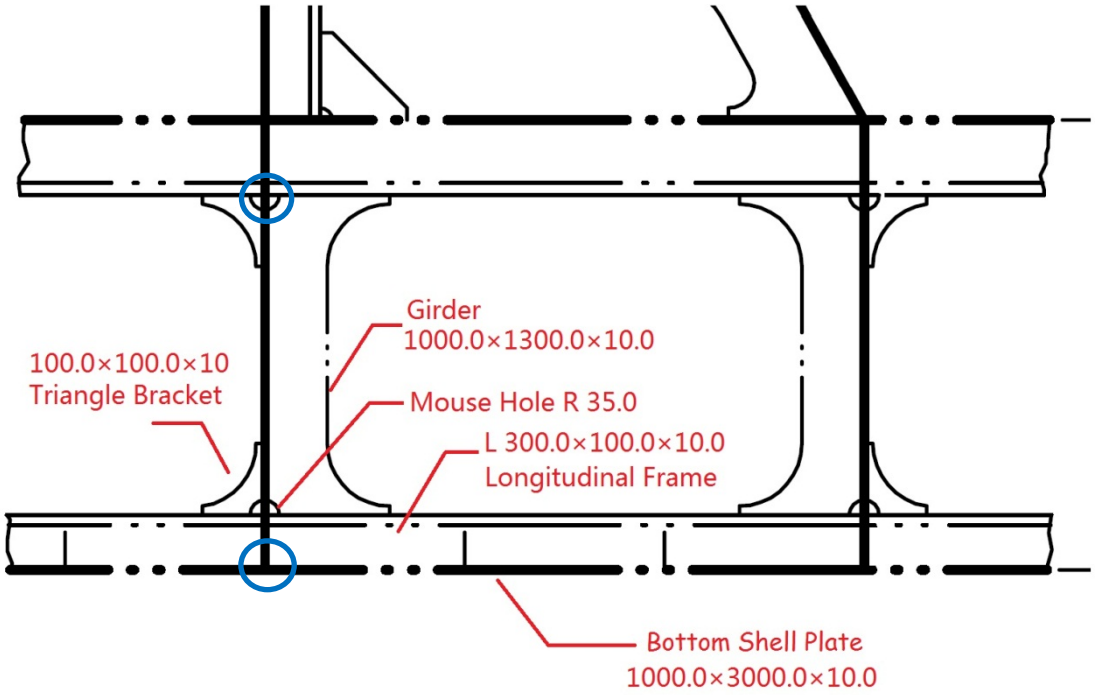

Figure 8.8 Dimensions on bottom longitudinal frames

The component can be considered as the cruciform having the geometry dimensions: height H 1.0 m and width 0.3 m, with the bracket 0.1 m (L=0.4m), assumed as the length of the cruciform corresponding to simple specimen. The thicknesses of the plate are 10mm separately; the thickness correction factor can be got by folding the flange. The Length Scale 'as' equals to 12.86 mm from the formula.

$$as = smallest\ of \quad ((300+100)/22\times(10/20)^{0.5},\quad 1000/3\times(10/20)^{0.87})$$

Here L is the length of Width+Bracket 400mm, and H is the height 1000mm;

the thickness correction factor is 1/2

Considering the critical distance point (1.2 mm) away from the corner, the value of SCF can be given as 2.22; if we check the LEFM curves against Length Scale, the value of SCF are found out equalling to 2.36.

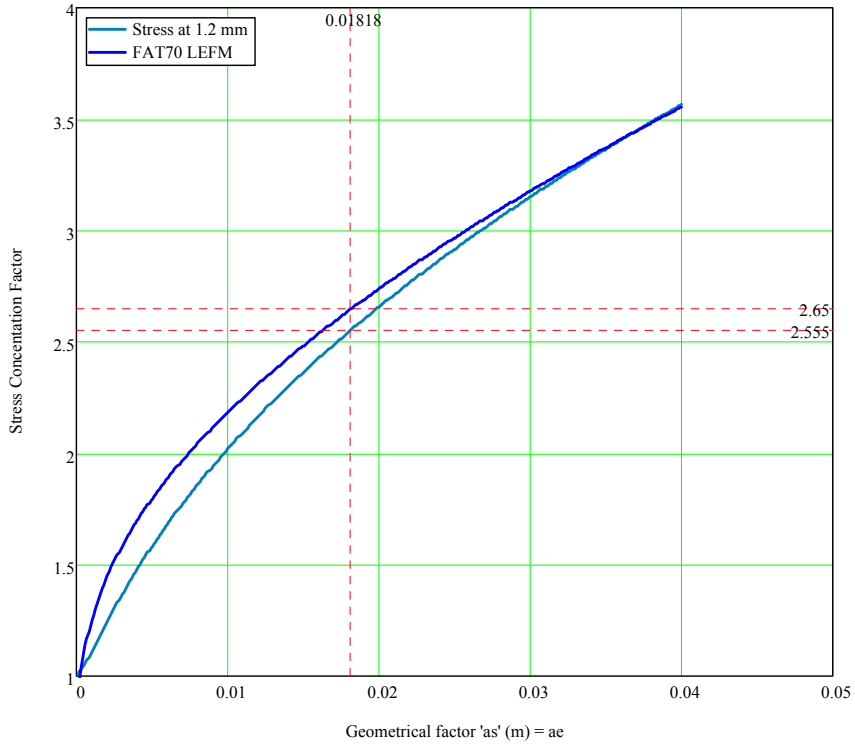

Figure 8.9 SCF Comparison of bottom longitudinal frame

Within the bottom shell longitudinal frames, the boundary condition is assumed symmetric between the stiffeners and between the web frames. The situation I case comparison will be on the ANSYS FE calculations. Both of the linear and quadratic extrapolation methods are got to take the hot-spot stress value, and the diagrammatic models are shown in Figure 8.10**Error! Reference source not found.**.

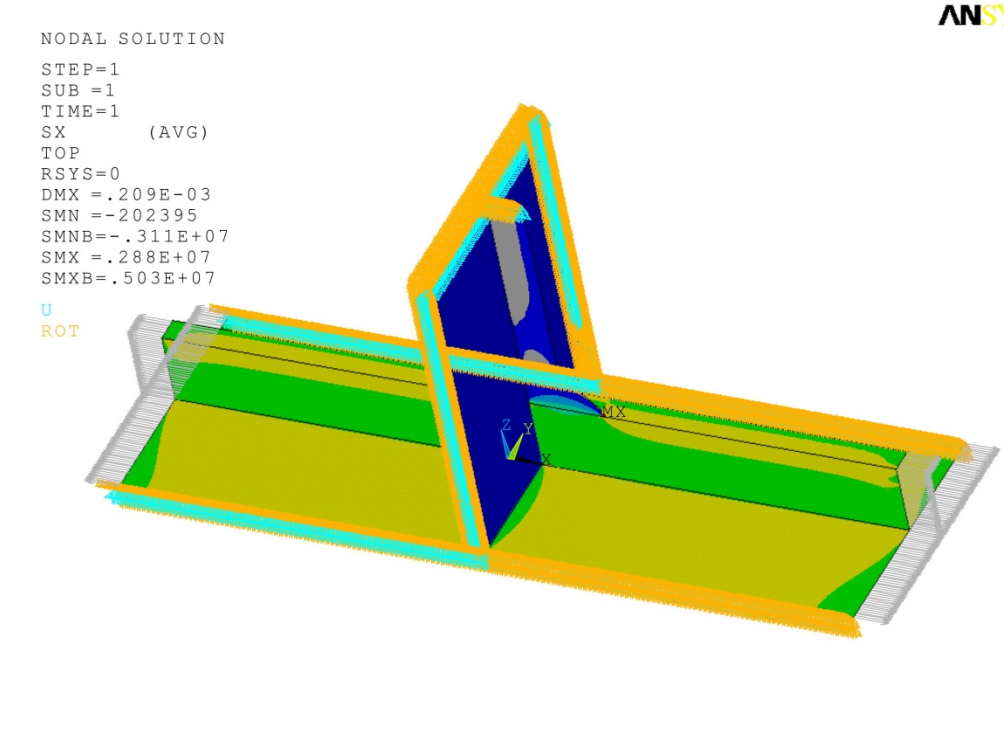

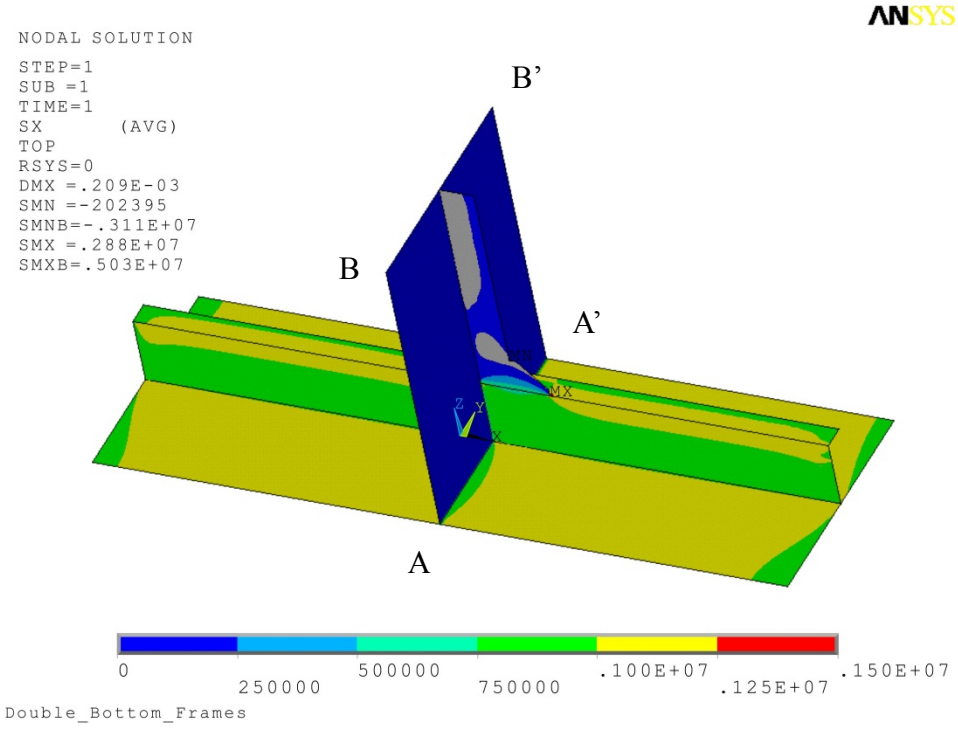

Figure 8.10 FE bottom longitudinal frames model

Moreover it should be confirmed that the shell FE mesh can be simulated by multi-surfaces; and the longitudinal plate is the relatively thick one, to be extended to the top-surface intersection. The mesh size for the FE model is 0.1t, which, based on the convergence discussion by authors in Chapter 4, will be fine enough to get the accurate stress concentration factors for design code purposes.

The hot spot stress based fatigue design is based on the linear or quadratic extrapolation method over 2 or 3 points in front of the crack initiation position (and on the surface). Based on the ANSYS calculation, the non-dimensional surface stress values (divided by nominal stress) are shown in Table 8.2.

Table 8.2
Surface Non-dimensional stress (divided by nominal one) for Extrapolations

	1st point	2nd point	3rd point	SCF
0.4/1.0t	2.089	1.641		2.39
4/8/12mm	2.089	1.715	1.592	2.71
0.5/1.5t	1.942	1.544		2.14
5/15mm	1.942	1.544		2.14

The stress concentration around the double bottom frame is predicted to have a value between 2.14-2.71; the SCF result found from the Length scale curve is 2.22, and from the LEFM is 2.36, in Figure 8.11.

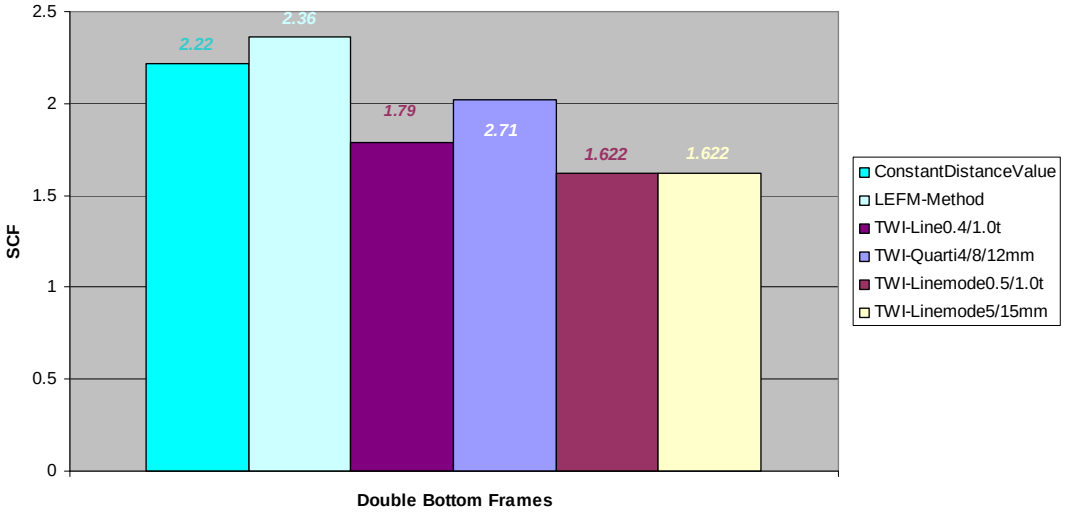

Figure 8.11 SCF results by various methods for the double bottom frames

Situation II: Bottom Longitudinal brackets Cracks

As shown in Figure 8.12, the cracks can be also found the connections of the girder and transverse plate, which can be recognized as secondary fatigue failure situation (Fatigue Failure Situation II). In this situation, the stress concentration will be found at the girder connection end, and the geometry of the frames will be the key factor affecting the crack generations. There may be the dimension definitions for the assumed cruciform, and rules for length scale measurement are also marked in Figure 8.12.

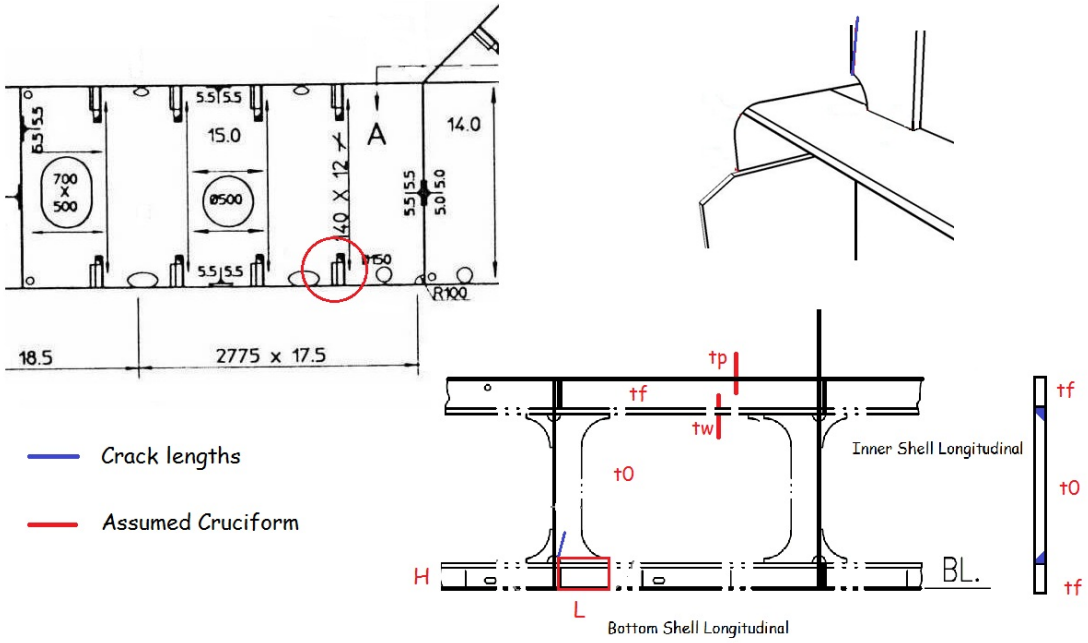

Figure 8.12 Situation II of cracks happen at bottom longitudinal brackets

For the case study of crack propagation along the girder, the major loading can be recognized as the tensile load on the transverse plate and the girder directions. Dimensions of the longitudinal detail are listed in Table 8.2.

The component can be considered to be a geometry transformation of a cruciform having: height H 0.3 m and width 0.3 m, with the bracket 0.1 m (L=0.4m), assumed as the length of the cruciform corresponding to simple specimen. The thicknesses of the plate are 10mm separately. The Length Scale 'as' equal to 18.18 mm based on the prediction formula, ignoring the thickness effect from the flange.

$$as = smallest\ of \quad ((300+100)/22, \quad 300/3)$$

Here L is the length of Width+Bracket 400mm, and H is the height of longitudinal frames 300mm

Considering the critical distance point (1.2 mm) away from the corner, the value of SCF can be given as 2.555; if we check the LEFM curves against Length Scale, the value of SCF are found out equalling to 2.65 in Figure 8.13.

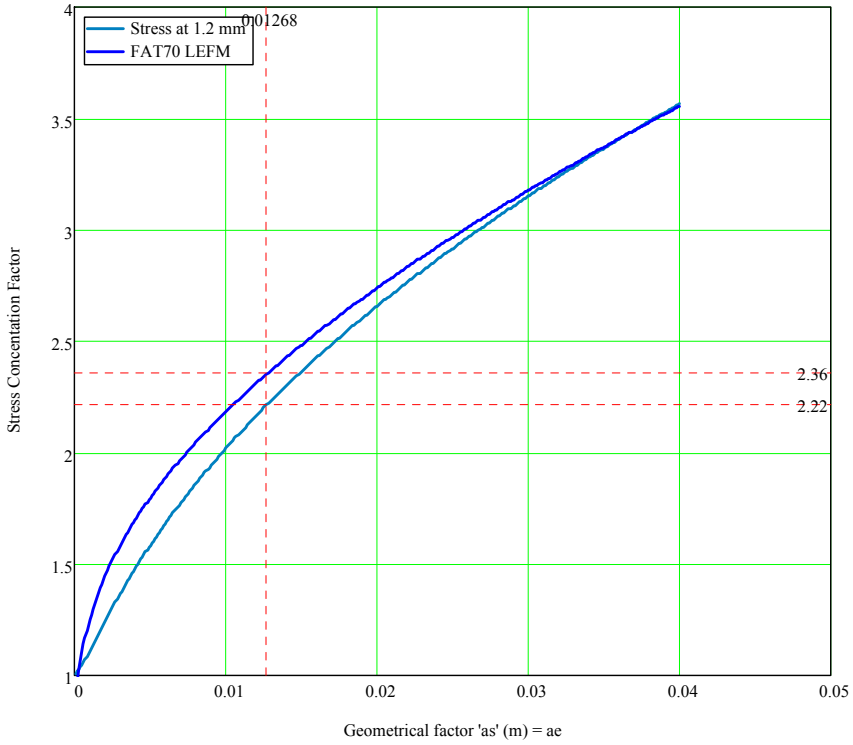

Figure 8.13 SCF Comparison of bottom longitudinal frame

8.2.2 Double Bottom Girders

The stool is to be fitted with diaphragms in line with the longitudinal double bottom girders for effective support of the corrugated bulkhead.

Where corrugations are cut at the lower stool, the weld connections of corrugations and stool side plating to the stool top plate is to be in accordance with.

The corrugated bulkheads used in bulk carriers are normally fitted with top and bottom stools.

Transverse bulkheads are constructed of corrugated steel plates, reinforced at the bottom and top connections with bottom and top stools.

The buckling analysis is to be carried out for the bottom panel between the hopper tank girder (margin girder) and the first double bottom girder inboard. The

allowable reduction (in mm) found by this analysis is to be applied for the other bottom plates as well.

The bottom girder structural details can be recognized as top deck girder connections, when the girder framing comes under heavy loading shown in Figure 8.14 and Figure 8.15, the girder buckled due to their reduced thickness. The supporting longitudinal girder gives rise to stress concentration locations requiring fatigue evaluation.

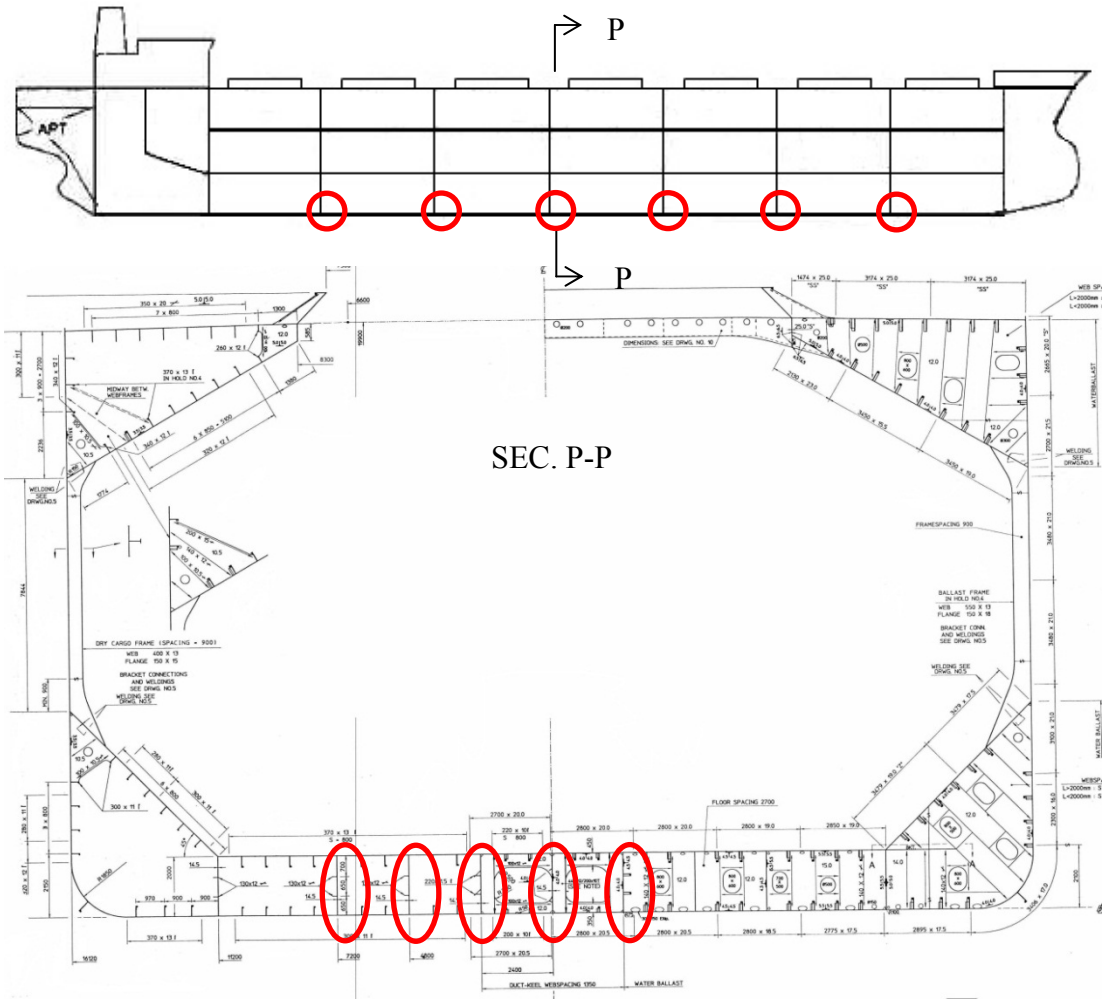

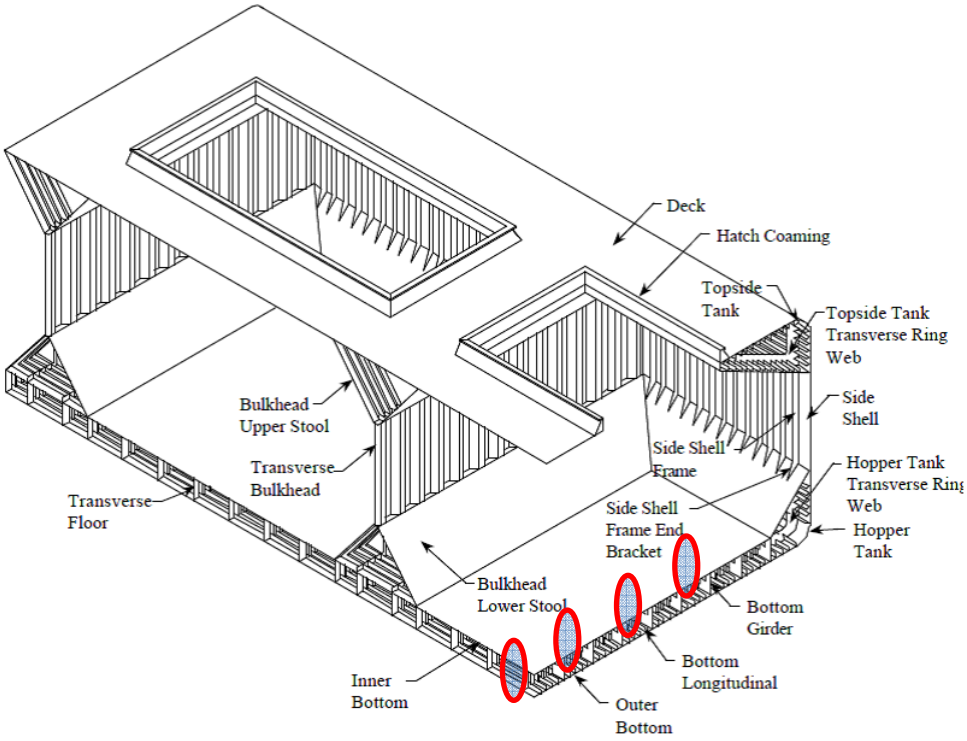

Figure 8.14 Sketch of Centre girder of Double bottom ballast tank

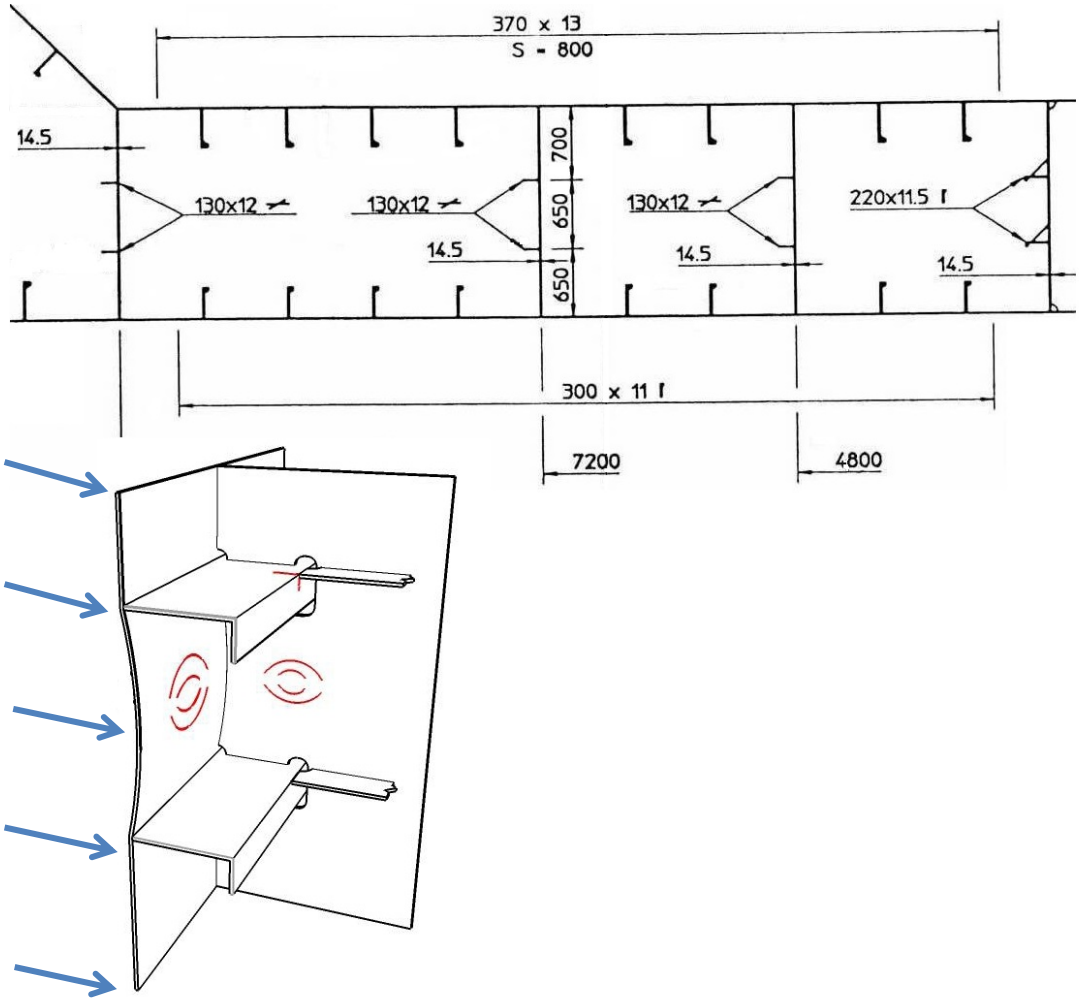

Figure 8.15 Detail description of Centre girder and web frame plating

Situation I: Cracks at the Connections of Centre line/side Girder

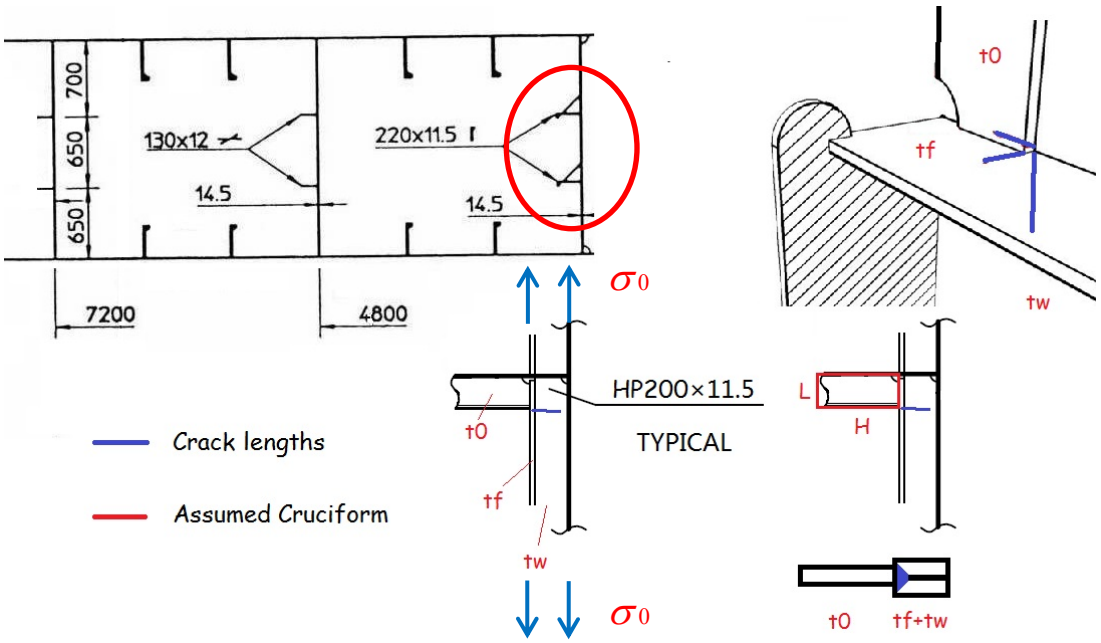

Figure 8.16 Situation I of Cracks at the Connections of Centre line/side Girder

Situation II: Cracks at the Connections of Centre line/side Girder

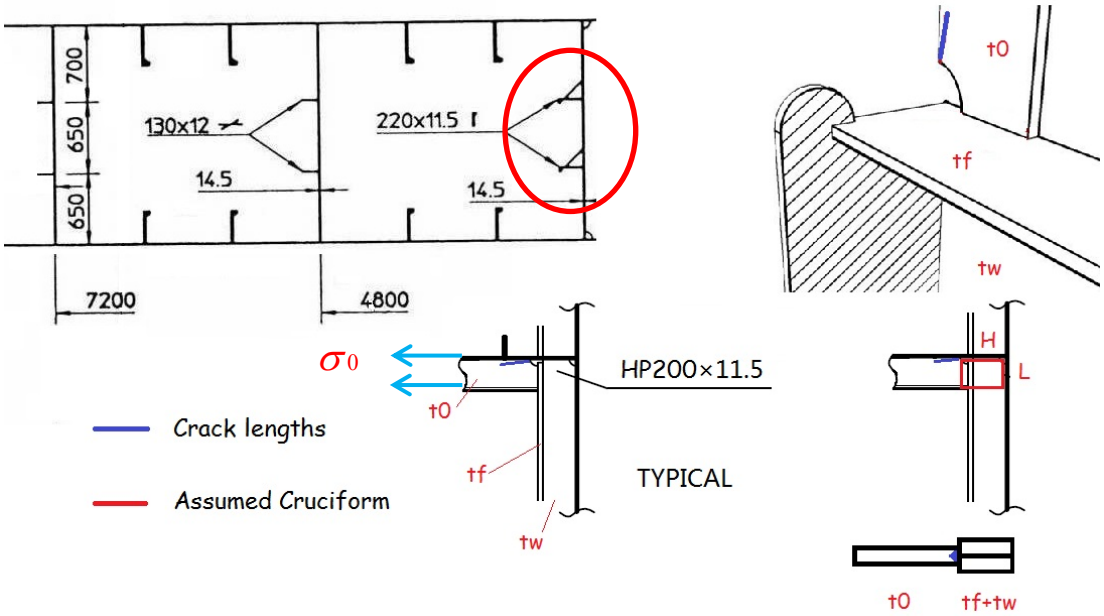

Figure 8.17 Situation II of Cracks at the Connections of Centre line/side Girder

8.2.3 Inner Double Bottom Frames

The structural details in the double-bottom construction are influenced by the lower water ballast load; fatigue cracks are tolerated at the connection between vertical brackets of the inner bottoms.

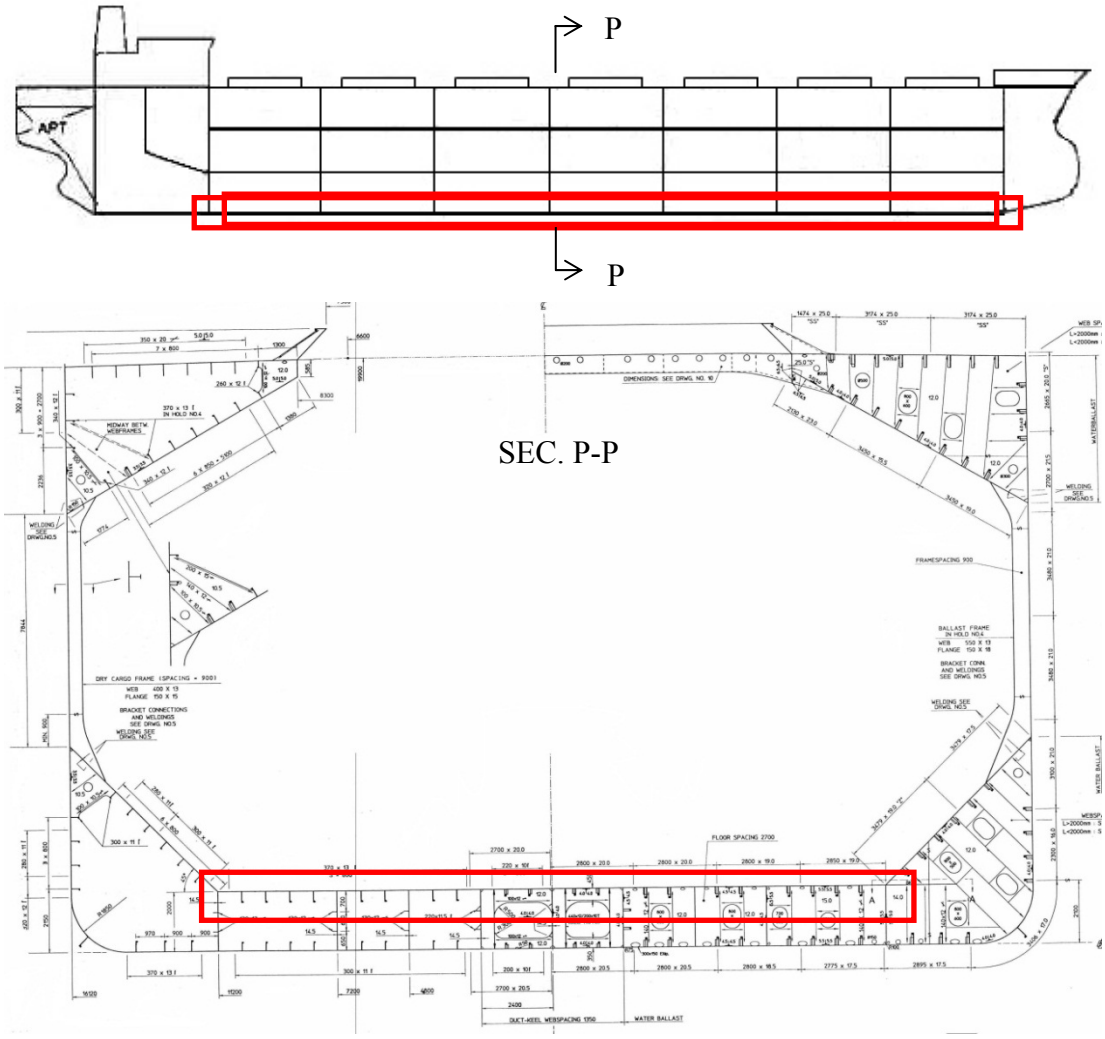

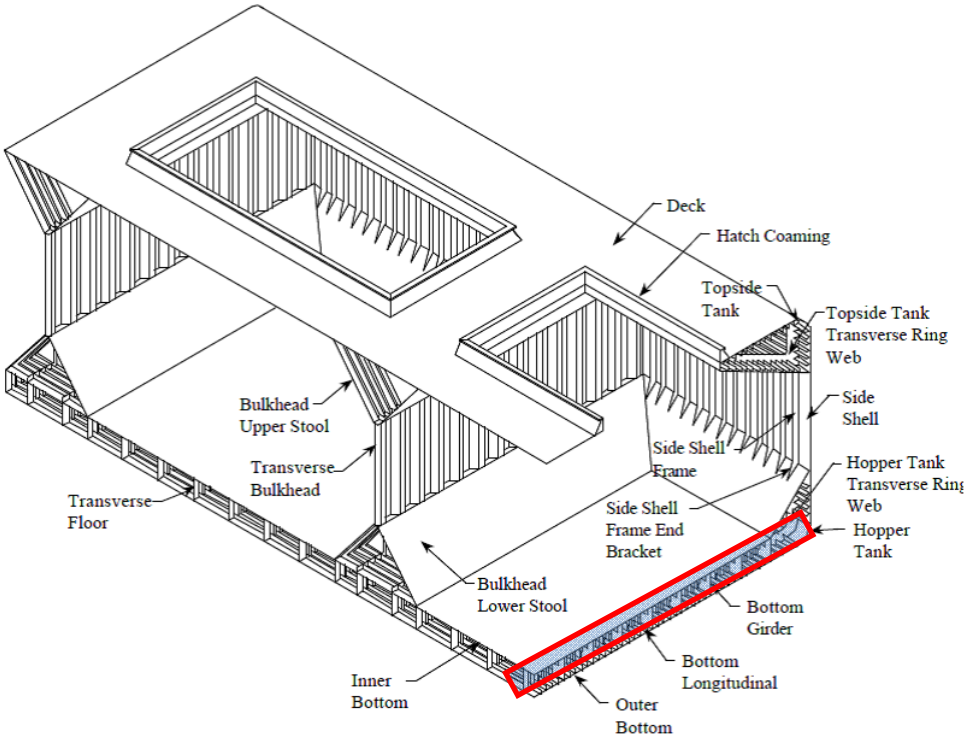

Figure 8.18 Sketch of Inner Bottom, Web frame plating

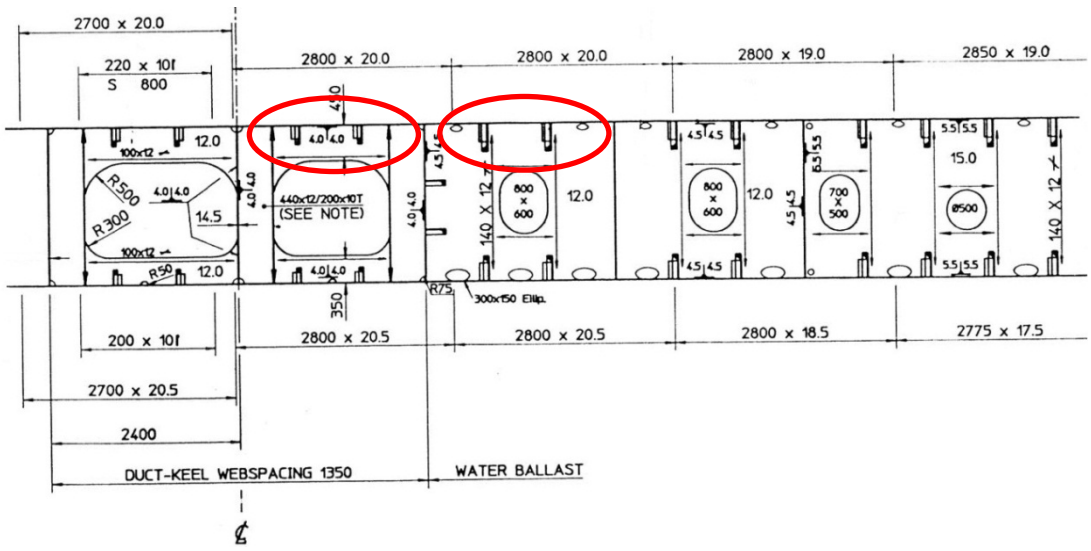

Figure 8.19 Detail description of Inner Bottom, Web frame plating

By comparing various stress amplitude values, large differences are found between our methods and extrapolated hot spot approaches. For the deck connections, the extrapolation method will give larger values. It is abnormal that the SCF increased to such high value at the connection of side frames and decks, because of that the fatigue cracks are not initiated from deck locations first. It is the disadvantage of the surface stress extrapolation. The Length Scale methods are less conservative.

A number of cracks exposed to fatigue failure can be found at the bulkheads of ships and the bulwark constructions, as shown in Figure 8.20

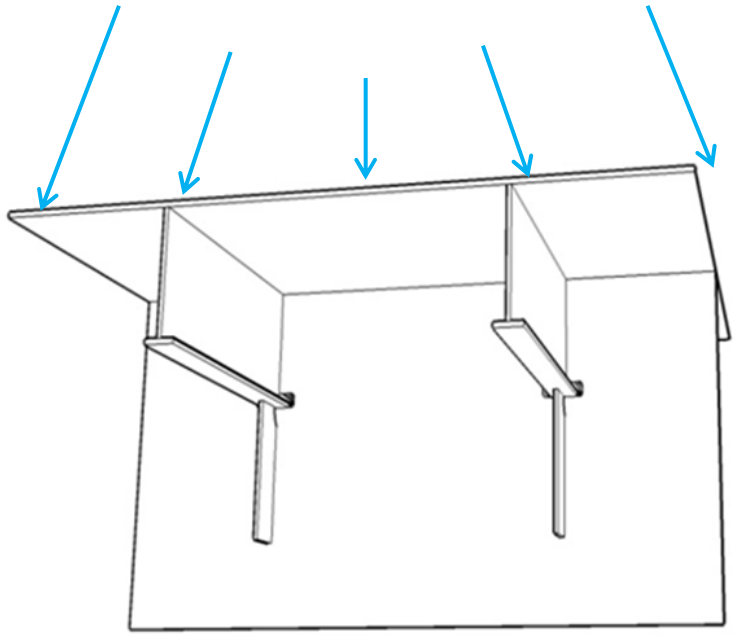

Figure 8.20 Gunwale Framing Constructions

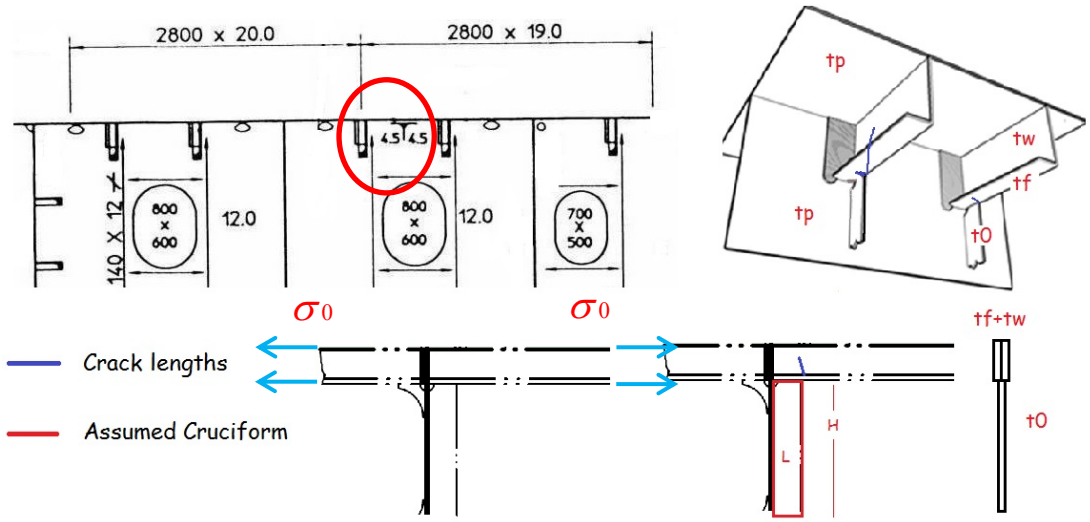

Figure 8.21 Cracks at Gunwale Framing Constructions

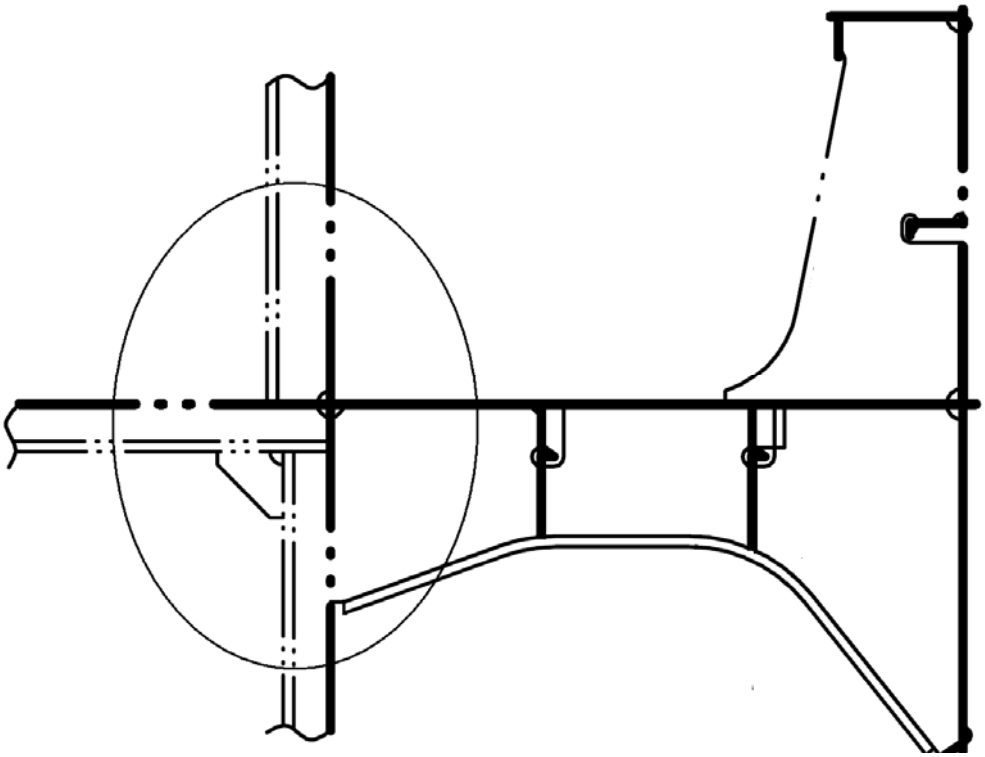

Figure 8.22 Gunwale Framing Constructions Details

The discontinuous stiffener flanges lead to stress concentrations. The rat (mouse) hole is necessary by the demand of fabricated manufacture process.

The FE model is shown in Figure 8.23.

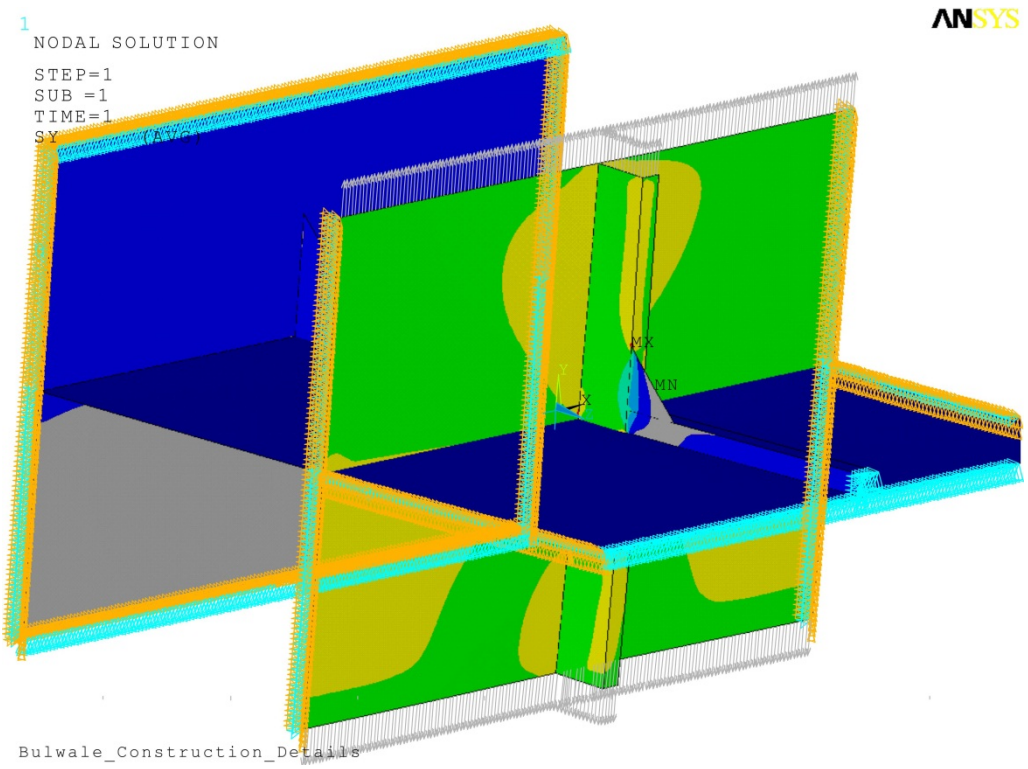

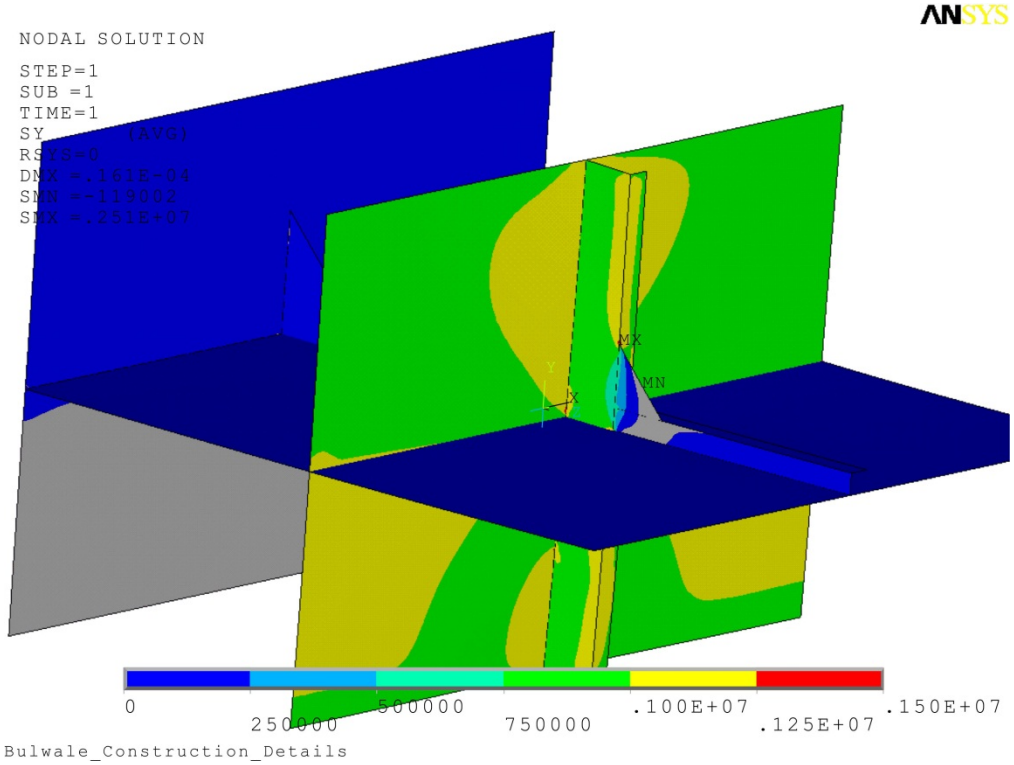

Figure 8.23 Gunwale Frames Constructions FE results

The chosen connection of a web frame corresponding to the side tank plate, where the width of plate included in full-scale specimen. The distance between sides longitudinal was 2000mm. The side shell was 10mm thick and the transverse frames are 10mm thick. L-section is used for the longitudinal stiffener: bracket $250mm \times 250mm$, thickness 10mm, and flat bar is $150 \times 90 \times 10mm$ used as buckling stiffener.

The shape can be found in the test specimen similar with the cruciform geometry, it provides guidance on possible theoretical prediction to achieve the stress concentration target. From the drawing of specimen, H is assumed as 0.4m and L is 2.0m approximately; the Length Scale can be derived as 12.86mm leading to SCF, 2.22, and 2.36 (LEFM).

$$as = smallest\ of \quad ((250+150)/22 \cdot (10/20)^{0.5}, \quad 2000/3 \cdot (10/20)^{0.87})$$

Here L is the length of Width+Bracket length 400mm, and H is the height 2000mm, the thickness correction factor is (10/20);

Alternatively, stress linearization leads to the exclusion of the local stress peak in plate or shell structures. No guides are available for determining usable stress value from these FEA results.

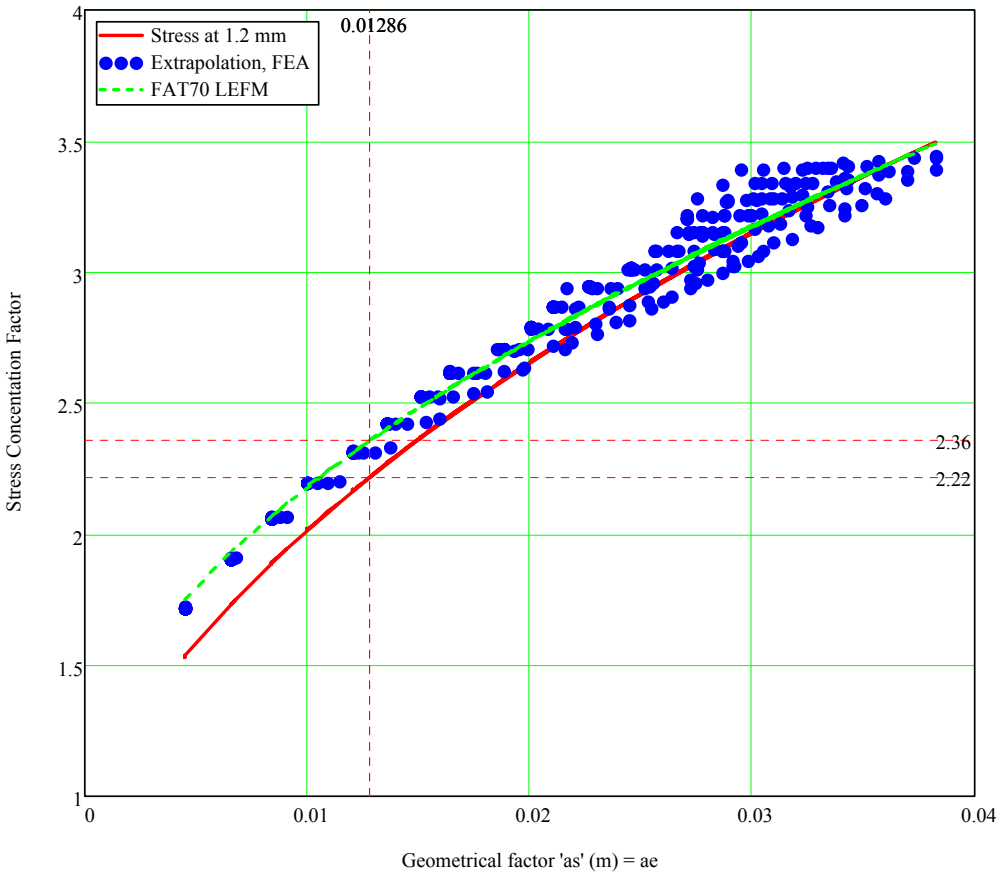

Figure 8.24 Comparison of SCF of Bulwale Construction Details

A comparison of the various stress amplitude values is shown in Figure 8.25, little differences are found between our methods and the extrapolated method in the detail.

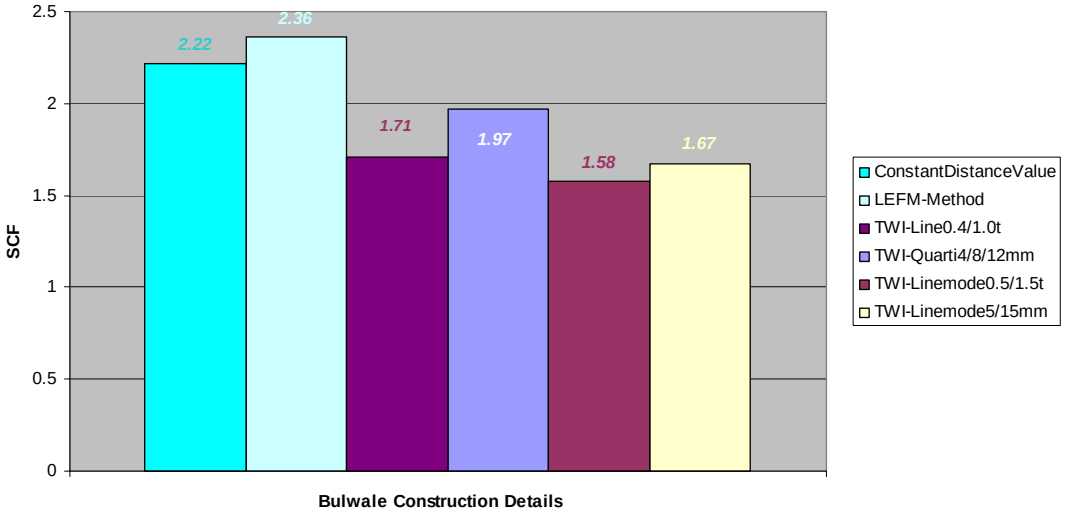

Figure 8.25 SCF results by various methods for the gunwale frames

8.2.4 Double Bottom Ballast Tank Longitudinal

The details of Oil Tanker are concluding connection and stiffener type of ballast tank and cargo tank; the gusset shape, gusset edge stiffening and knife edge crossings still remain as the most trouble structural details.

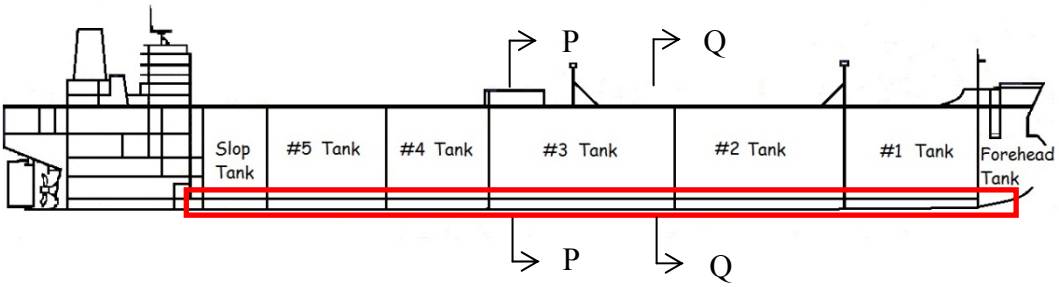

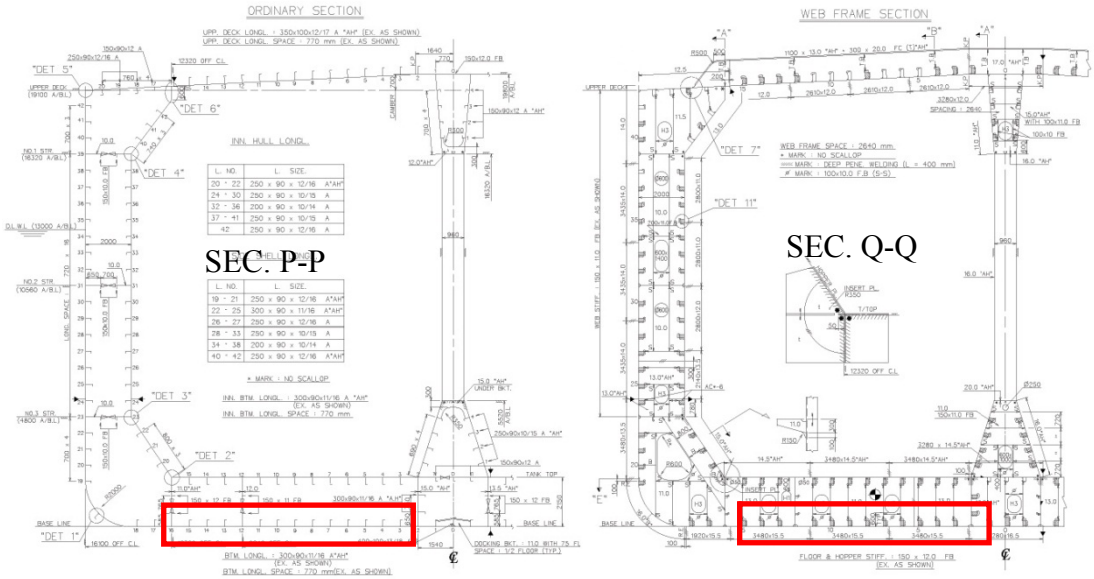
ORDINARY SECTION
SEC. P-P
WEB FRAME SECTION
SEC. Q-Q

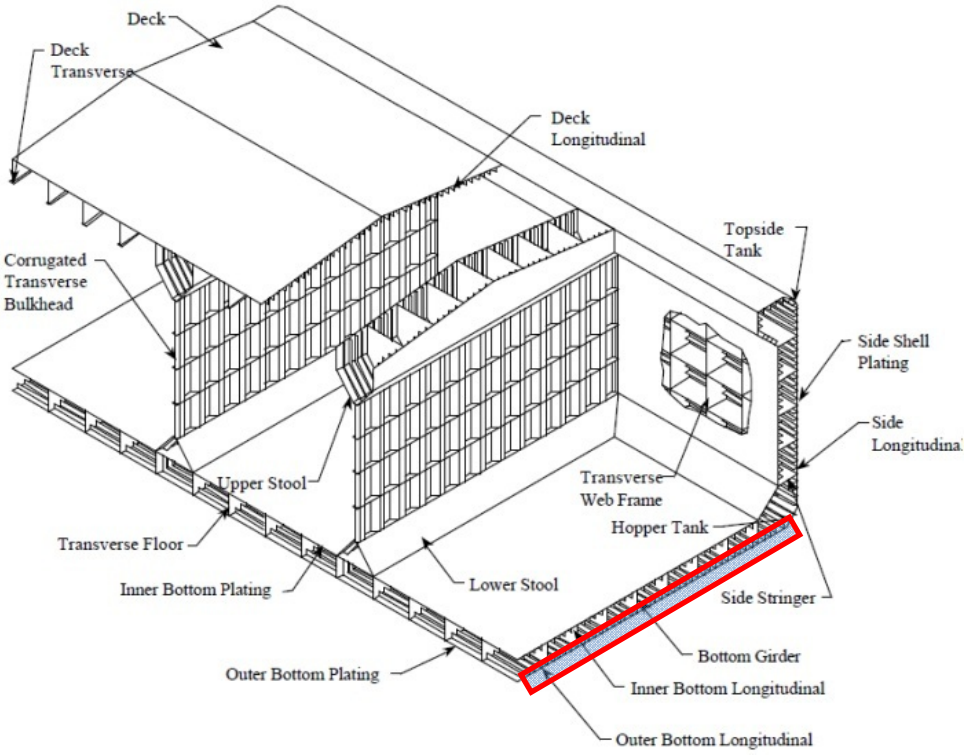
Deck
Deck Transverse
Deck Longitudinal
Topside Tank
Corrugated Transverse Bulkhead
Side Shell Plating
Side Longitudina
Upper Stool
Transverse Web Frame
Hopper Tank
Transverse Floor
Inner Bottom Plating
Lower Stool
Side Stringer
Bottom Girder
Outer Bottom Plating
Inner Bottom Longitudinal
Outer Bottom Longitudinal

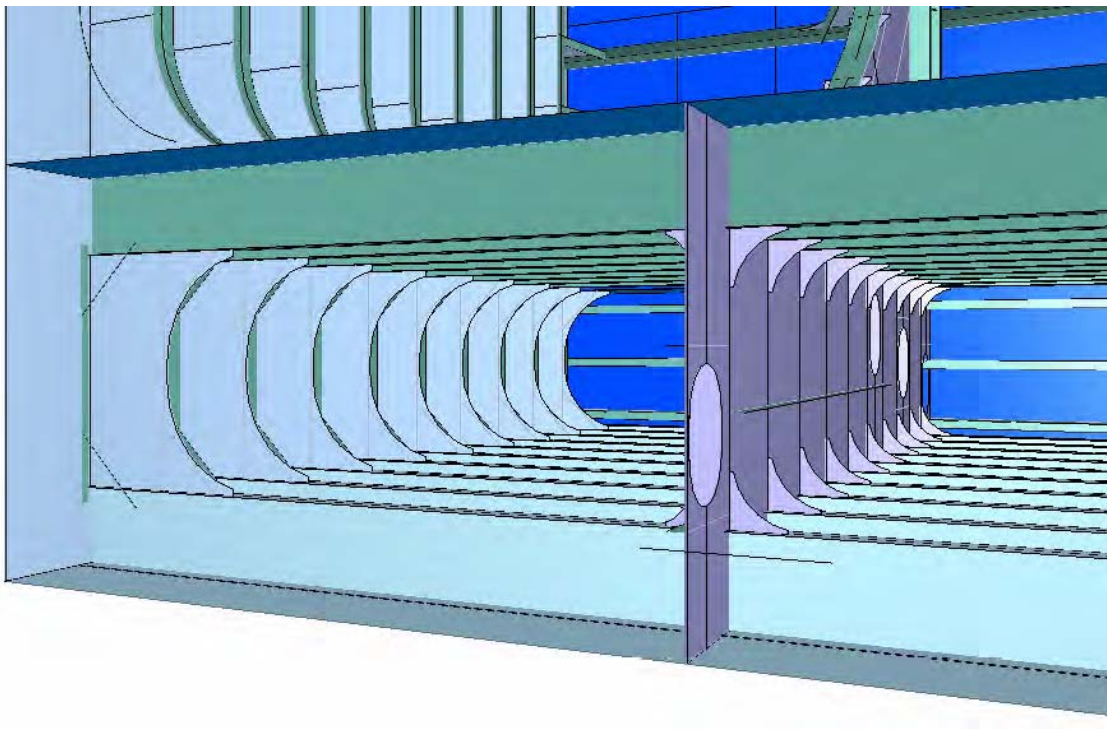

Figure 8.26 Sketch of Ballast Tank Bottom

The hydrodynamic pressure acting on the bottom shell is due to local wave loading, in Figure 8.27.

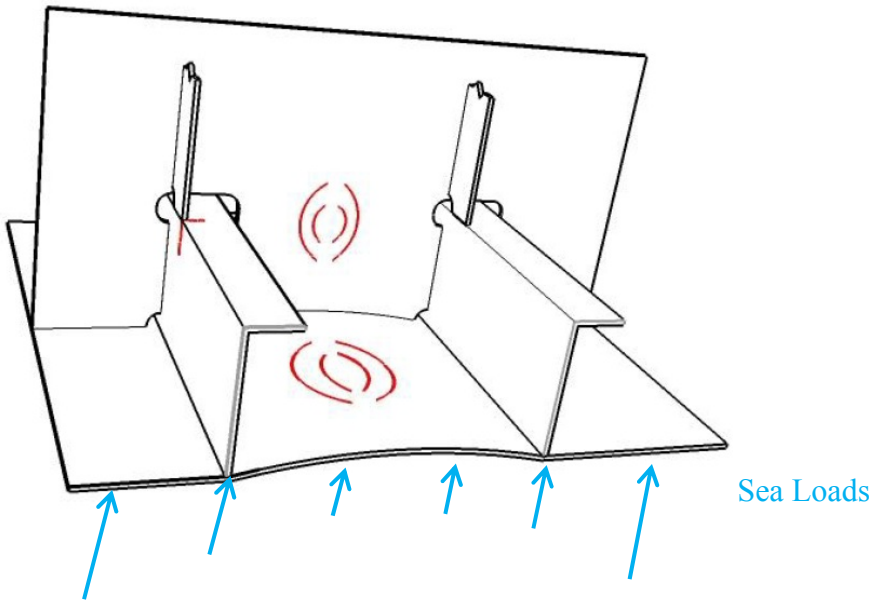

Figure 8.27 Sea Loads on the bottom shell of Bulk Carriers

Situation I:

As shown in Figure 8.28, the crack is recognized as that initiated from the connection of the flange and girder, and then propagates along the flange plate and longitudinal frames. It is implicitly assumed that the corner position is enough to prevent root cracking of bottom longitudinal fatigue problems, as situation I.

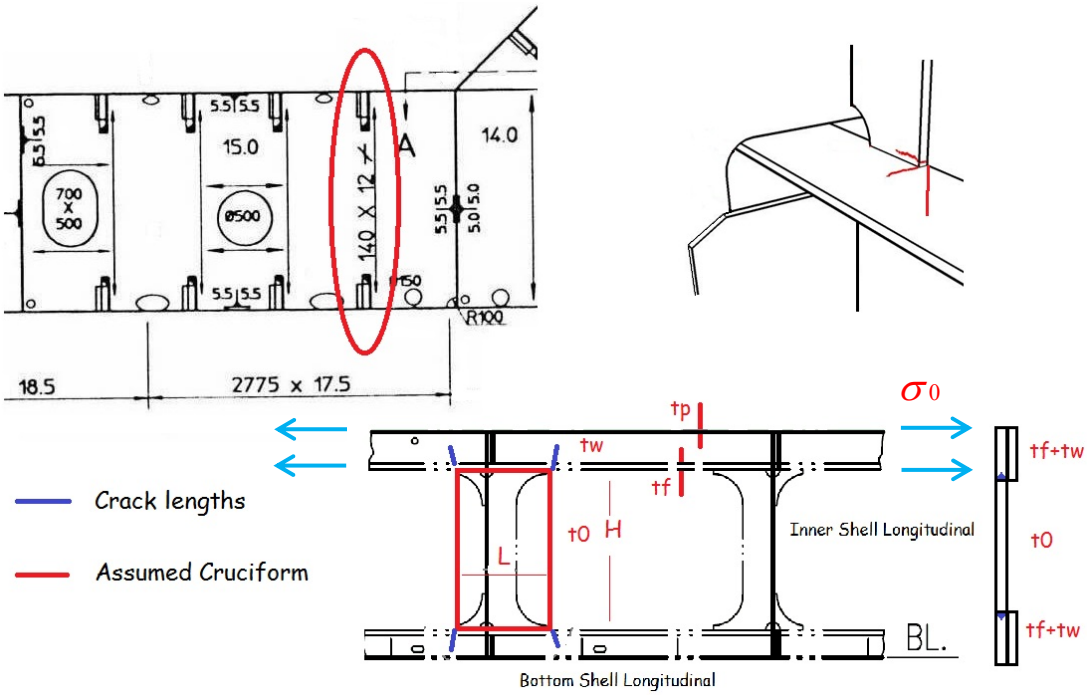

Figure 8.28 Situation I of cracks at bottom longitudinal frames

The stress concentration will be found at the connection end, and the geometry of bracket is the key factor affecting the crack initiations. For the case study of edge crack in the bottom longitudinal frames, the major loading can be recognized as the tensile load on the longitudinal. Even though, the bottom longitudinal can be addressed as the case of cruciform corner crack, for typical length scale measurements; and conversion rules have been given in Figure 8.28.

Dimensions of the longitudinal detail are listed in Table 8.3, and also marked in

Figure 8.29; the longitudinal stiffener is a web frame stiffener on flat plate.

Table 8.3

Dimensions of the longitudinal stiffener frame

Component	Dimensions (mm)
Bottom Shell Plate	1000.0×3000.0
Girder	1000.0×1300.0
Longitudinal Frame	*L* 300.0×100.0×10.0
Triangle Bracket	100.0×100.0×10.0
Mouse Hole	*R* 35.0

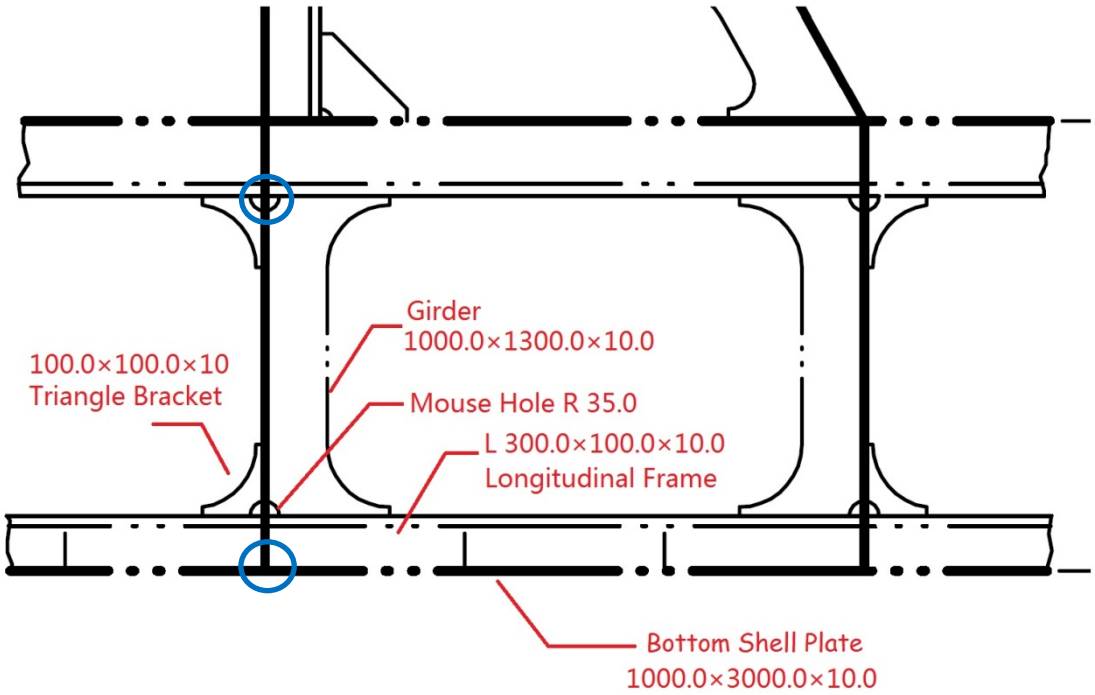

Figure 8.29 Dimensions on bottom longitudinal frames

The component can be considered as the cruciform having the geometry dimensions: height H 1.0 m and width 0.3 m, with the bracket 0.1 m (L=0.4m), assumed as the length of the cruciform corresponding to simple specimen. The

thicknesses of the plate are 10mm separately; the thickness correction factor can be got by folding the flange. The Length Scale 'as' equals to 12.86 mm from the formula.

$$as = smallest\ of\quad ((300+100)/22\times(10/20)^{0.5},\quad 1000/3\times(10/20)^{0.87})$$

Here L is the length of Width+Bracket 400mm, and H is the height 1000mm;

the thickness correction factor is $(10/20)$

Considering the critical distance point (1.2 mm) away from the corner, the value of SCF can be given as 2.22; if we check the LEFM curves against Length Scale, the value of SCF are found out equalling to 2.36.

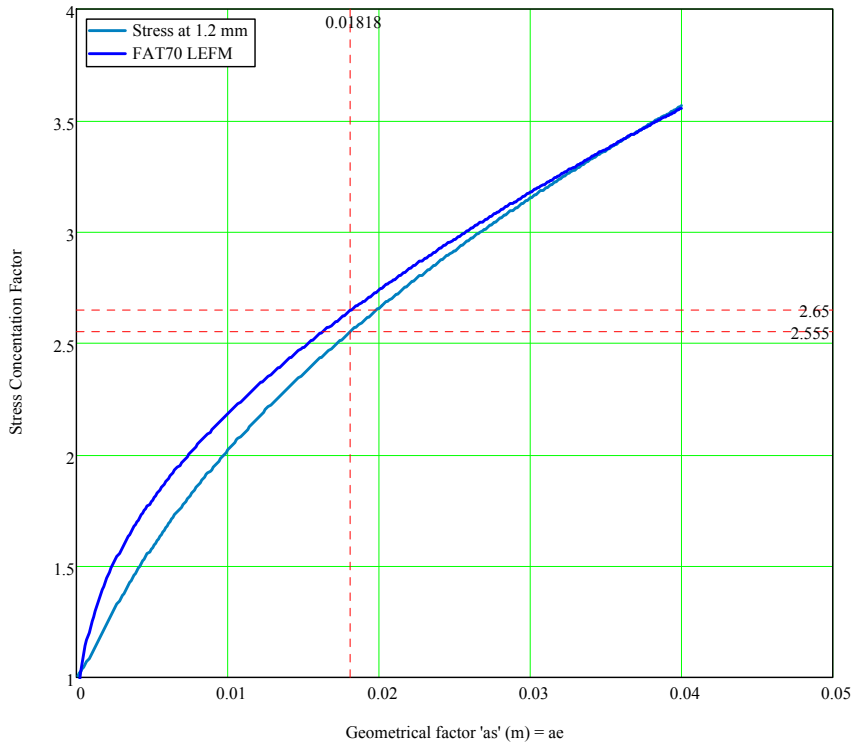

Figure 8.30 SCF Comparison of bottom longitudinal frame

Within the bottom shell longitudinal frames, the boundary condition is assumed symmetric between the stiffeners and between the web frames. The situation I case comparison will be on the ANSYS FE calculations. Both of the linear and quadratic extrapolation methods are got to take the hot-spot stress value, and the diagrammatic models are shown in Figure 8.31.

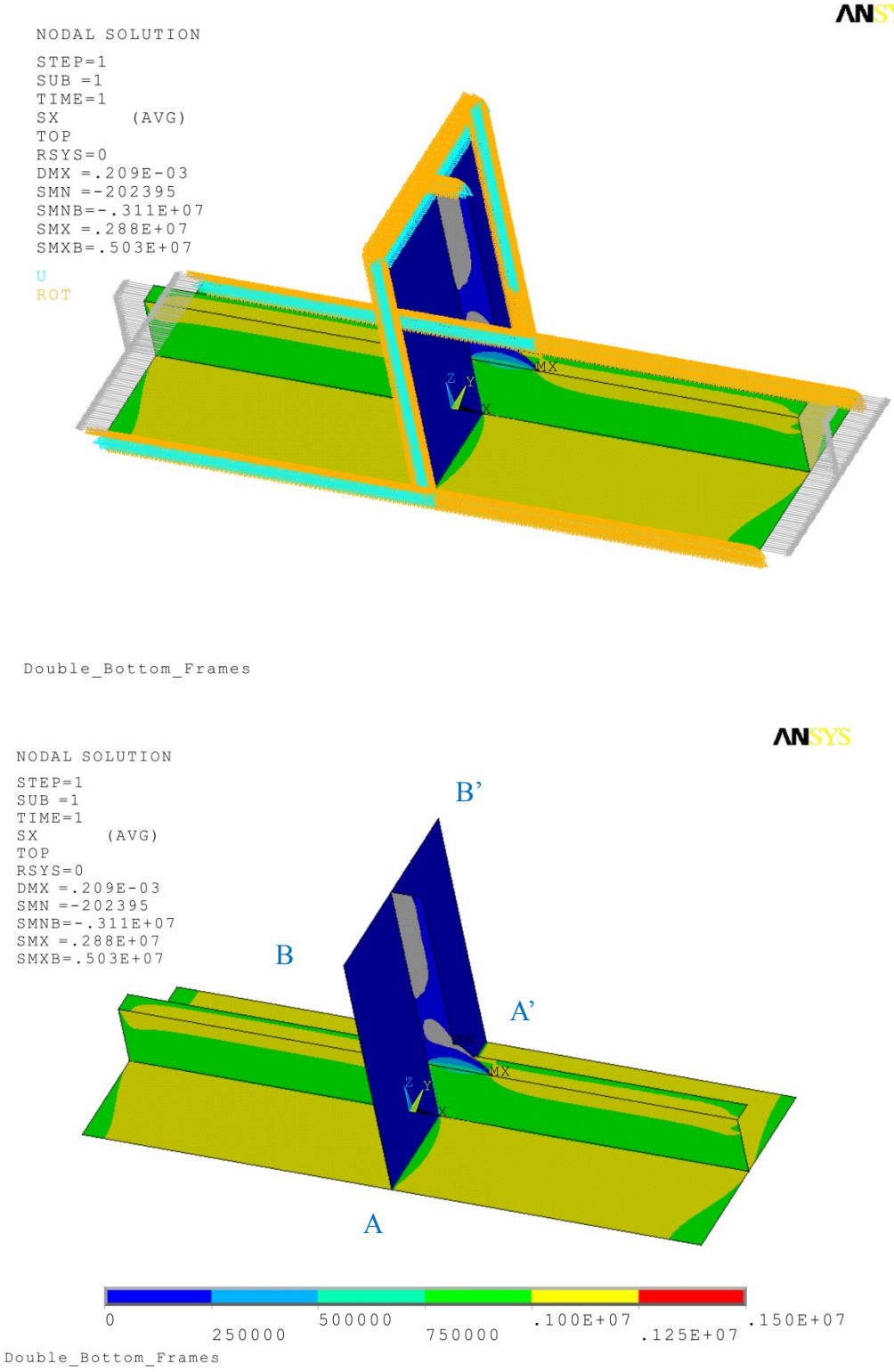

Figure 8.31 FE bottom longitudinal frames model

Moreover it should be confirmed that the shell FE mesh can be simulated by multi-surfaces; and the longitudinal plate is the relatively thick one, to be extended to the top-surface intersection. The mesh size for the FE model is 0.1t, which, based on the convergence discussion by authors in Chapter 4, will be fine enough to get the accurate stress concentration factors for design code purposes.

The hot spot stress based fatigue design is based on the linear or quadratic extrapolation method over 2 or 3 points in front of the crack initiation position (and on the surface). Based on the ANSYS calculation, the non-dimensional surface stress values (divided by nominal stress) are shown in Table 8.4.

Table 8.4
Surface Non-dimensional stress (divided by nominal one) for Extrapolations

	1st point	2nd point	3rd point	SCF
0.4/1.0t	2.089	1.641		2.39
4/8/12mm	2.089	1.715	1.592	2.71
0.5/1.5t	1.942	1.544		2.14
5/15mm	1.942	1.544		2.14

The stress concentration around the double bottom frame is predicted to have a value between 2.14-2.71; the SCF result found from the Length scale curve is 2.22, and from the LEFM is 2.36, in Figure 8.32.

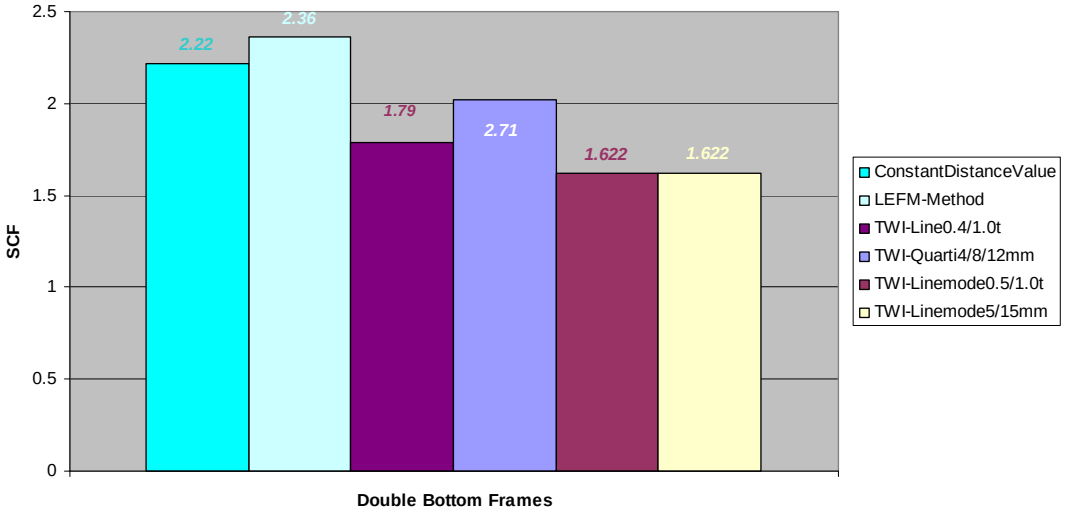

Figure 8.32 SCF results by various methods for the double bottom frames

Situation II:

As shown in Figure 8.33, the cracks can be also found the connections of the girder and transverse plate, which can be recognized as secondary fatigue failure situation (Fatigue Failure Situation II). In this situation, the stress concentration will be found at the girder connection end, and the geometry of the frames will be the key factor affecting the crack generations. There may be the dimension definitions for the assumed cruciform, and rules for length scale measurement are also marked in Figure 8.33.

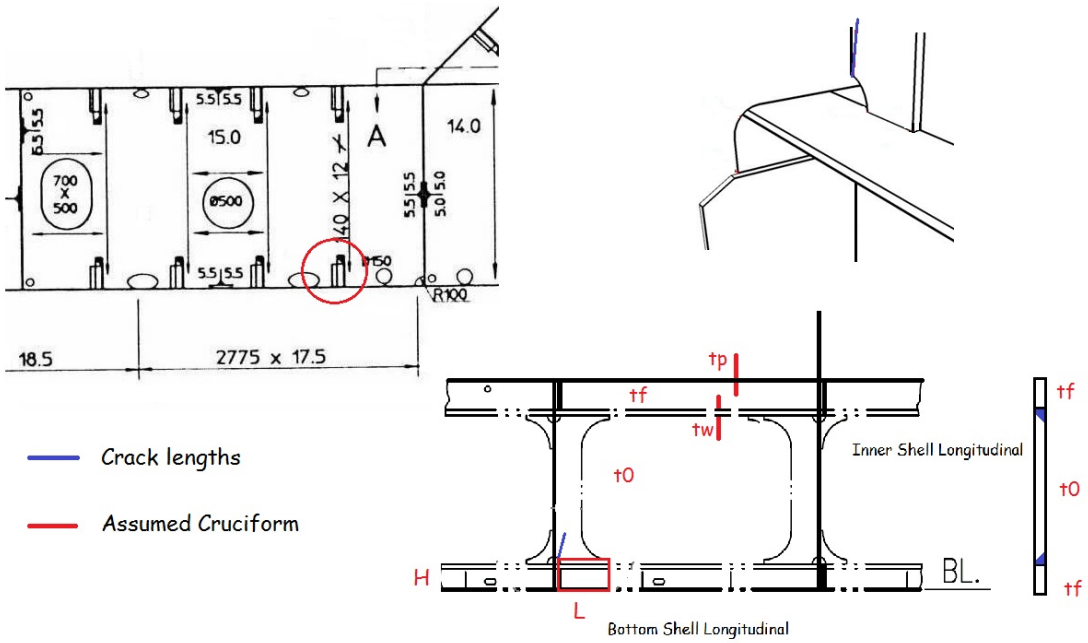

Figure 8.33 Situation II of cracks happen at bottom longitudinal brackets

For the case study of crack propagation along the girder, the major loading can be recognized as the tensile load on the transverse plate and the girder directions. Dimensions of the longitudinal detail are listed in Table 8.4.

The component can be considered to be a geometry transformation of a cruciform having: height H 0.3 m and width 0.3 m, with the bracket 0.1 m (L=0.4m),

assumed as the length of the cruciform corresponding to simple specimen. The thicknesses of the plate are 10mm separately. The Length Scale 'as' equal to 18.18 mm based on the prediction formula, ignoring the thickness effect from the flange.

$$as = smallest\ of\quad ((300+100)/22,\quad 300/3)$$

Here L is the length of Width+Bracket 400mm, and H is the height of longitudinal frames 300mm

Considering the critical distance point (1.2 mm) away from the corner, the value of SCF can be given as 2.555; if we check the LEFM curves against Length Scale, the value of SCF are found out equalling to 2.65 in Figure 8.34

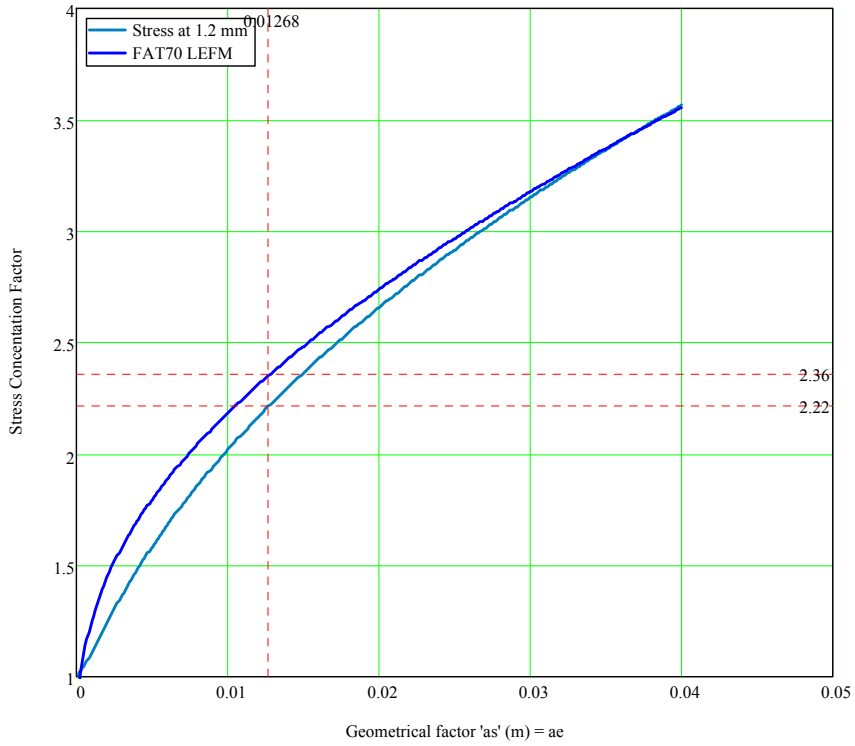

Figure 8.34 SCF Comparison of bottom longitudinal frame

8.2.5 Ballast Tank Side Shell

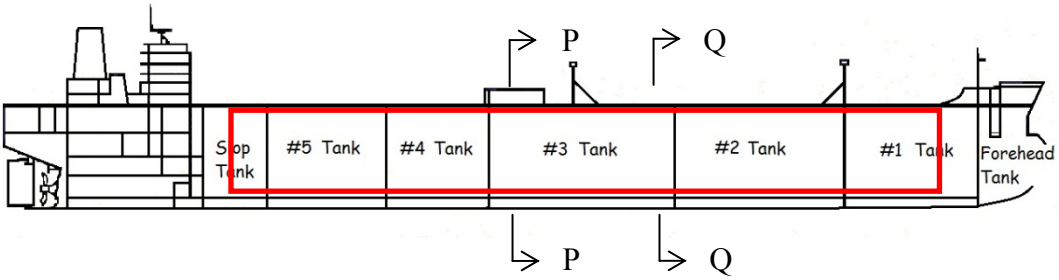

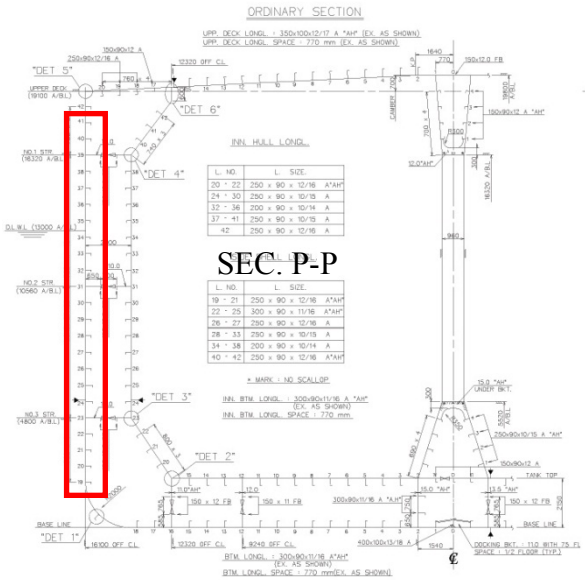

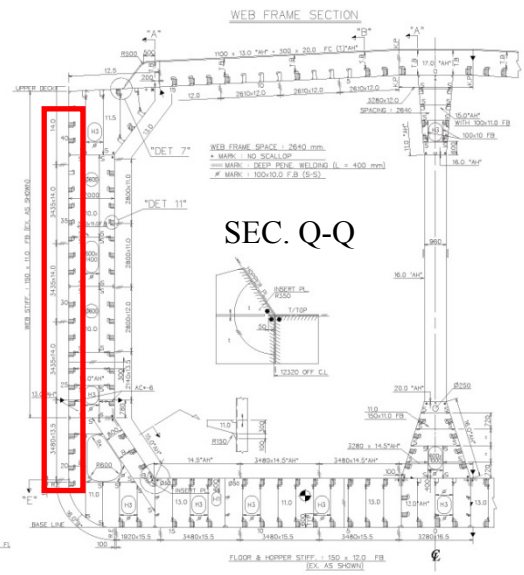

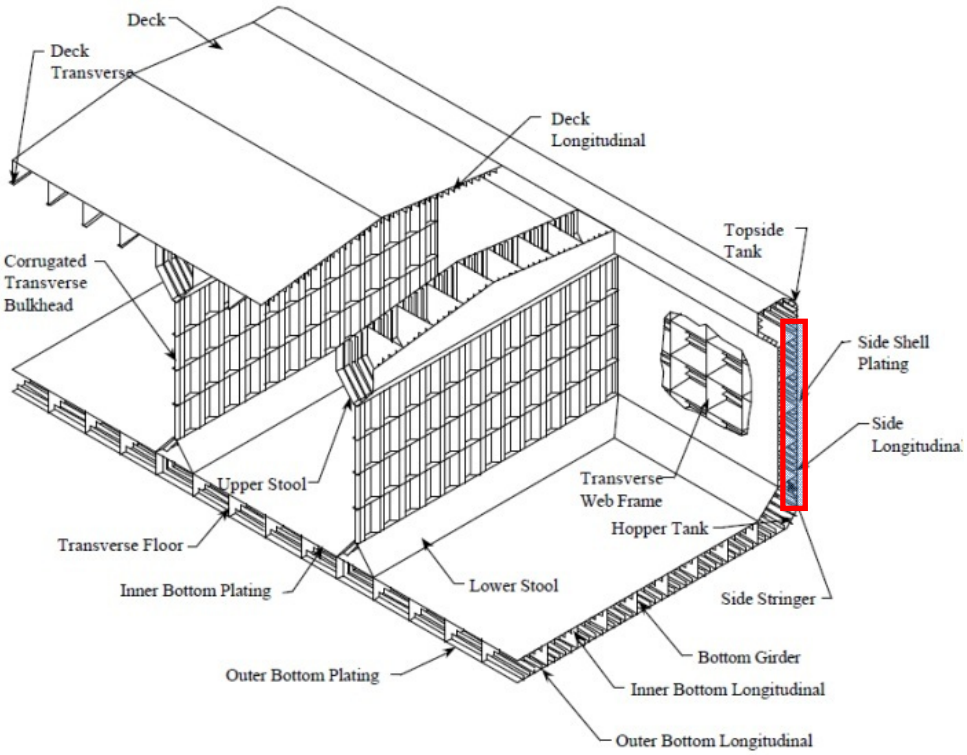

Figure 8.35 Sketch of Tank Side Shell

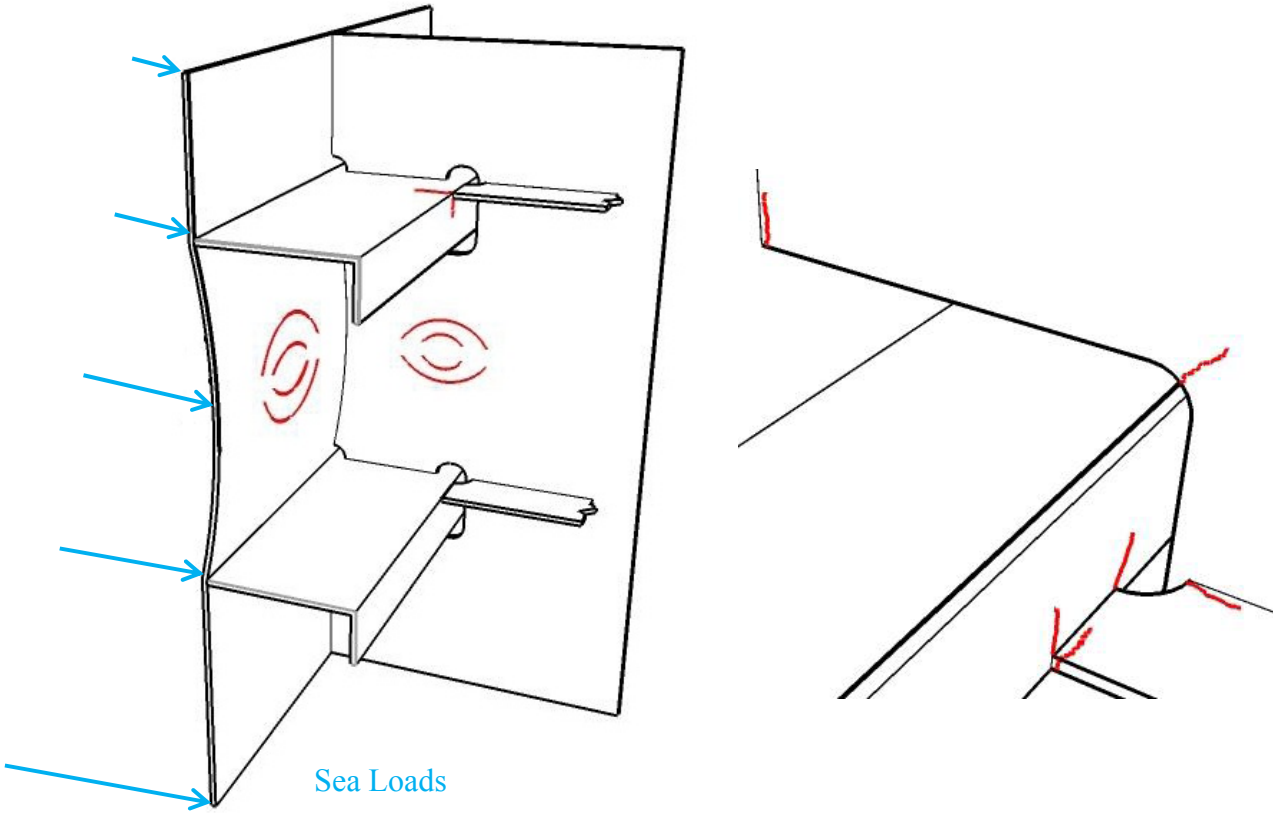

Figure 8.36 Sea Loads on the side shell of Tank

Situation I: Cracks at the connection of side shell longitudinal webs

Figure 8.37 shows a section through a ballast tank showing the connections by side bracket framing (30.000DWT_Transerve Bulkhead Construction). It is observed that the side frame components with double bracket design are favourable in terms of fatigue life.

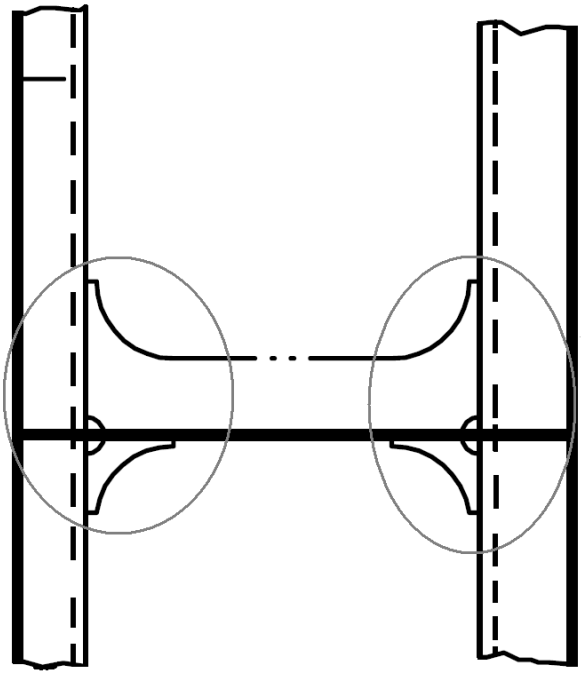

Figure 8.37 Transverse Side Plates Frames

This is especially true on tank ships where long spans of side framing can be supported by the flanged-triangular brackets. The transverse side tank frames can be considered as the cruciform geometry transformations. Dimensions of the side tank framing components have been listed in Table 8.5.

Table 8.5
Dimensions of the side tank framing constructions

Component	Dimensions (mm)
Side Plating	2000.0×3000.0×12.0
Longitudinal Bulkhead	2000.0×3000.0×12.0
Horizontal Stiffener	*L* 250.0×90×12.0
Longitudinal Side Frame	*L* 250.0×90×12.0
Strut	1500.0×250×10.0
Triangle Bracket I, II	300.0×300.0×10.0

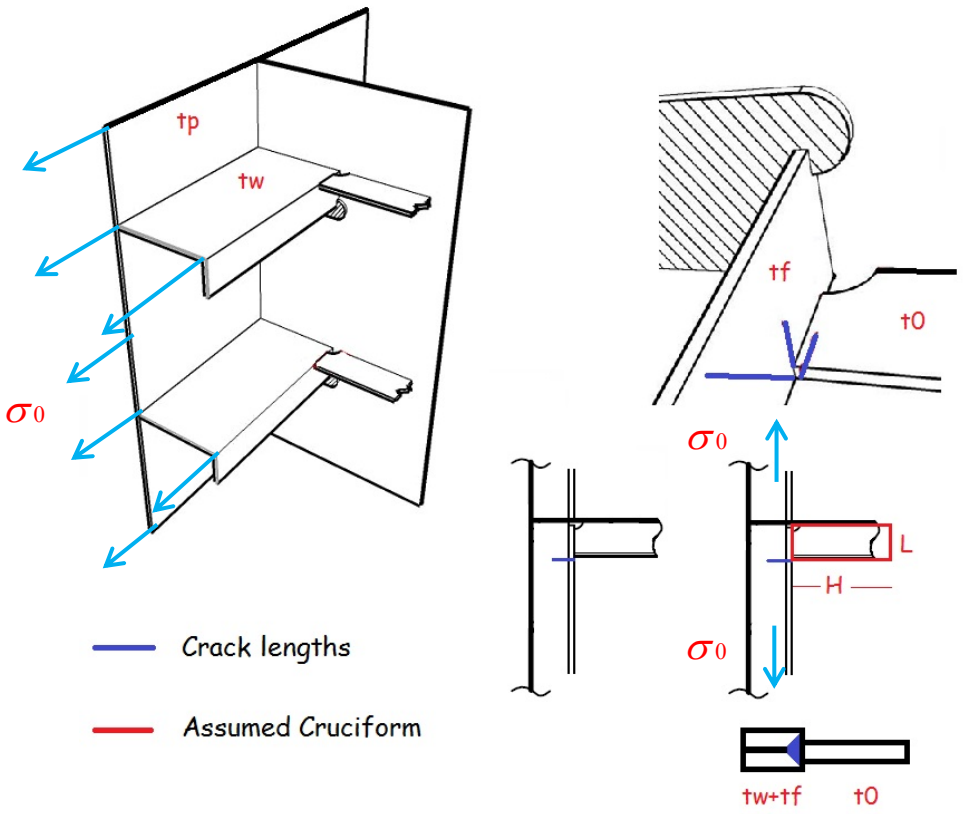

Figure 8.38 Situation I of Cracks at the connection of side shell longitudinal webs

The equivalent height and width of the cruciform specimen, corresponding to simple rectangular specimen, are 1.5 m and 0.25 m respectively, with the bracket 0.30 m on two sides. The strut stops the stress transferring through the longitudinal frames, as a result that we use the single bracket length to predict the Length Scale. The thickness correction should fold the thickness of flange to 24mm and divided by the thickness of bracket 10mm.

$$as = smallest\ of\quad ((300+250)/22\cdot(10/24)^{0.5},\quad 1500/3\cdot(10/24)^{0.87})$$

Here L is the length of With+Bracket length 550mm, and H is the height 1500mm,

the thickness correction factor is $(10/24)$

The Length Scale ‘as’ was predicted as 16.13 mm assuming folding the plate of

the flange as the double thickness. Considering the critical distance point (1.2 mm) away from the corner, the stress concentration factor can be found out equalling to 2.43, and LEFM is 2.54

A study is performed on the RISPECT components Level 3; using shell element models as shown in Figure 8.39. The SCF can be extrapolated from the surface FE points.

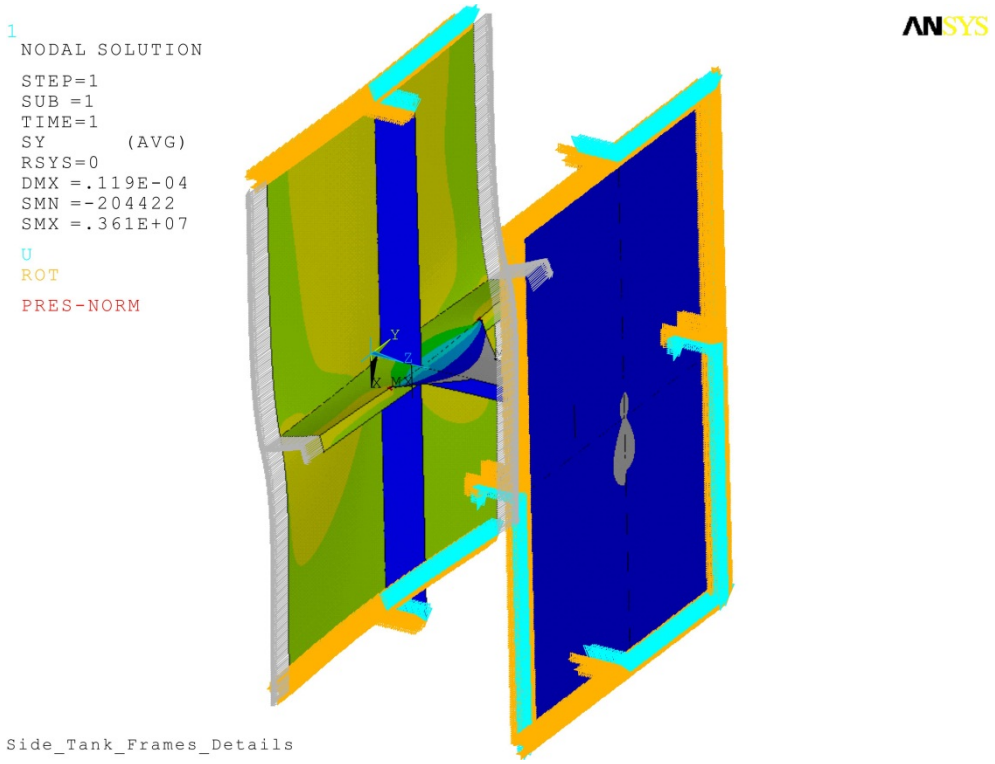

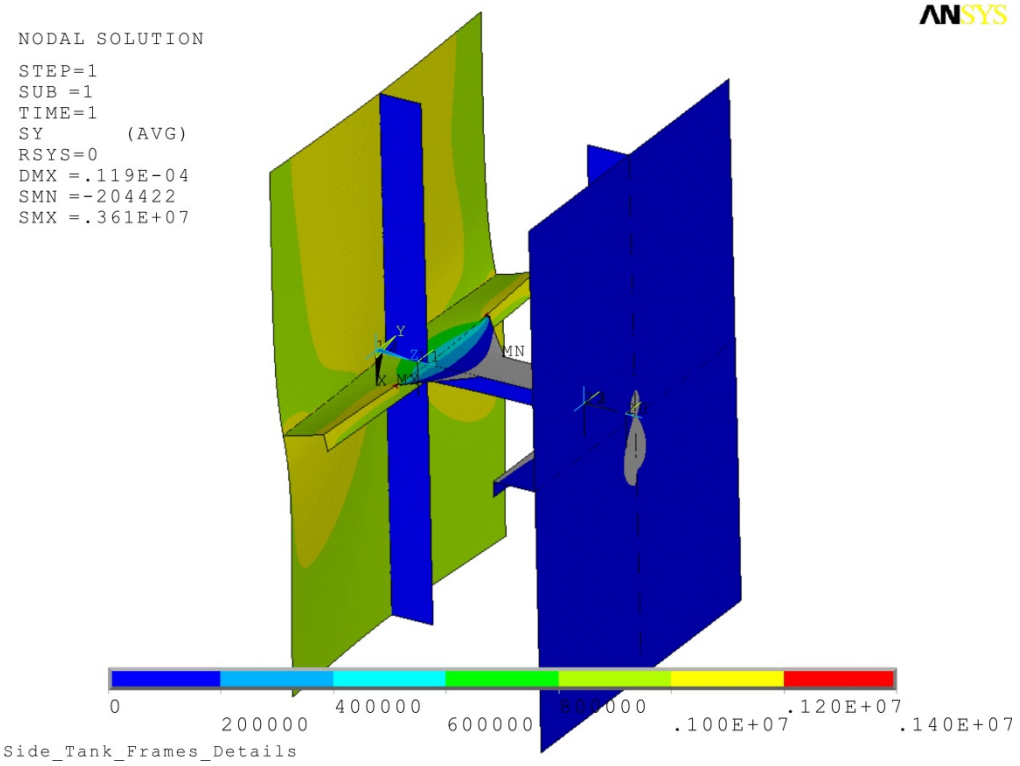

Figure 8.39 FE calculation results of the transverse side plate frames

The numerical results of side plates framing constructions and concentration factors are given in Figure 8.40.

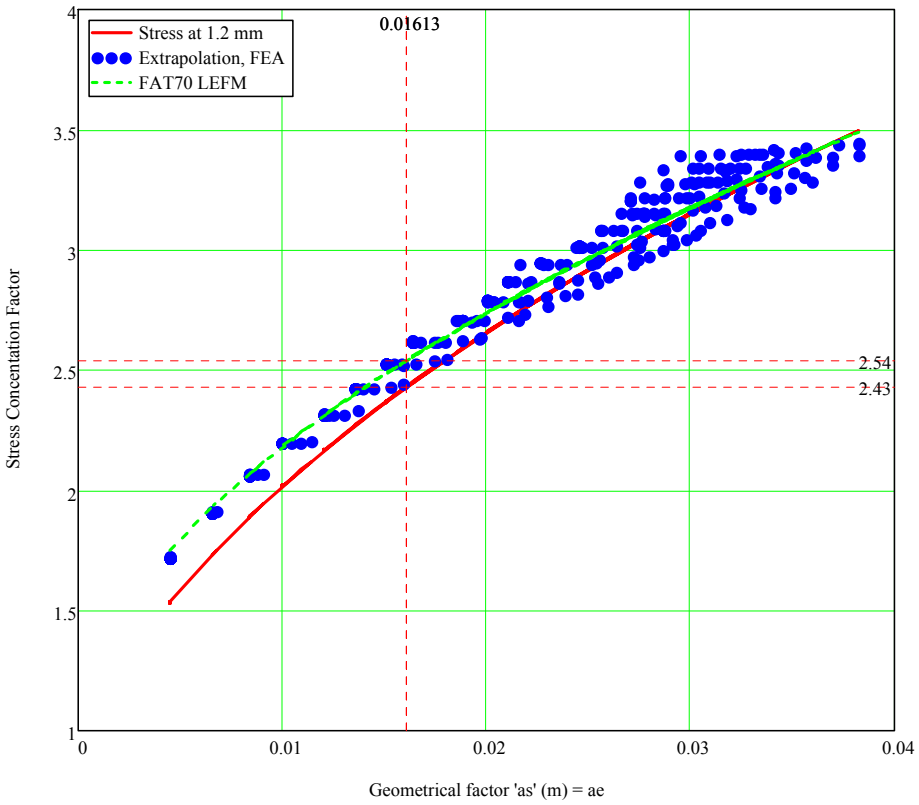

Figure 8.40 Comparison of SCF of Side Tank Frames Details

Table 8.6

Surface Extrapolation SCF values for the Specimen

	1st point (convert stress)	2nd point	3rd point	SCF
0.4/1.0t	1.72	1.32		1.99
4/8/12mm	1.83	1.47	1.32	2.39
0.5/1.5t	1.60	1.22		1.795
5/15mm	1.70	1.26		1.91

A comparison of the various stress amplitude values is shown in Figure 8.41, little differences are found between our methods and the extrapolated method in the detail.

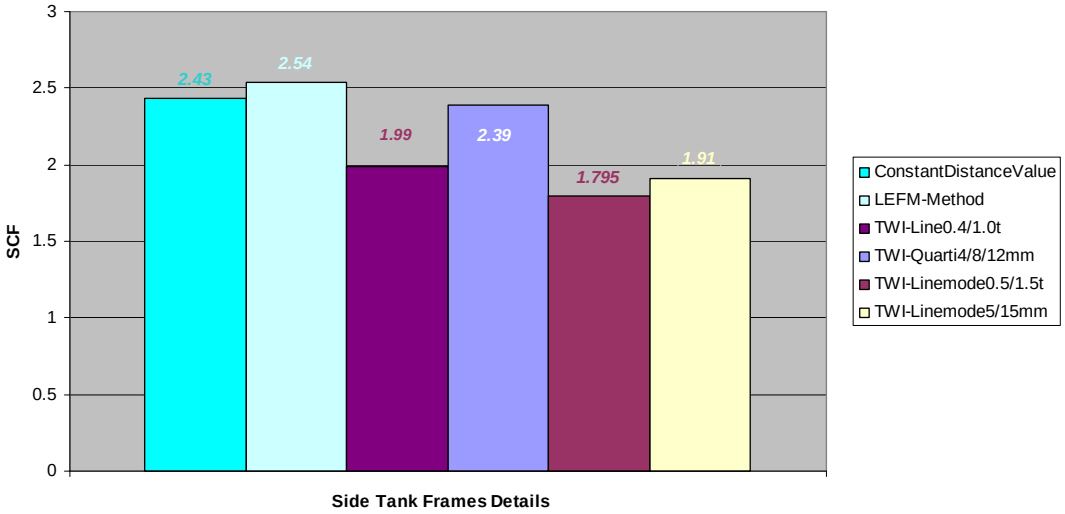

Figure 8.41 SCF results by various methods for the side frames

Situation II: Cracks at the connection of side shell longitudinal to vertical web frame

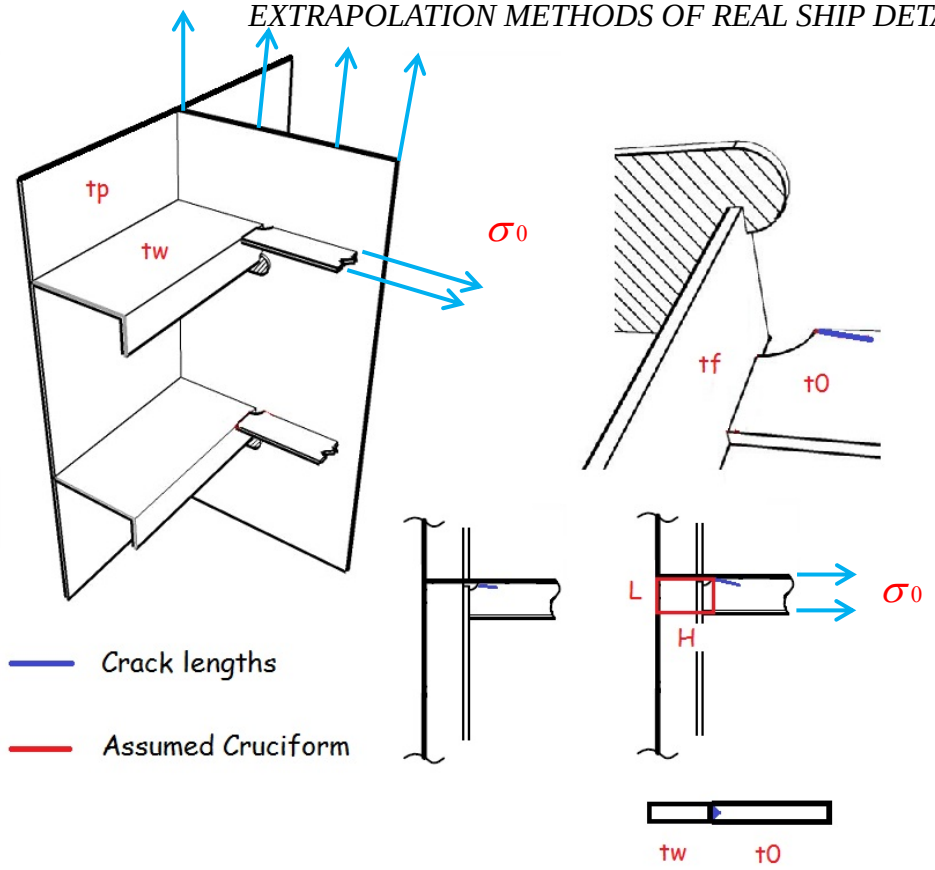

Figure 8.42 Situation II of Cracks at the connection of side shell longitudinal, to vertical web frame

8.2.6 Cargo Lower Stool Plates

Stool side plating is to align with the corrugation bulkheads, and side shell frames (of their brackets) are to align with the bulkhead lower stool to to provide vertical load transmission between these stiffening members.

The bulk cargo requires that the transverse bulkheads have lower and upper stools to improve loading and unloading of the bulk cargo and also to improve structural strength of transverse bulkheads. Scallops should be avoided in the way of the locations of the lower stool and double bottom.

In general, plate diaphragms or web frames are to be fitted in bottom stools in way of the double bottom girders and plate floors, although lower stool side plating

may not be surveyed visually anywhere between the inner bottom plating and the stool top plate in Figure 8.43.

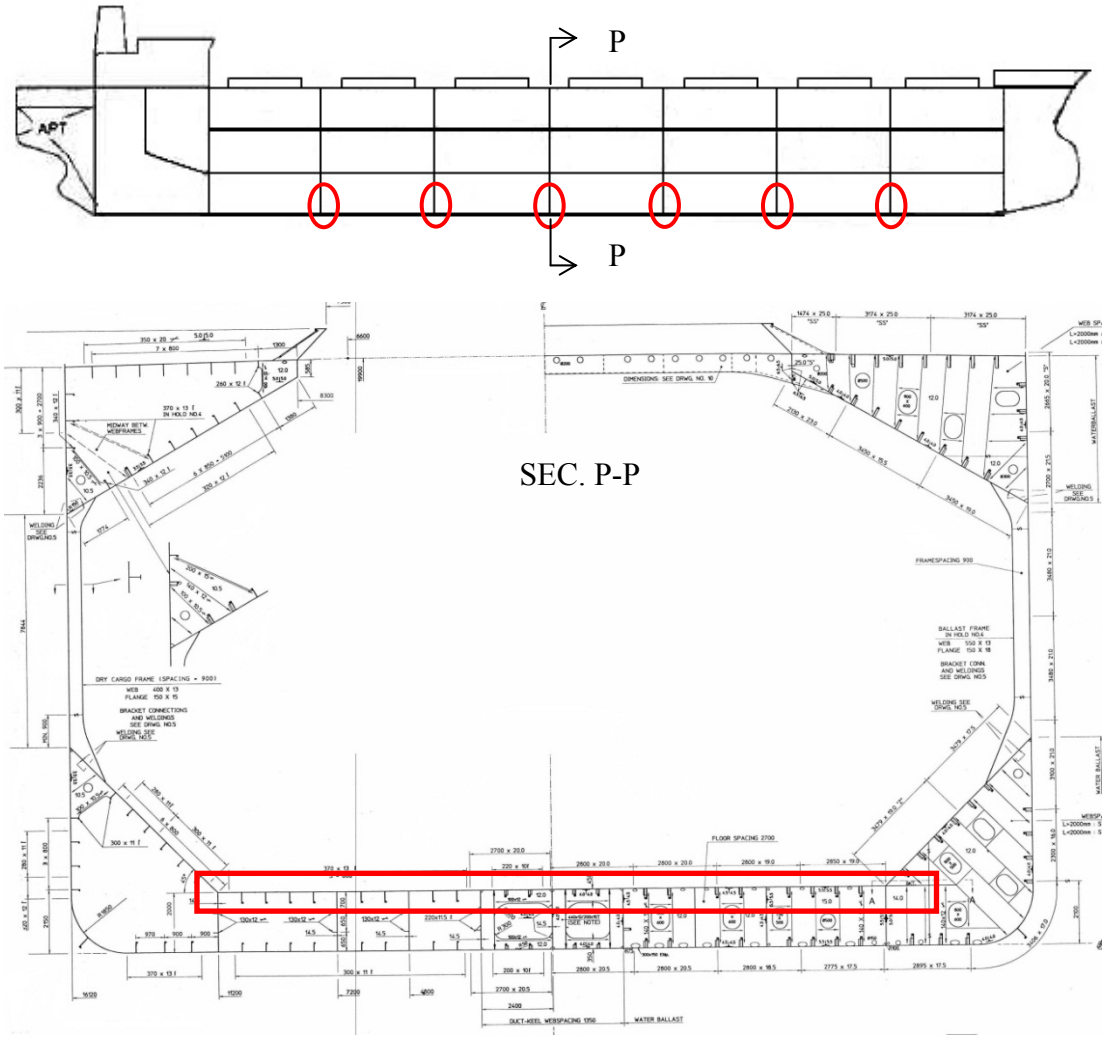

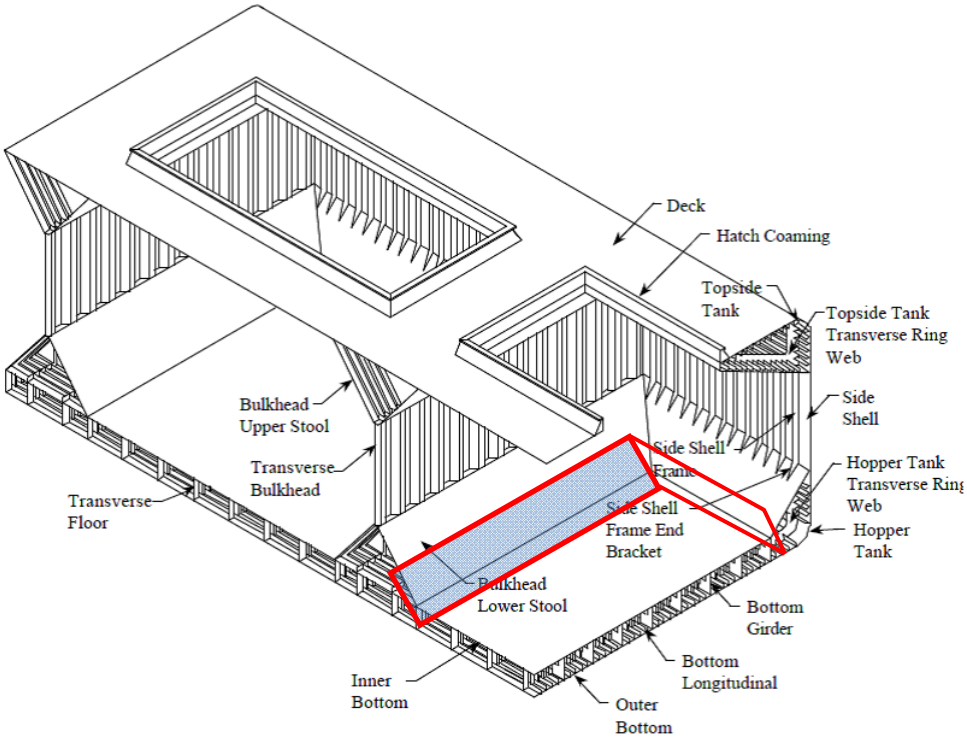

Figure 8.43 Sketch of lower stool plating in Cargo holds

The loading conditions should be considered in the rule criteria checking of local strength. Some Bulk Carriers have cargo holds designed to be partially filled with salt-water ballast. In order to identify whether a Bulk Carrier has this facility, it is necessary to check the Capacity Plan and/or the Trim and Stability booklet to identify which holds are designated for partial filling purposes.

The loading conditions of the hold mass curves should be included in the loading manual and loading instrument. In addition, careful planning is required in the loading of bulk carriers. Not only is it critical that the final departure condition be sound, but how the ship is loaded and offloaded is very important for a successful operation.

In addition to the loading condition of the carrier, careful planning must go into the sequence in cargo holds and during loaded and unloaded situations.

The full cargo mass in the considered cargo hold completely filled to the top of the hatch coaming with cargo density, whichever is the greater, is defined as M_{full}.

The conditions usually applicable to service are: Maximum DraughtFuel oil tank

in double bottom 100% full, ballast water tank in double bottom empty, shown in Figure 8.44 **Error! Reference source not found.**a); and 67% Maximum DraughtNot applicable (when No Multi-Port) is assigned Fuel oil tank in double bottom 100%, full Ballast water tank in double bottom empty, in Figure 8.44 b). Additional conditions applicable during loading and unloading are in harbour of 67% Maximum Draught in Figure 8.44 c).

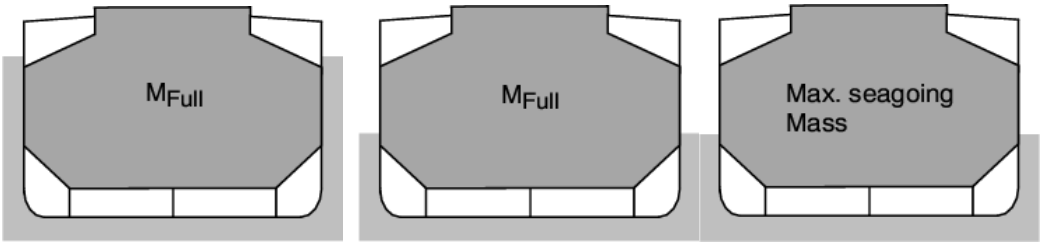

a), b), c)

Figure 8.44 Full Cargo Mass levels of the bulk carrier
http://www.veristar.com/bvrules/D_4_s3_4_5.htm

The actual cargo mass in a cargo hold is corresponding to a homogeneously loaded condition at maximum draught, noted by M_H in Figure 8.45.

The general conditions applicable to service features is Maximum DraughtAll double bottom tank empty; and the additional conditions applicable is Maximum DraughtApplicable to cargo holds which are intended to be loaded with high density cargo Fuel oil tank in double bottom 100% full Ballast water tank in double bottom empty. In operation, the maximum allowable cargo mass is limited to M_{HD}, which is in the considered hold for loading conditions with specified holds empty at maximum draught, as given in the Loading Manual.

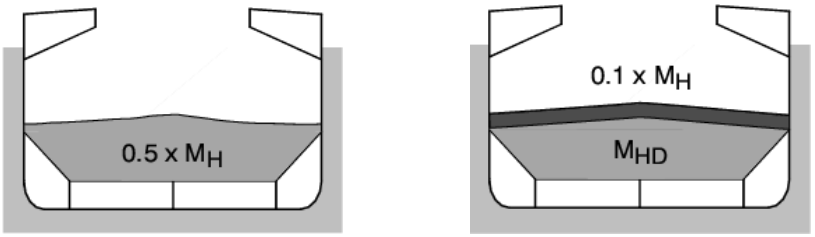

a), b)

Figure 8.45 Actual Cargo Mass levels of the bulk carrier
http://www.veristar.com/bvrules/D_4_s3_4_5.htm

The conditions of empty cargo mass in harbours are defined in Figure 8.46 that all double bottom tanks empty. It should be notated the No Multi-Ports is assigned in 83% Maximum DraughtNotApplicable of Figure 8.46 b; Maximum DraughtApplicable to cargo holds which are intended to be empty at maximum draught of Figure 8.46 c.

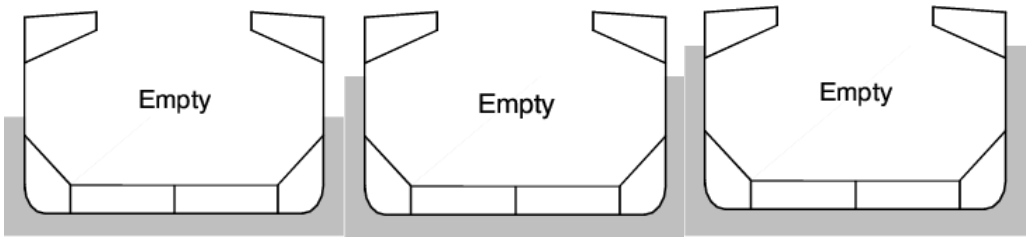

a), b), c)

Figure 8.46 Empty Cargo Mass levels of the bulk carrier
http://www.veristar.com/bvrules/D_4_s3_4_5.htm

Even more, shear and bending moment will be changed during the loading and unloading process. Shifts monitors or measurements will be necessary to confirm the weight of cargo loaded and to ensure that intermediate loading still satisfies the limitations based on local draft.

In general, the shell framing has been subjected to heavy loadings and the loads transferred through the bottom corner brackets have caused the box girder framing to buckle.

Brackets or deep webs are to be fitted to connect the lower stool to the bottom transverses.

Fatigue cracks of main cargo holds are found at the connections on the hopper sloping plating and lower stool plating in Figure 8.47, on the edge of the stoop plate along the surface of the surface of the cargo holds.

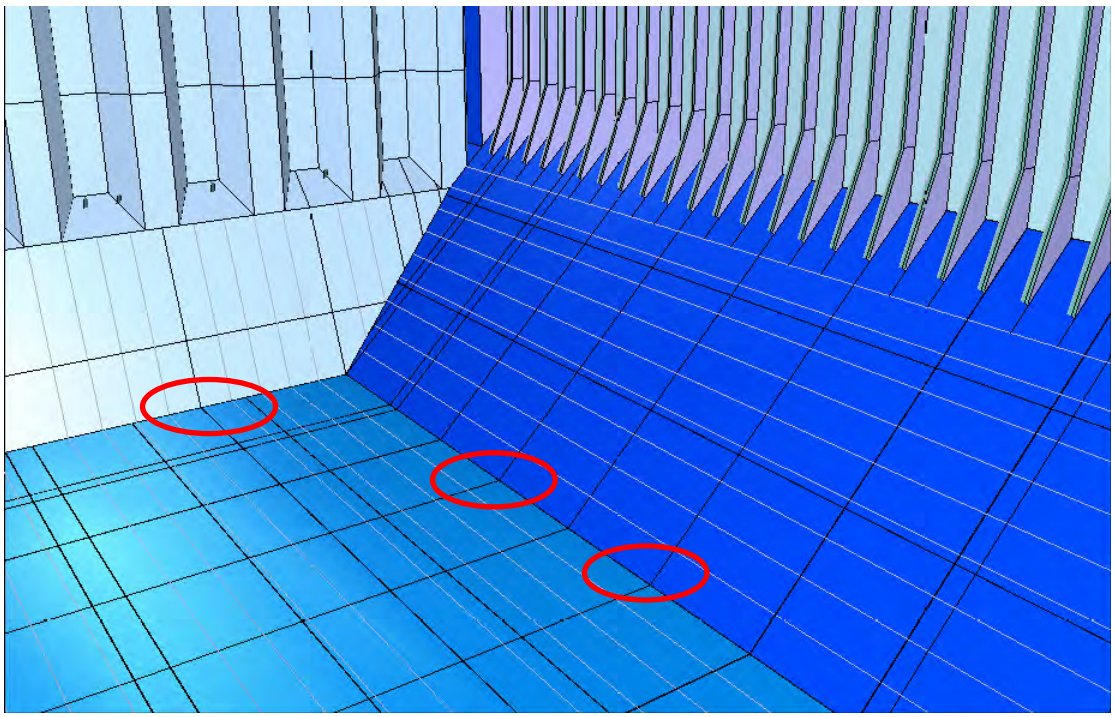

Figure 8.47 Fatigue cracks happened on the edge of the stoop plate

Note the cracks are to be in the structural configuration of the cargo hold bottom where the welded position. The weld connections are to be in accordance with the inner bottom plating of stool side plating and supporting floors, shown in Figure 8.48. They are caused by the critical pressure to the intersection of the girders or bending of the double bottom.

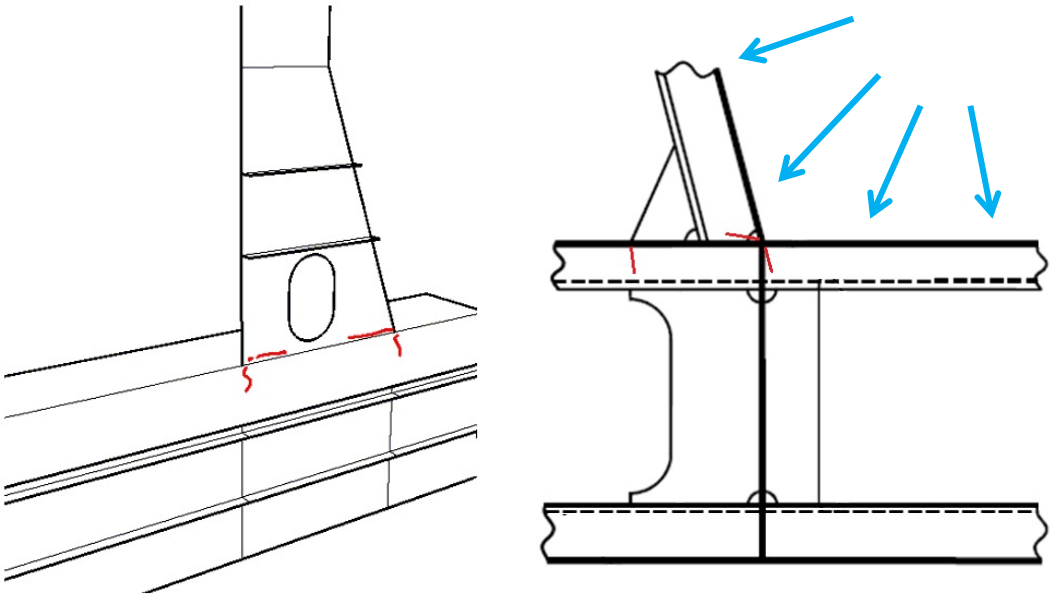

Figure 8.48 Crack positions on the cargo hold bottom plating

Situation I: Cracks along Hopper Sloping

It appears obviously that cracks propagate along the hopper sloping that large stresses occur at the connections that may lead to rupture of the bottom frames.

It is interesting to investigate if this stress concentration is caused by the right-angled configuration of the stool and if the fitting of a symmetric stool, that is, inclined in both holds, could smooth the stress flow at this area.

Conversion rules of the cargo hold lower stool are marked in Figure 8.49, and the assumed cruciform is to have a height in general of the length between two frames, and length of the bracket height. In particular, the thickness of main cruciform plate is to be of the 3 times of the one of upper strake of the lower stool, and the thickness of the attachment is doubled by folding the plate of the inner bottom longitudinal plate.

Detailed FE models have to be used when estimating stress concentration at

these locations accurately.

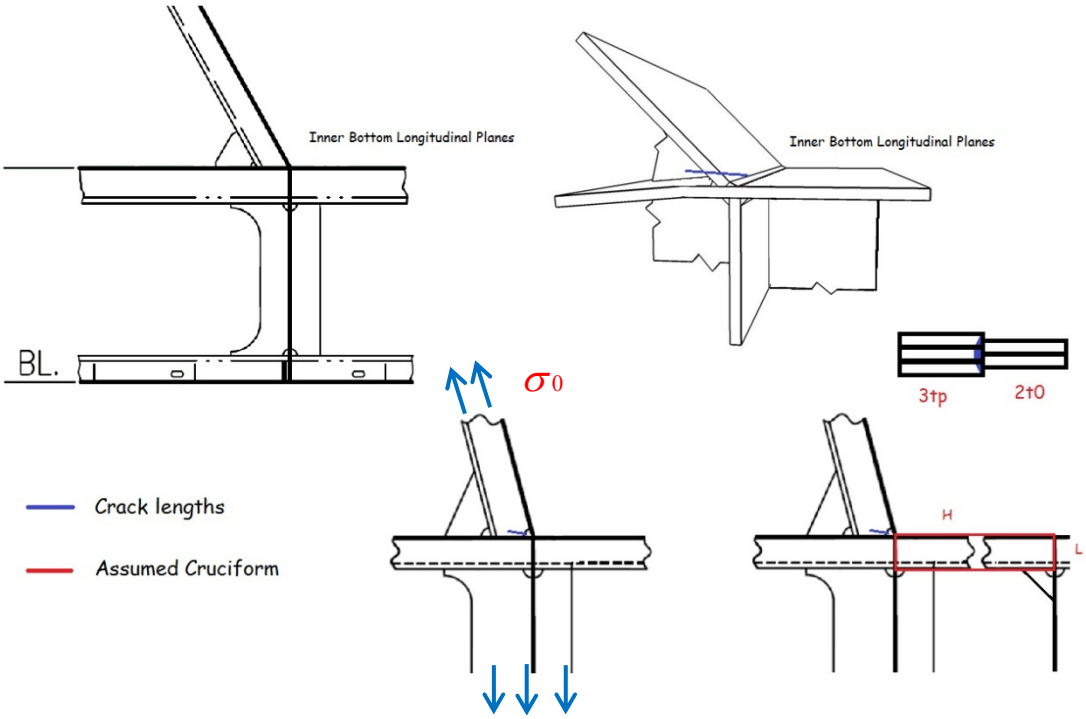

Figure 8.49 Situation II of cracks at alongside hopper sloping

In general terms, the ship is longitudinally stiffened except from the side shell between the hopper tank and the top-side tank that are transversely stiffened. Also, in some areas, such as between the centreplate and the first longitudinal girder in the double bottom, transverse stiffeners are located at half web spacing, except from specific locations.

The size of the selected vessel is justified by the fact that it is a very usual bulk carrier design placed between the existing bulk carriers' size extremes (cape and handy size), thus better allowing the generalisation of any obtained results from this work.

Situation II: Cracks into Double Bottom Components

In general, the ends of stool side ordinary stiffeners are to be attached to the floors of the bottom plates, or at the lower ends of the stool. The continuity of the stress flow is to be adequately broken at these locations. High stress concentrations occur at the intersection of the girders of the double bottom with the crack propagation into the floors; it appears that the lower stool connection suffers larger stresses that could herein become critical.

If applying transverse stresses directly to the bottom longitudinal, since it is to be recognized as the cruciform types based on the previous rules, show in Figure 8.50. The assumption can be recognized as 135 degree cruciform situation.

The height of the cruciform flange, H is the vertical height of the lower stool; the width is to be in line with stool connections to the inner bottom floors, and is to have a width of the mean depth of the sloping stool side approximately. The thickness of the stool plate is to be equal to the flange thickness, and the main cruciform plate is to be required 3 times of the inner bottom plating, the thickness correction is illustrated in Figure 8.50.

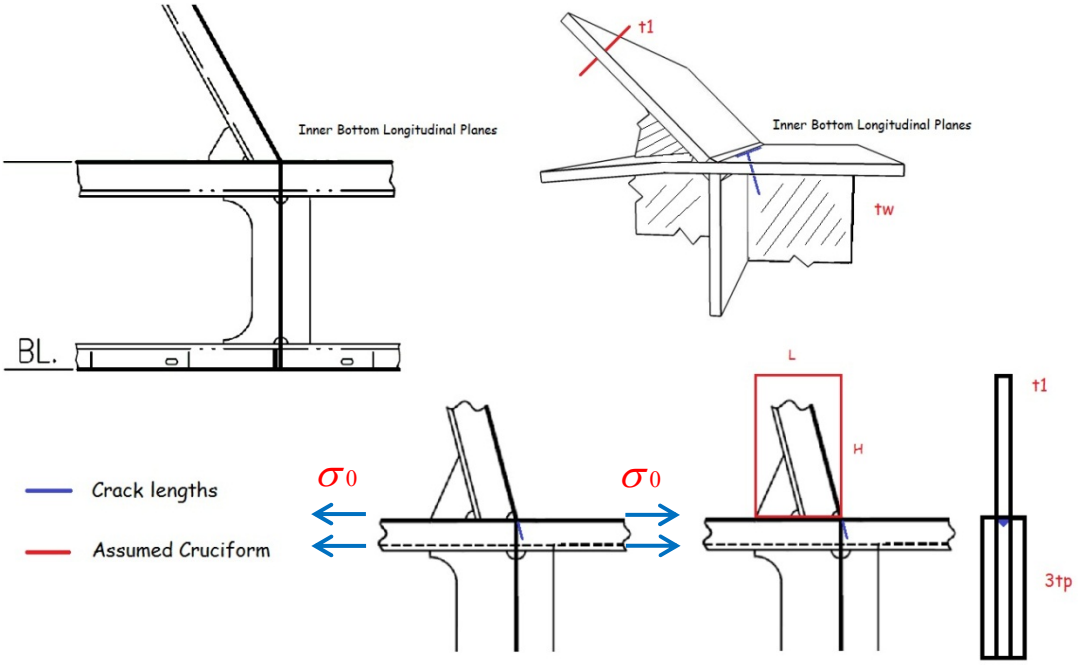

Figure 8.50 Situation I of cracks into the double bottom plates

Note that until now and in view of the experiences from historical accident data, it is expected that relevant bulk carrier designs of major shipbuilders are commonly cross checked by proper FE models both on the builder's and the classification society's side.

It is beyond the confirmations of the present study is recommended to use more dense mesh models of ship constructions, where having high stress concentrations.

The observations on the induced stresses at the lower stool plates show that the scantlings of a ship constructed are adequate to withstand the design loads according to rules.

8.2.7 Side Shell Frames

Frame brackets are the structural members connecting the lower end of side frames, or web frames with the tank top plating, floors or bottom plating. These structural members transfer the loading between side structure assemblies and bottom structure assemblies.

Special consideration to the side shell frames survey measurements may have been given by the Society, bracket cracks can decrease the service life of the ship component, and also can be attributed to instability of the side shell panel.

The fatigue configurations that occur often at the side frame bracket connections shown in Figure 8.51, especially in the mid ship/cargo section having high failure rates.

Where cracks close to the bracket end connection are found, the number of hold frames to be measured is to be increased; numbers of side frames to be measured are equivalent to those of the class renewal survey or intermediate survey corresponding to the ship's age.

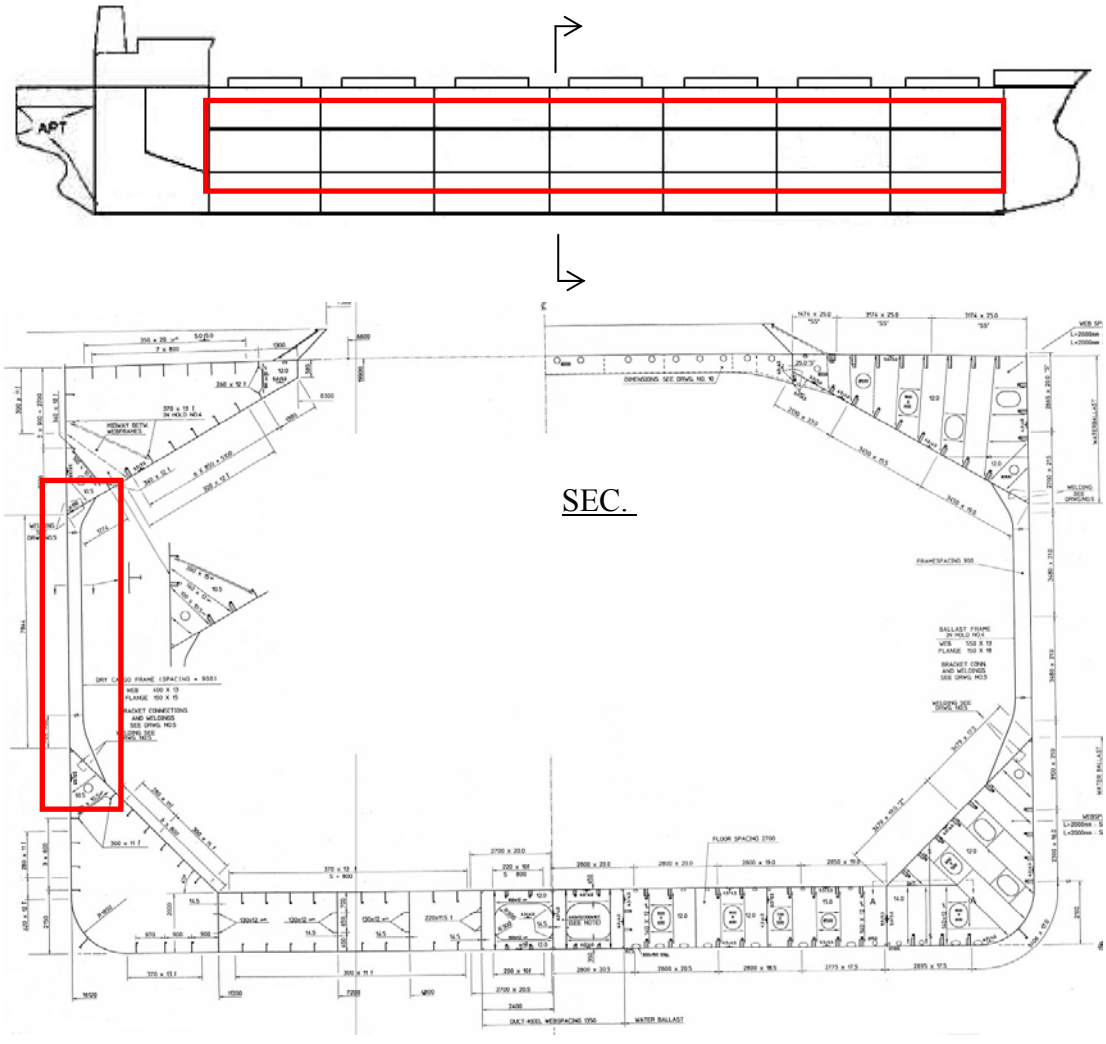

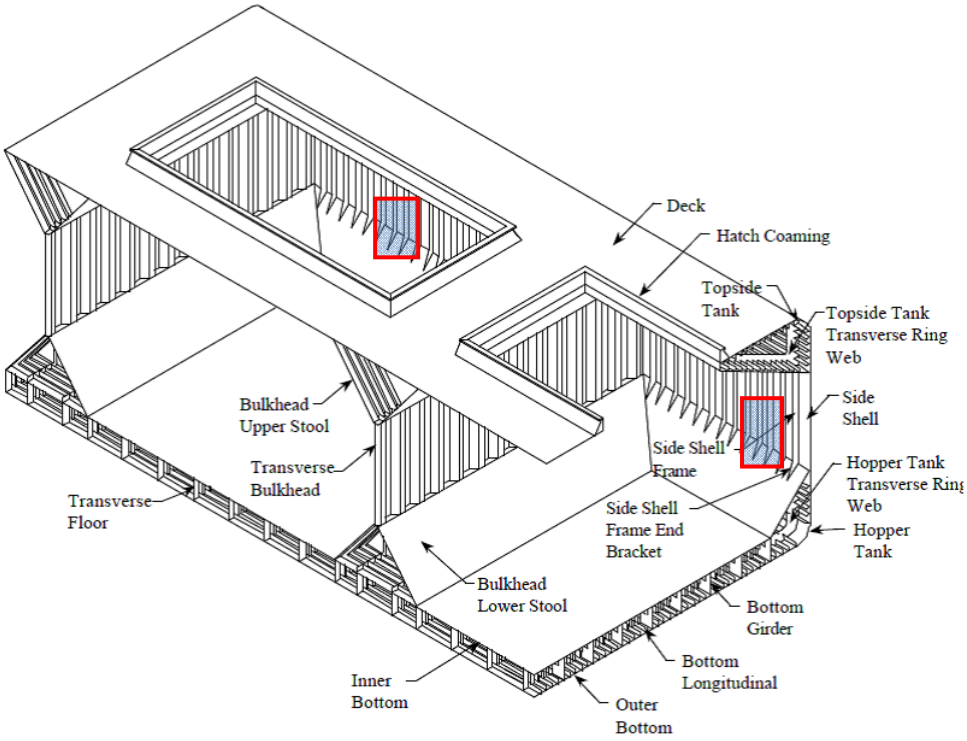

Figure 8.51 Sketch of Side shell frames

Figure 8.51 shows a frame bracket connecting the lower end of a side frame with the tank top plating of a transversely and longitudinally framed double bottom structures. There is a variety of construction forms used for side shell frames in bulk carriers. Some have faceplates (T-sections) on the side shell frames, some have flanged plates and some have bulb plates.

The use of faceplates and flanged sections is considered similar for gauging purposes in that both the web and faceplate or web and flange plate are to be gauged. If bulb plate has been used, then web of the bulb plate is to be gauged in the normal manner and the sectional modulus has to be specially considered if required.

The dimensions and shapes of our interested lower brackets are shown in Figure 8.52 as well. The bracket toes of inner skin, horizontal girders of transverse bulkhead or connections of the web and flange are potential crack positions.

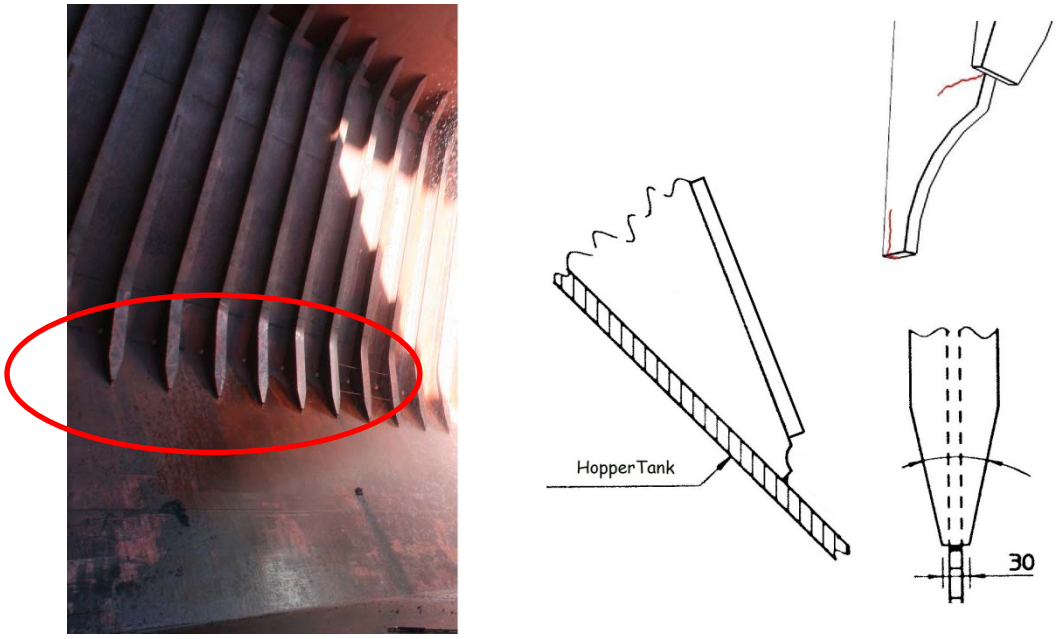

(http://www.maritime-executive.com/media/transfer/img/cargo_hold_cleaning_high_res.jpg)

Figure 8.52 Detail description of Side shell frames

Double continuous plate is to be adopted for the connections of frames and brackets to side shell, hopper and upper wing tank plating and web to face plates.

Situation I: Stool and Side Frame Connections

As shown in Figure 8.53, the crack is recognized as that initiated from the bracket toe of side shell frames, and then propagates along the inner plate and girder of the lower stool.

Figure 8.53 Structural reinforcement using Tripping Brackets
(LR, Thickness Measurement and close-up survey guidance Part1, 2012, P43)

It is implicitly assumed that the corner position is located at the end of the bracket connections, as situation I in Figure 8.54.

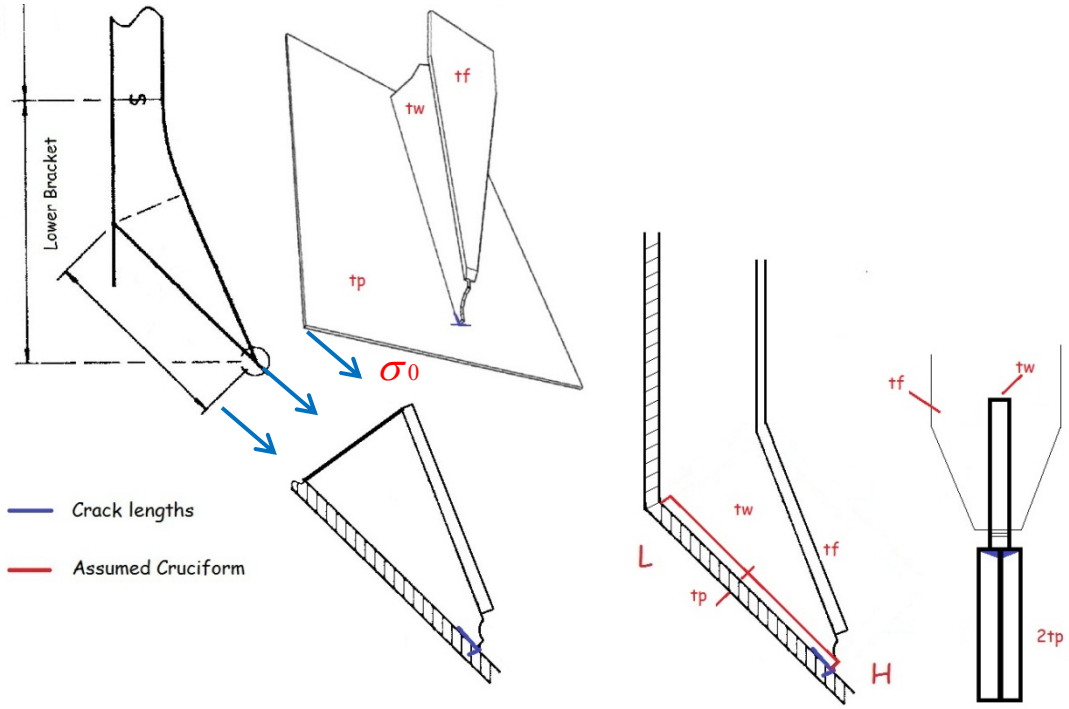

Figure 8.54 Cracks at connections of stool and side frame

Dimensions of the side shell frame are listed in Table 8.7, and also marked in Figure 8.55; the side shell frame is a web frame stiffener welded on stool plate, and a flange plate weld on the bracket.

Table 8.7

Dimensions of the side shell frame (of mid-sections Frames)

Component	Dimensions (mm)
Web Plate high bracket edge	840.0×15.0
Web Plate Length	2100.0×15.0
Web Plate low bracket edge	15.0×15.0
Flange Plate	150.0×21.0

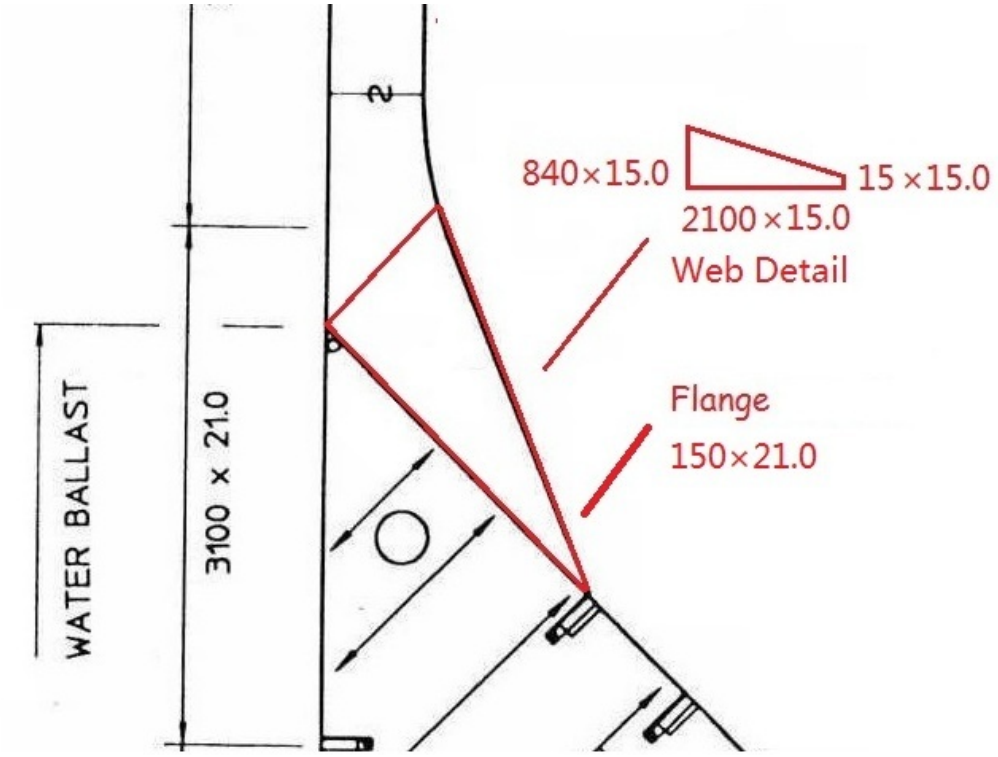

Figure 8.55 Dimensions on side shell frame

The hull form is such to prohibit an effective fillet weldment, edge preparation of the web of frame and bracket may be required, in order to ensure the same

efficiency as the weld connection stated above.

As a result, the component can be considered as the cruciform having the geometry dimensions: width 2.1 m (L=2.1m) and height H 15.0 mm, corresponding to the simple specimen.

In way of the foremost hold, side frames of asymmetrical section are to be fitted with doubling the thickness at the end of the bracket. The thickness of the web plate is 15mm, and the thickness of the stool plate is 10mm; the thickness correction factor of the side shell frame location can be got by folding the stool plate as $(15/20)$. The Length Scale 'as' equals to 3.89 mm from the formula:

$$as = smallest\ of \quad (2100/22\times(15/20)^{0.5},\quad 15.0/3\times(15/20)^{0.87})$$

Here L is the length of Wed plate 2100mm, and H is the height 15.0 mm;

the thickness correction factor is 15/20

Considering the critical distance point (1.2 mm) away from the corner, the value of SCF can be given as 1.466; if we check the LEFM curves against Length Scale, the value of SCF are found out equalling to 1.68 from Figure 8.56.

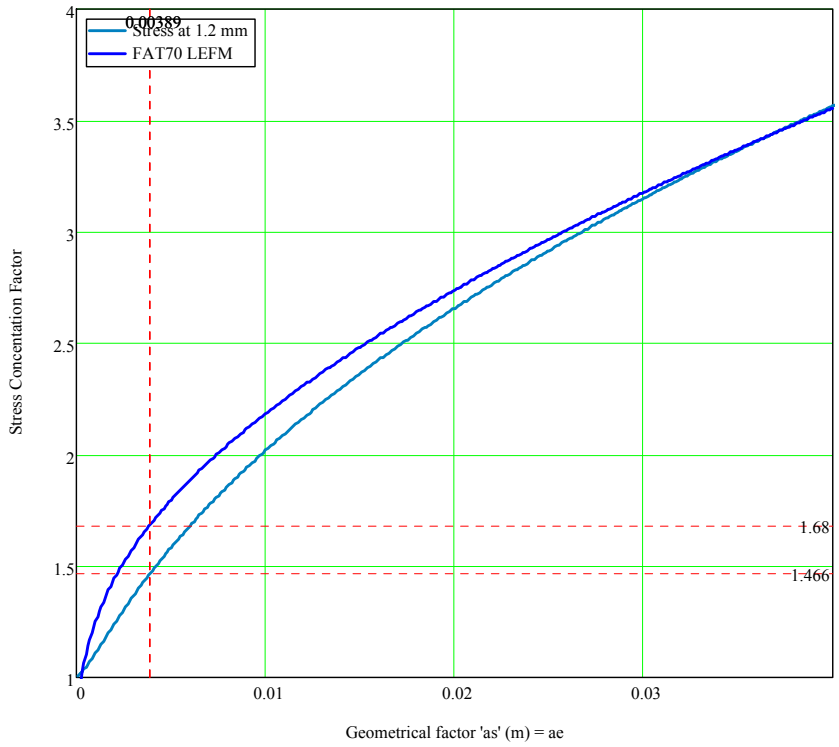

Figure 8.56 SCF Comparison of bottom longitudinal frame

Situation II: Bracket Toe Ends

The part of bracket component to be coated includes: the web and the face plate of the side frames; and the hold surface of side shell, hopper tank and topside tank plating, as applicable, over a width not less than 100 mm from the web of the side frame.

When lower end brackets are not assembled well with the flanges, the cracks are to be found at the toe connections in the design stage, shown in Figure 8.57.

http://www.dkfotinakis.com/pics/cat11big.jpg

Figure 8.57 The bulk carrier side shell frames and plating repairs

The loading conditions are to meet the outside sea pressure requirements, which can be converted to the pure tensile strength along the direction in Figure 8.58. Adequate cruciform structure in the bracket end is to be ensured: the flange is to be aligned with the attachment part, and the geometry of the bracket web is to extend up beyond the main plate which the cracks propagate in.

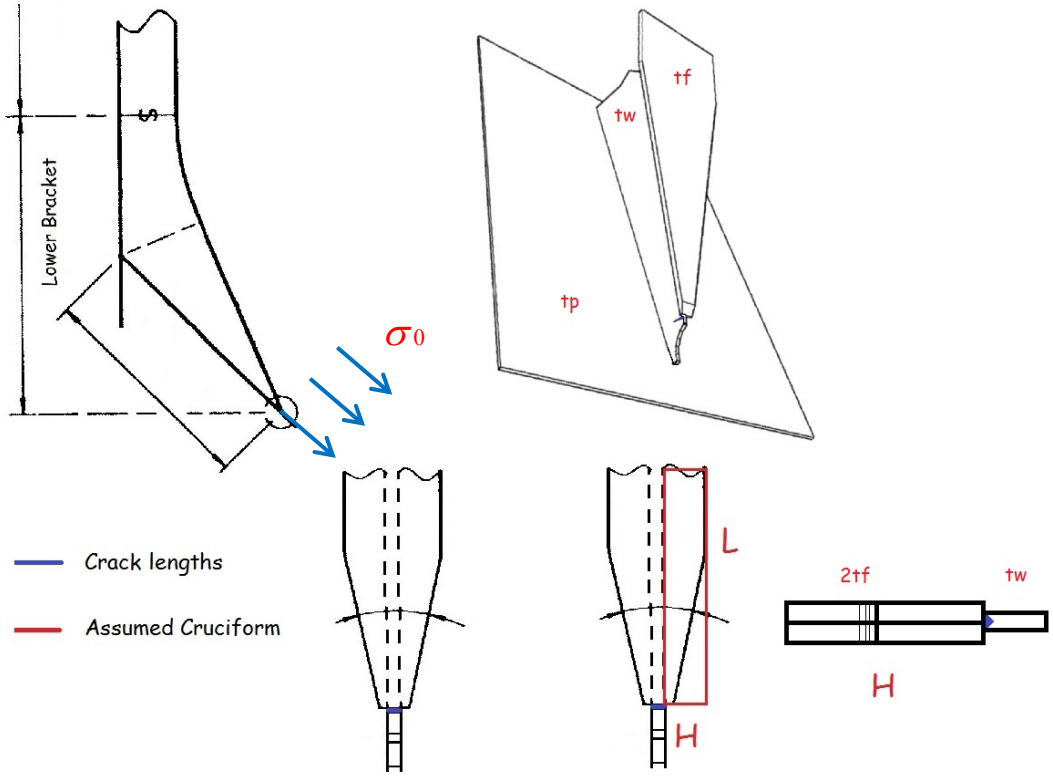

Figure 8.58 Cracks at End of the Bracket Toe

Dimensions of the side shell frame are listed in Table 8.8, and also marked in Figure 8.59; the side shell frame is a web frame stiffener welded on stool plate, and a flange plate weld on the bracket.

Table 8.8

Dimensions of the bracket end (of mid-sections Frames)

Component	Dimensions (mm)
Flange Plate long edge	150.0×21.0
Flange Plate short edge	30.0×15
Flange Plate	30.0×15.0
Thickness of Web Plate	15.0

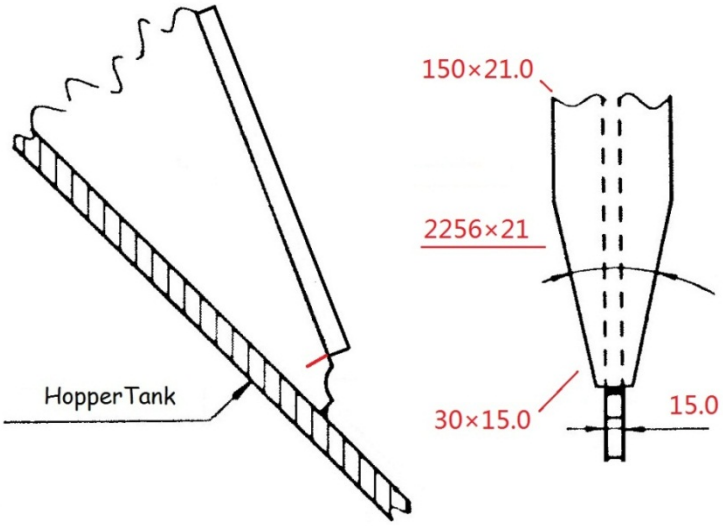

Figure 8.59 Dimensions of the bracket toe end

The component can be considered as the cruciform having the geometry dimensions: width 2.256 m (L=2.256m) and height H 15.0 mm, assumed as the length of the cruciform corresponding to simple specimen.

For alternative calculations, thickness factor may be used. The thickness of the flange plate is 21mm, and the thickness of the web plate is 15mm; the thickness correction factor can be got by folding the flange. The Length Scale 'as' equals to 12.24mm from the formula:

$$as = smallest\ of\ \ (2256/22\times(42/15)^{0.5},\ \ 15.0/3\times(42/15)^{0.87})$$

Here L is the length of Wed plate 2256mm, and H is the height 15.0 mm;

the thickness correction factor is 42/15

The actual section modulus of the brackets of the side frames is to be imagined about an axis parallel to the attached plate, based on the assumed shape in figure. Considering the critical distance point (1.2 mm) away from the corner, the value of SCF can be given as 2.18; if we check the LEFM curves against Length Scale, the value of SCF are found out equalling to 2.30.

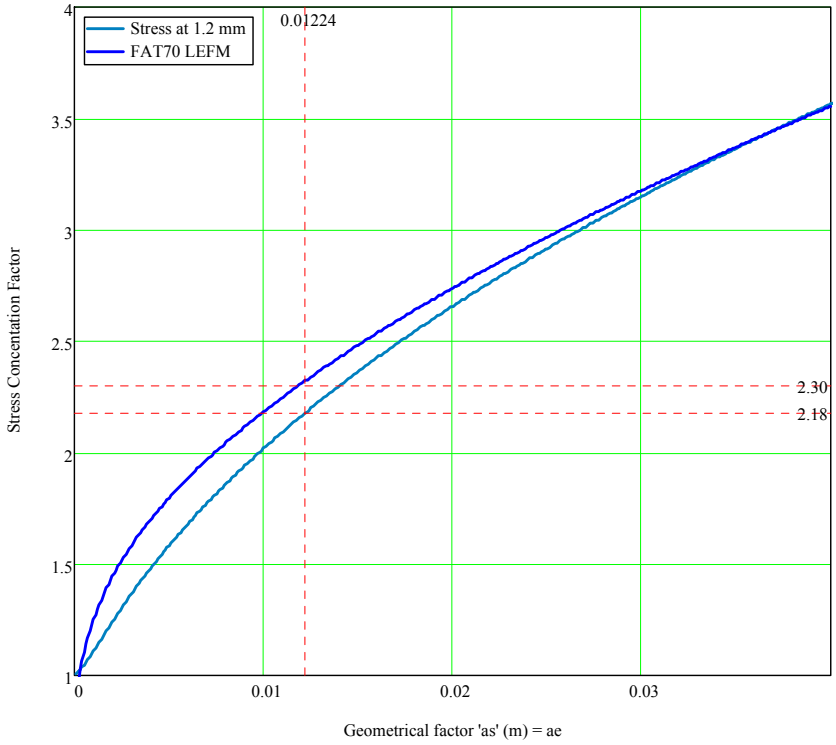

Figure 8.60 SCF Comparison of bottom longitudinal frame

8.2.8 Top Tank Longitudinals

The structural characteristic of deck design is the transverse connections of the decks and sides, which allows for flexibility.

The local web frame is easily buckled but there is no apparent impact loading on the shell plating. Possibly a large gunwale load caused the subsequent buckle in the web frame.

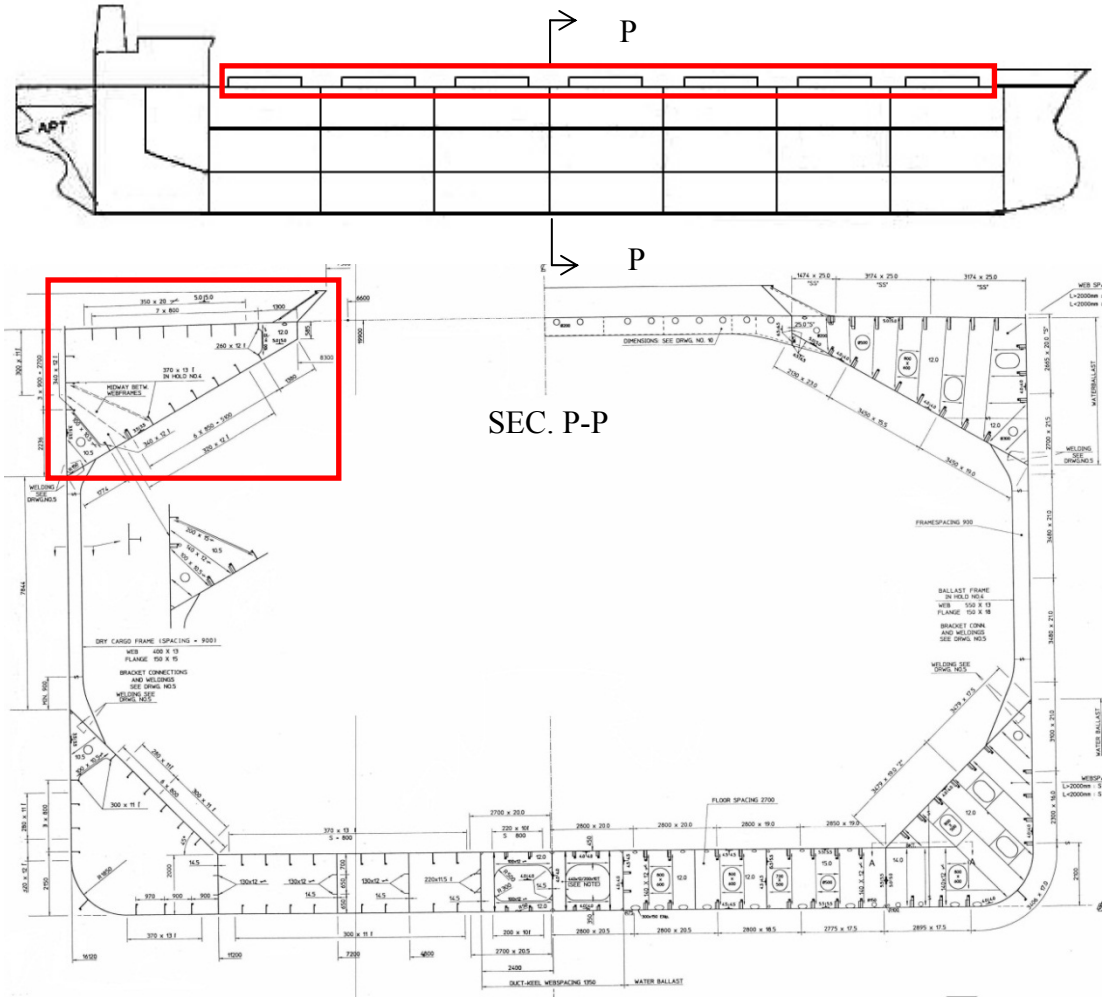
P
APT
P
SEC. P-P

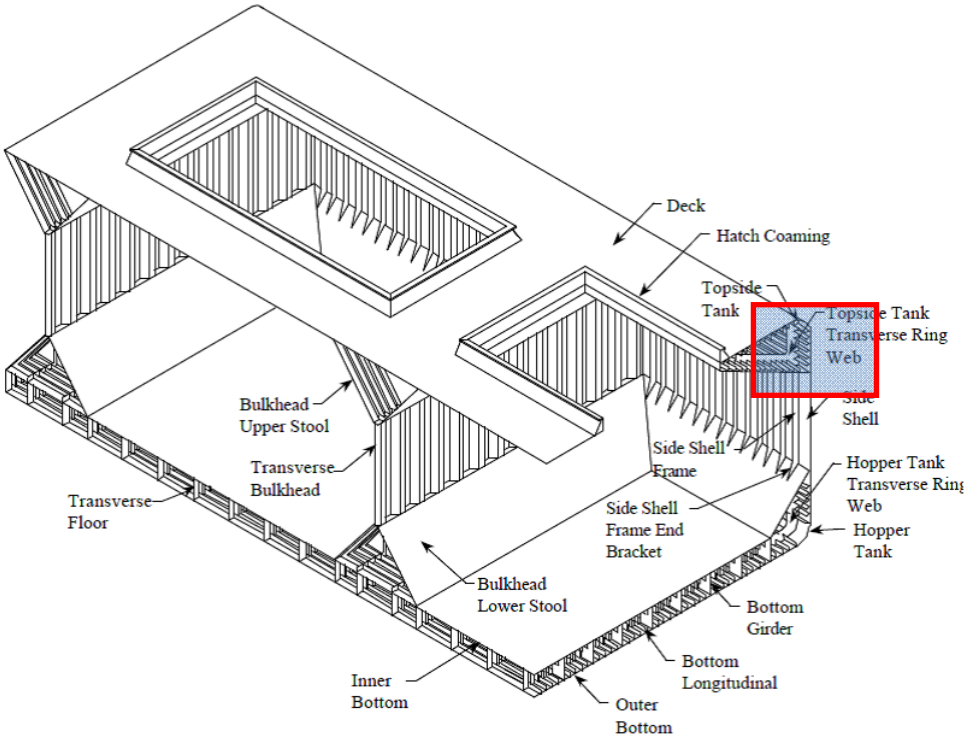

Figure 8.61 Sketch of ballast tank bottom longitudinal

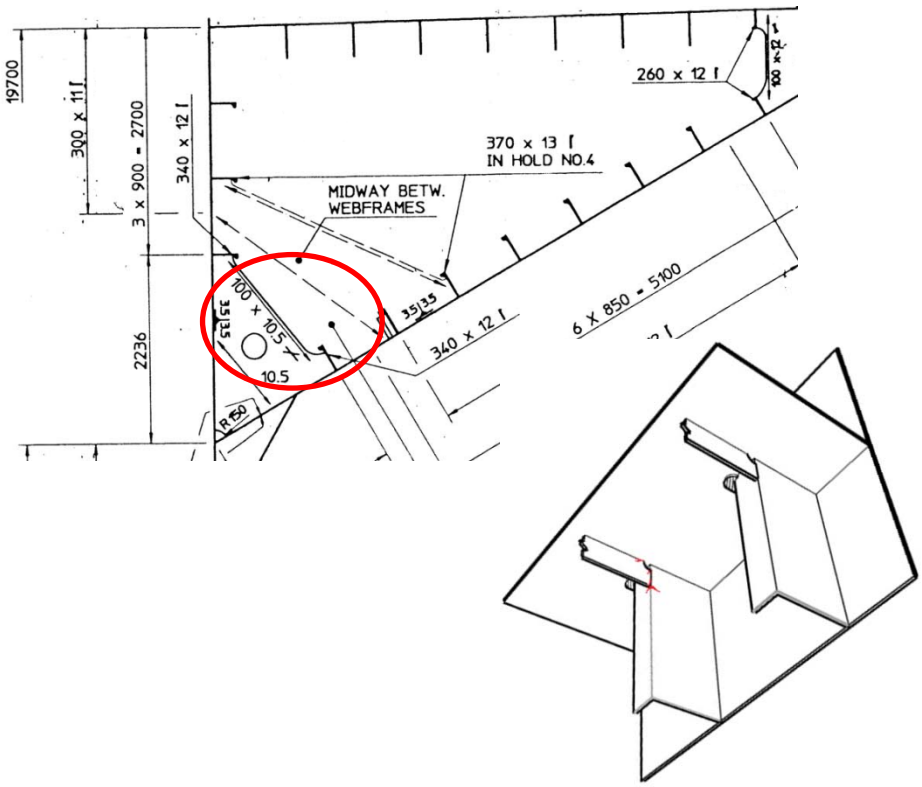

Figure 8.62 Detail description of Longitudinal, transverse web

Situation I:

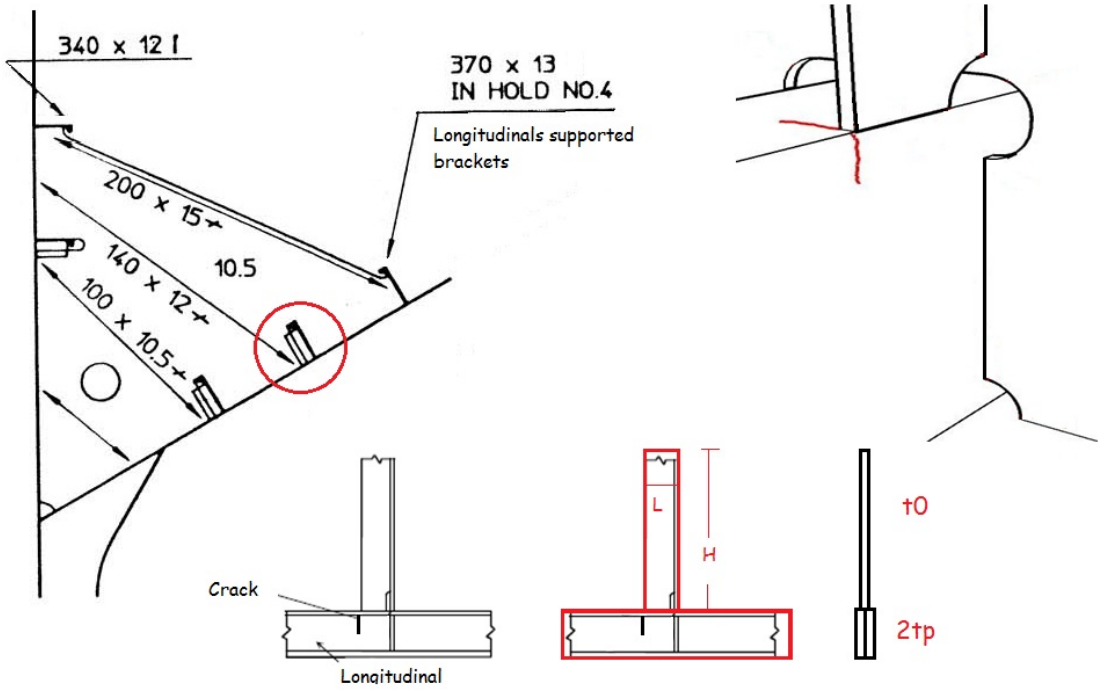

Figure 8.63 Situation I of Cracks happen at the connection of the flange and web plate in lowest longitudinal and vertical stiffener (axial loading),

Situation II:

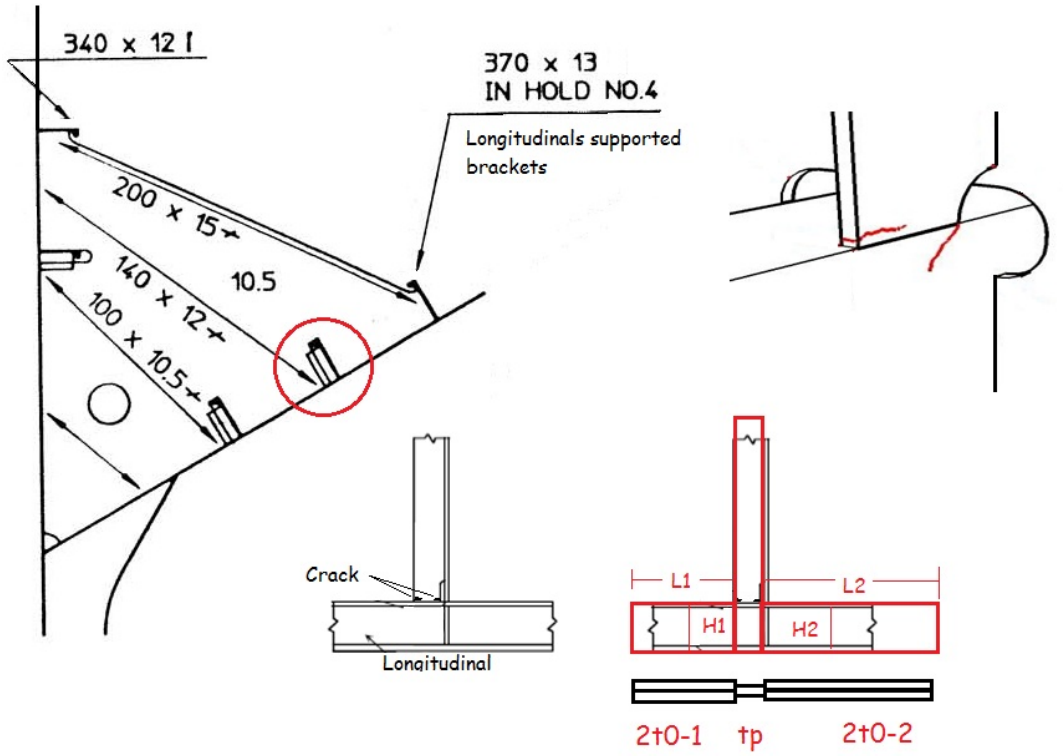

Figure 8.64 Situation II of Cracks happen at the connection of the flange and web plate in lowest longitudinal and vertical stiffener (pressures loadings),

Situation III:

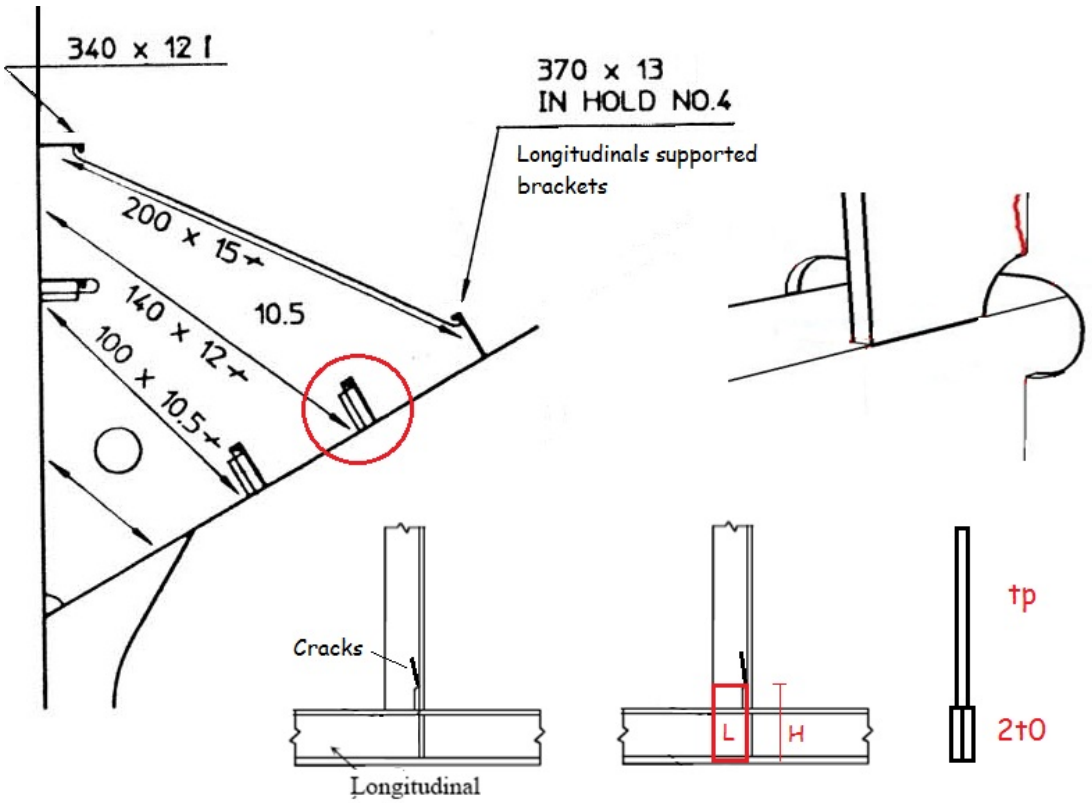

Figure 8.65 Situation III of Cracks happen in lowest longitudinal and vertical stiffener at transverse web frame (axial loading)

8.2.9 Deck Stiffening Connections

Strength decks form the principle members of the hull girder upper flange and usually the upper watertight boundary and may be subject to local water, cargo and equipment loadings, shown in Figure 8.66.

Other decks depend on the longitudinal extent, vertical distance from the neutral axis of the hull, and their effective attachment contribute to a lesser extent in resisting the longitudinal bending.

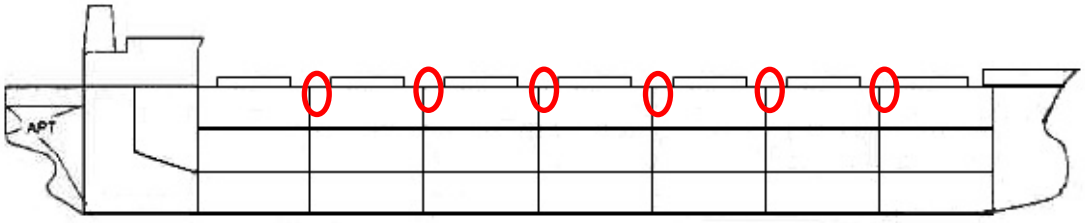
APT

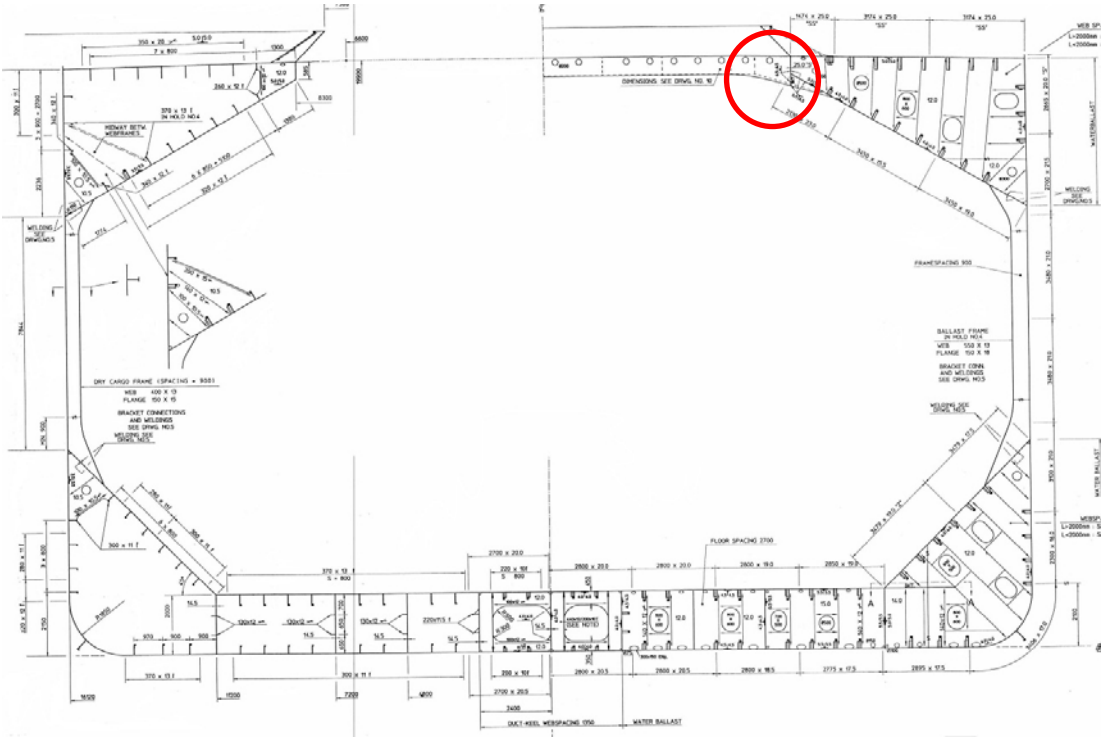

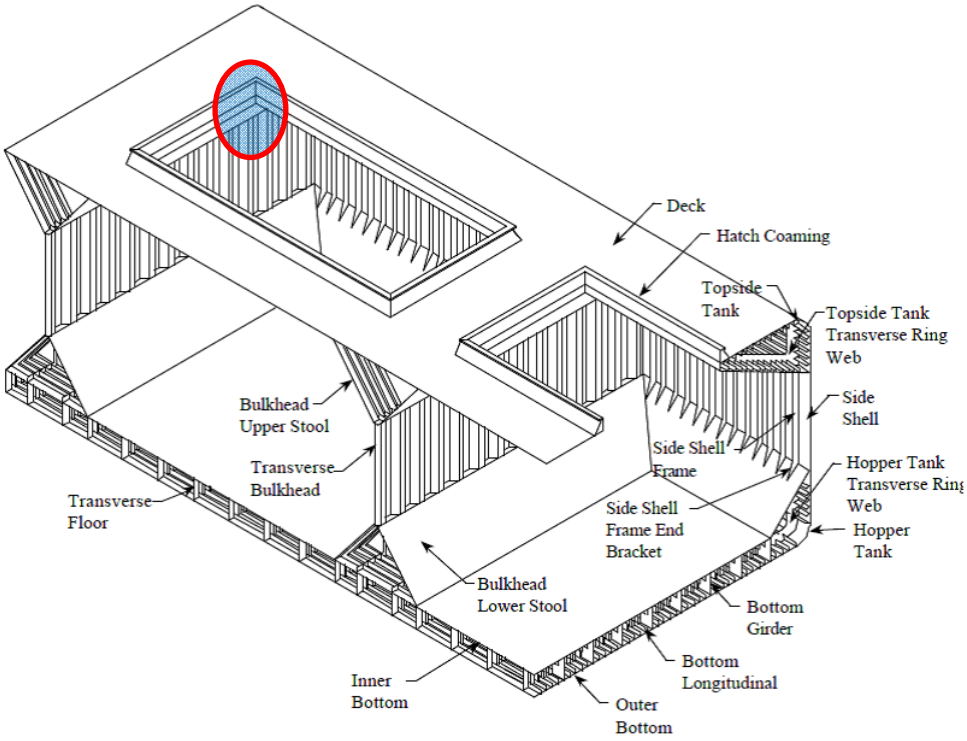

Figure 8.66 Main deck connections

This detail is from reference (30.000DWT_Transerve Bulkhead Construction), the main deck stiffeners had been reinforced with the 'rider plates' to improve the endurance under the loading and special attention given to the existing brackets.

Several failures occurred at the connection between the deck and side frames, serving as the end bracket for transverse main deck stiffening running from the side shell to the main deck, see Figure 8.67.

Figure 8.67 Stress fatigue crack found at cut-outs of Bulk carriers
(http://www.amteccorrosion.co.uk/papers/coatingfailuresguide.html)

Variations of the deck configurations included in the beam brackets observed by surveys are shown in Figure 8.68. The configurations that occur most often in the mid-ship/cargo section are the corner bracket connections, which have a high failure rate.

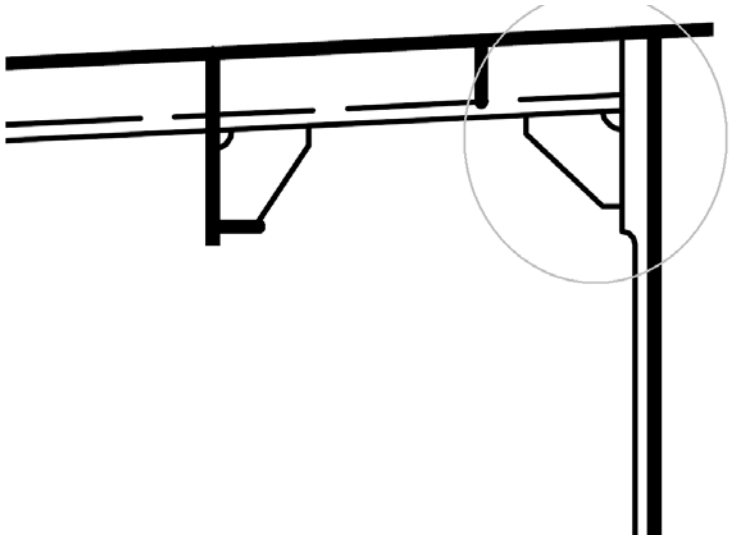

Figure 8.68 Deck Framed Connection

The chosen detail centres on the deck framing connection corner, where a

longitudinal stiffener passes through the bulkheads. Dimensions of the selected components are listed in Table 8.9 for the case study. The longitudinal stiffener is an angle section.

Table 8.9
Dimensions of Deck Connection

Component	Dimensions (mm)
Deck Plating	$2000.0\times1000.0\times12.0$
Side Plating	$2000.0\times3000.0\times12.0$
Deck Web Beam	L $250.0\times90.0\times12.0$
Main Frame	L $300.0\times100.0\times12.0$
Beam Bracket	$300.0\times25.0\times10.0$

Although some stiffeners had been reinforced with rider no attention had been given to the existing brackets.

The detail can be considered to the cruciform specimen geometry: height H=0.3 m and width W=0.3 m. The Length Scale 'as' was predicted as 17.60 mm, assuming double plate thickness by folding the web plate of the longitudinal stiffener. Considering the critical distance point (1.2 mm) away from the corner, the stress concentration factor is equal to 2.52; and LEFM is about 2.62.

$$as = smallest\ of\quad ((300+300)/22\cdot(10/24)^{0.5},\quad 2000/3\cdot(10/24)^{0.87})$$

Here L is the length of Width+Bracket length 600mm, and H is the height 2000mm,

the thickness correction factor is $(10/24)$

The numerical plotting results comparisons are given in Figure 8.69 by ANSYS; SCFs are extrapolated from the extrapolation points.

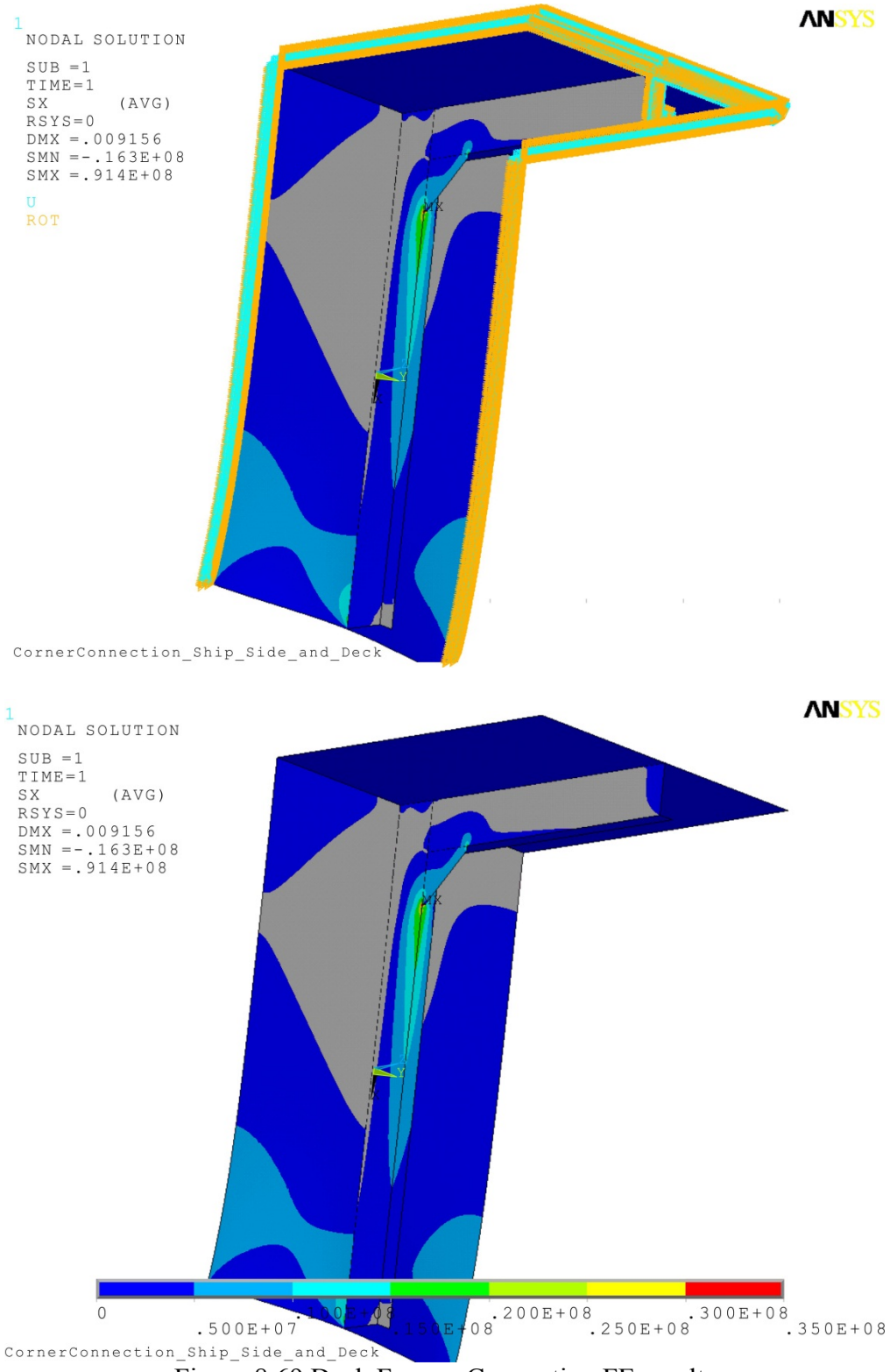

Figure 8.69 Deck Frames Connection FE results

The numerical results of side plates framing constructions and concentration factors are given in Figure 8.70.

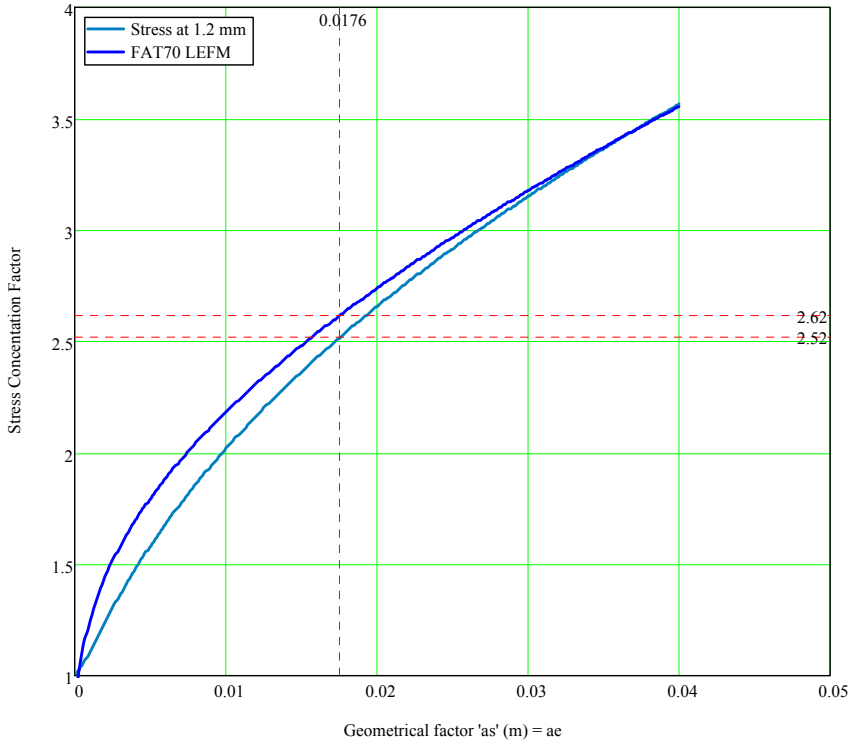

Figure 8.70 Comparison of SCF of Side Tank Frames Details

Comparison of various stress amplitude values are shown in Figure 8.71.

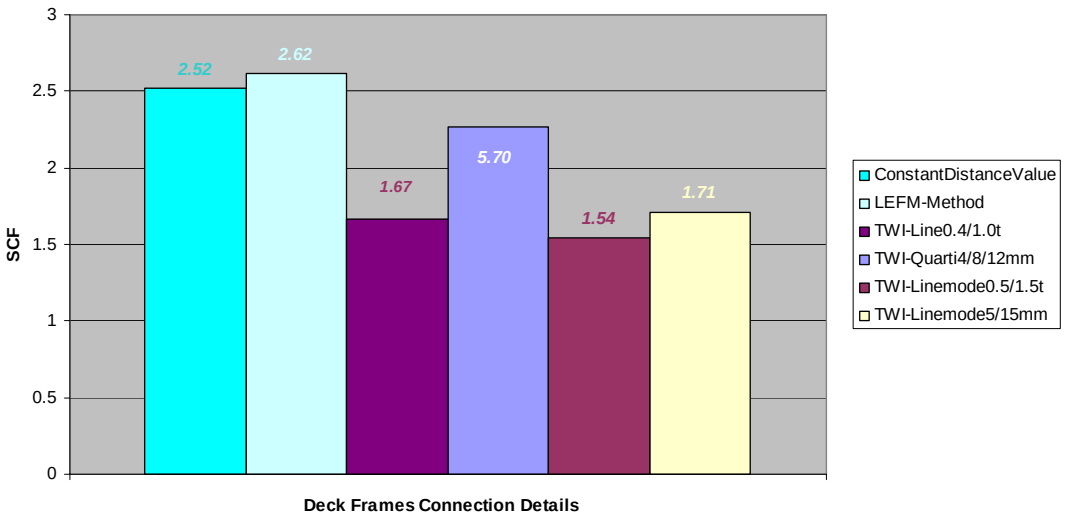

Figure 8.71 SCF results by various methods for the deck frames

8.3 Conclusions

The primary aim of the current chapter is to investigate the length scale method applications on the realistic engineering components, and more to check the validation of the method.

Case study SCF comparisons are listed for the connection detail in. According to the tested specimens selected from bulk carrier and tank, higher and more conservative SCFs have been obtained. Good application can be seen across the board in figures, with the primary source of variation being the computed values.

For full-scale detail fatigue analysis, the specimen can be simplified to focus on the locations where cracks happen. The connection can be related to the cruciform shape. This results in simple rules for the prediction of SCFs. The real structural verification has suggested that the length scale method can be efficient enough for the engineering fatigue analysis. In addition the length scale method will help and guide the engineers to solve the more complicated details efficiently. The approach will be more general applicable.

REFERENCES

1. Bea, R, et al. (1992-1996) Ship Maintenance Project. Ship Structure Committee, SSC-395, Washington D. C.
2. Burnside, OH, et al. (1984) Long-term Corrosion Fatigue of welded Marine Steel. Ship Structure Committee SSC-326.
3. Hobbacher A. Recommendations for Fatigue Design of Welded Joints and Components. IIW document XIII-2151r1-07 / XV-1254r1-07, 2007.
4. IACS. Common Structural Rules for Double Hull Oil Tankers. 2006
5. Lotsberg, I. and Einar Landet. (2004a), Fatigue capacity of side longitudinals in floating structures. OMAE-FPSO'04-0016, Int. Conf. Houston.

6. Lotsberg, I. Recommended Methodology for Analysis of Structural Stress for Fatigue Assessment of Plated Structures. OMAE-FPSO'04-0013, Int. Conf. Houston.
7. SR202 of Shipbuilding Research Association of Japan. Fatigue Design and Quality Control for Offshore Structures. International Institute of Welding (IIW) Document: IIW XIII-1414-91, 1991.
8. Yagi, J., Machida, S., Tomita, Y., Matoba, M., and Kawasaki, T. Definition of Hot Spot Stress in Welded Plate Type Structure for Fatigue Assessment. Journal of the Society of Naval Architects of Japan, Vol.169, p.311-318, 1992 (in Japanese), IIW-XIII-1414-91, International Institute of Welding, 1991.

CHAPTER 9

CONCLUSIONS AND RECOMMENDATIONS

9.1 Achievements

A new stress concentration and stress intensity factor assessment method has been established.

The main achievements are:

1. A singular stress field in the vicinity of a sharp corner is characterized by a length scale: ‘as’;
2. The length scale is related to the shape and dimensions of the structural detail;
3. The length scale is related to the stress intensity factor through the concept of an effective additional crack length: ‘ae’. For right angled corner or notches bigger than ‘as’, ‘ae’ is empirically found to be approximately equal to the length scale ‘as’;
4. The nature of the stress field can be defined by the length scale and this indicates to the stress analyst the mesh size required to capture the stresses as they tend to infinity at the singularity;
5.
6. Using Paris Law, the fatigue life of a detail is predicted from ‘ae’; and from usage of the fatigue life prediction ‘ae’ and hence ‘as’ is related to a fatigue SCF;
7. SCFs predicted from the length scale ‘ae’ are compared with SCFs predicted by conventional linear and quadratic extrapolation methods.

8. SCFs predicted from the length scale ‘ae’ are compared with SCFs predicted from the stress interpolated to 1.2mm from the corner.
9. Fatigue strength predicted using the length scale method has been compared with large scale experiments on ship structural details of HHI;
10. Alternatively the length scale indicates the distance away from the corner, where the stresses can be considered nominal values (i.e. values that are not substantially affected by the singularity).

9.2 Conclusions

The aim of the series of approaches review above is to provide effective fatigue design way; ignoring the time-consuming of FEM procedures and uncertainty of surface points’ extrapolation. The designer will spend less time to check structure fatigue analysis and verify in advance that the Length Scales are importance in stress concentration calculations.

Conclusions at algorithm level are already drawn in individual chapters, so an overview has been offered here to generalize what had been studied for future fellows. The main advantage of the Length Scale approach is the combination with fatigue assessment obtained in this research.

a) An analogy has been shown to exist between the well known Westergaard stress function and similar to sharp re-entrant corner. The closed form solutions to corner elasticity problems can be generated with Williams’ index for the similar traction-free crack problem.

The novel length scale raiser stress definitions are based on an approximate analytical frame, and the accuracy has been carefully checked against numerical analyses. The dimensional factor ‘as’ has been found to represent the stress field well in 70% of the numerical models and that makes an empirical formulation of practical interest.

Care is required to identify cases where the existing length scale method does not perform well. A case would be when there is significant bending, either in or out of plane.

The method works well for gusset attachment plates to longitudinal stiffeners, and other stiffened plate structural connections.

b) Although the extrapolation method (hop-spot method) is accepted by most classification societies, the accuracy of the SCF obtained from the extrapolation methods will clearly depend on the actual size of the prototype structure, the extrapolation points and the mesh size. It should be best to estimate effective applied reference stress; it may be possible, on basis of systematic studies using the geometry factor methods, to come up with simple guidance for SCFs of various welded connection configurations. The Length Scale can be used in a formula, which can be used to convert the geometry characteristics into an SCF.

c) Stresses determined at 1.2mm from the corner were also found to be a good indicator of the SCF.

d) For short cracks (roughly smaller than ‘as’) the length scale method needs to be modified to account for the K value tending to zero as the crack size tends to zero. This is a result of the 90-degree-corner stress singularity being slightly weaker (power = 0.455 for a right angled corner) than the crack singularity (power = 0.5).

e) The proposed method compared with the FE resulted in typical relative differences in the order of 1%. The method can be used to make useful predictions, even in the very short crack stage.

f) For more complex cases in real ship structural locations, multi stage approaches may be required as the crack grows and breaks flanges or moves from a web into shell plating.

g) It has been observed that the developed program can reasonably predict fatigue crack propagation behaviour in comparison with experiments.

In the experiments of the HHI bracket-type specimens, the real details were approximated to the cruciform and the SCF prediction formula using 'as' was found to result in a good estimate of fatigue life.

h) For full-scale ship hull construction, the applicability of the method has been discussed for details such as stiffened panels with corner connections, transverse frame structures and bracket attachments to the longitudinal stiffener flange.

i) From the results of the simulations and the experiments, it is shown that the length scale methodology in stiffener can offer good results. This may imply a possibility of avoiding, or at least better targeting of the details to subject to numerical FEA simulations.

It is apparent that not only SCFs but also stress intensity factors can be easily estimated using length scale methods. This could change the habits of designers, especially those working on stiffened plated structures at the preliminary design stage.

9.3 Future Works

Besides the achievements above, numerous tasks are still left for future scientific research. Actually the work is still ongoing, further understanding of the stress flow inside of the system for more cases studies.

Those involving out of plane bending will allow the clear SCF estimation for fatigue assessment in much more complicated realistic details.

Attachments to folded plates (e.g. stiffener flange-web-bracket connections) are more complex than the simple cruciform and need further research to fully understand the effects of the in-plane bending moments that result from the eccentric forces within these connections.

Thickness changes between the attached plate and the parent plate have been considered in this work but the analysis of cracks growing from one plate thickness into another, or moving through a junction of three plates requires further work.

The effects of shear forces need to be considered.

It is evident that there is also room for further progress in fatigue calculations out with this area:

a) Large cyclic straining of the material,
b) Residual stress effects
c) Corrosion of the surface.

APPENDIX A

ANALYTICAL STRESS FORMULA DERIVATION

Before we begin with the concept of the analytical stress derivations, the pertinent aspects of analytic and harmonic functions should be examined first.

An analytic function $f(z)$ can be regarded as a function of x and y having single-valued continuous partial derivatives. Thus:

$$\frac{\partial}{\partial x} f(z) = f'(z)$$
$$\frac{\partial}{\partial y} f(z) = if'(z) \qquad \text{A.1}$$

where $z = x + iy$

Now, let us assume the function $f(z)$ takes the form

$$f(z) = P(x,y) + iQ(x,y)$$
or simply $f(z) = P + iQ$ A.2

Accordingly

$$\frac{\partial f(z)}{\partial x} = \frac{\partial P(x,y)}{\partial x} + i\frac{\partial Q(x,y)}{\partial x}$$
$$\frac{\partial f(z)}{\partial y} = \frac{\partial P(x,y)}{\partial y} + i\frac{\partial Q(x,y)}{\partial y} \qquad \text{A.3}$$

And then

$$i\left(\frac{\partial P(x,y)}{\partial x} + i\frac{\partial Q(x,y)}{\partial x}\right) = \frac{\partial P(x,y)}{\partial y} + i\frac{\partial Q(x,y)}{\partial y} \qquad \text{A.4}$$

Equating the real and imaginary parts of the above expressions yields

$$\frac{\partial P(x,y)}{\partial x} = \frac{\partial Q(x,y)}{\partial y} \quad \text{and} \quad \frac{\partial P(x,y)}{\partial y} = -\frac{\partial Q(x,y)}{\partial x} \qquad \text{A.5}$$

The equations above are known as the Cauchy-Riemann equations, the functions P and Q are termed conjugate harmonic functions. It is evident that both

functions are real that the knowledge of one will enable the determination of its conjugate via the use of the Cauchy-Riemann equations.

In general, the theory of elasticity gives a full development of the equations for plane extension. The strain-displacement relationships and Hooke's law lead to compatibility equations:

$$\nabla^2(\sigma_x+\sigma_y)=(\frac{\partial^2}{\partial x^2}+\frac{\partial^2}{\partial y^2})(\sigma_x+\sigma_y)=0 \qquad \text{A.6}$$

The equilibrium equations are automatically satisfied by defining a stress function Φ, in terms of its relationship to the stresses, substituting the expressions for the stresses into the compatibility leading to

$$\nabla^4\Phi=\nabla^2(\nabla^2\Phi)=0 \qquad \text{A.7}$$

In the above expression Φ is a bi-harmonic function known as Airy's stress function, used in solving two dimensional boundary-value problems.

Indeed, considerable flexibility can be gained by adopting the complex stress function approach, since they are generally more concise and permit the solution of problems containing sharp corners, notches or cracks.

According to Muskhelishvili's complex stress function approach, it enables the Airy's stress function Φ to be written in terms of two complex functions, $\psi(z)$ and $\chi(z)$. The integral of the compatibility equations with respect to z is also another analytic function:

$$\int f(z)dz=\int(P+iQ)dz=p+iq=4\psi(z) \qquad \text{A.8}$$

We differentiate expression with respect to x, we get

$$\psi'(z)=\frac{\partial p}{\partial x}+i\frac{\partial q}{\partial y}=\frac{1}{4}f(z) \qquad \text{A.9}$$

$$\text{i.e.} \quad \frac{\partial p}{\partial x}+i\frac{\partial q}{\partial y}=\frac{1}{4}(P+iQ) \qquad \text{A.10}$$

Accordingly:

$$\frac{\partial p}{\partial x}=\frac{P}{4} \quad \text{and} \quad \frac{\partial q}{\partial x}=\frac{Q}{4} \qquad \text{A. 11}$$

Now since p and q are conjugate analytic function, they satisfy the Cauchy-Reimann equation, then it is possible to express Eqn. A.12 as

$$\nabla^2\Phi = 4\frac{\partial p}{\partial x} = 2(\frac{\partial p}{\partial x} + \frac{\partial q}{\partial y}) \quad \text{A.12}$$

Equivalently, the above expression can be written as

$$\nabla^2(\Phi - xp - yq) = 0 \quad \text{A.13}$$

Consequently, obtain an expression for the stress function Φ as being

$$\Phi = xp + yq + p \quad \text{A.14}$$

Clearly, p has its conjugate q, such that

$$\chi(z) = p_1 + iq_1 \quad \text{A.15}$$

Accordingly, any stress function can be written as

$$\Phi = \mathrm{Re}[\overline{z}\psi(z) + \chi(z)] \quad \text{A.16}$$

where $\psi(z)$ and $\chi(z)$ are suitably chosen analytic functions

It is worth nothing that the general expression for the stress function $F(z)$ is

$$F(z) = \Phi + i\Omega = \overline{z}\psi(z) + \chi(z) \quad \text{A.17}$$

And that it is always possible to obtain the equivalent Airy's stress function. The Westergaard semi-inverse method (Westergaard, 1939) constitutes another simple and versatile tool for solving a certain class of plane elasticity problems. It uses the Airy's stress function representation, in which the solution of plane elasticity problem is reduced to finding a function Φ which satisfies the bi-harmonic Equation and the appropriate boundary conditions. In conformity with Eqn. A.17 above, Westergaard defined Airy's stress function Φ for symmetric problems by

$$\Phi = \mathrm{Re}\,\overline{\overline{Z}}_I + y\,\mathrm{Im}\,\overline{Z}_I \quad \text{A.18}$$

Here Φ automatically satisfied bi-harmonic equation, the stress resulting to be

$$\begin{aligned}\sigma_x &= \mathrm{Re}\,Z_I - y\,\mathrm{Im}\,Z_I' \\ \sigma_y &= \mathrm{Re}\,Z_I + y\,\mathrm{Im}\,Z_I' \\ \tau_{xy} &= -y\,\mathrm{Re}\,Z_I'\end{aligned} \quad \text{A.19}$$

The constant term entering $\sigma_{1,2,3}$ in equation takes different values depending on the applied loads and the geometry of the cracked plate. Now any function Z_I which is analytic in the region except for a particular branch cut along a portion of the x-axis will have the form.

$$Z_I = \frac{g(z)}{[(z+b)(z-a)]^{1/2}} \qquad \text{A.20}$$

This will solve crack problems for a crack along the x-axis at $-a \le x \le a$, $y = 0$ and leads to boundary conditions of uniform biaxial stress σ at infinity

$$Z_I = \frac{\sigma z}{(z^2 - a^2)^{1/2}} \qquad \text{A.21}$$

For the problem of an infinite plate subjected to uniform in-plane shear stresses τ at infinity, the boundary conditions may be stated as

$$\begin{aligned} &\sigma_x = \sigma_y = 0 \\ &\tau_{xy} = \tau \text{ for } (x^2 + y^2)^{1/2} = \infty \end{aligned} \qquad \text{A.22}$$

The Westergaard function of the sliding mode is

$$Z_I = \frac{i\tau z}{(z^2 - a^2)^{1/2}} \qquad \text{A.23}$$

The study of stress and displacement fields near the crack tip is important, because these fields govern the fracture process that takes place at the crack tip. In this section we make a thorough study of the stresses near the crack tip.

If we place the origin of the coordinate system at the crack tip $z = a$ through the transformation

$$\zeta = z - a \qquad \text{A.24}$$

The Westergaard function for an infinite plate with a crack of length $2a$ subjected to equal stress infinity, takes the form as

$$Z_I = \frac{\sigma(\zeta + a)}{[\zeta(\zeta + 2a)]^{1/2}} \qquad \text{A.25}$$

Expanding equation we obtain

$$Z_I = \frac{\sigma(\zeta + a)}{(2a\zeta)^{1/2}}[1 - \frac{1}{2}\frac{\zeta}{2a} + \frac{1\cdot 3}{2\cdot 4}(\frac{\zeta}{2a})^2 - \frac{1\cdot 3\cdot 5}{2\cdot 4\cdot 6}(\frac{\zeta}{2a})^3 + ...] \qquad \text{A.26}$$

For small $|\zeta|, (when |\zeta| \to 0)$, that is the distance near to the crack tip at $x = a$, the Westergaard function can therefore be written:

$$Z_I = \frac{K}{(2\pi\zeta)^{1/2}} \qquad \text{A.27}$$

Or if we using polar coordinates, r, θ we have

$$\zeta = re^{i\theta} \tag{A.28}$$

And the stresses near the crack tip are

$$\begin{aligned}
\sigma_x &= \frac{K_I}{\sqrt{2\pi r}}\cos\frac{\theta}{2}(1-\sin\frac{\theta}{2}\sin\frac{3\theta}{2}) \\
\sigma_y &= \frac{K_I}{\sqrt{2\pi r}}\cos\frac{\theta}{2}(1+\sin\frac{\theta}{2}\sin\frac{3\theta}{2}) \\
\tau_{xy} &= \frac{K_I}{\sqrt{2\pi r}}\cos\frac{\theta}{2}\sin\frac{\theta}{2}\cos\frac{3\theta}{2}
\end{aligned} \tag{A.29}$$

Now suppose that the cracked plate is subjected to uniform stress σ and $k\sigma$ along *y* and *x* directions, respectively, at infinity. The stress field may be obtained by superimposing the stress field and the uniform field $\sigma_x = (k-1)\sigma$

Thus

$$\sigma_x = \frac{K_I}{\sqrt{2\pi r}}\cos\frac{\theta}{2}(1-\sin\frac{\theta}{2}\sin\frac{3\theta}{2}) - (1-k)\sigma \tag{A.30}$$

The quantity K_I is the opening stress intensity factor and expresses the strength of the singular elastic stress field. As shown by Irwin (1958), the equation applies to all crack-tip stress fields independently of crack/body geometry and the loading conditions.

Combined with the approaches of Williams and Westgaard described above, the study of stress and displacement fields near the crack initiation is important; we are trying to give a new stress formula for corner prediction (Xu and Barltrop, 2007, 2012[1]), although it is semi-analytical methodology, and the formula would be accepted by engineers more easily.

For illustration consider Z_I function, some of application cases are given below, such as a crack of length $2a$ in an infinite plate subjected to one direction uniform tension at infinity:

$$Z_I = \frac{pz}{\sqrt{z^2-a^2}} - \frac{1}{2}p \tag{A.31}$$

crack of length 2a in infinite plate subjected to partly uniform stress on the crack:

$$Z_I = \frac{2}{\pi}pa(\sqrt{\frac{a}{z}} - \arctan\sqrt{\frac{a}{z}}) \tag{A.32}$$

Using the ModeI Φ, the problem solved is that of a central crack of length, 2a,

opened by a pair of splitting forces P, acting against the crack surfaces at the position y=0, x=b.

$$Z_I = \frac{P}{\pi(z-b)} \cdot \frac{\sqrt{a^2-b^2}}{\sqrt{z^2-a^2}} \quad \text{A.33}$$

$$K = \frac{P}{\sqrt{\pi a}} \sqrt{\frac{a+b}{a-b}} \quad \text{A.34}$$

If we add a second pair of equal size splitting forces at the position $y=0, x=-b$, the total value of Z_I becomes

$$Z_I = \frac{2P}{\pi(z^2-b^2)} \cdot \frac{\sqrt{a^2-b^2}}{\sqrt{1^2-(a/z)^2}} \quad \text{A.35}$$

K value at each crack-tip is given by

$$K = \frac{2P}{\sqrt{\pi a}} \frac{a}{\sqrt{a^2-b^2}} \quad \text{A.36}$$

REFERENCES

1. H. M. Westergaard. Bearing pressures and cracks. Transactions, ASME, Journal of applied mechanics, 1939
2. G. R. Irwin. Fracture. Handbuch der physic, vol.VI, Springer, Berlin 1958
3. Li Xu and Nigel Barltrop. Analysis of Sharp Corners in Structural Details. Universities of Glasgow & Strathclyde, UK
4. Li Xu, Benqiang Lou and Nigel Barltrop, Considerations on the fatigue assessment methods of floating structure details, Journal of Engineering for the Maritime Environment 0(0) 1–12

APPENDIX B

Methods Adopted for K Calculations

B.1 Weight Function Method

Various analytical methods have also been used by several authors to develop approximate weight functions specifically. For deriving weight functions, proposed by Petroski and Achenbach, 1978 has attracted a lot of attention. However, it has been shown that the Petroski-Achenbach method can sometimes lead to inaccurate weight functions, dependent on the type of the reference stress field.

An appropriate reference stress intensity factor K, can often be found in the literature without, however, the crack opening displacements $u_r(x,a)$. Petroski and Achenbach proposed a general approximate crack opening displacement function $u_r(x,a)$ of the form

$$u_r(x,a) = \frac{\sigma_0}{\kappa\sqrt{2}}[4F\sqrt{a(a-x)} + \frac{G(a-x)^{3/2}}{\sqrt{a}}] \qquad \text{B.1}$$

Where, $F = K_r / \sigma_0\sqrt{\pi a}$

Thus, if the reference stress intensity factor K, and, as a consequence, the geometry correction factor fare known, the only unknown in Eqn.B.1 is the function G, which can be determined from the self-consistency of Eqn.B.2 resulting in:

$$K_r = \frac{\kappa}{K_r}\int_0^a \sigma_r(x)\cdot\frac{\partial u_r}{\partial a}dx \qquad \text{B.2}$$

However, the general weight function form of Eqn. B.2 seems to be adequate for many other crack configurations as demonstrated. The accuracy of weight functions approximated depends on the associated stress field $\sigma_r(x)$; it has been shown to be inaccurate for very non-uniform or discontinuous local reference stress

field $\sigma_r(x)$.

It was also pointed out that in some cases the three-term expression of Eqn.B.2 is not sufficient, requiring sometimes more than three terms.

For this reason Fett (1987) proposed a more general weight function in the form of expression Eqn.B.3

$$m(x,a)=\frac{2}{\sqrt{2\pi(a-x)}}[1+M_1(1-\frac{x}{a})+M_2(1-\frac{x}{a})^2+...+M_n(1-\frac{x}{a})^n] \qquad \text{B.3}$$

However, Shen and Glinka, 1991 found that a variety of existing weight functions has the same singular term and they can be accurately approximated by Eqn.B.4. Knowing the general weight function expression, the derivation of the weight function for particular geometrical configuration can be reduced to the determination of parameters M_1 M_2 and M_3.

$$m(x,a)=\frac{2}{\sqrt{2\pi(a-x)}}[1+M_1(1-\frac{x}{a})^{1/2}+M_2(1-\frac{x}{a})+M_3(1-\frac{x}{a})^{3/2}] \qquad \text{B.4}$$

The accuracy of the three parameters and consequently, accuracy of the weight function depends on the quality of the reference stress intensity factors. The method of derivation of these parameters M_1 M_2 and M_3 is discussed below.

Mathematically, the weight function $m(x,a)$, is the Green's function for the present boundary value problem scaled with respect to the crack dimension. It has been further shown by Niu and Glinka (1987, 1990) that the method makes it possible to derive a general weight function of the form Eqn. B.5

$$m(x,a)=\frac{2}{\sqrt{2\pi(a-x)}}[1+M_1(1-\frac{x}{a})+M_2(1-\frac{x}{a})^2] \qquad \text{B.5}$$

Knowing the 2-term general weight function expression, the derivation of the weight function for a particular geometrical configuration of cracked body can be reduced to the determination of parameters M_1 and M_2.

Although Eqn.B.3 of weight functions are admissible for crack problems, expressions of Eqn. B.4 and Eqn. B.5 are used more accuracy. Therefore, the general weight function forms of equations are tested to check the number of necessary terms required to sufficiently approximate known exact weight functions.

The principle of superposition allies on any linear elastic system. If two or more

different loadings are applied to the system, the effect of the combined loads is the sum of their individual effects. The principle of superposition enables us to relate K-values for different load cases when the geometries are the same.

Many authors also applied numerous weight functions of different mathematical forms available in technical journals and handbooks. The weight function $m(x,a)$ for an edge crack emanating from the weld toe in a T-butt joint was finally given in the polynomial form:

$$m(x,a)=(\frac{2}{\pi a})^{1/2}\frac{1}{\sqrt{1-x/a}}[1+m_1(1-\frac{x}{a})+m_2(1-\frac{x}{a})^2] \quad \text{B.6}$$

$$m_1=0.6147+17.1844\alpha^2+8.7822\alpha^6 \quad \text{B.7}$$

$$m_2=0.2502+3.2889\alpha^2+70.0444\alpha^6 \quad \text{B.8}$$

G. Glinka, 1991 generalized forms of mode I weight functions for the deepest point and the surface point of a surface, semi-elliptical crack in a flat plate. These expressions are subsequently used to determine weight functions and stress intensity factors for semi-elliptical cracks in plates, thin- and thick-walled cylinders.

$$m_A(x,a)=\frac{2}{\sqrt{2\pi(a-x)}}[1+M_{1A}(1-\frac{x}{a})^{1/2}+M_{2A}(1-\frac{x}{a})+M_{3A}(1-\frac{x}{a})^{3/2}] \quad \text{B.9}$$

$$m_B(x,a)=\frac{2}{\sqrt{\pi x}}[1+M_{1B}(\frac{x}{a})^{1/2}+M_{2B}(\frac{x}{a})+M_{3B}(\frac{x}{a})^{3/2}] \quad \text{B.10}$$

The weight function $m(x,a)$ does not depend on the stress distribution, but only on the geometry of the component. The limitation of the generalised method is that the determination of the parameters, which need more M values to apply to engineer conditions.

If the geometries are different then the principle does not strictly apply but may be used to obtain approximate solutions. Hence, the WF method enables an efficient and direct SIF calculation. However, the obvious disadvantage of this method is the number of reference stress intensity factors that has to be known and which could be difficult to find. However, the number of necessary reference SIF calculation can be decreased by using characteristic properties of weight functions.

The cracks propagate from the edge approaching to the centre of the plate till the failure of the whole plate, and the twin cracks growth will interact with each

other leading to the results similar with the ones from the semi-infinite plate.

B.1.1 Weight Function for double edge crack

Wigglesworth (1957) determined the crack opening displacement of the surface crack for a = 0 analytically. The solutions are given as a power series

$$u(\rho) = \sum_{n=0}^{\infty} A_n (1-\rho)^{n+1/2} \tag{B.11}$$

The coefficients up to the 12th order are

$$\begin{aligned} &A_0 = 1.0000 A_1 = -0.143719 A_2 = 0.019965 A_3 = 0.019665 \\ &A_4 = 0.011856 A_5 = 0.006254 A_6 = 0.002993 \\ &A_7 = 0.001256 A_8 = 0.000390 A_9 = -0.00001 \\ &A_{10} = -0.000172 A_{11} = -0.000213 A_{12} = -0.000212 \end{aligned} \tag{B.12}$$

The reference stress intensity factor associated with weight functions and relation form of the equations necessary for derivation of parameters $M_1, M_2 \ldots$.

The weight function for a double edge crack was derived using reference stress intensity factors according to general weight functions definitions. The final expressions for the weight function parameters are

$$\begin{aligned} M_1\left(\frac{a}{2b}\right) = {} & 0.08502 - 0.02230 \cdot \left(\frac{a}{2b}\right) - 1.41028 \cdot \left(\frac{a}{2b}\right)^2 + 4.64559 \cdot \left(\frac{a}{2b}\right)^3 \\ & + 19.6924 \cdot \left(\frac{a}{2b}\right)^4 - 148.266 \cdot \left(\frac{a}{2b}\right)^5 + 336.837 \cdot \left(\frac{a}{2b}\right)^6 \\ & - 336.591 \cdot \left(\frac{a}{2b}\right)^7 + 127.009 \cdot \left(\frac{a}{2b}\right)^8 \end{aligned} \tag{B.13}$$

$$\begin{aligned} M_2\left(\frac{a}{2b}\right) = {} & 0.2234 - 0.6146 \cdot \left(\frac{a}{2b}\right) + 11.1687 \cdot \left(\frac{a}{2b}\right)^2 - 56.5326 \cdot \left(\frac{a}{2b}\right)^3 \\ & + 151.937 \cdot \left(\frac{a}{2b}\right)^4 - 182.634 \cdot \left(\frac{a}{2b}\right)^5 + 86.4731 \cdot \left(\frac{a}{2b}\right)^6 \end{aligned} \tag{B.14}$$

$$\begin{aligned} M_3\left(\frac{a}{2b}\right) = {} & 0.4983 + 0.7512 \cdot \left(\frac{a}{2b}\right) - 10.5597 \cdot \left(\frac{a}{2b}\right)^2 + 47.9251 \cdot \left(\frac{a}{2b}\right)^3 \\ & - 115.933 \cdot \left(\frac{a}{2b}\right)^4 + 131.976 \cdot \left(\frac{a}{2b}\right)^5 - 59.8893 \cdot \left(\frac{a}{2b}\right)^6 \end{aligned} \tag{B.15}$$

It has been shown that the integration technique is accurate and easier from the view of the mathematical derivation. Much more efficient and easier method for stress intensity factor calculation should be found for engineering fatigue application, such as using the length scale function method.

B.1.2 Weight Function for edge crack in infinite plane

Observing the numerical points carefully, the trend of the results looks similar with that of the shape edge crack in an infinite width plane. As a reason, to give additional checks of the weight functions, the stress intensity factors were plotted in Figure B.1 for pure tension, by application of finite element calculations, and also comparing with the boundary collocations function F

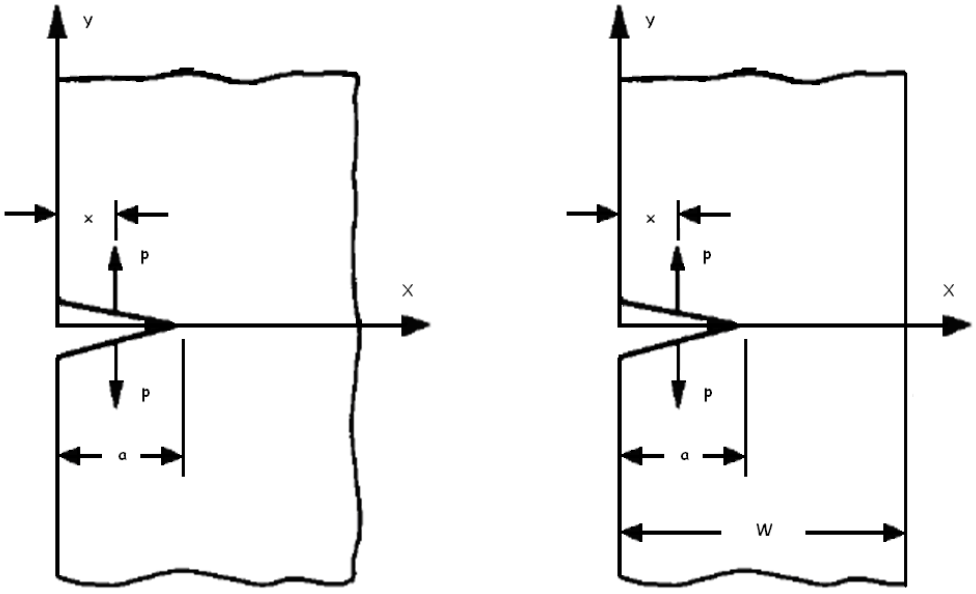

a) b)

Figure B.1 Weight function notation for edge crack in bodies:
(a) in a semi-finite plate; (b) in a finite width plate

It is therefore of practical significance to develop weight function solutions for both embedded cracks in infinite body and in semi-infinite body, which will enable the determination of stress intensity factor.

The weight function for an edge crack in a semi-infinite plate (Figure B.1.a) is derived analytically by Sih in the form

$$m(x,a)=\frac{2}{\sqrt{\pi a(1-(\frac{x}{a})^2)}}[1.3-0.3(\frac{x}{a})^{5/4}] \quad \text{B.16}$$

The least square fitting of B.5 expression to general weight function form resulted in the determination of the factors in front of the terms in equations.

$$m(x,a)=\frac{2}{\sqrt{2\pi(a-x)}}[1+0.569300(1-\frac{x}{a})+0.279375(1-\frac{x}{a})^2] \quad \text{B.17}$$

here: $M_1=0.569300; M_2=0.279375$ B.18

Or

$$m(x,a)=\frac{2}{\sqrt{2\pi(a-x)}}[1+0.0719768(1-\frac{x}{a})^{1/2} + 0.246984(1-\frac{x}{a})+0.514465(1-\frac{x}{a})^{3/2}] \quad \text{B.19}$$

here: $M_1=0.0719768; M_2=0.246984; M_3=0.514465$ B.20

An accuracy comparison of different weight function formula changing, calculated using Eqn. B.16 and B.20 to the theoretical points of crack length ratio, is shown in Figure B.2.

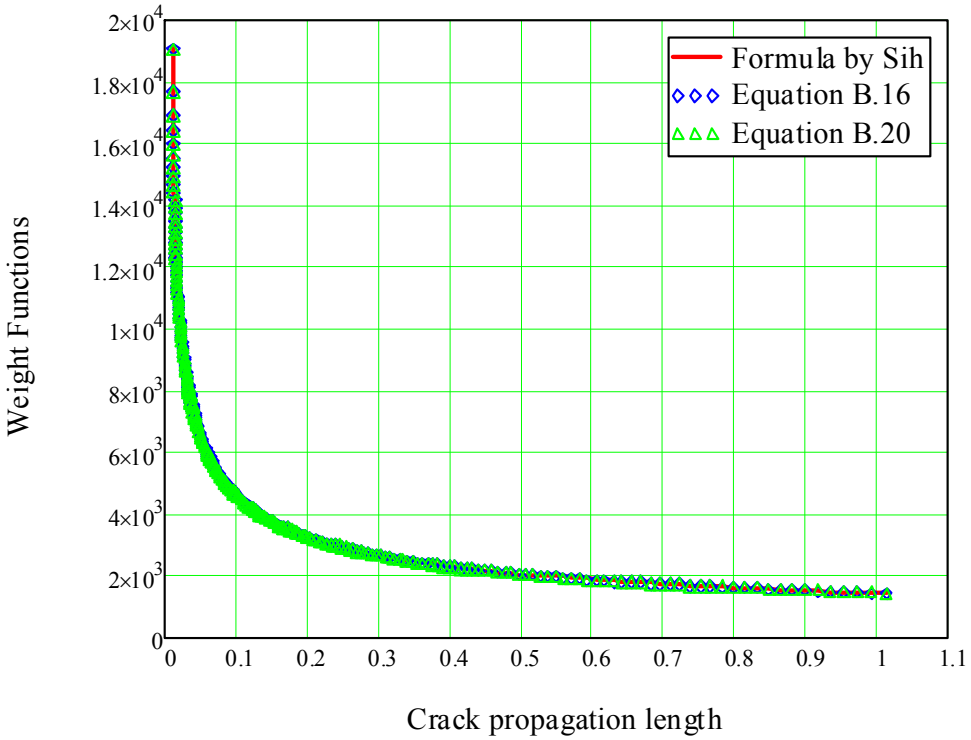

Figure B.2 Comparison of weight functions for single edge crack in a semi-infinite width plate

B.1.3 Weight Function for edge crack in finite plane

The other analytical weight function for single edge crack in a finite width plate (Figure B.1.b) was given by Kaya and Erdogan (1980) that

$$m(x,a)=\frac{2}{\sqrt{\pi a}}\frac{G(\frac{x}{a},\frac{a}{2b})}{(1-a/2b)^{3/2}\sqrt{[1-\left(\frac{x}{a}\right)^2]}} \qquad \text{B.21}$$

The unknown functions in weight function can be expressed by combined formula of fitting parameters and the geometric ratio.

$$G(\frac{x}{a},\frac{a}{2b})=g_1(\frac{a}{2b})+g_2(\frac{a}{2b})\cdot\frac{x}{a}+g_3(\frac{a}{2b})\cdot\left(\frac{x}{a}\right)^2+g_4(\frac{a}{2b})\cdot\left(\frac{x}{a}\right)^3 \qquad \text{B.22}$$

There are 4 corrective function factors in the function above, which has make determination, application and correction of the functions more complicated, and more than the numerical factor in front of the ratio be known.

$$g_1(\frac{a}{2b}) = 0.46 + 0.36 \cdot \frac{a}{2b} + 0.84 \cdot (1 - \frac{a}{2b})^5 + 0.66 \cdot (\frac{a}{2b})^2 \cdot (1 - \frac{a}{2b})^2 \quad \text{B.23}$$

$$g_2(\frac{a}{2b}) = -3.52 \cdot (\frac{a}{2b})^2 \quad \text{B.24}$$

$$g_3(\frac{a}{2b}) = 6.17 - 28.22 \cdot \frac{a}{2b} + 34.54 \cdot (\frac{a}{2b})^2 - 14.39 \cdot (\frac{a}{2b})^3 - (1 - \frac{a}{2b})^{3/2} - 5.88 \cdot (1 - \frac{a}{2b})^5 - 2.64 \cdot (\frac{a}{2b})^2 \cdot (1 - \frac{a}{2b})^2 \quad \text{B.25}$$

$$g_4(\frac{a}{2b}) = -6.63 + 25.16 \cdot \frac{a}{2b} - 31.04 \cdot (\frac{a}{2b})^2 + 14.41 \cdot (\frac{a}{2b})^3 + 2 \cdot (1 - \frac{a}{2b})^{3/2} + 5.04 \cdot (1 - \frac{a}{2b})^5 + 1.98 \cdot (\frac{a}{2b})^2 \cdot (1 - \frac{a}{2b})^2 \quad \text{B.26}$$

For the model, the general form of weight function is considered 2-term reference general Eqn.B.27; the derivation of point load weight function can then be simplified using this general expression.

$$m(x,a) = \frac{2}{\sqrt{2\pi(a-x)}}[1 + M_1(1 - \frac{x}{a}) + M_2(1 - \frac{x}{a})^2] \quad \text{B.27}$$

The derivation of weight function for an edge crack should be reduced to the derivation of parameters $M_1, M_2 \ldots$ along the entire crack front. The values for the unknown parameters M_1 and M_2 are not constant values like the situation in semi-finite plate, that is because the effect of the width in semi-infinite plate can be recognized as zero, while the influence should be separated by sub-interval crack in finite width plate. And the unknown factors M_1 and M_2 could be expressed as the function the crack ratio as following

$$M_1(\frac{a}{2b}) = 0.6147 + 17.1844 \cdot (\frac{a}{2b})^2 + 8.7822 \cdot (1 - \frac{a}{2b})^6 \quad \text{B.28}$$

$$M_2(\frac{a}{2b}) = 0.2502 + 3.2899 \cdot (\frac{a}{2b})^2 + 70.0444 \cdot (1 - \frac{a}{2b})^6 \quad \text{B.29}$$

B.2 Boundary Collocation Function

Even more, for a finite width plate containing edge crack shown in Figure B.3,

several reference solutions have been referred. For this kind of crack model, the stress intensity factor can be known for pure tension; and knowledge of solution (bending) allows being determined.

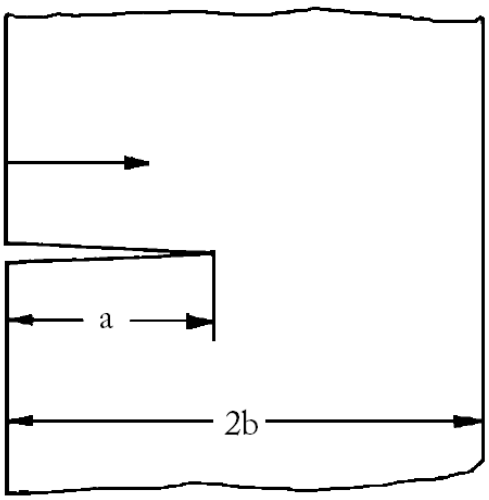

Figure B.3 Geometry of edge crack embedded in finite width strips

Tada and Fett etc. (1991) derived stress intensity factors for constant crack surface loads and quadratically distributed stresses. For $\sigma = \text{costant}$, one can fit the geometric function $F(a/b)$, as shown in Eqn. B.30.

$$F(a/b) = 1.122\frac{0.026778\left(0.427103 + a/b\right)^{-2.73895} + 0.26514a/b + 0.72475}{\left(1 - a/b\right)^{3/2}} \qquad \text{B.30}$$

The most accuracy results are given by least square fitting method (Gross 1964 and Brown 1966) in Eqn. B.31.

$$F(a/b) = 1.12 - 0.23(a/b) + 10.6(a/b)^2 - 21.7(a/b)^3 + 30.4(a/b)^4 \qquad \text{B.31}$$

The tension loaded edge crack several geometric functions have been compiled in handbook. One of them is given by Eqn. B.32.

$$F(a/b) = 0.265(1 - \frac{a}{b})^4 + \left(0.857 + 0.265\frac{a}{b}\right)\cdot(1 - \frac{a}{b})^{-3/2} \qquad \text{B.32}$$

One of expression is given by transcendental function, which referred the geometric function from the solution of central crack in a plate. In his viewpoint, the

geometric function is separated by the analytical expression and folded influences multiplied by function factors in Eqn. B.33.

$$F(a/b)=\sqrt{\frac{2b}{\pi a}\tan\frac{\pi a}{2b}}\cdot\frac{0.752+2.02(\frac{a}{b})+0.37(1-\sin\frac{\pi a}{2b})^3}{\cos\frac{\pi a}{2b}} \quad \text{B.33}$$

As the reference load case bending is used exclusively and for the geometric function F a solution based on the Boundary Collocation Method is applied, which for the edge crack in pure bending for any a/b is given by Eqn. B.34.

$$F(a/b)=\sqrt{\frac{2b}{\pi a}\tan\frac{\pi a}{2b}}\cdot\frac{0.923+0.199(1-\sin\frac{\pi a}{2b})^4}{\cos\frac{\pi a}{2b}} \quad \text{B.34}$$

Or $F(a/b)=\sqrt{\frac{\tan\lambda}{\lambda}}\cdot\frac{0.923+0.199(1-\sin\lambda)^4}{\cos\lambda}$

$\lambda=\pi a/2b$

The result by least square fitting method is presented of pure bending loaded condition in Eqn. B.35.

$$F(a/b)=1.122-1.40(a/b)+7.33(a/b)^2-13.08(a/b)^3+14.0(a/b)^4 \quad \text{B.35}$$

In case of pure tension of double crack in the plate, the solutions can be referred that from the case of central crack in plate. The solutions are compared with the geometric function F given by Eqn. B.36.

By asymptotic approximation, Benthem (1975) and Koiter derived the geometric function, F as

$$F(a/b)=\frac{1.122-0.561(a/b)-0.015(a/b)^2+0.091(a/b)^3}{\sqrt{1-a/b}} \quad \text{B.36}$$

Divided the central cracks to the both sides of the plate, the formula of Eqn. B.37 is completely identical for the modification of the Irwin's interpolation formula by Tada 1973.

$$F(a/b)=\frac{1.122-0.561(a/b)-0.205(a/b)^2+0.471(a/b)^3-0.19(a/b)^4}{\sqrt{1-a/b}} \quad \text{B.37}$$

The solutions of edge crack propagating in the rectangle strip has provide

various analysis results for difficult crack ratio shown in Figure B.4

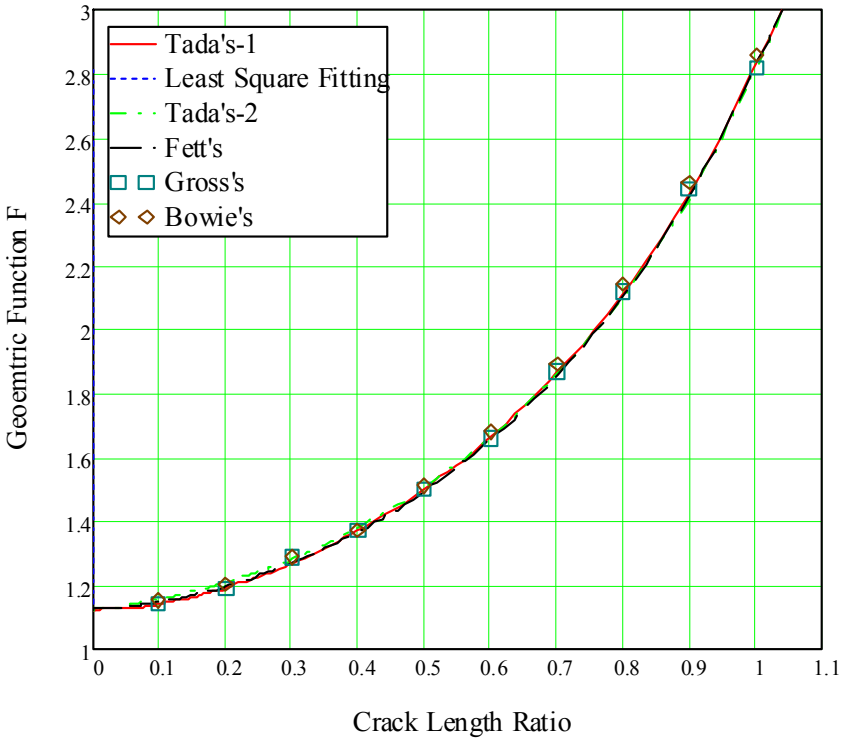

Figure B.4 Geometric function curves of the central crack in plate strip

Figure B.5 illustrates a plate containing a central crack. For this kind of crack model, the stress intensity factor is known for pure tension; and knowledge of a non-symmetrical solution (or bending) allows BC to be determined.

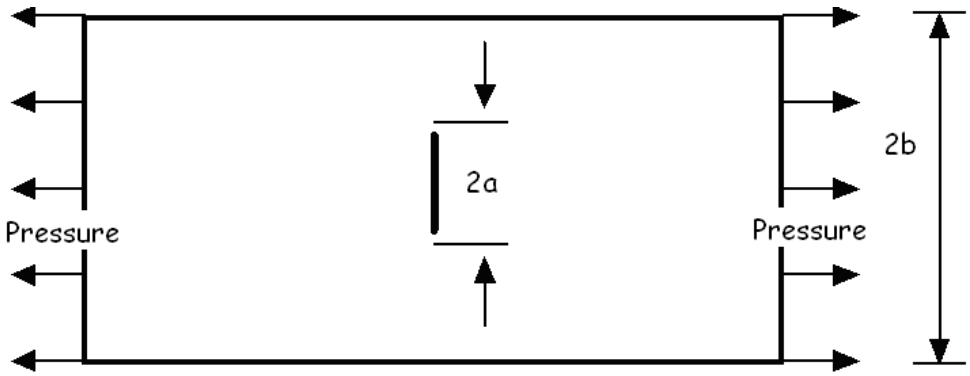

Figure B.5 Geometrical data of a rectangular plate with a central crack

It can be noted by comparing the result that geometric function corresponds to

the exact correction, equations below of a finite width strip approximate form having acceptable accuracy. Irwin (1957) gave approximate solution by periodic crack solutions (Eqn. B.38)

$$F(a/b) = \sqrt{\frac{2b}{\pi a}\tan\frac{\pi a}{2b}} \qquad \text{B.38}$$

Based on the Isida' series solution 1970, Brown et al also got least square fitting solution by the following form (Eqn. B.39):

$$F(a/b) = 1 + 0.128(a/b) - 0.288(a/b)^2 + 1.525(a/b)^3 \qquad \text{B.39}$$

Feddersen (1966) guessed empirical formula, based on the Isida's results, the accuracy of the formula is better than 0.3% even for the crack exceeding the half length of plate; it is more concise equation (Eqn. B.40) comparing with others.

$$F(a/b) = \sqrt{\sec\frac{\pi a}{2b}} \qquad \text{B.40}$$

Koiter 1965 used asymptotic approximation method got the solution (Eqn. B.41):

$$F(a/b) = \frac{1 - 0.5(a/b) + 0.326(a/b)^2}{\sqrt{1 - a/b}} \qquad \text{B.41}$$

Tada (1986) based on the works of Isdia, modified the solutions of Koiter's and Feddersen's and gave the empirical solution; the two equations can gave out more than 0.3% accuracy results for any a/b:

$$F(a/b) = \frac{1 - 0.5(a/b) + 0.370(a/b)^2 - 0.044(a/b)^3}{\sqrt{1 - a/b}} \qquad \text{B.42}$$

$$F(a/b) = \left(1 - 0.025(a/b)^2 + 0.06(a/b)^4\right)\sqrt{\sec\frac{\pi a}{2b}} \qquad \text{B.43}$$

As a consequence, it was just illustrated that basic solutions were used with proper central crack case calculation, which can be applied in the similar cases of component having internal crack in the plate; the stress intensity factor calculation can be recognized as the combination of the two cases of different crack lengths in centre of plate. Examples a symmetric crack in the shape of strip should be considered as well for the special problems. The solutions will provide approximate analyses for more difficult situations shown in Figure B.6

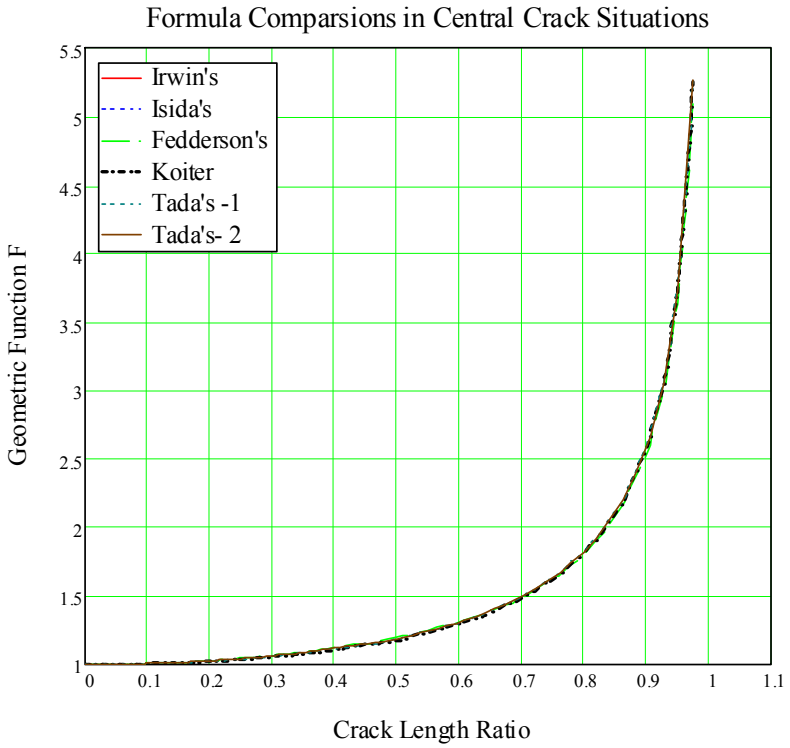

Figure B.6 Geometric function curves of the central crack in plate strip

Based on the numerical and empirical results of SIF in tension (or bending loads) reported herein, SIF of engineering components (such as naval or offshore structures) are assumed to be predicted.

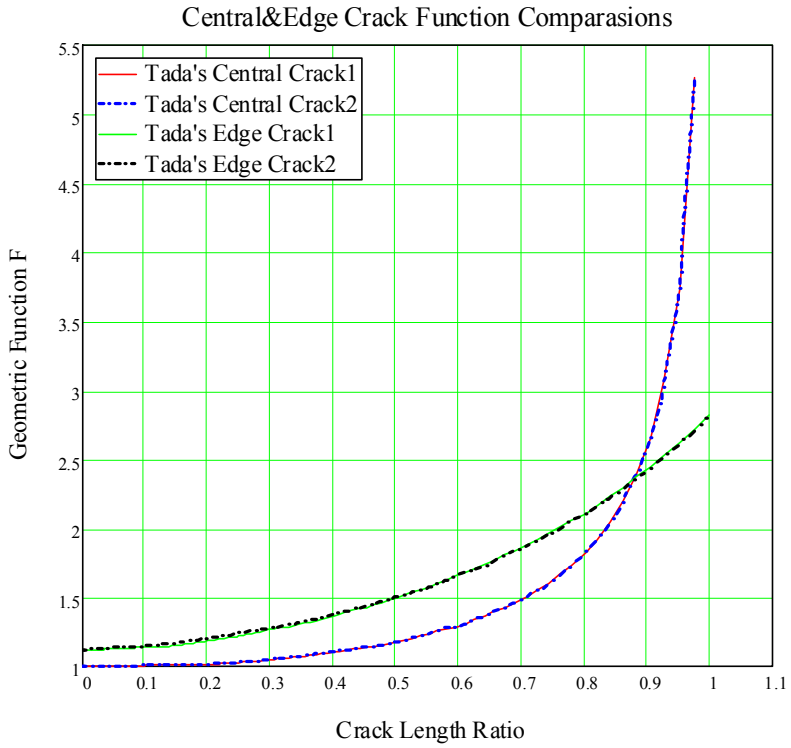

Figure B.7 Geometric function curves of the central crack in plate strip

B.3 Relationship between BCM and WF

The weight function method can be used to obtain stress intensity factors under complex loading conditions. It should be noted that the type of stress distribution can be given by nonlinear expressions. The boundary collocation method can be regarded as a relatively simple extension of weight function method.

Mathematically, the weight function can be considered as a generalized Green's function for the stress intensity factor problem. It has been found that the weight function can often be represented by Eqn. B.44

$$m(x,a)=\frac{2}{\sqrt{2\pi(a-x)}}[1+M_1(1-\frac{x}{a})^{1/2} + M_2(1-\frac{x}{a})+M_3(1-\frac{x}{a})^{3/2}] \quad \text{B.44}$$

An important feature is that weight functions can be applied for wide variety of crack configurations. By using the general expression, the determination of weight function reduces to the determination of three parameters M_1, $M_2 and$ M_3.

The stress intensity factor may be good to compare with indication of the state of the stresses at the crack tip. If the reference stress intensity factors are known, these three parameters can be obtained with the help of assumed conditions.

In the current analysis, the following additional condition Eqn.B.45 is used, where $x = 0$ at the open end of the crack.

$$\left.\frac{\partial m(x,a)}{\partial x}\right|_{x=0} = 0 \qquad \text{B.45}$$

The condition, as opposed to the null second derivative condition at $x = 0$ proved analytically by Fett, 1997; was found to improve the accuracy of the derived weight functions.

In order to determine the weight function $m(x,a)$; two reference stress intensity factors are required. The stress intensity factor described for uniform stress distribution $\sigma(x) = \sigma_0$ in Eqn.B.46:

$$K_1 = Y_0(a)\sigma_0\sqrt{\pi a} \qquad \text{B.46}$$

Similarly, the stress intensity factor results for linearly varying stress distribution $\sigma(x) = \sigma_0(1 - x/a)$ in Eqn.B.47:

$$K_2 = Y_1(a)\sigma_0\sqrt{\pi a} \qquad \text{B.47}$$

Substituting these values plus the third condition into the above form of the weight function, the BCM equations with corresponding stress distribution, three equations solving unknowns of M_1, M_2 *and* M_3 are established in Eqn.B.49-B.51:

$$M_1 = \pi\sqrt{2}\left[\frac{14}{3}Y_0 - \frac{25}{3}Y_1\right] - \frac{64}{9} \qquad \text{B.48}$$

$$M_2 = \frac{5}{3}\left[\frac{\pi}{\sqrt{2}}\left(24Y_1 - 12Y_0\right) + 7\right] \qquad \text{B.49}$$

$$M_3 = -5\pi\sqrt{2}\left[2Y_1 - Y_0\right] - \frac{16}{3} \qquad \text{B.50}$$

This approach was developed for crack problems with prescribed stress

boundary conditions.

B.4 Summary of Elasto-Plastic Fracture Mechanics

The linear elastic analysis of the stress field in body with or without cracks, dealt with in the preceding, applies to ideal brittle materials for which the amount is negligible, of inelastic deformation near the tip. The singular stress fields represent the asymptotic fields from the distance tending to zero, and their realm of applicability is confined to a very small region around the crack tip. In other words, under the applied loading, the plastic zone configuration influences the strength of the deformation field and the stress distributions.

Little progress has been made on the important problems of tensile loadings opening a crack, although the anti-plane strain case is now well understood for both perfectly plastic (Hult and McClintock, 1956) and strain hardening (Neuber, 1961; Rice, 1967) materials, and some useful approximate models (Irwin, 1960 and Dugdale, 1960) have been proposed for tensile cases.

In the present we present an elementary analysis of the elastic-plastic stress field. It includes J-integral explanation, energy release rate G calculation and the plastic zone of Irwin and Dugdale.

For crack problems, Rice introduced the two-dimensional version of the conservation law, a path independent line integral, defined as the J-integral. It has come to receive widespread acceptance as an elastic-plastic fracture parameter.

The J-integral appeared in the works of provided the primary contribution toward the application of the path independent integrals to stationary crack problems in nonlinear elastic solids (shown in Figure B.8). In an effort to establish path independence for the J-integral the deformation theory of plasticity has been invoked.

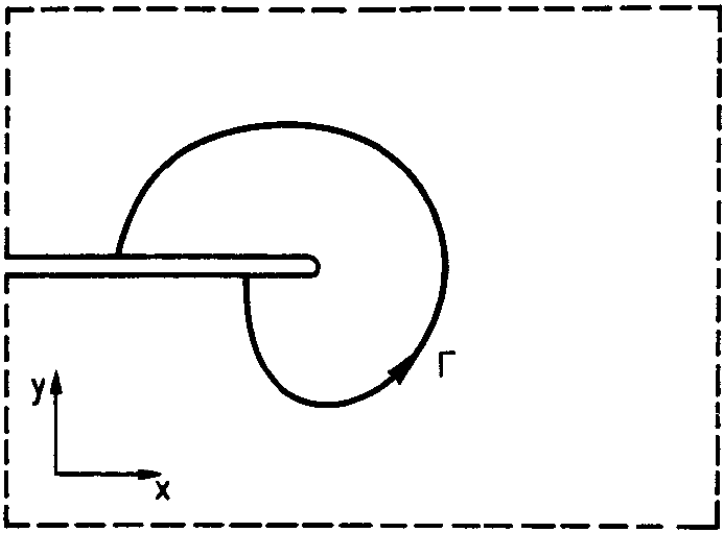

Figure B.8 Arbitrary path Γ integrals to stationary crack problem

The definition of the J integral in two-dimensional problems, and its physical interpretation in terms of the rate of potential energy with respect to an incremental crack. The potential energy $\Pi(a)$ of the body is given by

$$\Pi(a) = \int_A w dA - \int_\Gamma T_k u_k ds \qquad \text{B.51}$$

where A is the area of the body and s is the boundary

Under the previous assumptions differentiation of Eqn. B.51 with respect to crack length a yields, we get

$$J = -\frac{d\Pi}{da} \qquad \text{B.52}$$

For any path of integration surrounding the crack tip, it is expressed the J-integral as the rate of decrease of potential energy with respect to the crack length, and holds only for self-similar crack growth.

The integration path may be taken close or far away from the crack tip, and can be selected to make the calculation of the J-integral easy. Tractions and displacements are assumed to be independent of crack length.

$$J = \int_\Gamma [W(\varepsilon) dy - T \cdot \frac{\partial u}{\partial x} ds] \qquad \text{B.53}$$

having the same value for any path surrounding the tip

The utility of the method rests in the fact that alternate choices of integration

paths often permit a direct evaluation of J. In linear elastic analysis, and under pure modes, J can be used for the computation of stress intensity factor K below:

$$K = \sqrt{EJ} \qquad \text{(Plane stress)} \tag{B.54}$$

$$K = \sqrt{EJ(1-\upsilon^2)} \quad \text{(Plane stain)} \tag{B.55}$$

The path independent nature of the integral allows the integration path to be taken close or far away from the crack tip. The utility of the path independent integral lies largely in the fact that its value may be simply determined for a variety of cases and configurations.

Recently, the J-integral has been used to study three-dimensional nonlinear finite deformation of an elastoplastic body, dynamic fracture, thermal fracture (Nakamura etc, 1986), fracture in viscoplastic materials (Dexter, R. J, 1993), and creep and fatigue crack growth analysis (Dowling, 1976 and Riedel, 1980).

In early studies (Irwin, 1960), energy release rate is defined G in terms of the behaviour at the crack tip; it is also found a trend for G (Rice 1963) to decrease with increase of plate thickness, also found that G value to increase when the crack and plate size are increased.

The energy release rate and the corresponding stress intensity factor are determined for each crack extension increment in several possible crack propagation directions. It can be evaluated from the maximum energy release G criterion, where the released strain energy dW per crack extension da is dissipated.

$$G = -\frac{dW}{da} \tag{B.56}$$

If W_N is the energy in original configuration of crack tip elements, while W_D is the energy in subsequent configuration of these elements with virtually extended crack tip δa . Then for virtual crack extension da it follows:

$$G = \frac{dW}{da} = \frac{W_D - W_N}{\delta a} \tag{B.57}$$

The relationship between G and K of an isotropic material is established by using Irwin's crack closure integral (Irwin, 1958).

$$G = \frac{(1-\upsilon^2)}{E} K_I{}^2 + \frac{(1-\upsilon^2)}{E} K_{II}{}^2 \tag{B.58}$$

By using the instantaneous energy release rate, the virtual crack closure

technique (VCCT) is a very efficient method for determining the stress intensity factor for any given virtual crack extension. This technique was originally proposed by Rybicki and Kanninen (1977), is a very attractive SIF extraction technique, a relatively easy algorithm of application capability of FEM relating with the energy release rate.

Simplified model for plane stress yielding which avoids the complexities of a true elastic-plastic solution was introduced by Dugdale, 1960. The model applies to thin plates in which plane stress conditions dominate, and to materials with elastic-plastic behaviour which obey the yield criterion. For lower stress levels, or for which the plastic zones are much smaller than the plate thickness, it was found that the yield regions through the thickness remain almost the same; this is consistent with plane strain deformations.

Yielding leads to stress redistribution and modifies the size and shape of the plastic zone shown in Figure B.9. However, we can obtain some useful results regarding the shape of the plastic zone from the approximate calculation.

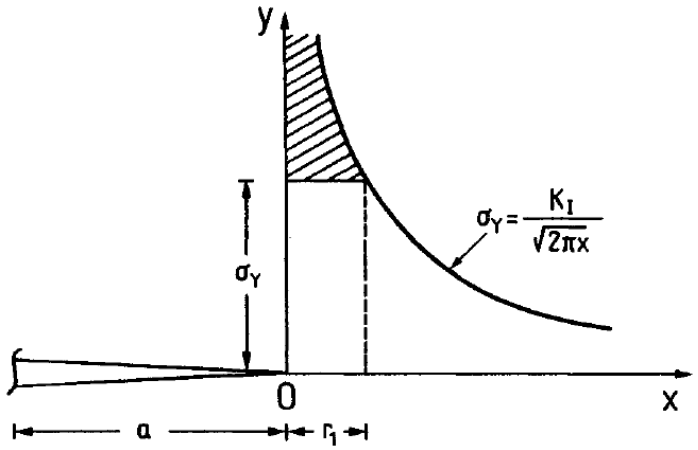

Figure B.9 Plastic zone of an elastic-plastic analysis of the stress field

It can be remembered even that, clearly demonstrated by the analytical approaches, Irwin's contention is that if a crack extends by a small amount r_y. Thus, as a result of the crack-tip plasticity, the displacement is larger and the stiffness of the plate is lower than in the elastic case.

Or if based on the solution by Nikishkov and Vainshtok (1980), the stress

intensity factor could be expressed as following:

$$KI = \frac{1}{2}\sqrt{E^*}(\sqrt{J_1 - J_2 - G_3} + \sqrt{J_1 + J_2 - G_3}) \quad \text{B.59}$$

$$KII = \frac{1}{2}\sqrt{E^*}(\sqrt{J_1 - J_2 - G_3} - \sqrt{J_1 + J_2 - G_3}) \quad \text{B.60}$$

$$KIII = \sqrt{2\mu G_3} \quad \text{B.61}$$

Where

$$E^* = E[\frac{1}{1-\nu^2} + (\frac{\nu}{1+\nu})\frac{\varepsilon_{33}}{\varepsilon_{11} + \varepsilon_{22}}] \quad \text{B.62}$$

This argument is supported by the following fundamental properties of J: (1) J is path independent for linear or nonlinear elastic material response; (2) J is equal to $-d\Pi / da$ for linear or nonlinear elastic material response; (3) K can be related to the crack-tip opening energy relationship by a simple relation of the form $K = \sqrt{EJ}$; (4) J can be calculated by FEM easily.

As discussed already, the increase in cracked area due to a virtual crack extension of Δa and energy approach is simple. In more complicated analysis, the J-integral has to be applied to some point on the crack front if the local value of the energy release rate is sought, and the increase in cracked area has to be calculated.

Consider the case of a smooth specimen containing a crack and having an applied stress range $\Delta\sigma$, combining the linear elastic stress intensity equations, J loses its potential energy interpretation, but retains physical significance as a measure of the crack tip strain field, is expressed as follows:

$$\Delta J_e = \frac{Y^2 \Delta\sigma\pi(a + a_0)}{E} \quad \text{B.63}$$

$$\Delta J_e = 2\pi Y^2 W_e(a + a_0) \quad \text{B.64}$$

where We is the elastic strain energy density, ($\Delta\sigma^2 / 2E$)

An approximate solution for J_p of the exponential plastic case may be obtained based on an estimate that has been made by Shih and Hutchinson (1975) for tension loaded cracked members.

$$\Delta J_p = 2\pi Y^2 f(n) W_p(a + a_0) \quad \text{B.65}$$

The quantity W_p is the plastic strain energy density, which may be expressed in

terms of n, stress ($\Delta\sigma$) and plastic strain range (Δe_p), causing Eqn. 3.109 to yield:

$$\Delta J_p = 2\pi Y^2 f(n)\frac{\Delta\sigma\Delta e_p}{n+1}(a+a_0) \qquad \text{B.66}$$

For combined elastic-plastic deformation, the last total J may be approximated to express as:

$$\Delta J = 2\pi Y^2(a+a_0)[\frac{f(n)}{n+1}\{\frac{\Delta\sigma\Delta eE}{E}\}-\{\frac{2f(n)}{n+1}-1\}\frac{\Delta\sigma^2}{2E}] \qquad \text{B.67}$$

To estimate the extent of the plastic zone in front of the crack, Irwin presented a simplified model for the determination of the plastic zone attending the crack tip under small-scale yielding. Using the approximate solution and found that the distance r_p from the crack tip to the point of the yield stress is exceeded.

Introducing the expressions for the singular principal stresses into the von Mises yield criterion expressed, we obtain the following expression of the plastic zone

$$r_p(\theta) = \frac{1}{4\pi}(\frac{K_I}{\sigma_Y})^2(\frac{3}{2}\sin^2\theta+1+\cos\theta) \qquad \text{B.68}$$

for plane stress

and

$$r_p(\theta) = \frac{1}{4\pi}(\frac{K_I}{\sigma_Y})^2[\frac{3}{2}\sin^2\theta+(1-2\upsilon)^2(1+\cos\theta)] \qquad \text{B.69}$$

for plane stress, where σ_Y is the yield stress

These observations propose that the effect of plasticity makes the plate behave as if it had a crack longer than actual crack size. The extent of the plastic zone along the crack axis ($\theta = 0$) is given by

$$r_p(0) = \frac{1}{2\pi}(\frac{K_I}{\sigma_Y})^2 \qquad \text{B.70}$$

for plane stress

Since internally applied forces are in static equilibrium, the distribution of stress in the sheet must be independent of elastic constants. We assume that plastic concentration in front of the crack; and which has an effective length which exceeds that of the physical crack by the length of the plastic crack.

It is apparent in this determination that the equilibrium condition along the y

direction is violated, since the actual elastic stress distribution inside the plastic zone is replaced by constant stress.

REFERENCES

1. A.C. Kaya and F. Erdogan. Stress intensity factors on COD in an orthotropic strip, internat. J. fracture 6. 171-190 (1980)
2. C.F. Shih and J.W. Hutchinson. Fully Plastic Solutions and Large Scale Yielding Estimating for Plane Stress Crack Problems. Division of Engineering and Applied Physics. Harvard University, Cambridge, Massachusetts 02138, Report No. DEAP-S-14, July 1975.
3. Dexter, R. J. and O'Donoghul, P. E., Computational procedures and energy integral for dynamic fracture in visco-plastic materials., Engineering Fracture Mechanics, 1993, 44, 591-607
4. Dowling, N. E. and Begley, J. A., Fatigue crack growth during gross plasticity and the J-Integral., ASTM STP, 1976, 590, 82-103
5. Dugdale, D.S., 1960. Yielding of steel sheets containing slits. J. Mech. Phys. Solids 8 (2), 100–104.
6. Feddersen, C. E. Plane strain crack toughness testing of high strength metallic materials, by W.F. Brown and J.E. Srawley, Am. Soc Test. Mater. Spec. Tech Publ. No. 410, (1966)
7. Fett T. Disappearing first derivative of weight functions. Engng Fract Mech 1997;57:583–7.
8. G. P. Nikishkov and V. A. Vainshtok. ’Method of virtual crack growth for determining stress intensity factors KI and KII, Strength of Materials, 12, 696-701 (1980).
9. G. R. Irwin, Fracture, Handbud der Physik. 6,551 (1958).
10. G. R. Irwin, Plastic zone near a crack and fracture toughness. Proc. 7th Sagamore Ordnance Material Conf., Syracuse University, NY (1960)
11. G. Shen and G. Glinka, Universal features of weight functions for cracks in mode 1, Eng. Fract. Mech. (1991)
12. H. Tada, "'The stress analysis of cracks handbook", Del Research Corporation

(1986).

13. Irwin, G. R., Analysis of stresses and strains near the end of a crack transversing a plate, Transactions of the ASME, Journal of Applied Mechanics, 1957, 24, 361.
14. J. R. Rice, A path independent inte8ral and the approximate analysis of strain concentrations by notches and cracks. I. Appl. Mech. Tmns. ASME, 85, 588 (1963).
15. J.P. Benthem, Three-dimensional state of stress at the vertex of aquarter-infinitecrack in ahalf-space Report WTHD Nr. 74, Department of Mechanical Engineering, Delft University of Technology (September 1975).
16. L. A. Wigglesworth, Stress distribution in a notched plate. Muthematika 4, 76-96 (1957)
17. Nakamura, T., Shih, C. F. and Freund, L. B., Analysis of a dynamically loaded three-point-bend ductile fracture specimen, Engineering Fracture Mechanics, 1986, 25, 323-339
18. Petroski HJ, Achenbach JD. Computation of the weight function from a stress intensity factor. Eng Fract Mech 1978;10:257–66.
19. Riedel, H. and Rice, J. R., Tensile crack in creeping solids., ASTM STP, 1980, 700, 112-130.
20. Rybicki EF, Kanninen MF. A finite element calculation of stress intensity factors by a modified crack closure integral. Engng Fract Mech 1977; 9:931–8
21. Shen G, Glinka G. Determination of weight functions from reference stress intensity solutions. Theor Appl Fract Mech 1991;15:237–45
22. T. Fett, C. Mattheck and D. Munz, On the calculation of crack opening displacement from the stress intensity factor. Engng Fracture Mech. 27, 697-715 (1987).
23. T. Fett, Conditions for the determination of approximative COD fields. Enging. Fract. Mech, 39 (1991), pp. 905–914.
24. X. Niu and G. Glinka, The weld prolile effect on stress intensity factors in weldments. ht. J. Fracture 35,3-20 (1987).
25. X. Niu and G. Glinka, Weight functions for edge and surface semi-elliptical

cracks in flat plates and plates with comers. Engng Fracture Mech. 36, 459-476 (1990).

APPENDIX C

FEA Applications in LEFM

C.1 Terminology of Finite Element Method

In the finite element method, the actual continuum or body of matter is represented as an assemblage of subdivisions called finite elements, taking solid mechanics as the example. These elements are considered to be interconnected at specified joints called nodes or nodal points. The nodes usually lie on the element boundaries where adjacent elements are considered to be connected. Since the actual variation of the stress field variable (e.g., displacement, stress, or velocity) inside the continuum is not known, we assume that the variation of the field variable inside a finite element can be approximated. The approximating function (also called interpolation model) is defined in terms of the values of the field variables at the nodes. By solving the field equations, which are generally in the form of matrix equations, the nodal values of the field variable will be known.

Once these are known, the approximating functions define the field variable throughout the assemblage of elements. The solution of continuum problem by the finite element method always follows an orderly step-by-step process. With reference to static structural stress problems, the step-by-step procedure can be stated as follows (S. S. Rao, 2004):

Step (I): Discretization of the simulation area, the first step in the finite element method, is to divide the structure (or solution region) into subdivisions or elements. Hence, the structure (plate or solid) is to be modelled with suitable elements. The number, type, size, and arrangement of the elements are to be decided.

$$q(x_i) = \sum_{i=1}^{n} N_i q_i \qquad \text{C.1}$$

Where n is the number of nodes for each element, q_i are nodal values of q, and N_i are element shape functions.

Step (II): Selection of proper interpolation and displacement model, since the displacement solution of real component under some specified load conditions cannot be predicted exactly, we assume some suitable solution to approximate the unknown results. The assumed ones must be simple from a computational standpoint, but it should satisfy certain convergence requirements. In general, the solution or the interpolation model is taken in the form of a polynomial.

Step (III): Derivation of element stiffness matrices and load vectors, from the model assumed above, the element stiffness matrix $[k^e]$ and the load vector are to be derived by using either equilibrium conditions or a suitable variational principle, the general formula of stiffness matrix is

$$k^e = \int B^T E B dV \qquad \text{C.2}$$

where B is the strain-displacement matrix, E is the material property matrix, and dV is an increment of the element volume V. To obtain B for the element by deriving shape function matrix N.

Step (IV): Assemblage of element equations to obtain the overall equilibrium equations, here the individual element stiffness matrices and load vectors are to be assembled in a suitable manner and the overall equilibrium equations have to be formulated as

$$[K]\{v\} = \{P\} \qquad \text{C.3}$$

where $[K]$ is the assembled stiffness matrix, $\{v\}$ is the vector of nodal displacements, and $\{P\}$ is the vector of nodal forces for the complete structure.

Step (V): Solution for the unknown nodal values; the overall equilibrium equations have to be modified to account for the boundary conditions of the problem. After the incorporation of the boundary conditions, the equilibrium equations can be used to solve the unknown values (like displacement). For linear problems, the vector displacement can be solved very easily. However, for nonlinear problems, the solution has to be obtained in a sequence of steps, with each step involving the

modification of the stiffness matrix $[K]$ and/or the load vector $\{P\}$.

Step (VI): Computation of structural stresses (or strains) at the nodes, from the known nodal displacements $\{v\}$, if required, the element stresses can be computed by using the equations of structural mechanics.

$$\sigma = [D][B]\left[\overline{d_i}\right]$$
$$\varepsilon = \sum [B_i]\left[\overline{d_i}\right] \qquad \text{C.4}$$

The terminology used in the previous six steps has to be modified if we want to extend the concept to other fields. For example, we have to use the term continuum or domain in place of structure, field variable in place of displacement, characteristic matrix in place of stiffness matrix, and element resultants in place of element strains. The application of the steps of the finite element analysis is illustrated with the help of the following schematic outline.

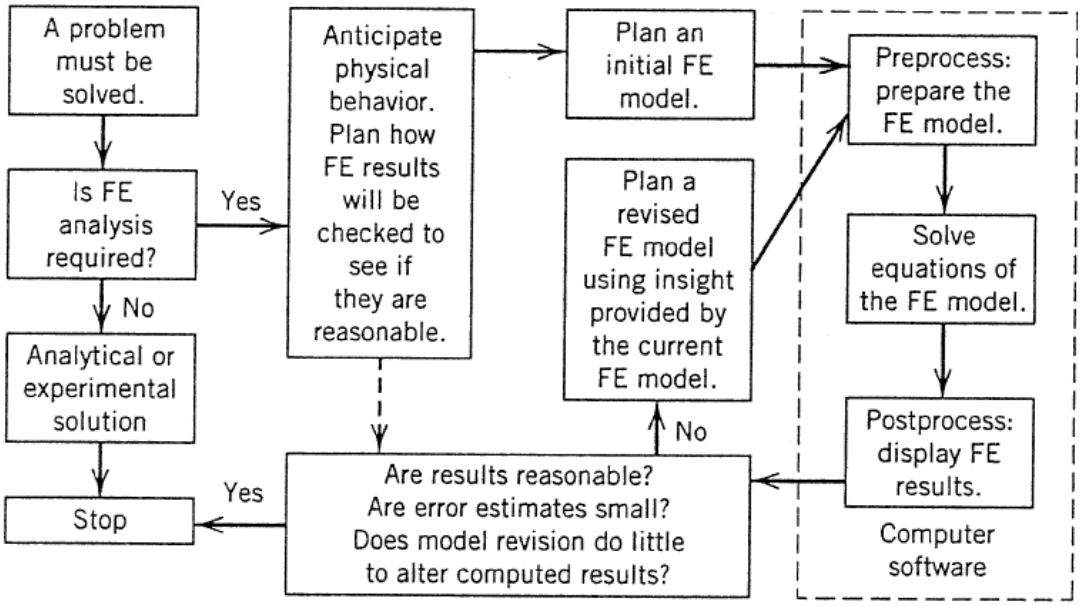

Figure C.1 Outline of the whole process in FE analysis project (S. S. Rao, 2004)

By now, there are commercial simulation software using the technologies of Finite Elements, and are capable of performing static (stress) analysis, (more such as thermal analysis, modal analysis, frequency response analysis, transient simulation and also coupled field analysis). The most frequent used ones are ANSYS (ANSYS

Inc, US, 1970), ABAQUS (Dassault Systèmes Simulia Corp. US, 1978), NASTRAN (MSC.Software Corporation, US, 1960s) and so on. It is convenient to use the general-purpose package, and for some professional manufacturing production analysis, engineers prefer to use some special ones such as SESAM (DNV), FAD (LR) etc.

ANSYS (or ABAQUS, NASTRAN) is a general-purpose finite-element package solving a wide variety of mechanical problems, all of them can be accepted to solve the fatigue and fracture problems.

SESAM is a life cycle management system, developed by DNV, delivering strength assessment and operational management from design to operation. It covers a structure's entire life cycle delivering engineering software support in design, structural re-analysis systems, modifications and repair, input to the operational phase, emergency response and decommission; FDA is similar software for production cycles developed by LR; they are used in naval architecture and offshore engineering widely.

This calculation method will be applied through our results verification and careful observation of structural calculations gained further insight into research serving life of ship structures.

C.2 Solid and Shell Elements Considerations

As assessing above, the typical stress equilibrium equation has been given. In the finite element method, the solution region is considered as built up of sub-regions elements. As an example of application of finite element method, it might be used to represent a complex geometrical shape, considering such as the bottom structure (or side ones) of ship. It is very difficult to find the exact response (like stresses and displacements) of the part under any specified loading condition. In each piece or element, a convenient approximate solution is assumed and the conditions of overall equilibrium of the structure are derived.

The satisfaction of these conditions will yield an approximate solution for the displacements and stresses. And each kind of elements or the dimensions of the

elements should be considered, considering the consuming of the calculation.

The term of ‘solid element’ is used to mean a three-dimensional solid that is unrestricted as to shape, loading, material properties. A consequence of this generality is that six possible stresses (three normal and shear) must be taken into account; the displacement field involves all three possible components. Typical finite element of 3D solids are tetrahedral and hexahedra showing in Figure C.2, with three translational DOF per node.

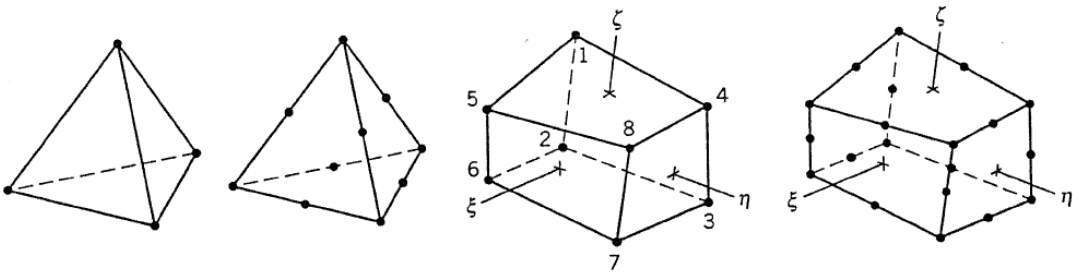

Figure C.2 Common tetrahedral and hexahedra 3D elements

With n the number of nodes per element, and translational DOF, these relations for 3D solids and solids of revolution are as follows:

$$\varepsilon_{6\times1} = B_{6\times3n} \cdot d_{3n\times1}$$
$$k_{3n\times3n} = \iiint B^T E_{6\times6} B dxdydz \qquad \text{C.5}$$

Additional 3D elements are of course possible and are described the documentation of commercial software. Some elements may have nodes at the middle of each face, in addition to midedge nodes. The analysis should consult the documentation, in case even the basic elements describe above the special features. Typical 3D elements do not use rotational DOF; accordingly, rotational DOF must be suppressed in the global equations. In examining computed displacements and stresses it is helpful to view results from different directions and on different cross sections. Most often, peak stresses appear on the surface of a solid; therefore a plot of surface stresses must be examined.

Problems of beam bending, plane stress, plates and so on, can all be regarded as special case of 3D physical problems. In fact, this would be a simplification by using 2D elements. 3D solid models are the hardest to prepare, the most tedious to check

for errors, and the most demanding of computer resources; as a reason 2D elements would become elongated in modelling plates, and shells.

A plate is a thin solid and might be modelled by 3D solid element. But a solid element is wasteful of DOF, as it computes transverse normal stress and transverse shear stresses, all of which are considered negligible in a thin plate. Also, thin 3D element invite troubles produces by ill-conditioning, plane element may be able to display states of constant σ_x σ_y and τ_{xy} if it is to pass patch tests; plate element may be able to display these states in each $z =$ constant layer (in Figure C.3).

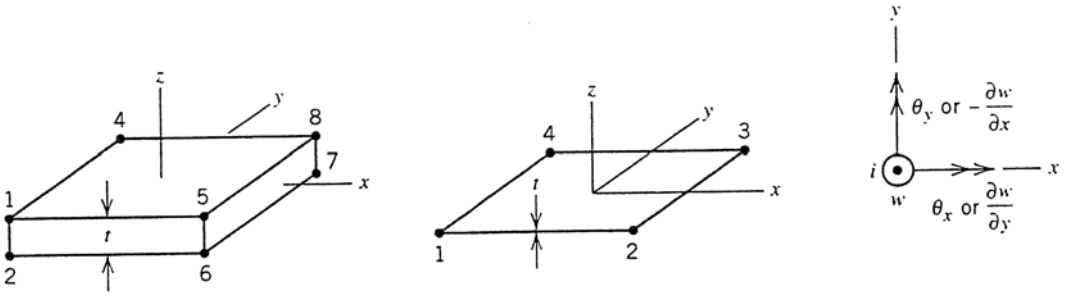

Figure C.3 The comparable solid and plate element, viewed normal to xy plane

For two-dimensional steady-state problem, the governing differential equation is

$$\frac{\partial}{\partial x}(k_x \frac{\partial T}{\partial x}) + \frac{\partial}{\partial y}(k_y \frac{\partial T}{\partial y}) + \dot{q} = 0 \qquad \text{C.6}$$

and the boundary conditions are

$$T = T_0(x, y)$$

$$k_x \frac{\partial T}{\partial x} l_x + k_y \frac{\partial T}{\partial y} l_y + q = 0 \qquad \text{on the boundary} \qquad \text{C.7}$$

$$k_x \frac{\partial T}{\partial x} l_x + k_y \frac{\partial T}{\partial y} l_y + h(T - T_\infty) = 0$$

A Mindlin element is based on nodal values, if all interpolations use the same polynomial, then for an element of n nodes; the N_i are given for a four-node quadrilateral element, an eight-node quadrilateral is also popular, based on the same N_i used for a plane eight-node.

$$N_1 = \frac{1}{4}(1-\xi)(1-\eta) \qquad N_2 = \frac{1}{4}(1+\xi)(1-\eta)$$
$$N_3 = \frac{1}{4}(1+\xi)(1+\eta) \qquad N_4 = \frac{1}{4}(1-\xi)(1+\eta) \qquad \text{C.8}$$

Accordingly, the behaviour of the Mindlin plate element can be reduced from the behaviour of the corresponding plane element provided that all terms of the integrand and integrated by the same quadrature rule; integration of $B^T EB$ with respect to z is done explicitly. Integration in the plane of the element is done numerically if the element is isoparametric.

$$\begin{Bmatrix} w \\ \theta_x \\ \theta_y \end{Bmatrix} = \sum_{i=1}^{n} \begin{bmatrix} Ni & 0 & 0 \\ 0 & Ni & 0 \\ 0 & 0 & Ni \end{bmatrix} \begin{Bmatrix} w_i \\ \theta_{xi} \\ \theta_{yi} \end{Bmatrix} = Nd \qquad \text{C.9}$$

Classical plate theory uses polar coordinates for circular plates. In FE analysis, it is simple by making shell elements flat rather than cylindrical of conical. Each such element is thus a flat annular ring. The geometry of a shell is defined by its thickness and its mid-surface, which is curved surface in space. Load is carried by a combination of membrane action and bending action. A thin shell can be very strong if membrane action dominated, in the same way that a wire can carry great load in tension but only small load in bending. A wire must have a different shape for every different distribution of lateral load if there is to be no bending.

Equations that describe the behaviour of shells of other shapes are considerably more complicated, so that shell solutions for engineering purposes must usually be obtained by FE analysis. Advantages of a flat element include simplicity of element formulation, simplicity in the description of element geometry, and the element's ability to represent rigid-body motion without strain.

Commercial software does some checking automatically. These checks involve computing a numerical value from the input data and comparing it with one or more stored values that define limits of acceptability. Software often allows a 'check run' that stops short of solving global equations or even generating them. Errors that may be detected by automatic data checks include the following: nodes are not connected

to any element; nodes are close together or coincident but not connected; elements share a node but do not use the same set of DOF at the node; The poisson's ratio should be in the range of $0 < \upsilon < 0.5$; the elements should not have too large aspect ratio or corner angles that differ too greatly; Side node may curve the side too greatly or be too far from mid-side; the linear element in space is too greatly warped; that is, its node are too far above or below the mean plane; a curved shell element spans too great an arc.

The FE method is not very good at calculating peak stress at holes, fillets, and so on. Often a stress raiser is small, being roughly the size of an element that would be used if the stress raiser were absent. The stress raiser is not modelled, but nominal stresses at its location are calculated by FE analysis. Then if a tabulated SCF for the local geometry and stress field is available, one need only multiply the nominal stress by the SCF to obtain the peak stress.

In an axially symmetric problem, radial and circumferential normal stress should be equal on the axis of revolution. None of these conditions is likely to be met perfectly. The amount of imperfection is a measure of discretizeion error, or is perhaps a warning of an error in the FE model. One would also suspect a error in modelling if there are unexpected stress gradients or stress concentrations. Inevitably, there will be disagreements between FE results and other results (analytical results, experimental, and formulas from handbooks) used for comparison. Reasons for any substantial disagreement must be sought. FE results are not necessarily when there is disagreement, but experience shows that most users are entirely too willing to accept computed results as face value. Close inspection of results shows how the FE model can be improved. A need for mesh refinement is indicated in regions where stress contours display considerable inter-element discontinuity.

Application of commercial software ANSYS, which supplies several meshing tool for meshing elements, can optimum our calculation in Figure C.4:

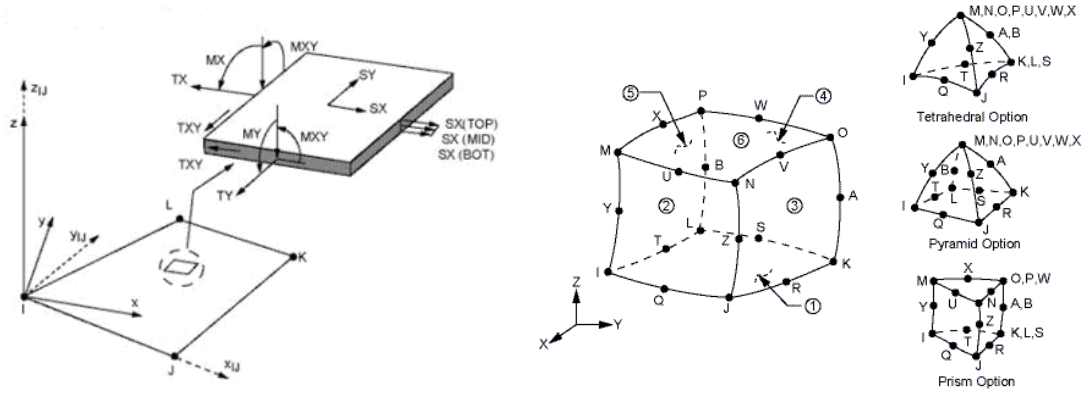

Figure C.4 Illustration of (a) Shell 63 input data; (b) Solid 95 geometry (ANSYS 13.0 User Manual)

Several requirements have to be satisfied for performing acceptable calculations related to discontinuities in the vicinity and the stress gradient close to the hot spot. However, the 20 node solid elements (Solid95) used for finite element modelling and the stresses obtained at midpoints of the first elements are normally slightly exaggerated due to the singularity at the weld toe and latter are somehow corrected by linear extrapolation applied for stress rising.

C.3 MPC Technology

The displacement based on finite element formulation occurs in the solution of structural static problems. The method is, however, general and can be also applied for solving multi-point constraint conditions on primary variables of finite element method (Mark Ainsworth, 2001, and Libor Jendele, Jan Cervenka, 2009). The fact significantly reduces computer storage requirements, which will be called Complex Boundary Conditions, or Multi-points Constraints.

The types of Von-Neumann boundary conditions have no impact on dimension n in FEA. Constraints can also be more complicated, such as those modelling rigid parts, or those transmitting motion between flexible bodies. Structural component may be consisted of rigid parts and moving parts connected together by rotational or sliding connections.

Here discussing a solution for implementing Dirichlet BCs form, each degree of

structural freedom is a linear combination with other degrees of freedom. The important point about implementing equations is that the boundary conditions are already utilized by assembling the equation system. It means that if we have m of these BCs, then the final dimension of the matrix K becomes only $n \times m$.

Let us suppose that all structural constraints are specified; mathematically, this is expressed as

$$u_l = u_{l0} + \sum \alpha_{lk} u_k \qquad \text{C.10}$$

The constraint may be as simple as that of identical displacements between nodes. The simply form of single boundary condition after manipulation is written as following:

$$\sum_{j=1}^{n} (K_{ij} + K_{ij}\alpha_{ij}\delta_{ij}) u_j = r_i - K_{il} u_{l0} \qquad i = 1,...,n \qquad \text{C.11}$$

The set of equations have already used to solve unknown displacements, which will be preceded to the case of multiple boundary conditions.

Redundant conditions are ignored and contradictory conditions are fulfilled after their summation. Therefore, before any such set of conditions is used, it is necessary to detect and fix all redundant and contradictory multiple conditions.

This is easily done in the case of a simple set of conditions, which can be written in vector form:

$$\bar{u}_l = \bar{u}_{l0} + A\bar{u}_k \qquad \text{C.12}$$

The above relationship represents a system of algebraic linear equations. The system is typically non-symmetric, sparse and has different numbers of rows (the number of conditions) and columns (the number of master and slave DOFs). It is often known which DOF is dependent (or slave) and which is independent (or master) previously.

The Multi-points Constraints are successfully implemented in the finite element package ANSYS; Multipoint constraint element (MPC184 in ANSYS) comprising a general constraint class that apply kinematic constraints between nodes. The elements are loosely classified here as ‘constraint elements’.

C.4 Singular Element in LEFM

It can be noticed that a slightly higher stress concentration effect occurs at the specimen mid-thickness point with respect to the specimen free surfaces (V Saouma, D Schwemmer, 1984). In equation C.9 if the stresses are to be singular, then [B] (FE theory has been described in Appendix C. 4) has to be singular as the two other components are constants. Consequently, if [B] is to be singular then the determinant of Jacobian Matrix, J-Matrix must vanish to zero at the crack tip.

$$J = \begin{bmatrix} \frac{\partial x}{\partial \xi} & \frac{\partial y}{\partial \xi} \\ \frac{\partial x}{\partial \eta} & \frac{\partial y}{\partial \eta} \end{bmatrix} \qquad \text{C.13}$$

Now considering a rectangular element of length L along its first side (1-2-3, in Figure C.5), we can readily see that both off-diagonal terms ($\partial y/\partial \xi$ and $\partial x/\partial \eta$) are zero.

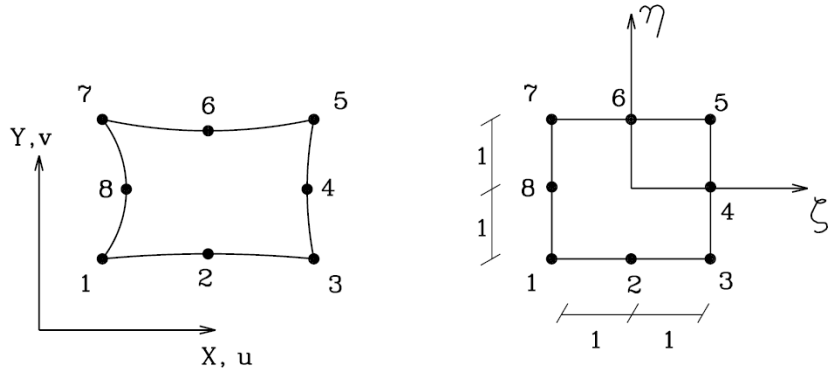

Figure C.5 Quadratic Finite Element: Global and Parent Element

Thus, for the determinant of the Jacobian to be zero we must have either one of the diagonal terms equal to zero.

It will suffice to force $\partial x / \partial \xi$ to be zero. Making the proper substitution for $\partial x / \partial \xi$ at $\eta = -1$, we have:

$$\left.\frac{\partial x}{\partial \xi}\right|_{\eta=1} = \frac{1}{4}(2+4\xi)L + \frac{1}{2}(-4\xi)x_2 \qquad \text{C.14}$$

After simplification and considering the first corner node (where $\eta = \xi = -1$), we would have:

$$x_2 = L/4 \qquad \text{C.15}$$

Thus all the terms in the Jacobian Matrix vanish if and only if the second node is located at $L/4$ instead of $L/2$, and subsequently both the stresses and strains at the first node will become singular. Thus singularity at the crack tip is achieved by shifting the mid-side node to its quarter-point position, see Figure C.6.

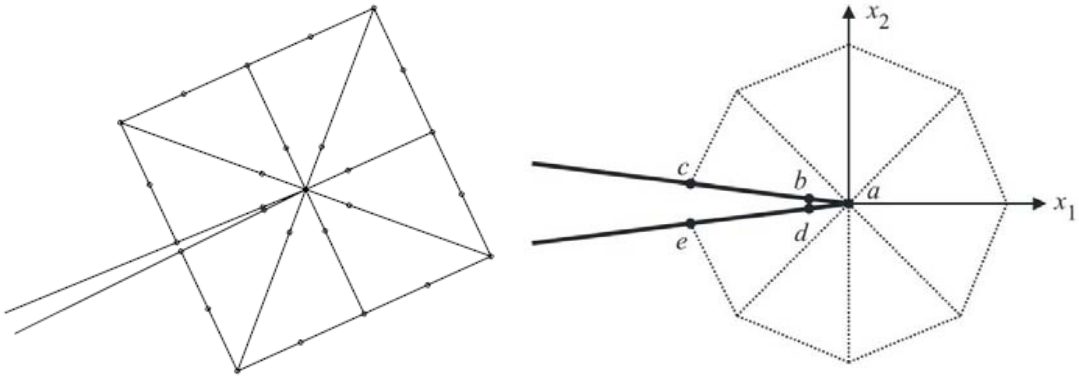

a) b)

Figure C.6 (a) Finite element discretization of the crack tip using singular elements;
(b) Displacement correlation method from quarter point singular elements

For the quarter-point singular element, in two dimensions, the displacement field is given by:

$$u' = \bar{u}'_A + (-3\bar{u}'_A + 4\bar{u}'_B - \bar{u}'_C)\sqrt{r/L} + (2\bar{u}'_A + 2\bar{u}'_C - 4\bar{u}'_B)\, r/L \quad \text{C.16}$$

$$v' = \bar{v}'_A + (-3\bar{v}'_A + 4\bar{v}'_B - \bar{v}'_C)\sqrt{r/L} + (2\bar{v}'_A + 2\bar{v}'_C - 4\bar{v}'_B)\, r/L \quad \text{C.17}$$

Herein, u' and v' are the local displacements of the nodes along the crack in the singular elements. Equating the terms of equal power 1/2 in the preceding two equations, the $\sqrt{r}$ term vanishes, and we can obtain the two stress intensity factors for mixed mode problems:

$$\begin{Bmatrix} K_I \\ K_{II} \end{Bmatrix} = \frac{1}{2}\frac{2G}{\kappa+1}\sqrt{\frac{2\pi}{L}}\begin{bmatrix} 0 & 1 \\ 1 & 0 \end{bmatrix}\begin{bmatrix} -3\bar{u}'_A + 4(\bar{u}'_B - \bar{u}'_D) - (\bar{u}'_C - \bar{u}'_E) \\ -3\bar{v}'_A + 4(\bar{v}'_B - \bar{v}'_D) - (\bar{v}'_C - \bar{v}'_E) \end{bmatrix} \quad \text{C.18}$$

Thus it can be readily seen that the extraction of the SIF can be accomplished through a 'post-processing' routine following a conventional finite element analysis in which the quarter point elements have been used.

C.5 J-integral Calculation Path

As describe before in Appendix C.4 Singular Element in LEFM, *J*-integral is a special powerful parameter to predict crack propagation value, especially for nonlinear elastic cracked body. Crack energy flow package can deal with two types of crack calculation *LEFM* and *EPFM*: they offer full control of the nodes in front of the crack tip and integrate the rate of the total potential energy. Even if the special crack tip elements are valid for elastic-plastic analysis, the results will be satisfactory.

It was found that the applied *J* vs. displacement for shell cracks bridged by stiffener, or girder can be calculated incorporating all sections. Standard crack calculation by *J*-integral will use high order element; the node information will be summed along the selected path (shown in Figure C.7). The innermost ring contains "collapsed" elements to represent the singularity in the crack tip stress field.

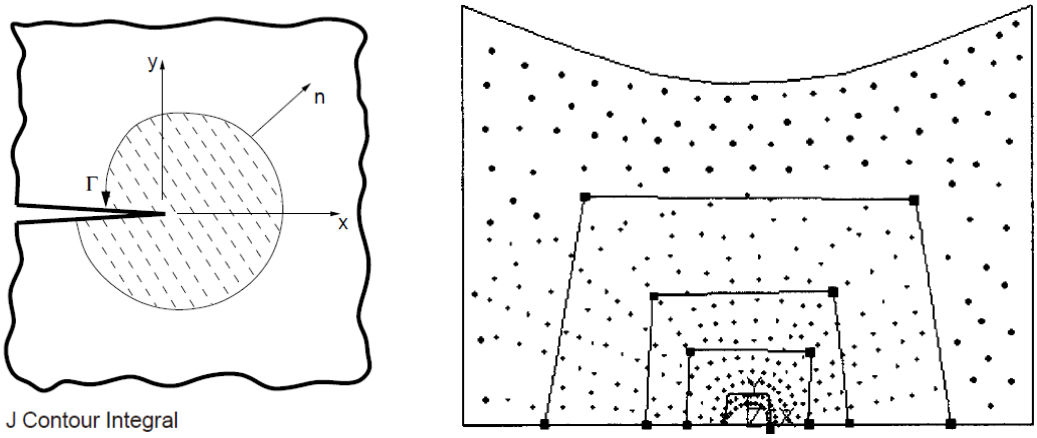

Figure C.7 Available FE **J** integral path around the crack tip region (ANSYS 13.0 User Manual)

The *J*-integral can be determined from analytical derivations or displacement measured. The energy release rate for the general multi dimension case can then be written in the matrix notation as the discretized form is given by

$$J = \int_{\Gamma} W dy - \int_{\Gamma} T \frac{\partial u}{\partial x} ds = \sum_{i=1}^{n} [\sigma_{ij} \frac{\partial u_j}{\partial x_1} - w\delta_{1i}] \frac{\partial q}{\partial x_i} w_{iw} A_{ie} \qquad \text{C.19}$$

Walterset al. (2006) also reported mixed mode stress intensity factors for three-dimensional cracks using a two-state interaction integral method. Shih and Hutchinson (1976) proposed a general method to compute *J*, later developed further and validated in the General Electric Corporation of a handbook (1981).

Many methods and models have been presented for estimation of J-integral. Consequently FE is accepted to estimate J along the crack front for the comparison purpose.

If an analysis is being performed by the finite element method, the formulas of the energy release rate have to be put into the finite element framework. One of discretized forms of the *J*-integral was provided by Shih et al (1986), the numerical method for evaluating *J*-integral can be written as:

$$J = \sum_{AorV} \sum_{P=1}^{m} \{[(\sigma_{ij} \frac{\partial u_j}{\partial x_1} - w\delta_{1i}) \frac{\partial q}{\partial x_1}] \det(\frac{\partial x_j}{\partial \xi_k})\}_p w_p - \sum_{crackface} (\sigma_{2j} \frac{\partial u_j}{\partial x_1} q) w \qquad \text{C.20}$$

where m is the number of Gaussian points for each element, w and w_p are weighting factors, σ_{ij} are stress components, u_j, are displacement members, x_i, are

global coordinates, ξ_i , are local coordinates, δ_{ij} , is the *Kronecker* delta.

The 3D implementation will be a little more complicated than the 2D situations; however, the principal is the same for path simulations. For the 3D crack problems, domain integral representation of the J-Integral is a volume integration, which again is evaluated over a group of elements.

It consists of path operations necessary to compute the J-Integral; one contour path was used around the crack tip to calculate J.

C.6 Fracture FE Case Study

Consider a finite plate in tension with a central crack as shown in Figure 1, the plate is made of steel with Young' modulus E=200GPa and Poisson's ratio v=0.3. Let b=0.2m, a=0.02m, Pressure=100MPa. Determine the SIFs (stress intensity factors) using 2D facture, and J-integral analysis.

An analytical solution given by W.D.Pilkey (Formulas for Stress, Stain, and Structural Matrices) is

$$K_I = C\sigma\sqrt{\pi a} \qquad \text{C.21}$$

$$C = 1.12 - 0.23(a/b) + 10.6(a/b)^2 - 21.7(a/b)^3 + 30.4(a/b)^4$$

where $\eta = \dfrac{a}{b}$

Use of this section yields $K_I = 25.680MPa \cdot \sqrt{m}$

Linear elastic and fracture mechanics (LEFM) and Plane stress assumption is used, the SIFs at a crack tip may be computed using the ANSYS commend (KCALC). The right-half model is used to calculate the SIF for 2D model refer to the model of "ANSYS TUTORIAL". (Using the APDL to finish the calculation) shown in Figure C.8 and Figure C.9

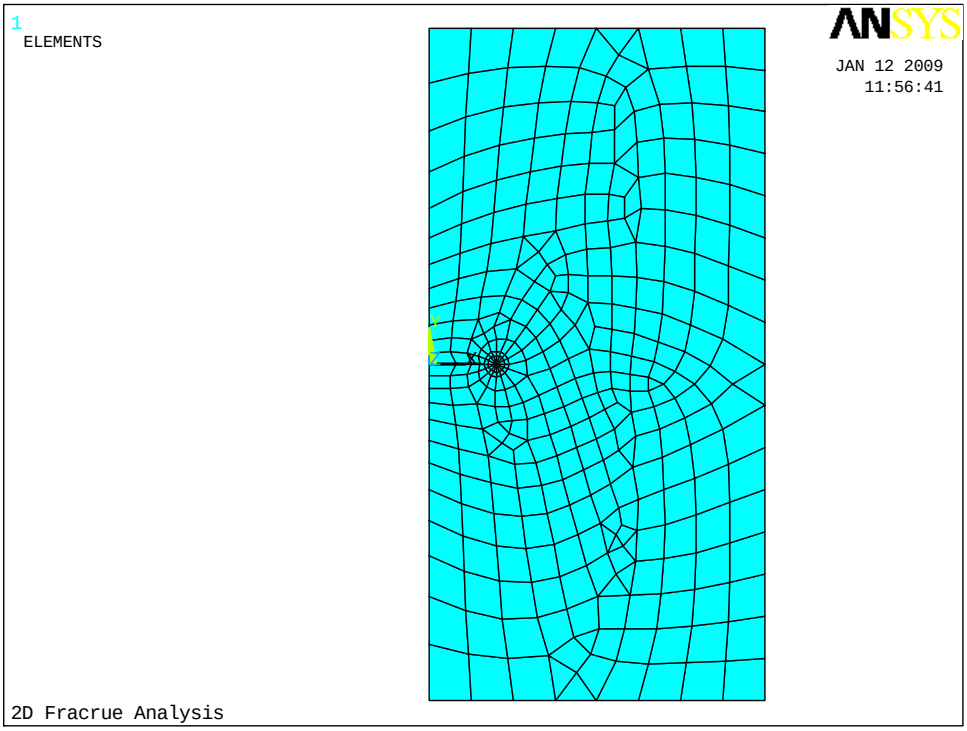

Figure C.8 The right-half model for 2D calculation

The crack-tip region is meshed using quarter-point (singular) 8 node quadrilateral elements (Shell93). The whole process was finished by GUI in "ANSYS TUTORIAL-2D FRACTURE ANALYSIS" in Figure C.9.

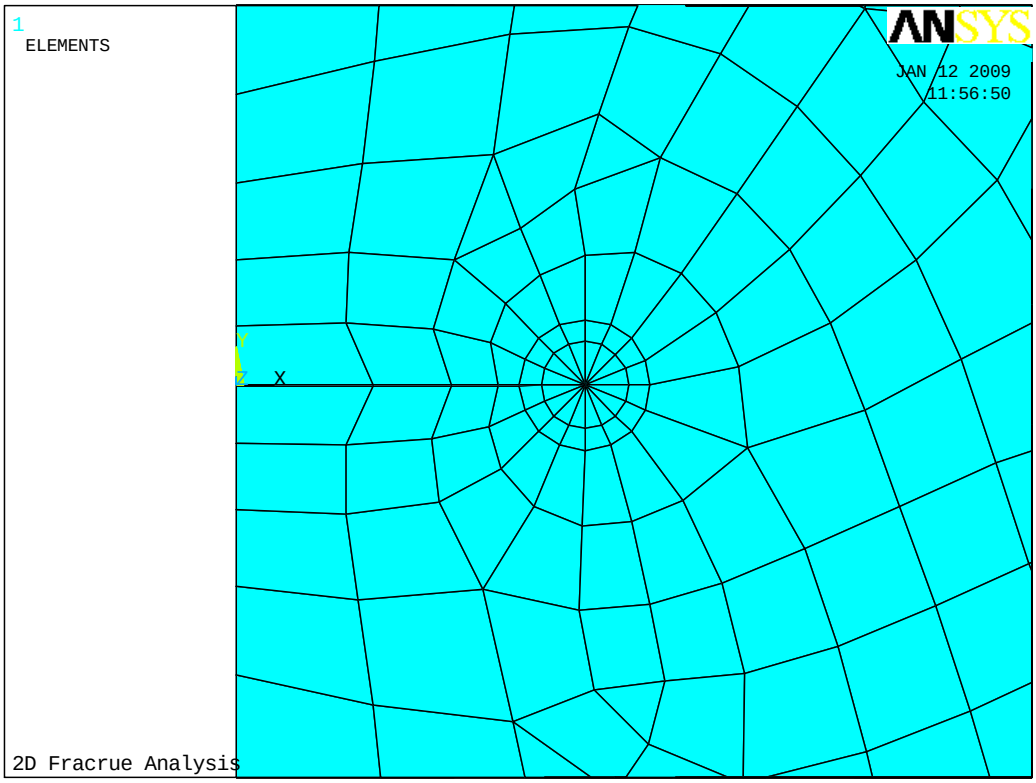

Figure C.9 the detail information of half model for 2D calculation

Classical fracture theory defines 3 fundamental modes (I The opening mode; II the edge-sliding mode; III the tearing mode) based on macroscopic relative displacement profiles. For this finite cracked sheet with uniform normal stress problem, only the first-mode fields are present.

It is general noticed that smooth and silky corresponding to the crack propagation by fatigue of corresponding to brittle fracture. Any cracking can be brought back to the one of the three simple stress modes or their superposition. There are thus three elementary failure modes of cracking shown in Figure C.10.

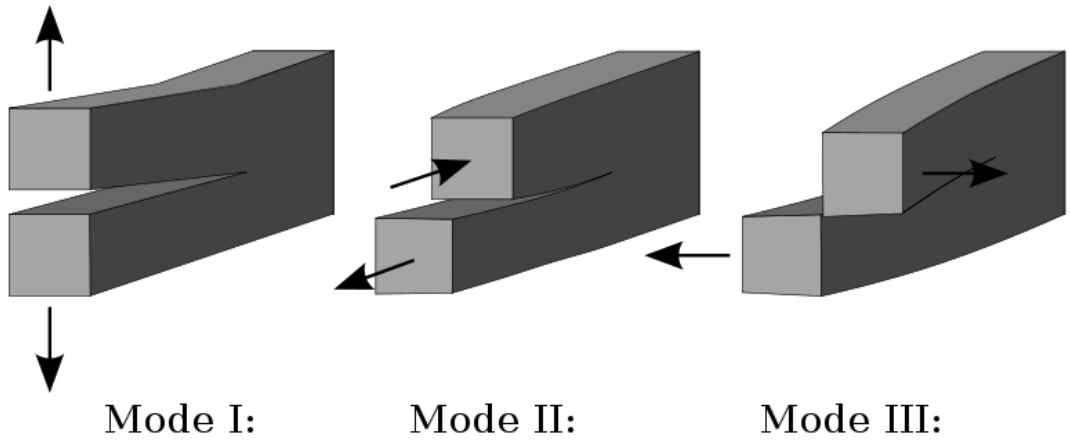

Figure C.10 Fracture failure modes with related loading situations

Mode I: mode of crack opening, where displacements with the lips of the crack are perpendicular to the direction of crack propagation;

Mode II: mode of in-plane shear, where displacements with the lips of the crack are parallel to the direction of crack propagation;

Mode III: mode of out-of-plan shear, where displacements with the lips of the crack are parallel to the crack front.

The stress intensity factor calculation equation for Mode I:

$$K_I = C_1 \sigma a^{1/2}; \quad K_{II} = K_{III} = 0 \qquad \text{C.22}$$

J-Integral method

$$J = \int_\Gamma W dy + \int_\Gamma (t_x \frac{\partial u_x}{\partial x} + t_y \frac{\partial u_y}{\partial y}) ds \qquad \text{C.23}$$

where

$$\int_\Gamma W dy = \frac{(1+\upsilon)(1-2\upsilon)}{4E} K_I^2 \qquad \text{C.24}$$

$$\int_\Gamma (t_x \frac{\partial u_x}{\partial x} + t_y \frac{\partial u_y}{\partial y}) ds = -\frac{(1+\upsilon)(3-2\upsilon)}{4E} K_I^2 \qquad \text{C.25}$$

and

$$J = \frac{K_I{}^2 \left(1-\nu^2\right)}{E} \qquad \text{C.26}$$

Due to the symmetry of the problem, a quarter models can be used in this report for 3D and J-integral methods shown in Figure C.11.

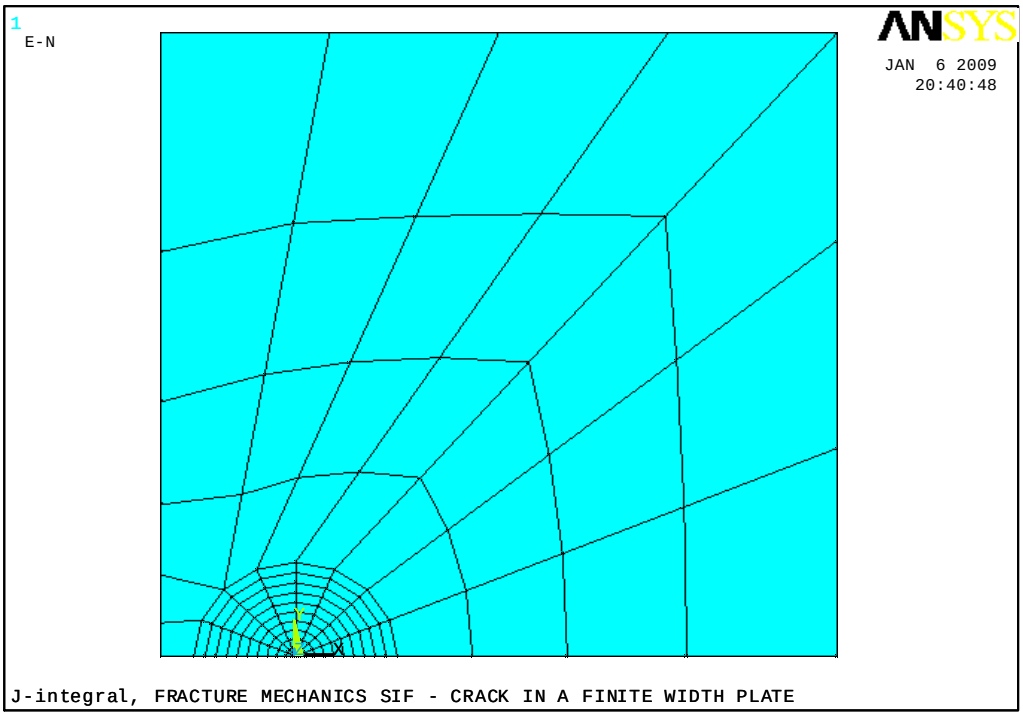

Figure C.11 the quarter model for 3D calculation

This variable, stress intensity factor is the function of the crack length a, component geometry and the applied loading; although, the numerical value has an accuracy of better than 0.5% for any value of ratio a/b, the process is time-wasting work. Obviously, it can be considered as the natural endurance ability to the fatigue strength.

REFERENCES

1. Libor Jendele, Jan Cervenka, on the solution of multi-point constraints-Application to FE analysis of reinforced concrete structures, Computers and Structures, 970–980
2. Mark Ainsworth, Essential boundary conditions and multi-point constraints in finite element analysis, Computer Methods in Applied Mechanics and Engineering: 6323-6339

3. Singiresu s. Rao, The Finite Element Method in Engineering, Elsevier Science & Technology Books. ISBN: 0750678283
4. V Saouma, D Schwemmer, Numerical evaluation of the quarter point crack tip singular element, International Journal of Numerical Methods in Engineering 20(1984): 1629-1641

APPENDIX D

Special Technology in Fatigue and Fracture Analysis

D.1 VCCT Technology

The stress intensity factor at the crack front was computed using the virtual crack closure technique (VCCT). This technique was originally proposed by Rybicki and Kanninen (1977), is a very attractive SIF extraction technique, a relatively easy algorithm of application capability of FEM.

$$G_i = \frac{K_i}{E} or \frac{K_i}{E}(1-\upsilon^2) \qquad \text{D.1}$$

The idea (E.F. Rybicki and M.F. Kanninen, 1977) presented in technical paper is based on the calculation of the energy release rate, using Irwin assumption that the energy released in the process of crack expansion is equal to work required to close the crack to its original state as the crack extends by a small amount.

We note that deLorenzi (deLorenzi, H.G., 1985) has shown that the energy release rate is given by

$$G = \frac{1}{\Delta A}\int (\sigma_{ij}\frac{\partial u_j}{\partial x_1} - w\delta_{i1})\frac{\partial \Delta x_1}{\partial x_i} dA \qquad \text{D.2}$$

for a unit crack growth extension along x_1

It is shown in Figure D.1 that FE model in the vicinity of a crack tip before the virtual crack closure.

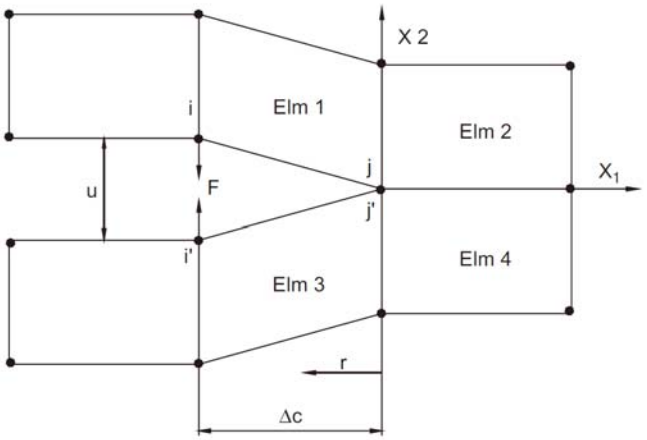

Figure D.1 2D finite element model in the vicinity of a crack tip before the virtual closure

For the finite element calculation, similar procedure can be applied to put the nodes in pairs to calculate the strain energy release rate. The translation vector always indicates corresponding nodes.

D.2 Paris Law Formulas

It is submitted that physical modelling of fatigue crack growth remains uniquely unsuccessful. But that should not worry us too much, since Fracture Mechanics analysis methods allow the prediction of growth rates of structural cracks from simple lab test configurations. It saves us from being required to have an understanding of the detailed micro-physics of crack growth.

The formula sets up a theoretical framework accounting for effects believed to be important, which efforts can be refined. Overview, reference states that the evaluation of failure analyses was hampered by a combination of a limited data base and uncertainties in experimental inputs. For those reasons, it should not be inferred that discrepancies between theory and experience reveal an inherent deficiency of fracture mechanics.

Most proposals were judged to be too empirical and received sceptically by many

experts in the field. Usually ΔK is a function of the crack length under a cyclic stress or displacement. The number of fatigue-crack growth rate relations in the literatures is enormous, but the first such relation was attributed to Head. Table D.1 gives list of some crack-growth rate relations that have been proposed since the early 1960's. This list is just a slight section summary of the all major relations currently used today.

Table D.1

Evolution of some typical crack-growth rate relations

Table-lookup procedure	Peoples	Dates
$dc/dN = C\Delta K^n$	Paris, Gomez and Anderson	1961
$dc/dN = C\Delta K^n(\Delta K_{\max})^m$	Paris and Erdogan	1963
$dc/dN = f(\Delta K, R, K_c)$	Forman, Kearney and Engle	1967
$dc/dN = f(\Delta CTOD)$	Tomkins	1968
$dc/dN = C(\Delta K_{eff})^n$	Elber	1970
$dc/dN = f(\Delta K, R)$	Walker	1970
$dc/dN = C(\Delta J_{eff})^n$	Dowling and Begley	1976
$dc/dN = f(W_{eff})$	Ogura et al.	1985
$dc/dN = f(\Delta K, R)$	Miller and Gallagher	1981

D.3 SN Assessment Employing FE-SAFE

The section above has described the process of calculating fatigue lives from linear FE-SAFE commercial packages. For FE analyses ANSYS may be used to model a series of ship structures, with the stress results being written for each event and FE-SAFE will analyze the sequence of stresses, and get the fatigue life of the real ones. Its focus has been to provide useful information to the design engineer when fatigue failure may be a concern.

The fatigue analysis requires accurate stress information, and inadequate meshing will give accurate stresses rarely. Sensitivity analysis, where fatigue lives

are calculated for the same model with different mesh densities, it is recommended using FE-SAFE to predict the fatigue life.

It can be separated into 3 areas: materials definition, loading analysis, and results evaluation. In the previous examples, loading was applied in the form of static load on the steel material, and analysis assumes that linear relationship between load and stress responses.

By introducing the stresses from calculating software, graphics may not be able to plot fatigue life contour plots on a linear scale because the contour algorithms cannot cope with the large range of numbers, which may encompass several orders of magnitude. Contour plots of fatigue life provide the clear indication of fatigue lives and the location of crack initiation sites.

The SN approach is effective method for fatigue assessment when fatigue life may be defined as a crack reaching the physically final crack. The statistical evaluation of the test results is given by Fricke (2004), using again a fixed slope exponent of the SN curve. For the lower-bound SN curve (97.7%) in the following form

$$\log N = \log a - m \log \Delta\sigma_n \qquad \text{D.3}$$

If the constant amplitude fatigue limit of the resistance SN curve corresponds to endurance less than 10^8 cycles, the fatigue resistance curve has to be modified according to:

$$\log N = \log \bar{a} - m \log \Delta\sigma \qquad \text{D.4}$$

N = predicted number of cycles to failure for stress range $\Delta\sigma$

$\Delta\sigma$ = stress range

m = negative inverse slope of S-N curve

$\log \bar{a}$ = intercept of log N-axis by S-N curve

$$\log \bar{a} = \log a - 2s \qquad \text{D.5}$$

a = constant relating to mean S-N curve

s = standard derivation of $\log N$

The slope of the fatigue strength curves for details assessed on the basis of

normal stresses is m=3.00. The constant amplitude fatigue limit is 5×10^6 cycles. The slope of the fatigue strength curves for details assessed on the basis of the shear stresses is m=5.00, but in this case the fatigue limit corresponds to an endurance of 10^8 cycles. FE-SAFE analysis is discussed in this section, have been comprised in this section by following:

(a) Several options accounting for mean stress are available; the elastically-calculated FEA nodal stress tensor is read;

(b) The stress tensor is multiplied by the time history of the applied loading, to produce a time history of the stress tensor;

(c) The time histories of the in-plane principal stresses are calculated. (The out-of-plane stress is checked for possible contact loading);

(d) The time histories of the three principal strains can be calculated from the stresses;

(e) For SN curve analysis a plane perpendicular to the surface is defined, and the time history of the stress normal to this plane is calculated;

(f) On the fatigue damage is calculated. For the individual fatigue cycles are identified using a 'Rainflow' cycle algorithm, the fatigue damage is calculated and the total damage is summed. The plane with the shortest life defines the plane of crack initiation, and this life is written to the output file;

(g) During the calculation, FE-SAFE may modify the endurance limit amplitude. If any cycle is damaging, the endurance limit amplitude is no calculated fatigue damage on the component, and the damage curve extended to this new endurance limit.

The availability of commercial FE tools is limited while the stress intensity factor calculations that are available are usually quite expensive and difficult to use in the hands of designers. Currently, fatigue life approach has been adopted for conducting FE analysis. It would of course be possible to use FEA to calculate the stresses or strains responses for each point in the load history.

And more that the failure behaviour of complex structures determined in numerical analyses may differ from the actual failure behaviour due to varying residual stresses.

REFERENCES

1. E.F. Rybicki, M.F. Kanninen, A finite element calculation of stressintensity factors by a modified crack closure integral, Eng. Fract. Mech. 9 (1977) 931–938
2. Fricke W, Doerk O, Gru¨ nitz L. Fatigue strength investigation and assessment of fillet welds around stiffener and bracket toes. Proceedings of the OMAE Specialty Conference on FPSO systems, OMAE-FPSO'04-0010, Houston, TX, ASME International Petroleum Technical Institute; 2004.
3. H. G. deLorenzi, "Energy Realease Rate Calculations by the Finite Element. Method,"Engineering Fracture of Mechanics, Vol.21, pp. 129-143
4. Rybicki EF, Kanninen MF, A finite element calculation of stress intensity factors by a modified crack closure integral. Engng Fract Mech 1977; 9:931-8